Development of Gene Therapy for Recessive Dystrophic Epidermolysis Bullosa

Christos Georgiadis

Institute of Child Health

University College London

A thesis submitted for the degree of Doctor of Philosophy

Declaration

I, Christos Georgiadis, confirm that the work presented in this thesis is my own. Where information has been derived from other sources, I confirm that this has been indicated in the thesis.

Abstract

Recessive dystrophic epidermolysis bullosa (RDEB) is a debilitating genetic cutaneous blistering condition caused by loss-of-function mutations in *COL7A1,* encoding type VII collagen (C7), central in anchoring fibril (AF) formation at the dermal-epidermal junction (DEJ). Presently no curative treatments exist for RDEB. Reconstitution of *COL7A1* expression in autologous primary keratinocytes (KC) and fibroblasts (FB) by *ex vivo* gene therapy was hypothesised to restore C7 expression and AF construction at the DEJ and ameliorate the RDEB skin phenotype.

Feasibility of this approach was demonstrated using a therapeutic grade, self-inactivating-lentiviral vector, encoding codon-optimised *COL7A1* (LV-COL7) to transduce primary RDEB KCs and FBs. Expression and secretion of full-length *de novo* C7 was confirmed, with transduced cells exhibiting supranormal levels of protein expression and functional recovery in *in vitro* migration assays. A human:murine chimeric preclinical RDEB skin graft model was developed to assess functional correction mediated by the transduced cells *in vivo*. RDEB grafts lacking C7 expression exhibited severe blistering recapitulating the disease phenotype. Gene-modified grafts, showed C7 deposition at the DEJ, with re-establishment of basement membrane zone integrity. Functional correction was confirmed by an abundance of *de novo* synthesised AF structures throughout the DEJ securing dermal-epidermal attachment. Gene-corrected FBs were shown to mediate a superior therapeutic benefit.

In addition, an alternative strategy was developed using zinc finger nucleases (ZFN) for the targeted editing of *COL7A1* and site-specific restoration of endogenous C7 expression. Incorporation of ZFNs into non-integrating lentiviral vectors (NILV) resulted in a marked improvement of their cleavage activity. ZFN-mediated disruption of *COL7A1* in KCs confirmed at both genomic and protein level initially enabled the *in vitro* modelling of RDEB, with observed regression of migration speeds. A dsDNA donor repair template was designed and codon optimised for co-delivery with the ZFNs. Sequencing across the ZFN binding site confirmed site-specific template insertion by targeted homologous recombination.

In conclusion, gene correction of primary RDEB cells by LV-COL7 can mediate restoration of protein and structural defects in an RDEB model forming the proposal for therapeutic application in man. Furthermore, development of an alternative site-specific targeting strategy for correction of *COL7A1* provides a promising insight into the realm of patient-tailored therapy.

Publications arising

The results described in Chapters 3 and 4 of this thesis are published in:

Georgiadis C, Syed F, Petrova A, Abdul-Wahab A, Lwin SM, Farzaneh F, Chan L, Ghani S, A. Fleck RA, Glover L, McMillan JR, Chen M, Thrasher AJ, McGrath JA, Di WL and Qasim W. Lentiviral engineered fibroblasts expressing codon optimized *COL7A1* restore anchoring fibrils in RDEB. J Invest Dermatol. 2016 Jan;136(1):284-92. doi: 10.1038/JID.2015.364

The results described in Chapters 3 and 4 of this thesis have significantly contributed towards:

A prospective phase I study of lentiviral-mediated COL7A1 gene-corrected autologous fibroblast therapy in adults with recessive dystrophic epidermolysis bullosa (LENTICOL-F)
ClinicalTrials.gov Identifier: (NCT02493816)
Investigator: Professor John McGrath, Professor of Molecular Dermatology and Consultant Dermatologist
Co-applicants: Dr Jemima Mellerio, Professor Waseem Qasim, Dr Wei-Li Di, Professor Adrian Thrasher
Institution: St John's Institute of Dermatology, Division of Genetics and Molecular Medicine
Grant: £499,320 (01/02/2015 – 31/01/2018) Sohana Research Fund

Acknowledgments

I would like to start by thanking my principal supervisor Wei-Li Di for her tremendous support throughout this project. There was never a time when she was too busy to offer to help or discuss my work and troubleshoot with me. Her passion about research, especially when it involved dermatology made her a fantastic supervisor, which I can truthfully say I am extremely grateful to have had. Wei-Li has also been especially encouraging, giving me countless opportunities to present my work in both national and international conferences, which I have found truly rewarding. Of course, an equal part in the completion of this project has been played by Waseem Qasim. He has been instrumental in seeing the bigger picture, challenging your thoughts, and bringing you down to earth when needed first thing on a Monday. His faith and perseverance with this project has seen it now enter a phase I clinical trial within a matter of 4 years. I would also like to thank Adrian Thrasher for his guidance and encouragement. Furthermore, I would like to acknowledge my funding from the UCL IMPACT CHRAT studentship, the Bogue fellowship and the NIHR GOSH BRC doctoral training support fund.

I am also truly grateful to my host at the University of Minnesota, Jakub Tolar, who gave me the opportunity to carry out some fascinating research in his lab. He is an inspirational individual who sees no obstacles in research and is ready to tackle anything; although I believe that has something to do with typically responding to emails at 4am. It was a great experience spending those few months in such a beautiful part of the world and learning the ways of a well-managed US lab. In hindsight though, I am gutted I did not take his advice as to what time of the year to best visit Minnesota. He had warned me my ears would fall off. .

However the experience of a PhD involving countless hours in the lab is not devoid of great friendships. I would particularly like to thank Emma for being my first port of call when I started, and even more so for providing comic relief when most needed. Also both Ben and Ulrike for being fantastic friends and because let's face it. . it's slim pickings in the lab at 11pm. Also Sian for her constant supply of baked goods and motivational thesis writing treats, such as the world's smallest whisky bottle (I've been saving this thimbleful for this day). Nancy and Ekaterina for passing down all their Western blot knowledge and Claire for her help with NGS. Sameer of course, for being such a selfless person and a fantastic colleague, always there to help, make you laugh with his online purchasing disasters and share his lunch with you in times of desperation. A special thanks goes to coffee. I'm also indebted to all my non-science friends who have been considerate enough to ignore me for the past few months, but who will hopefully also be patient enough to endure a bit more science blurb until I am slowly weaned off.

Most importantly though, I would like to thank my mum and brother for their unconditional and constant support. It's been a tough journey but we have held it together, as this would have otherwise been impossible without you. And of course Nastia, I honestly have the utmost respect for you and I'm truly appreciative of all you help and commitment. Thank you.

Dedicated to my dad.

ABSTRACT **3**

ABBREVIATIONS **17**

CHAPTER 1 INTRODUCTION **20**

1.1 EPIDERMOLYSIS BULLOSA: OVERVIEW AND CLASSIFICATION 20

1.2 STRUCTURE OF THE HUMAN SKIN 22

1.2.1 Human epidermis *23*

1.2.2 Basement membrane zone *26*

1.2.3 Human dermis *28*

1.3 MOLECULAR CHARACTERISATION OF EPIDERMOLYSIS BULLOSA SUBTYPES 29

1.3.1 Simplex EB *29*

1.3.2 Junctional EB *30*

1.3.3 Kindler syndrome *30*

1.4 DYSTROPHIC EB 31

1.5 TYPE VII COLLAGEN 33

1.5.1 Non – Collagenous domain 1 (NC-1) *34*

1.5.2 Triple helical domain *35*

1.5.3 Non – Collagenous Domain 2 (NC-2) *36*

1.5.4 Organisation into anchoring fibrils (AFs) *36*

1.5.5 Type VII collagen involvement in SCC progression *38*

1.6 CURRENT THERAPIES FOR RDEB 39

1.6.1 Conventional treatments for RDEB *39*

1.6.2 Replacement therapies for RDEB - recombinant protein therapy *40*

1.6.3 Cell therapies for RDEB *42*

1.6.3.1 Epidermal grafting and intradermal administration of allogeneic cells 42

1.6.3.2 Bone marrow transplantation of allogeneic stem cells 44

1.6.4 Gene therapies for RDEB *46*

1.6.4.1 Phage mediated gene therapy 46

1.6.4.2 γ-retroviral mediated gene therapy 47

1.6.4.3 Lentiviral mediated gene therapy 49

1.6.5 Alternative therapeutic options *51*

1.7 LENTIVIRAL GENE THERAPY 51

1.8 HIV LIFECYCLE 53

1.8.1 Viral attachment *53*

1.8.2 Viral entry *53*

1.8.3 Reverse transcription *54*

1.8.4 Nuclear import *54*

1.8.5 Proviral integration *55*
1.8.6 Transcription *55*
1.8.7 Nuclear export *55*
1.8.8 Translation viral assembly and budding *56*
1.9 DEVELOPMENT OF LENTIVIRAL VECTORS 58
1.10 ZINC FINGER NUCLEASES AS A HIGHLY TARGETED GENE-EDITING TOOL 61
1.10.1 Zinc finger protein structure and their development *61*
1.10.2 Zinc Finger Nuclease complexes for induction of DNA breaks *63*
1.10.3 ZFNs and their use in the clinic *64*
1.10.4 ZFNs for the in vitro modelling and treatment of genetic diseases *65*
1.10.5 Modes of delivery of ZFN to mammalian cells *66*
1.10.5.1 DNA plasmid/mRNA 66
1.10.5.2 Adeno-Associated Viruses (AAV) 66
1.10.5.3 Non-integrating Lentiviral Vectors (NILV) 67
1.10.5.4 ZFN proteins 68
1.10.6 Emergence of newer systems *68*
1.11 PROJECT AIMS 70
Hypothesis *71*
Objectives *71*
CHAPTER 2 MATERIALS AND METHODS 73
2.1 MATERIALS 73
2.1.1 Reagents *73*
2.1.3 Kits *75*
2.1.4 Buffers *75*
2.1.5 Culture media *77*
2.1.6 Antibodies *78*
2.1.7 Mammalian and murine cells *80*
2.1.8 Mouse Strains *81*
2.1.9 Primers *81*
2.1.10 Parental plasmids *82*
2.1.11 Generated plasmids *83*
2.1.12 E. coli bacterial competent cell strains *84*
2.2 METHODS 84
2.2.1 Growth of E. coli bacterial cells *84*
2.2.2 Preparation of JM109 competent cells *84*
2.2.3 Bacterial transformation *85*
2.2.4 Isolation of primary keratinocytes and fibroblasts from skin biopsies *85*

2.2.5 Irradiation of mouse 3T3 cells 85
2.2.6 Culture of mammalian cell lines 86
2.2.7 Culture of human keratinocytes 86
2.2.8 Culture of human fibroblasts 86
2.2.9 Freezing and recovery of cells 86
2.2.10 Restriction endonuclease DNA digestion 87
2.2.11 Filling in of 5' DNA overhangs 87
2.2.12 Exonuclease removal of 3' DNA overhangs 87
2.2.13 Dephosphorylation of 5' DNA termini 87
2.2.14 Agarose gel electrophoresis 88
2.2.15 Agarose gel purification of digested DNA fragments 88
2.2.16 Ligation of digested DNA fragments 88
2.2.17 Introduction of silent mutations by site directed mutagenesis 88
2.2.18 Genomic DNA extraction 89
2.2.19 TOPO-TA cloning 89
2.2.20 96-well sequencing reaction and DNA precipitation 89
2.2.21 Cell sorting by limiting dilution and FACS 90
2.2.22 Plasmid DNA preparation 90
2.2.23 Lentiviral vector production 90
2.2.24 Vector titration 91
2.2.25 Viral vector transduction of keratinocytes and fibroblasts 92
2.2.26 Flow cytometry for detection of GFP 92
2.2.27 Flow cytometry for detection of C7 92
2.2.28 Quantitative PCR (qPCR) 93
2.2.29 p24 ELISA 93
2.2.30 Detection of mismatches by nuclease S CEL-I assay 94
2.2.31 High-throughput next generation sequencing 95
2.2.32 In situ immunofluorescence staining 95
2.2.33 SDS-PAGE immunoblotting 95
2.2.34 In vitro wound healing scratch assay 96
2.2.35 In vitro two-dimensional migration assay 97
2.2.36 Bioengineered skin equivalent preparation and grafting on immunodeficient mice 97
2.2.37 Immunofluorescent and histological staining of bioengineered grafted tissue 98
2.2.38 Preparation of skin grafts for transmission electron microscopy (TEM) 99
2.2.39 Statistical analysis 99

CHAPTER 3 RESTORATION OF C7 EXPRESSION IN RDEB CELLS USING *COL7A1* EXPRESSING LENTIVIRAL VECTOR 100

3.1 HIV-1 LENTIVIRAL VECTOR CARRYING CODON-OPTIMISED *COL7A1* TRANSGENE UNDER THE CONTROL OF INTERNAL PGK PROMOTER 101

3.2 PRODUCTION OF PGK-COL7A1 EXPRESSING LENTIVIRAL VECTOR 103

3.3 TRANSDUCTION EFFICIENCY OF LV-COL7 VECTOR IN PRIMARY RDEB KERATINOCYTES AND FIBROBLASTS 105

3.4 RESTORATION OF C7 PROTEIN EXPRESSION IN RDEB KERATINOCYTES AND FIBROBLASTS TRANSDUCED WITH LV-COL7 VECTOR 108

3.4.1 Confirmation of C7 expression in gene modified RDEB cells by in situ immunofluorescence staining 108

3.4.2 Confirmation of C7 protein production in gene modified RDEB cells by Western blot 110

3.4.2.1 Antibody specificity against full-length C7 protein 110

3.4.2.2 Expression of full-length C7 in LV-COL7 transduced RDEB keratinocytes 111

3.4.2.3 LV-COL7 mediated C7 restoration in gene modified primary RDEB fibroblasts 114

3.5 FUNCTIONAL CORRECTION IN LV-COL7 TRANSDUCED RDEB KERATINOCYTES AND FIBROBLASTS 117

3.5.1 Improved cell migration in RDEB keratinocytes transduced with LV-COL7 117

3.5.2 Normalisation of RDEB fibroblast migration following correction by LV-COL7 119

3.6 DISCUSSION 121

CHAPTER 4 FUNCTIONAL EVALUATION OF GENE MODIFIED RDEB CELLS IN *IN VIVO* HUMAN:MURINE CHIMERIC SKIN GRAFT MODEL 123

4.1 HISTOLOGICAL FEATURES OF BIOENGINEERED HUMAN SKIN GRAFTS 124

4.1.1 Identification of the human skin graft and distinction from mouse tissue using human-specific tissue markers 124

4.1.2 Detection of human C7 protein in bioengineered human grafts 126

4.1.3 Epidermal differentiation markers in human and mouse skin 129

4.2 DEVELOPMENT OF AN *IN VIVO* PRE-CLINICAL RDEB HUMAN:MURINE CHIMERIC SKIN GRAFT MODEL 131

4.2.1 Formation of bioengineered RDEB skin equivalents 131

4.2.2 Human:murine chimeric skin graft model for the in vivo assessment of RDEB gene therapy 133

4.3 FUNCTIONAL RECOVERY OF C7 IN RDEB SKIN GRAFTS GENETICALLY CORRECTED BY LV-COL7 135

4.3.1 Restoration of C7 expression in graft generated by LV-COL7 corrected RDEB patient fibroblasts 135

4.3.2 Assessment of C7 function in an in vivo human:murine skin graft model 141

4.4 ANCHORING FIBRIL FORMATION IN GENE CORRECTED GRAFTS CONFIRMED BY TRANSMISSION ELECTRON MICROSCOPY 145

4.4.1 Amelioration of tissue cleavage through functional C7 anchoring fibril formation in graft generated from LV-COL7 gene corrected fibroblasts 145

4.4.2 Anchoring fibril formation in graft generated using a combination of LV-COL7 transduced RDEB keratinocytes and fibroblasts 149

4.5 DISCUSSION 152

CHAPTER 5 GENOME EDITING AS A TOOL FOR ESTABLISHING AN *IN VITRO* RDEB MODEL AND CORRECTING MUTATIONS IN *COL7A1* 155

5.1 TARGETED DISRUPTION OF *COL7A1* BY DNA PLASMID-BASED ZFN DELIVERY 156

5.2 DISRUPTION OF *COL7A1* IN KERATINOCYTES BY LENTIVIRAL-BASED ZFN DELIVERY - GENERATION OF AN *IN VITRO* RDEB CELL MODEL 157

5.2.1 Improvement of ZFN delivery efficiency by incorporation of ZFN sequences into a non-integrating lentiviral platform 157

5.2.2 Efficiency of NHEJ-mediated cleavage in keratinocytes transduced with NILV-ZFNs 158

5.2.3 Assessment of NILV-ZFN cleavage frequency in single cell clones 160

5.2.4 NILV-ZFN treated NTERT clones result in significant C7 disruption 162

5.2.5 Alteration of migration speed in cells transduced with NILV-ZFNs 164

5.2.6 Restoration of C7 expression in NILV-ZFN COL7A1 knockout cells following transduction with LV-COL7 166

5.3 GENE EDITING IN *COL7A1* BY HOMOLOGOUS RECOMBINATION-MEDIATED REPAIR FOLLOWING CO-DELIVERY OF NILV-ZFNS AND HOMOLOGOUS DONOR TEMPLATE 167

5.3.1 The design and subcloning of a homologous donor template 167

5.3.2 Integration of donor template into "recipient" genomic DNA by HDR pathway following NILV-induced DSBs 170

5.3.3 SDM modification in the donor template eliminates unwanted cleavage mediated by NILV-ZFNs 172

5.4 RESTORATION OF C7 EXPRESSION AT DEJ OF *IN VIVO* HUMAN:MURINE RDEB SKIN GRAFT MODEL FOLLOWING *COL7A1* GENE EDITING IN RDEB FIBROBLASTS 174

5.5 DISCUSSION 177

CHAPTER 6 DISCUSSION 181

6.1 PROPOSAL OF AN AUTOLOGOUS GENE THERAPY FOR RDEB 181

6.2 OVERCOMING THE OBSTACLES OF GENE TRANSFER TO EPITHELIAL CELLS USING 3RD GENERATION LENTIVIRAL VECTORS 182

6.3 LENTIVIRAL VECTOR CAVEATS- IN SEARCH OF OPTIMISATION STRATEGIES 185
6.4 DETERMINING THE FUNCTIONAL PROPERTIES OF *DE NOVO* SYNTHESISED C7 187
6.5 DEVELOPMENT OF A RDEB HUMAN:MURINE CHIMERIC MODEL ALLOWS FOR *IN VIVO* EVALUATION OF GENE CORRECTED CELLS 189
6.6 FIBROBLASTS DEMONSTRATE DESIRABLE CHARACTERISTICS MAKING THEM SUITABLE THERAPEUTIC CANDIDATES 190
6.7 PERSONALISED MEDICINE FOR RDEB - GENOME EDITING AS A TOOL FOR THE CORRECTION OF *COL7A1* MUTATIONS 192
6.8 CONCLUDING REMARKS 198
REFERENCES 200

List of Figures

FIGURE 1.1 SCHEMATIC OF HUMAN SKIN. 23
FIGURE 1.2 BASEMENT MEMBRANE ZONE. 28
FIGURE 1.3 TISSUE CLEAVAGE SITES IN EB SUBTYPES. 31
FIGURE 1.4 PROPORTION OF MUTATIONS IN *COL7A1* GENE 32
FIGURE 1.5 SCHEMATIC REPRESENTATION OF THE STRUCTURAL ORGANISATION OF THE TYPE VII COLLAGEN PRO-A1(VII) POLYPEPTIDE EXONS 34
FIGURE 1.6 ORGANISATION OF TYPE VII COLLAGEN INTO ANCHORING FIBRILS. 37
FIGURE 1.7 HIV-1 LIFECYCLE IN HOST MAMMALIAN CELL. 57
FIGURE 1.8 REVERSE TRANSCRIPTION OF HIV-1. 58
FIGURE 1.9 ZINC-FINGER NUCLEASE STRUCTURE. 62
FIGURE 1.10 HOMOLOGOUS DIRECTED REPAIR AFTER DELIVERY OF DONOR TEMPLATE TO ZFN TREATED MAMMALIAN CELLS. 64
FIGURE 1.11 GENE MODIFICATION STRATEGIES FOR THE CORRECTION OF AUTOLOGOUS RDEB CELLS 72
FIGURE 2.1 SCHEMATIC OF THE SURVEYOR NUCLEASE CEL-I ASSAY FOR THE DETECTION OF ZFN ACTIVITY. 94
FIGURE 3.1 2ND AND 3RD GENERATION SIN LENTIVIRAL PACKAGING PLASMIDS. 102
FIGURE 3.2 CONFIRMATION OF LV-COL7 PLASMID BY RESTRICTION DIGESTION ANALYSIS. 103
FIGURE 3.3 TRANSFECTION AND TRANSDUCTION EFFICIENCY OF LV-GFP VECTOR IN HEK-293T CELLS. 104
FIGURE 3.4 FLOW CYTOMETRY ANALYSIS OF LV-COL7 TRANSDUCED PRIMARY RDEB KERATINOCYTES FOR CONFIRMATION OF C7 EXPRESSION. 105
FIGURE 3.5 INTRACELLULAR C7 EXPRESSION IN LV-COL7 TRANSDUCED RDEB FIBROBLASTS. 107
FIGURE 3.6 CELL PROLIFERATION AND VIABILITY FOLLOWING ESCALATED DOSE OF LV-COL7 TRANSDUCTION 108
FIGURE 3.7 RESTORATION OF C7 PROTEIN EXPRESSION IN RDEB KERATINOCYTES TRANSDUCED WITH LV-COL7 109
FIGURE 3.8 RESTORATION OF C7 PROTEIN EXPRESSION IN PRIMARY RDEB FIBROBLASTS TRANSDUCED WITH LV-COL7. 110
FIGURE 3.9 ANTIBODY ASSESSMENT FOR DETECTION OF C7 EXPRESSION IN WT AND RDEB KERATINOCYTES. 111
FIGURE 3.10 EXPRESSION OF C7 IN CELL LYSATE AND CULTURE MEDIA OF RDEB KERATINOCYTE LINE POST LV-COL7 TRANSDUCTION. 112
FIGURE 3.11 C7 EXPRESSION IN PRIMARY RDEB PATIENT (BT) KERATINOCYTES AND FIBROBLASTS. 114
FIGURE 3.12 RESTORATION OF PROTEIN EXPRESSION IN RDEB PATIENT (EB8) & (CK) FIBROBLASTS FOLLOWING LV-COL7 TRANSDUCTION. 115
FIGURE 3.13 DURABILITY OF C7 EXPRESSION IN RDEB CORRECTED FIBROBLASTS *IN VITRO* 116
FIGURE 3.14 EFFECT ON RDEB KERATINOCYTE MIGRATION FOLLOWING RESTORATION OF C7 PROTEIN EXPRESSION. 118
FIGURE 3.15 EFFECT OF LOSS AND RESTORATION OF C7 EXPRESSION ON RDEB PATIENT (CK) AND (EB8) FIBROBLASTS. 120
FIGURE 4.1 MORPHOLOGICAL STAINING OF SKIN BY H&E AND SPECIES-SPECIFIC ANTIBODIES DIFFERENTIATES BETWEEN HUMAN AND MOUSE TISSUE. 125

FIGURE 4.2 DETECTION OF SPECIES-SPECIFIC C7 EXPRESSION IN HUMAN AND MOUSE TISSUE. 128
FIGURE 4.3 HUMAN SPECIFIC C7 RECOGNITION IN SKIN USING MAB-C7-LH7.2 IMMUNOFLUORESCENT STAINING. 129
FIGURE 4.4 EPIDERMAL MATURATION AND DIFFERENTIATION MARKERS IN HUMAN AND MOUSE TISSUE. 130
FIGURE 4.5 HUMAN:MURINE CHIMERIC SKIN GRAFT MODEL. 132
FIGURE 4.6 ASSESSMENT OF C7 EXPRESSION AND GRAFT MORPHOLOGY USING LV-COL7 TRANSDUCED KERATINOCYTES IN PRE-CLINICAL HUMAN:MURINE CHIMERIC SKIN GRAFT RDEB MODEL. 134
FIGURE 4.7 CONFIRMATION OF BIOENGINEERED HUMAN SES GRAFTED ON NSG MICE BY H&E AND HUMAN SPECIFIC ANTIBODY STAINING. 137
FIGURE 4.8 RESTORATION OF C7 EXPRESSION AT THE DEJ OF THE TRANSDUCED GRAFT MEDIATED BY LV-COL7 GENE CORRECTION OF RDEB PATIENT FIBROBLASTS. 138
FIGURE 4.9 EXPRESSION OF EPIDERMAL MATURATION AND DIFFERENTIATION MARKERS IN GRAFTS GENERATED FROM PRIMARY RDEB PATIENT (CK) KERATINOCYTES AND FIBROBLASTS. 140
FIGURE 4.10 VERIFICATION OF HUMAN ORIGIN OF BIOENGINEERED SES GRAFTED ON NSG MICE BY MORPHOLOGICAL AND SPECIES SPECIFIC STAINING. 142
FIGURE 4.11 RESTORATION OF C7 EXPRESSION IN GRAFT GENERATED BY THE COMBINATION OF LV-COL7 TRANSDUCED KERATINOCYTES AND FIBROBLASTS. 143
FIGURE 4.12 EXPRESSION OF MATURATION AND DIFFERENTIATION MARKERS IN PATIENT (BT) & (EB8) BIOENGINEERED SKIN GRAFTS. 144
FIGURE 4.13 ULTRASTRUCTURAL MORPHOLOGY OF GRAFTS GENERATED FROM RDEB PATIENT (CK) CELLS IMAGED BY TEM. 145
FIGURE 4.14 FUNCTIONAL CORRECTION OF DEJ THROUGH LV-COL7 MEDIATED RESTORATION OF TYPE VII COLLAGEN ANCHORING FIBRILS IN GENE CORRECTED FIBROBLAST GRAFT 148
FIGURE 4.15 ULTRASTRUCTURAL MORPHOLOGY OF GRAFTS GENERATED FROM PATIENT (BT) AND (EB8) CELL COMBINATION IMAGED BY TEM 150
FIGURE 4.16 RESTORATION OF ANCHORING FIBRIL FORMATION FOLLOWING LV-COL7 MEDIATED CORRECTION OF RDEB PATIENT KERATINOCYTES AND FIBROBLASTS. 151
FIGURE 5.1 CEL-I ASSAY FOR THE DETECTION OF ZFN-MEDIATED CLEAVAGE IN HACAT KERATINOCYTES 157
FIGURE 5.2 SCHEMATIC OF 2ND GENERATION NILV TRANSFER AND PACKAGING SYSTEM. 158
FIGURE 5.3 CEL-I ASSAY CONFIRMING NHEJ IN BULK POPULATION OF NILV-ZFNS TRANSDUCED NTERTS. 159
FIGURE 5.4 DETECTION OF NILV-ZFN INDUCED MUTATIONS BY SANGER SEQUENCING. 161
FIGURE 5.5 DETECTION OF MUTATIONS IN SELECTED CLONES OF NILV-ZFN TRANSDUCED NTERTS BY CEL-I NUCLEASE ASSAY. 162
FIGURE 5.6 DISRUPTION OF C7 EXPRESSION FOLLOWING NILV-ZFN. 163
FIGURE 5.7 C7 EXPRESSION IN NTERTS FOLLOWING NILV-ZFN MEDIATED DISRUPTION OF *COL7A1.* 163
FIGURE 5.8 ASSESSMENT OF MIGRATION IN NTERT KERATINOCYTES FOLLOWING NILV-ZFN TRANSDUCTION CAUSING DOWNREGULATION OF C7 165
FIGURE 5.9 RESTORATION OF C7 EXPRESSION IN NILV-ZFN CL4 CELLS TRANSDUCED WITH LV-COL7 167
FIGURE 5.10 DONOR TEMPLATE DESIGN. 168

FIGURE 5.11 ZFN BINDING SITE MODIFICATION OF DONOR TEMPLATE SEQUENCE BY SITE DIRECTED MUTAGENESIS 169
FIGURE 5.12 CONFIRMATION OF TEMPLATE INTEGRATION IN NILV-ZFN + NILV-TEMPLATE TRANSDUCED NTERTS BY KPNI DIGESTION 171
FIGURE 5.13 CONFIRMATION OF HDR-MEDIATED TEMPLATE INTEGRATION BY SDM AND KPNI SITE DETECTION IN NTERT CLONES USING SANGER SEQUENCING. 172
FIGURE 5.14 IDENTIFICATION OF TEMPLATE INTEGRATION SEQUENCES IN NILV-ZFNS + NILV-TEMPLATE CLONES AFTER TOPO-TA SUBCLONING 173
FIGURE 5.15 CORRECTION OF RDEB PATIENT FIBROBLASTS BY TALENS LEADS TO DEPOSITION OF HUMAN C7 AT THE DEJ. 176

List of Tables

TABLE 1.1 SUMMARY OF MOLECULAR AND CLINICAL FEATURES OF EB. 21
TABLE 2.1 LIST OF PRIMARY ANTIBODIES USED IN THIS STUDY. 78
TABLE 2.2 LIST OF SECONDARY ANTIBODIES USED IN THIS STUDY. 79
TABLE 2.3 LIST OF WT MAMMALIAN AND MURINE CELLS. 80
TABLE 2.4 LIST OF RDEB HUMAN PATIENT AND MURINE MODEL CELLS. 80
TABLE 2.5 LIST OF PCR, QPCR AND SDM PRIMERS USED. 81
TABLE 3.1 TITRATION BY QPCR OF LV-GFP AND LV-COL7 VECTORS PRODUCED USING TWO DIFFERENT TRANSFECTION REAGENTS. 104
TABLE 5.1 MUTATION ANALYSIS BY HIGH-THROUGHPUT SEQUENCING OF POLYCLONAL NILV-ZFN TRANSDUCED NTERT POPULATION. 160

Abbreviations

a.a.	amino acid
AAV	adeno-associated virus
Ad	adenovirus
ADA	adenosine deaminase
AF	anchoring fibril
α-SMA	alpha smooth muscle actin
AUC	area under the curve
BM	none marrow
BMDF	bone marrow derived fibroblasts
BMT	bone marrow transplantation
BMZ	basement membrane zone
bp	base pair
BSA	bovine serum albumin
C7	type VII collagen protein
CA	capsid
CCR	chemokine receptor
cDNA	complementary DNA
CGD	chronic granulomatous disease
cl	clone
CMV	cytomegalovirus
CpG	cytosine nucleotide adjacent to guanine nucleotide
cPPT	central polypurine tract
CRISPR	clustered regularly interspaced short palindromic repeats
DAPI	4'-6'-diamidino-2-phenylindole
DDEB	dominant dystrophic epidermolysis bullosa
DEB	dystrophic epidermolysis bullosa
DEJ	dermal epidermal junction
DMEM	Dulbecco's Modified Eagle Medium
DMSO	dimethyl sulphoxide
DNA	deoxyribonucleic acid
dNTP	deoxyribonucleotide triphosphate
DSB	double stranded DNA break
EBS	epidermolysis bullosa simplex
ECM	extracellular matrix
EF1α	elongation factor 1 alpha
EGF	epidermal growth factor
eGFP	enhanced green fluorescent protein
EGR1	early growth response protein 1
ELISA	enzyme-linked immunosorbent assay
FACS	fluorescence activated cell sorting
FB	fibroblast
FCS	foetal calf serum
Gly-X-Y	glycine-proline-hydroxyproline
GVHD	graft versus host disease

H&E	haematoxylin and eosin
HD	hemidesmosome
HDR	homology directed repair
HIV	human immunodeficiency virus
HLA	human leukocyte antigen
HMGB1	high mobility group box 1
HPLC	high performance liquid chromatography
HR	homologous recombination
HSPC	hematopoietic stem and progenitor cell
ICC	immunocytochemistry
IDLV	integrase deficient lentiviral vector
IL2Rγ	interleukin 2 receptor common gamma chain
IN	integrase
indels	insertions/deletions
IP	infectious particle
iPSC	induced pluripotent stem cell
JEB	junctional epidermolysis bullosa
K	keratin
kb	kilobase
KC	keratinocyte
kDa	kilodalton
KF	keratin filament
LD	lamina densa
LL	lamina lucida
LTR	long terminal repeat
LV	lentivirus
MA	matrix
mAb	monoclonal antibody
MFI	mean fluorescence intensity
MLV	murine leukemia virus
MN	melanin
MOI	multiplicity of infection
MoMLV	Moloney murine leukemia virus
mRNA	messenger RNA
MS	missense mutation
MSC	mesenchymal stem cell
NC-1	non-collagenous domain
NHEJ	non-homologous end joining
NILV	non-integrating lentiviral vector
NS	nonsense mutation
NSG	NOD.Cg-*Prkdc*^{scid} *Il2rg*^{tm1Wjl}/SzJ
pAb	polyclonal antibody
PAGE	polyacrylamide gel electrophoresis
PAM	protospacer adjacent motif
PBS	primer binding site/phosphate buffered saline
PCR	polymerase chain reaction
PEI	polyethylenimine
PGK	phophoglycerate kinase

PIC	preintegration complex
polyA	polyadenylation
PPT	polypurine tract
PTC	premature termination codon
PV	plasmalemal vesicle
PVDF	polyvinylidene fluoride
qPCR	quantitative PCR
rAAV	recombinant AAV
RCL	replication competent lentivirus
RDEB	recessive dystrophic epidermolysis bullosa
RNA	ribonucleic acid
RRE	Rev response element
RSV	Rous sarcoma virus
SCC	squamous cell carcinoma
SCID	severe combined immunodeficiency dissorder
SDM	site directed mutagenesis
SDS	sodium dodecyl sulphate
SE	skin equivalent
SFFV	spleen focus-forming virus
sgRNA	short-guide RNA
SIN	self-inactivating
SNP	single nucleotide polymorphism
SSA	single strand annealing
SSB	single stranded DNA break
TALEN	transcription activator-like effector nuclease
TCR	T-cell receptor
TEM	transmission electron microscopy
TU	transducing unit
UT	untransduced
VSV-G	vesicular stomatitis virus glycoprotein
WAS	Wiskott-Aldrich syndrome
WPRE	woodchuck hepatitis virus posttranscriptional regulatory element
WT	wild-type
ZF	zinc finger
ZFN	zinc finger nuclease
ZFP	zinc finger protein
Ψ	RNA encapsidation signal

Chapter 1 Introduction

1.1 Epidermolysis bullosa: overview and classification

Epidermolysis bullosa (EB), first described by Koebner H. et al in 1886 (Köbner, 1886) constitutes a clinically and genetically heterogeneous group of mechanobullous blistering disorders of the skin (Uitto et al., 2010), leading to tissue separation either spontaneously or following minor friction or trauma. A number of therapeutic approaches have been envisaged for the treatment of the disease although none have resulted in a cure with treatment predominantly revolving around pain management and palliative wound care.

Almost eighty years later in 1962, Pearson classified EB into the three main types still used to date. According to the distinct ultrastructural level within which blistering occurs in patient skin, EB can be categorised as epidermolytic (simplex), lucidolytic (junctional) and dermolytic (dystrophic) EB with a fourth subtype recently added in 2008, Kindler syndrome (KS), carrying a unique clinical phenotype characterised by blistering arising in multiple levels within the skin (Pearson, 1962).

Clinical symptoms are dependent on the type of EB, but predominantly include blistering of the skin, dystrophy of the nails and teeth, deformity of the limbs and erosions of the alimentary canal. Each of the aforementioned subtypes is further ordered on the basis of its severity; ranging from mild topical blistering in EB simplex (EBS) to whole body tissue separation and highly aggressive metastatic skin cancer with a low survival rate in dystrophic EB (DEB). At the molecular level, a range of genes have been reported to result in deleterious mutations carried over in a dominant or recessive inheritance pattern giving rise to dysfunctional proteins, the location of which directly corresponds to the position of ultrastructural cleavage **(Table 1.1)**.

Table 1.1 Summary of molecular and clinical features of EB.

Type	EBS			JEB		DEB		KS
Major	Suprabasal		Basal	Gen.	Loc.	DDEB	RDEB	Gen.
Subtype	Loc.	Gen. severe	Gen. intermediate	Severe, intermediate, PA, LO	Inversa	Gen.	Gen. severe Gen. intermediate Loc. Gen.other	
Mode of inheritance	AR, AD			AR		AD	AR	AR
Onset	Birth (some cases 12-18months)			Birth		Birth		Birth
Clinical features	Blisters/erosions/crusts, nail dystrophy, keratoderma, mechanical fragility, oral cavity erosions, occasional growth retardation			Blisters/erosions/crusts, dystrophic nails (may be absent) scarring, atrophy,exuberant granulation tissue, scarring alopecia, mechanical fragility, oral cavity erosions, mild scarring/microstomia/ankyloglosia, dental abnormalities, defective enamel, cases of growth retardation, severe anaemia, gastrointestinal tract involvement		Blisters/erosions/crusts, dystrophic nails (may be absent), milia scarring, atrophy, scarring alopecia (RDEB),, mechanical fragility, oral cavity, severe erosions/ scarring /microstomia/ankyloglosia, dental abnormalities, severe caries (RDEB), severe of growth retardation (RDEB), severe anaemia (RDEB), severe acral musculoskeletal deformities (RDEB), gastrointestinal and genitourinary tract involvement, ocular keratitis, squamous cell carcinoma		Atrophic scarring, dystrophic or absent nails, granulation tissue, keratoderma, poikiloderma, photosensitivity, gingival hyperplasia, colitis, squamous cell carcinoma
Level of skin cleavage	Intraepidermal (epidermolytic)			Intra lamina-lucida (lamina lucidolytic)		Sub-lamina densa (dermolytic)		Mixed
Ultrastructural site of skin findings	Basal layer, above level of HD attachment plaque, Basal keratinocytes, at interface between granular & cornified cell layer			Lamina lucida		Sub- lamina densa		Mixed
Other findings	Dense, circumscribed clumps of keratin filaments, reduced integration of keratin filaments with HD, absent or reduced keratin filaments within basal KC			Markedly reduced or absent HD, absent sub-basal dense plate	HDs may be normal or reduced in size & number	Normal or decreased number of AFs, electron dense stellate bodies within basal layer	Absent or rudimentary appearing AFs (reduced in RDEB-O) electron dense stellate bodies within basal layer	Increased frequency of caries, pseudosyndactyly
Mutational analysis	*TGM5, PKP1, DSP, ITGA6, ITGB4*	*KRT5, KRT14, PLEC1, DST*		*LAMA3, LAMB3, LAMC2*	*LAMA3, LAMB3, LAMC2, COL17A1 ITGA3, ITGA6, ITGB4*	*COL7A1*		*FERMT1*
Types of mutations	Spl, Del, NS, MS, In-frame Indels			MS, NS Ins, Spl		NS, Spl	MS, NS, Del, Ins, Spl	NS, Del, Spl, Ins, Indels
Proteins affected	Keratins 5 & 14, plectin, plakophilin-1, desmoplakin, bullous pemphigoid antigen-1, a6β4 integrin			Laminin-332, type XVII collagen, a6β4 integrin, integrin a3 subunit		Type VII collagen (C7)		Fermitin family homolog 1 (kindlin-1)

Key: *AR*, Autosomal Recessive; *AD*, Autosomal Dominant; *HD*, Hemidesmosome; *AF*, Anchoring Fibril; *KC*, Keratinocyte; *Spl*, Splice site mutation; *Del*, Deletion; *NS,* Nonsense mutation; *MS*, Missense mutation; *Indels* insertion/deletion, Gen, generalised; Loc, localised; PA, pyloric atresia; LO, late onset. (Construction of summary table based on published data (Fine et al., 1991, Fine et al., 2008, Fine et al., 2014)).

1.2 Structure of the human skin

The human skin consists of three distinct layers starting from the subcutaneous fatty layer which lies below the dermis and ultimately the epidermis. Each of these is composed of distinct cell types conferring different properties to the skin **(Figure 1.1)**. The epidermis is the most superficial layer acting as a protective barrier against chemical, natural such as UV, physical and a wide range of environmental insults while keeping essential body fluids in. The epidermis, comprised largely of keratinocytes, is subdivided into five distinct *strata*. The outermost layer is the *stratum corneum* comprised of terminally differentiated anucleated keratinocyte cells, key components of the skin barrier, creating a tough structure acting as a first line of defence. Below are the *stratum granulosum*, *spinosum* and *basale* predominantly composed of keratinocytes at earlier stages of differentiation. Additional cell populations including melanocytes, Langerhans' cells and Merkel cells are situated amongst the keratinocytes and contribute to the functional and protective properties of the epidermis. The basal layer is attached to the underlying dermis of connective tissue through the basement membrane.

The dermis consists mainly of fibroblasts and to a lesser extent mast cells and histocytes (monocytes/macrophages), and contributes largely towards water retention due to the large amount of produced macromolecules (polysaccharides and proteins). The dermis further functions as a supporting matrix via the production and association with two types of protein fibre, namely elastin and collagen, providing the bulk and tensile strength required (McGrath, 2008). Below the dermis is the subcutaneous fat layer aiding in the protection and insulation of the underlying organs while also facilitating energy retention.

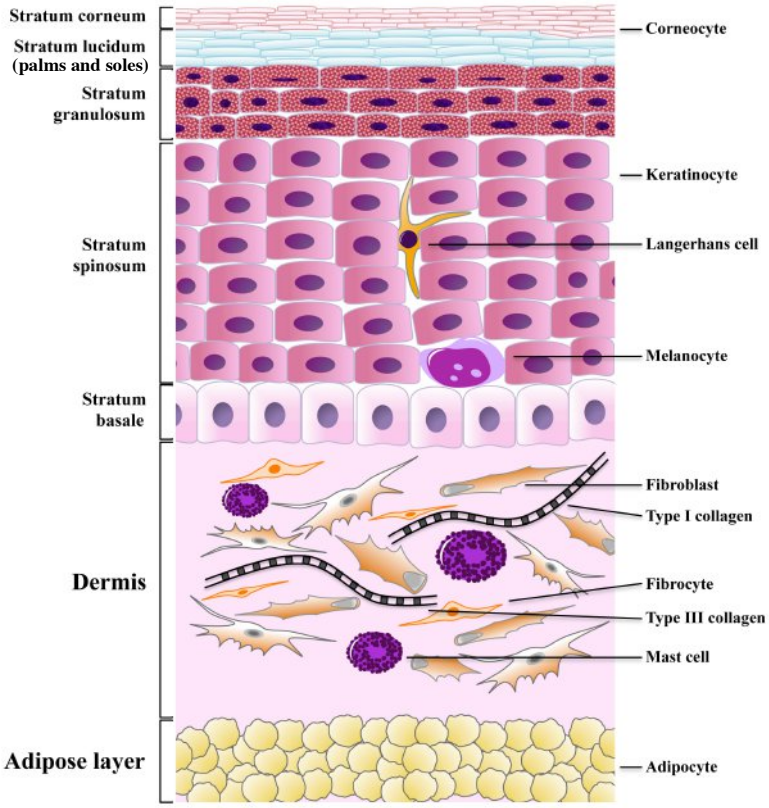

Figure 1.1 Schematic of human skin.
Structure of the epidermis connecting to the underlying dermis at the basement membrane zone before interaction with adipose layer. Distinct keratinocyte morphology following differentiation through 5 *strata* can be seen while dermis is largely populated by fibroblast cells.

1.2.1 Human epidermis

Keratinocytes, as part of their normal growth and differentiation cycle undergo a four-step process. Basal keratinocytes forming the deeper-most layer of the epidermis contain a dense network of keratin filaments providing intracellular cytoskeletal support. Keratins form the largest subgroup of intermediate filament proteins providing structural support to the epidermis accounting for up to 85% of the mass of a fully differentiated keratinocyte (Fuchs, 1995). Of the approximately 30 identified keratin filaments, 18 of those are expressed in skin. Classed into types I, acidic low molecular weight proteins keratins K9-20, and II, basic high molecular weight proteins K1-8, based on their keratin chain arrangement and biochemical properties are commonly co-expressed as heterodimeric pairs. Their structure is intended to have a cytoprotective function on the epithelial cells, which is highlighted by the fact that mutations in keratins leading to cytolysis can have detrimental effects on tissue integrity resulting in blistering disorders such as EBS. Mitotically active basal keratinocytes, interconnected by membrane junctions termed desmosomes, comprise of equal proportions of K5 and partner keratin K14 tightly regulating squamous cell differentiation (Nelson and Sun, 1983, Moll et al.,

1982). By modulating signalling pathways through the interaction with kinases, receptors and adaptors (Pallari and Eriksson, 2006) they are able to regulate events involved in protein synthesis, cell growth and differentiation (Koch and Roop, 2004, Alam et al., 2011). The levels of the K5/K14 pair gradually decresase with progression of keratinocytes to a more differentiated state while K1/K10 expression in turn increases with its synthesis only occurring in postmitotic keratinocytes (Coulombe et al., 1989). One of the main signals involved in the basal to suprabasal switch is coordinated by the Notch signalling pathway with Notch ligands DELTA1 and receptors located in the basal and spinous layers, respectively (Blanpain and Fuchs, 2009). This in turn leads to two key processes enabling progression of keratinocytes through the stages of epidermal stratification, delamination and asymmetric cell division. During asymmetric division, two resulting cells are generated, a committed suprabasal daughter cell and a proliferative basal cell (Lechler and Fuchs, 2005). Additional secreted factors promoting basal cell proliferation also come from the underlying dermal fibroblasts such as fibroblasts growth factor-7 (FGF-), FGF-10, insulin-like growth factors, epidermal growth factor (EGF) and transforming growth factor- α (TGF-α) (Hsu et al., 2014).

In the suprabasal or spinous epidermal layers keratinocytes are in a postmitotic state although remain metabolically active producing K1/K10 cytoskeletal filaments and aggregating the cytokeratins together to form tonofibrils, mediating the development of desmosomes. Initiation of involucrin production, a substrate for transglutaminase-mediated enzymatic crosslinking, is additionally carried out within the spinous layer which will assist in the release of lipids in the intercellular spaces during later stages of differentiation (Rice and Green, 1979, Carroll et al., 1993).

Production of keratins ceases in the further differentiated granular layer where keratinocytes now switch to the production of filaggrin and loricrin, essential for epidermal homeostasis regulation. Keratohyalin granules within the granular layer contain the precursor of filaggrin, profilaggrin, which following proteolytic cleavage can assist in water retention and skin barrier function. Loricrin is produced for subsequent use by the terminally differentiated corneocytes aiding in their interconnection for the formation of a strong skin barrier. Keratin filaments also undergo reorganisation with dense packing to survive the subsequent lytic stage of the keratinocytes. Epidermal differentiation and development of distinct *strata* is additionally regulated by a calcium gradient which increases throughout the basal and spinous layers reaching a maximum in the granular layer. Calcium concentrations can induce terminal differentiation, resulting in metabolically inactive, flattened and anucleated cellular cytoskeletons known as squames comprising the *stratum corneum*, which will eventually be sloughed (Elias et al., 2002). This 10-20 μm thick layer forms the outermost protective barrier

of the skin often compared to a “brick and mortar” structure with high water impermeability achieved by the accumulation of lipid molecules secreted from exocytosis of lamellar bodies and the arrangement of the dead cells (Denda et al., 1994, Potts and Francoeur, 1991).

Epidermal stem cells are crucial for the maintenance of tissue homeostasis for the continual self-renewal, turnover and repair following injury of the epithelial tissue. The typical turnover rate of keratinocytes is around 2 to 3 weeks for their progression from the basal to the cornified layer. Epithelial stem cells can be located in the outer sheath region of the hair follicle also known as the bulge, considered the deepest and most protected area of the skin. This specialised portion of the hair follicle, also termed a stem cell niche, provides the balanced microenvironment required to support stem cell maintenance and differentiation. The abundance of hair follicles on the body and therefore stem cell-containing bulge regions demonstrates the magnitude of the skin’s regeneration capacity.

Their close proximity to sebaceous glands also allows for their migration upwards for differentiation into sebocytes, besides their downward migration for renewal of the hair follicle itself, facilitating the passing of hair through the follicles by the oils released. Generation of new hair is carried out by a subset of differentiated stem cells with a finite number of divisions, the transit-amplifying cells. The bulge cells will also periodically migrate to the basal epidermal layer thereby populating the region with transient amplifying cells. However bulge stem cells are not involved in normal maintenance of the epidermis, and will transiently contribute to interfollicular homeostasis only in injury (Ito et al., 2005). Transformation of oncogenic RAS gene in the bulge stem cells, coupled with inactivation of tumour suppressors p53, TGF-β or BRCA1 have been linked to development of aggressive squamous cell carcinoma (SCC) (Ratushny et al., 2012).

Other major stem cell niches include the sebaceous gland and the basal interfollicular epithelium which as with the bulge derived stem cells can be characterised by the expression of K5, K14 and p63 (Blanpain and Fuchs, 2009). Of particular importance to the maintenance of epidermal homeostasis are the interfollicular keratinocytes which reside in the rete ridges which serve as a protective niche (Jones et al., 1995, Li et al., 1998). The high clonogenic capacity of these cells coupled with the ability to propagate them *in vitro* has allowed for the generation of skin grafts which have successfully become commonplace clinical treatment for burn patients (Green, 1991).

1.2.2 Basement membrane zone

Located immediately below the epidermis, is a sheet of extracellular matrix (ECM) proteins that make up the basement membrane zone (BMZ) **(Figure 1.2)**. Attachment to the BMZ is conferred by rivet-like structures in the basal keratinocyte layer known as hemidesmosomes (HDs). HDs, which are found on the inner surface of the keratinocyte basal pole, comprise of four single-span transmembrane proteins, the 180 kDa bullous-pemphigoid antigen (BPAG2, BP180, type XVII collagen), two α6β4 integrin subunits forming the core of the HD junction and CD151 protein arranged in a two-plaque structure (Tsuruta et al., 2008). The α6β4 integrin in turn interacts with the keratin intermediate filaments consisting of basal K5/K14 through the association with two members of the plakin family, plectin and dystonin (230 kDa BPAG1e, BP230) at the inner hemidesmosomal plaque (Fine et al., 2008, Shimizu, 1998). Association with the keratin cytoskeleton is a unique feature of α6β4 amongst integrins, which would typically interact with actin (Jones et al., 1998). In addition to HDs, a separate group of actin cytoskeleton-associated matrix adhesion proteins known as focal contacts are also found within the BMZ. Although not shown to be as crucial in mediating adhesion as HDs, their involvement has been associated with signalling pathways and regulation of cell migration (Tsuruta et al., 2011).

Type VII collagen (C7) is one of the main contributors of dermal-epidermal adhesion forming "wheat stack" shaped, centrosymmetrically banded semicircular loop structures known as anchoring fibrils (AFs), after antiparallel dimerisation of two fibrils at their carboxyl (C)-terminus. These can be seen extending from their amino (N)-terminus which indirectly bind to hemidesmosomal α6β4 integrin via the bridging activity of laminin-332 in the *lamina densa* (Rousselle et al., 1997), where they protrude down to the papillary dermis encircling dermal type I and III collagen amongst other fibrous elements before terminating back in the *lamina densa* (Shimizu et al., 1997).

Failure to generate functional C7 AFs at the DEJ results in the dystrophic form of EB (DEB). This can be caused by either missense or splice-site mutations, or small insertions/deletions resulting in nonsense or frame shift mutations in *COL7A1* (Varki et al., 2007) with over 600 distinct variants presently described (Human Gene Mutation Database).

Subjacent to the HD below the basal keratinocyte membrane are the subbasal dense plate, a 40 nm wide electron-lucent zone termed *lamina lucida* sparsely populated with laminins and a tightly packed electron-dense layer, the *lamina densa* composed of type IV collagen, laminin-332, nidogen and perlecan (Adachi et al., 1997). Hemidesmosomal abnormalities with

mutations in either of collagen XVII, integrin α6β4 or laminin-332 can lead to blister formation in the *lamina lucida* below the HD, characteristic of JEB.

One of the major proteins within the BMZ specifically found at the bordering region of *lamina lucida* and *lamina densa* is laminin-332 (previously known as laminin 5, Kalinin). Laminins comprise a family of trimeric glycoproteins with an α-chain, a β-chain and a γ-chain bound through disulfide bonds, confering structural integrity within the ECM via integrin and syndecan receptor-mediated interaction and binding of cell membrane and ECM molecules. The ECM of the BMZ, comprised mostly of laminins but also collagens, fibrin, fibronectin, perlecan and nidogen, although originally thought to only act as a supportive matrix with filtering properties has now been described extensively for its roles in the regulation of cell growth, division, differentiation, migration and apoptosis (Gumbiner, 1996, Aumailley and Smyth, 1998). Approximately 15 different laminin isoforms have been discovered in the ECM with laminins-332 and -511 being specific to the BMZ (Miner and Yurchenco, 2004).

Laminin-332 (containing α3, β3and γ2 chains) encoded for by gene *LAMA3, LAMB3, LAMC2*, in particular is known to interact with α6β4 and α3β1 integrins in HDs and focal contacts, respectively, and with thin anchoring filaments composed of type IV and type XVII collagen traversing the basal *lamina*. Upon secretion, laminin-332 is subjected to extensive proteolysis with specific cleavage of its subunits, each in turn acquiring binding, processing or regulatory properties. Both N-terminus of β3 and with lower affinity γ2 subunits of laminin-332 have been reported to directly interact with the N-terminus of type VII AFs (Chen et al., 1999, Tsuruta et al., 2008). It is widely accepted that dysregulation of laminin-332 directly correlates with progression to tumour formation through modulation of cell adhesion and migration. A recent report has described the development of SCC tumourigenesis through the support and signaling of laminin-332 and C7 (Waterman et al., 2007). Specifically, the individual VIII domain of the β3 subunit was shown to promote tumour progression following binding to C7 resulting in activation and upregulation of phosphoinositol-3-kinase (PI3K) thereby protecting the cell from apoptosis.

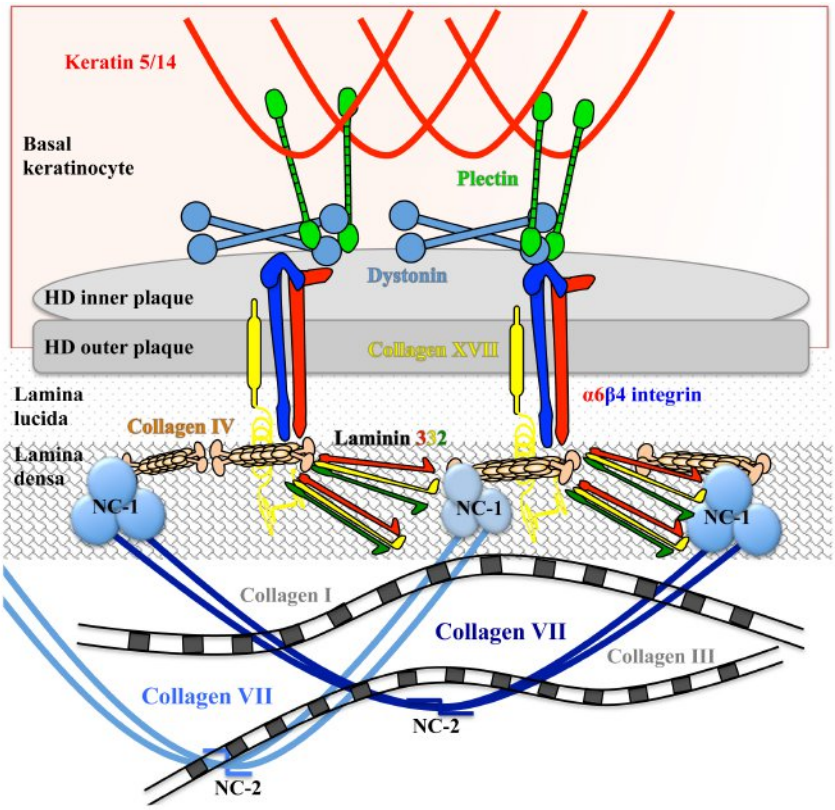

Figure 1.2 Basement membrane zone.
Protein interactions within the basement membrane zone. Hemidesmosome (HD) structure at the basal pole of the keratinocyte attached to *lamina lucida* and *densa* region of the BMZ mediated by keratin 5/14 and α6β4 integrin interaction. Adhesion to underlying papillary dermis conferred by non-collagenous (NC-1) domain of C7 interaction to laminin-332 and type IV collagen looping around interstitial collagens type I and III.

1.2.3 Human dermis

Located below all layers of the tightly packed epidermis and the BMZ is the dermis divided into two morphologically distinct regions, the uppermost papillary and lower, reticular, dermis. The two are distinguished by the arrangement and density of collagen fibres with a sparser distribution within the superficial papillary dermis. The dermis provides the skin with its tensile strength and flexibility while being home to a vast number of sweat glands, sebaceous glands, nerve endings, hair follicles and blood vessels providing nutrients to both dermis and epidermis. The dermis is populated by three main cell types, namely fibroblasts, macrophages and adipocytes, playing a crucial role in the synthesis of dermal proteins which provide the structural framework, phagocytosis of cellular and pathogenic debris and energy storage. Within the papillary region, finger like projections known as dermal papillae act to increase the contact surface area with the epidermis and in addition contain receptors sensitive to touch and pressure termed Meissner corpuscles amongst others signalling temperature, pain and itching. The

reticular region of the dermis is predominantly comprised of bundles of collagen and elastic fibres interspaced with sebaceous glands, sweat glands, blood vessels and hair follicles. Dermis contains glycosaminoglycans and specifically hyaluronic acid provides the dermis with its water retention properties maintaining the correct hydration and salt balance to the skin (Waller and Maibach, 2006).

The collagen bundle fibres of the dermis comprise of type I and III collagen and to a lesser extent type V as well as fibril-associated collagens with interrupted triple helices (FACIT) collagens, types XII, XIV, XVI and VI which do not aggregate to form fibrils but can instead bind the surface of type I and III collagen (Ruggiero et al., 2005). Type III is crucial in the early developmental stages of the skin and colocalises with the most abundant collagen, type I although the ratio shifts during adolescence to a higher proportion of type I collagen (Cuttle et al., 2005). Their organisation is tightly regulated and can be arranged in both perpendicular and horizontal fashion.

1.3 Molecular characterisation of Epidermolysis Bullosa subtypes

Abnormalities in a number of proteins of the epidermis, BMZ and dermis can have a detrimental effect on the integrity of the skin structure resulting in tissue separation. Protein anomalies within the skin clinically manifest with epidermal blistering ranging from mild to life-threatening whole body tissue separation. The tendency is for the blistering severity to be augmented the deeper the cleavage occurs within the dermal-epidermal region. Out of the numerous skin diseases known, EB constitutes the largest heterogeneous group of incurable severe skin blistering disorders differentiated based on the level of cleavage within the skin **(Figure 1.3)**.

1.3.1 Simplex EB

Epidermolysis bullosa simplex (EBS) is the most frequent type of EB characterised by fragility of the skin, leading to non-scarring blisters due to injury of the skin surface. The prevalence is about 1:17,000 in the UK. It is an autosomal dominant skin disease caused by mutations in keratin-5 and -14, resulting in the disruption of the intermediate filament network above the DEJ (Bolling et al., 2011, Rugg et al., 2007, Yasukawa et al., 2006). Its phenotype is predominantly mild with erosions confined to the hands and feet but in rare cases it may be fatal (Bruckner et al., 2011, Pfendner and Bruckner, 1993).

1.3.2 Junctional EB

Two main types make up the junctional form of EB (JEB); generalised severe (lethal) and generalised (non-lethal) previously known as Herlitz and non-Herlitz, respectively. They differ in severity but share common genetic mutations. The onset of generalised severe JEB is at birth with blistering covering most of the body and mucosal membranes, leading to not only malnutrition due to irritation of the buccal cavity and digestive track but also scaring and in severe cases fusion of affected limbs. This disorder manifests at the level of the basal keratinocytes or HDs where separation of the basement membrane of the epidermis within the *lamina lucida* occurs. The two types differ in the extent of damage caused by a reduction of HDs and anchoring filaments, or their complete absence in lethal cases. JEB carries an autosomal recessive inheritance pattern and has been most commonly associated with mutations in four genes. *LAMB3* mutations account for up to 70% of the cases, and to a lesser extent *COL17A1, LAMC2* and *LAMA3* (Aumailley et al., 2005, Varki et al., 2006). With the exception of the *COL17A1* encoded protein collagen XVII which forms one of the structural components by interacting with α6β4 integrin to make up HDs (Charlesworth et al., 2003), the aforementioned genes encode proteins integral to the assembly of the laminin-332 heterotrimer, essential for the association of the epidermal to the dermal layer offering strength and stability to the structure (Aumailley et al., 2005).

1.3.3 Kindler syndrome

A more recently recognised EB subtype sometimes considered a distinct type of EB due to the variability in the location of blistering within the BMZ is Kindler syndrome. This rare autosomal recessive blistering disorder with only 250 cases reported arises from premature termination of translation of kindlin-1 protein caused by mutations in the FERMT1 gene (Jobard et al., 2003). Expression of kindlin-1 is localised to basal epidermal keratinocytes where it functions as a focal adhesion adaptor protein. Loss of the protein leads to disorganisation of keratinocytes affecting cytoskeletal architecture and anchoring to β1 integrin (Has et al., 2011). The disease is associated with epithelial microblister formation and soft tissue scarring, pigmentation anomalies (poikiloderma), photosensitivity and predisposition to epithelial skin carcinoma during the later stages of life (Bruckner-Tuderman and Has, 2014).

1.4 Dystrophic EB

Dystrophic EB encompasses the most severe forms of cutaneous blistering disorders with a high mortality rate in the early years of life with no effective treatment currently available. It has been estimated to affect 6 per 1,000,000 patients worldwide with ~800 reported cases in the UK (Pfendner and Lucky, 1993a, Horn et al., 1997, McKenna et al., 1992). Patients suffering from DEB are challenged by lifelong skin fragility, susceptibility to shearing upon minimal friction and reduced epidermal barrier function resulting in vulnerability to mucosal membrane infections (Fine et al., 2008). Associated complications can present themselves in the form of joint contractures and growth retardation or more destructive outcomes such as mutilating scarring deformities of the limbs and life threatening skin carcinomas (Bruckner-Tuderman, 2009, Burgeson, 1993, Fritsch et al., 2008, Kadler et al., 2007).

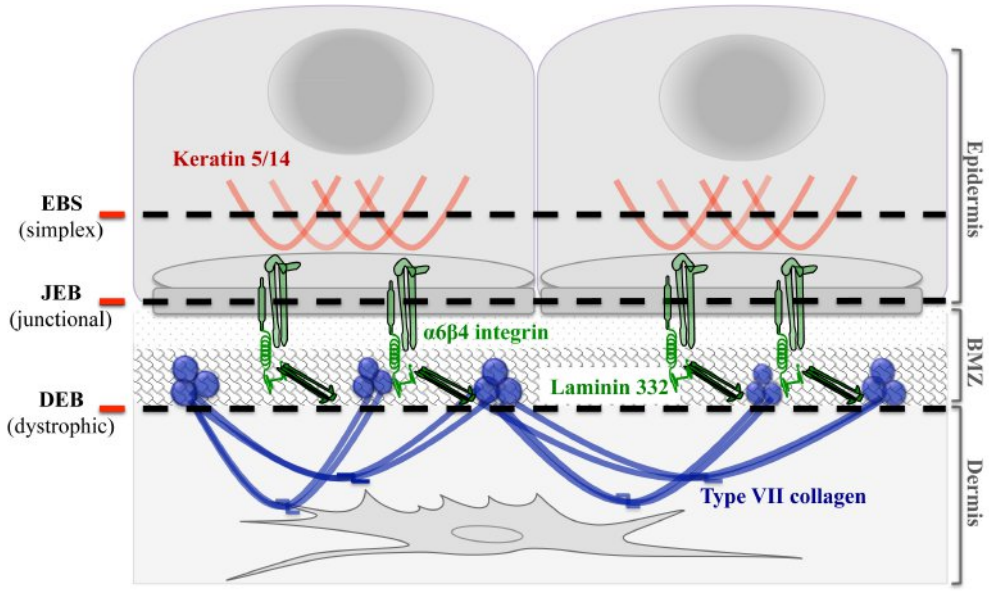

Figure 1.3 Tissue cleavage sites in EB subtypes.
Level of tissue cleavage by the three main types of Epidermolysis Bullosa (Simplex, Junctional, Dystrophic) and their key corresponding affected proteins.

Dystrophic EB is subdivided into two types according to the current classification system based on its inheritance pattern. These can be either dominant (DDEB) or recessive dystrophic epidermolysis bullosa (RDEB). RDEB is further divided into several subtypes including severe generalised, (RDEB sev-gen), previously referred to as Hallopeau-Siemens type (RDEB-HS), generalized other (RDEB-O) (or non-Hallopeau-Siemens RDEB-non-HS), generalised intermediate and localised. The level of tissue cleavage in all major types and subtypes of DEB is identical, localised to the *lamina densa* of the DEJ. DDEB is the mildest of the dystrophic

types with blistering confined predominantly to the hands, elbows, knees and feet with relatively fast healing time but with significant scarring. RDEB-O shares common clinical manifestations with DDEB but affected areas can also include the trunk. RDEB-sev gen, on the other hand, is placed at the top of the severity scale associated with the demise of the individual by the third to fourth decade of life. It manifests in severe blistering affecting the whole skin surface of the body and further spreads to the ocular, nasal, oropharyngeal, gastrointestinal, genitourinary and musculoskeletal systems (Fine et al., 1991) with fusion of the tongue to the floor of the mouth, erosions of internal organ lining and mutilating scarring of the limbs causing fusion of fingers and toes known as "mitten" hand and feet deformity, a hallmark of this disorder (Pfendner and Lucky, 1993a). Dystrophic EB patients account for approximately 25% of all EB sufferers. Patients suffering from the recessive form of this disorder have been associated with a 70% chance of developing SCC by the age of 45 with a subsequent mortality rate of 90% (Ayman et al., 2002, Fine et al., 2009, Pfendner and Lucky, 1993a).

The gene responsible for all three types of DEB is *COL7A1* encoding the protein type VII collagen, alpha 1. It plays a critical role in the association of the epidermal layer to the underlying dermis by functioning as an AF between the external epithelia and the underlying stroma. To date, over 600 mutations including missense, nonsense, splicing, small insertions or deletions in the *COL7A1* gene have been reported (Varki et al., 2007) **(Figure 1.4)**.

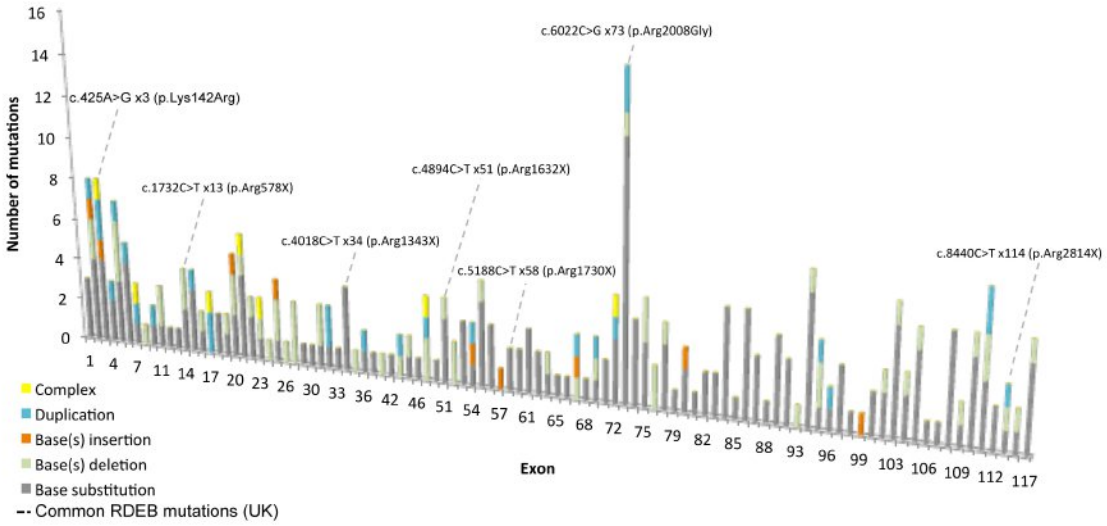

Figure 1.4 Proportion of mutations in *COL7A1* gene.
Frequency of mutation types reported at each exon of the *COL7A1* gene with commonly found mutations in the UK marked by dotted line.

1.5 Type VII collagen

Since its discovery in 1983 by Bentz *et al.* the *COL7A1* gene has been extensively studied due to its direct correlation with DEB (Bentz et al., 1983).

Chromosomal mapping of the human type VII collagen gene (*COL7A1*) was carried out and was found to be at locus 3p21 in the short arm of chromosome 3 (Parente et al., 1991). The gene contains 9,287 base pairs and has 10 splice variants (Ensembl). It codes for 2,944 amino acids (a.a.) spanning over 118 exons, the largest number of exons in a single gene at the time of its discovery, but with relatively small intervening introns resulting in a moderately compact gene (Christiano et al., 1994b). At the amino acid level, the mouse C7 polypeptide exhibits 84.7% homology in the nucleotide sequence and 90.4% identity at the protein level when compared to human (Kivirikko et al., 1996).

The protein product of the gene is C7 measuring at 295 kDa and is the main constituent of AFs securing the association of the epidermis to the underlying dermis. C7 is produced and secreted almost exclusively by basal keratinocytes and dermal fibroblasts, albeit at much lower abundance from the latter (Parente et al., 1991). The presence of this protein has also been detected by immunofluorescence in foreskin, placenta, skeletal muscles, chorioamnion, cornea, oral mucosa, cervix, kidney cortex, liver, lung, stomach, elastic cartilage and large intestine (Sakai et al., 1986).

Type VII collagen along with type IV collagen belongs to the group of non-fibrillar collagens and is characterised by its heterogeneous supramolecular organisation (Christiano et al., 1994b). It is encoded by the *COL7A1* gene, which features a large triple helical collagenous domain flanked by two non-collagenous domains on either terminus giving rise to monomeric polypeptide pro-α1 (VII) chains, the building blocks for the generation of functional AFs **(Figure 1.5)**.

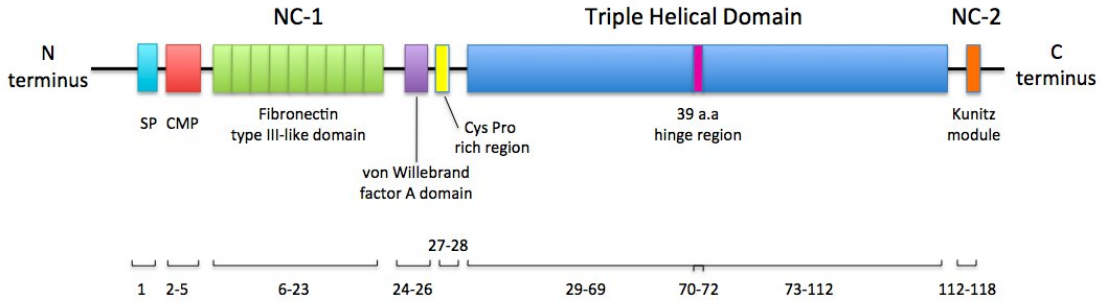

Figure 1.5 Schematic representation of the structural organisation of the type VII collagen pro-α1(VII) polypeptide exons.
The N terminus of the amino acid sequence codes for a 5' UTR signal peptide which is followed by a non-collagenous domain (NC-1) spanning across 26 exons, approximately 145 kDa in size, and consisting of sub domains with homology to known adhesive molecules. These are a cartilage matrix protein (CMP) like domain, followed by nine consecutive fibronectin type III modules, a von Willebrand factor A domain and a cysteine, proline rich region. The triple–helical domain (84 exons) flanked by the two non-collagenous regions is made up of Gly-X-Y repeats with a large 39 a.a. interruption forming a collagenous hinge region susceptible to proteolytic digestion with pepsin. The polypeptide ends with the second non-collagenous domain (NC-2) made up of seven exons and about 30 kDa in size containing a segment resembling the Kunitz protease inhibitor molecule.

1.5.1 Non – Collagenous domain 1 (NC-1)

The amino terminus of the pro-α1 (VII) chain initiates with the 5' untranslated region (U) signal peptide and predicted signal peptidase cleavage site encoded by the first of 118 exons (Christiano et al., 1992, Christiano et al., 1994b).

Exons 2-5 residing at the amino terminal of the non-collagenous domain 1 central region, were sequenced to reveal that the 85 amino acids shared a 38.8% homology with cartilage matrix protein. The major segment making up the NC-1 is comprised of nine consecutive repeat sequences. These submodules exhibit features of adhesive proteins which were verified by sequencing, displaying a 23.2% homology to fibronectin type III domains (FNIII) (Christiano et al., 1992). Each fibronectin type III like submodule is approximately 90 amino acids in size and encoded by two separate exons, which has also been characterised in other genes (Christiano et al., 1992). This includes the FNIII-like repeats in the a13 chain of VI and the a1 chain of XII collagen (Christiano et al., 1992, Chu et al., 1990).

This is followed by a 123 amino acid segment encoded by three separate exons, found to be homologous to the A domains of von Willebrand factor (21.1%) (Christiano et al., 1992). These type-A-like motifs have been thought to be involved in its binding to collagen and platelet glycoprotein 1B (Mohri et al., 1989).

The final two exons of NC-1, 27 and 28, encode a cysteine, proline rich domain, 173 and 36 bp in size making up the 85 amino acid segment which has yet to be described in other protein sequences (Christiano et al., 1994b, Christiano et al., 1992).

1.5.2 Triple helical domain

The 1530 amino acid central segment of the pro-α1 (VII) makes up the collagenous triple helical domain consisting of numerous repeats of Gly-X-Y although including a number of interruptions within the amino acid sequence. Although it would be possible to have more than 400 combinations of Gly-X-Y triplets, it appears that only a limited number of them occur with many of them never observed (Ramshaw et al., 1998).

The most frequent combination found in the coding sequence is Gly – Proline – Hydroxylisine or Hydroxproline (Hyp), derived from posttranslational modification of Pro and Lys, which provides maximal stability to the triple-helical structure (Jones and Miller, 1991). The main factors providing the support to the helix are the close packing of the triple chain which is held together by hydrogen bonds combined with the high content of the imino acids Pro and Hyp (Ramshaw et al., 1998). Within the helix, each of the amino acids making up the triplet retains a distinct position with glycine securely buried avoiding contact with solvent, whereas residues Y and predominantly X being highly exposed to solvents (Jones and Miller, 1991, Ramshaw et al., 1998). Usually, when residues X and Y are not occupied by imino acids which confer stability to the helix, but with a combination of the 20 standard amino acids, they have been shown to be involved in binding to other collagen molecules forming fibrils or other ECM molecules and may also play a role in recognition (Ramshaw et al., 1998).

Most of the exons making up the uninterrupted regions of the triple helix were found to contain base pairs in numbers of multiples of nine, which is the required size to encode the stable amino acid triplet Gly-X-Y (Christiano et al., 1992) some of which are commonly found in the triple helix coding regions of fibrillar collagen and not usually associated with non-fibrillar collagen genes (Vuorio and de Crombrugghe, 1990).

It has further been shown that the 19 interruptions, typical in non-fibrillar collagens, which may be due to insertions or deletions of the amino acid in the Gly-X-Y repeat sequence in the majority of cases correspond to exons which are not multiples of 9 bp (Chung and Uitto, 2010, Uitto et al., 2010). Eleven of these interruptions were caused by small 1 to 2 amino acid imperfections, while a further seven were due to insertions of up to 10 amino acids. The largest non-triple helical interruption in the collagenous sequence is 39 amino acid residues in length and located approximately at the centre of the domain, termed the hinge region, contributing

towards the flexibility of the protein structure. Its sequence reveals its distribution across three separate exons and its susceptibility to proteolytic cleavage by pepsin (Christiano et al., 1994a).

The *COL7A1* triple helix region exhibits further similarity in its pattern to fibrillar collagen genes as none of the codons in the coding region are split by introns as opposed to what is commonly observed in non-fibrillar collagens where the exons begin and end with split codons even in exons encoding uninterrupted Gly-X-Y repeats (Christiano et al., 1994b, Vuorio and de Crombrugghe, 1990).

1.5.3 Non – Collagenous Domain 2 (NC-2)

The carboxyl terminal of the pro-α1 (VII) chain ends with a second, much smaller in size non-collagenous domain NC-2. It is perceived that upon secretion, this domain is responsible for the associations of the homotrimeric monomer into antiparallel dimers. This is then followed by the proteolytic removal of the NC-2 regions, which assists in stabilising the dimers by the formation of disulfide bonds (Greenspan, 1993, Rattenholl et al., 2002). The enzyme shown to be responsible for the cleavage of NC-2 is procollagen C-proteinase/BMP-1[2] (PCP) although the reason behind this processing is not known (Colombo et al., 2003, Rattenholl et al., 2002).

The 30 kDa non-collagenous domain is distributed over seven exons, the first one being a fusion or junctional exon of the collagenous and NC-2 domains (Greenspan, 1993, Christiano et al., 1994b). A cysteine residue Cys-2634 residing in the triple-helical domain closest to NC-2 has been suggested to interact with the first Cys-2802 or second cysteine Cys-2804 within the NC-2 sequence forming intermolecular disulfide bonds stabilising the 60 nm overlap region observed in the anti-parallel dimer formation (Morris et al., 1986, Christiano et al., 1994a, Colombo et al., 2003).

The remaining exons together form a conserved motif which appears to be homologous to Kunitz-type serine protease inhibitors (Greenspan, 1993). This is thought to be responsible for directing the formation of pro-α1 (VII) dimers or possibly be involved in the regulation of the cleavage of NC-2, post dimerisation (Lunstrum et al., 1987).

1.5.4 Organisation into anchoring fibrils (AFs)

Three identical pro-α1(VII) chains associate through their carboxy-terminal ends and their collagenous domains, resulting in a homotrimer with a characteristic triple-helical conformation. Upon secretion into the extracellular space, newly synthesised homotrimers,

known as procollagens, assemble into 785 nm anti-parallel dimers through a 60 nm overlap of their carboxy-terminal sequences (Burgeson et al., 1990). Proteolytic cleavage at the C-terminus region where the triple-helical domain meets the NC-2 domain promotes the stabilisation of the dimer by intermolecular disulfide bonds, which further offers protection against collagenase digestion (Bachinger et al., 1990). This is followed by the highly organised lateral aggregation of multiple dimer molecules to form cross-striated, centro-symetric banded AF structures, containing large globular NC-1 domains at both ends of the structure (Bachinger et al., 1990, Villone et al., 2008) **(Figure 1.6)**.

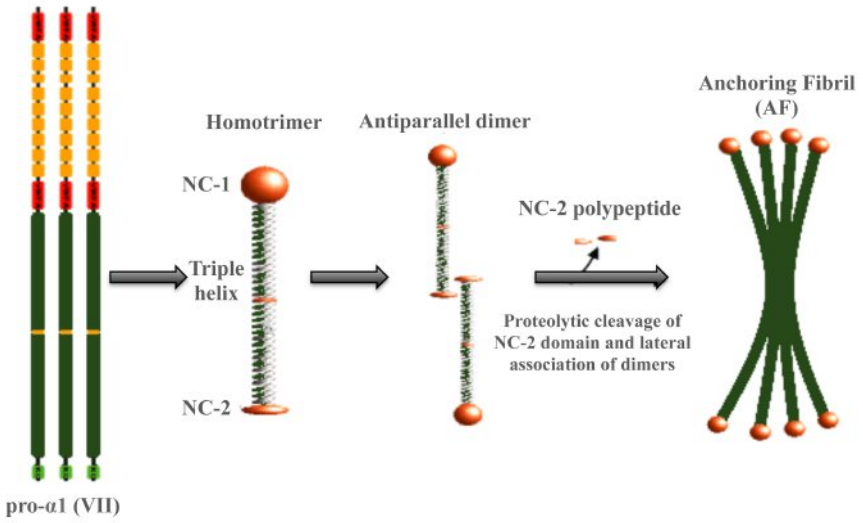

Figure 1.6 Organisation of type VII collagen into anchoring fibrils.
Three monomeric polypeptide chains of type VII α1 procollagen assemble into a triple helix. Antiparallel dimer formation by proteolytic cleavage of NC-2 domain of homotrimers. Lateral aggregation of mature dimers into AFs. (Schematic adapted from (Bruckner-Tuderman, 2009)).

Type VII collagen is the major if not exclusive component of AFs (Sakai et al., 1986). They are specialised fibrous structures crucial to the preservation of the structural integrity of skin securing the connection between the epidermis and the underlying dermis at the BMZ. These can be seen extending from their amino (N)-terminus of the NC-1 homotrimer portion where it interacts with macromolecular components of the BMZ and indirectly binds to hemidesmosomal α6β4 integrin via the bridging activity of laminin-332 in the *lamina densa* (Rousselle et al., 1997, Villone et al., 2008). It was originally proposed that the opposite end of the dimer binds to basement membrane-like patches within the papillary dermis, termed anchoring plaques, also containing type IV collagen and laminin-332 therefore securing the *lamina densa* to the underlying connective tissue matrix (Uitto and Christiano, 1992). Rotary-shadowed imaging has revealed the "trident" structure of the three NC-1 domain arms,

maximising the interactions of the AFs with the constituents of the *lamina densa* (Burgeson et al., 1990).

More recent studies have described the existence of a second and possibly sole manner of attachment, whereby the AF heterodimers protrude down into the papillary dermis forming U-shaped looped structures with both NC-1 ends inserted into the *lamina densa* resulting in physical entrapment of separate components of the dermal connective tissue, chiefly being type I and III collagen fibrils amongst other fibrous elements (Uitto et al., 1992, Uitto and Christiano, 1992, Villone et al., 2008).

The flexibility of the AFs is believed to be due to the highly conserved discontinuities within the repeating Gly-X-Y sequence of each pro-α1 (VII) chain (Christiano et al., 1994a).

Mutations in *COL7A1* can cause abnormal or loss of function of C7 protein, leading to a reduced number, rudimentary structure, or entire absence of AFs at the DEJ, and morphological alteration of the skin (Dang and Murrell, 2008).

Routine diagnosis for the distinction of the type of DEB involves transmission electron microscopy (TEM) of skin biopsy at birth and full sequence analysis of the gene. In suspected cases of DDEB sequencing is primarily limited to exons 73, 74 and 75 which have been linked to 75% of cases with full exome sequencing implemented if no mutation is identified. In RDEB, there is no such restriction as mutations could occur in any of the 118 exons always requiring the use of full exome sequencing, although there have been reports of hot-spot mutations in different ethnic groups (Murata et al., 2004).

1.5.5 Type VII collagen involvement in SCC progression

It has been well documented that the propensity of developing SCC above the age of 30 is substantially elevated in RDEB patients as opposed to those affected by other forms of EB with a mortality rate of 55% to as high as 80% in severe-generalised RDEB (Fine and Mellerio, 2009, Fine et al., 2009). One of the explanations for SCC development has been the persistent wounding and scarring suffered by these patients, which can deplete basal stem cell progenitors and stimulate a pre-malignant microenvironment (Smoller et al., 1990, Goldberg et al., 1988). Additional factors affecting cell cycle regulation such as mutated p53, reduced expression of insulin growth factor-binding protein 3 and elevated matrix metalloproteinase (MMP-7) expression have been linked to SCC in RDEB patients (Martins et al., 2009).

Over the past decade there has been considerable interest in the elucidation of the involvement of C7 expression, or lack of, in the progression to SCC. It was originally postulated that the greater the disease severity and therefore the lower amounts of C7 present, the higher the risk of SCC development (Martins et al., 2009, Pourreyron et al., 2007). This hypothesis was questioned by evidence from RDEB patient keratinocytes assessed on a murine skin model, suggesting the requirement of the NC-1 domain of C7 for downstream activation of Ras-driven tumourigenesis. This was shown to be linked to the fibronectin-like domains of NC-1 associated with laminin-332 promoting cell invasion, whereas entirely absent C7 failed to mount an oncogenic response (Ortiz-Urda et al., 2005).

More recent studies have demonstrated that contrary to Ortiz-Urda *et al.*, patients lacking entire C7 expression or the NC-1 domain were still predisposed to malignant transformation. In addition, the SCC cases reported were shown to be Ras independent (Pourreyron et al., 2007). This observation was further supported by Rodeck *et al.* obtaining similar findings and Fine et al. indicating that dominant-DEB patients carrying an unaffected *COL7A1* allele will seldom develop SCC (Rodeck and Uitto, 2007, Fine and Mellerio, 2009).

Further *in vitro* work has linked C7 to SCC, with its loss resulting in an increase of migration and invasion. This was determined to be caused by deregulation of epithelial keratinocyte differentiation through upregulation of CXCL10-CXCR3-phopholipase C-β4 (PLC-β4) signaling (Martins et al., 2009). Similarly, cancer-associated fibroblasts play a role in cancer invasion by providing oncogenic signals, which in a paracrine fashion can promote tumor progression in RDEB keratinocytes (Ng et al., 2012).

1.6 Current therapies for RDEB

1.6.1 Conventional treatments for RDEB

The current treatment options for RDEB are based on wound protection and pain management through the use of specially designed non-adherent dressings, which are secured with layers of gauze and elastic bandaging to provide padding and sturdiness (Kirkorian et al., 2014). The sloughing of the epidermis, the regular draining of blister fluid and erosions of the oesophagus limiting iron absorption result in a significant drop in haemoglobin levels also lead to the development of RDEB-associated chronic anaemia and therefore delay of wound healing. Iron and vitamin supplementation, nutritional support, and in severe cases gastrostomy are crucial as feeding may be incredibly cumbersome due to blistering along the entirety of the alimentary tract. In addition, balloon dilatation enabling the stretching of oesophageal strictures can

facilitate the passing of food (Pfendner and Bruckner, 1993, Pfendner and Lucky, 1993a, Pfendner and Lucky, 1993b).

A huge wealth of research is directed towards developing safer and more effective drug treatments to manage symptoms and prevent SCC progression. These include anti-itch, anti-fibrosis, anti-inflammatory, anti-microbial and wound healing promoting drugs. Recalcitrant pruritus poses one of the major challenges in the management of RDEB causing wound breakdown and hence cutaneous damage. Coupled with the acute dryness of the skin making the wounded area itchy this evokes scratching which contributes to bacterial colonisation. Patients are typically treated with antibiotics and antifungals and bathed in low concentration bleach solutions to manage pathogenic infections while given antihistamines and moisturisers containing benzalkonium chloride and chlorhexidine dihychloride, topical emollients and steroids for the reduction of itching and moistening of the skin.

The economic burden of this debilitating disorder is estimated at around £25 million per year in the UK with specialised dressings costing in the range of £250,000 per patient per year (www.debra.org.uk).

RDEB has received a vast amount of interest from the scientific community worldwide with generous support from charities attempting to tackle this disorder at the molecular level via a wide array of therapeutic approaches. These come in the form of protein, cell and stem cell, and gene therapy amongst others, a number of which have displayed encouraging results.

1.6.2 Replacement therapies for RDEB - recombinant protein therapy

Protein replacement therapy for RDEB is currently gaining momentum with immediate prospects of initiating clinical trials aided by the commercial backing of Shire's recent acquisition of Lotus Tissue repair specialising in the production of recombinant human C7 protein (rC7). The call for this type of therapy was proposed in order to circumvent the potential side effects and safety concerns associated with grafting or injecting localised cell therapies or more invasive transplantation procedures in addition to minimising the complexity of administration for the clinicians. Since the first successful *in vivo* study of its kind for RDEB initiated in 2004 by Woodley *et al.* a number of publications have arisen, demonstrating the efficacy of recombinant C7 protein in restoring functional expression following intradermal, intravenous or topical administration (Remington et al., 2009, Woodley et al., 2004a, Woodley et al., 2013, Nystrom et al., 2013). These studies were all performed on mice which were either immunocompromised and wounded to assess healing (Woodley et al., 2004a, Woodley et al.,

2013) or on RDEB recapitulating murine models expressing either none or 10% C7 at the BMZ (Remington et al., 2009, Nystrom et al., 2013). Recombinant human C7 was obtained by purification and precipitation of culture media from lentivirally transduced fibroblasts with full-length *COL7A1* cDNA (Woodley et al., 2004a).

The principal study confirmed the deposition of human C7 in athymic nude mice following intradermal injection of 20 μg of rC7 (Woodley et al., 2004a). Expression persisted for 3 months with an approximate 15% reduction overall. This was followed by intradermal injections of rC7 in RDEB skin equivalents grafted on mice further confirming functional correction of the disease with amelioration of subepidermal blistering accounted for by the assembly of human C7 AFs. Supporting evidence from two recent studies performing intradermal rC7 injections into *Col7a1*$^{-/-}$ *null* (Remington et al., 2009) or hypomorphic RDEB mouse models expressing 10% of wild-type (WT) C7 levels (Nystrom et al., 2013) came to similar conclusions demonstrating incorporation of the protein at the mouse DEJ and generation of AFs with signs of expression at distal sites from the injection with a significant improvement of the RDEB phenotype. An alteration to the protocol was carried out by Remington *et al*., 2009, whereby a monomeric type VII procollagen, instead of the 900 kDa trimer, was injected which could potentially reduce the efficacy of AFs assembly *in vivo*.

Although C7 is known to have a slow turnover (Burgeson, 1993), repeated and multiple site administration would be required clinically. It was estimated that an analogous dose in a 4 kg infant would be 100 mg of rC7 in 300 ml buffer over multiple time points (Bruckner-Tuderman, 2009). A subsequent drawback of this therapeutic approach was the activation of an immunogenic response by the formation of circulating auto-antibodies against human C7 (Remington et al., 2009, Woodley et al., 2004a, Woodley et al., 2007a). Although they did not appear to bind to the DEJ or prevent the formation of AFs in mice, it is unknown what effect they may have in humans as it could trigger the development of autoimmune blistering such as that seen in EB acquisita. In mice, treatment with anti-CD40L mAb appeared to impede anti-human C7 antibodies (Remington et al., 2009).

The small diffusion radius, most likely a consequence of the large size of C7 hampering its diffusion to neighboring wounded sites coupled with the requirement for multiple injections in severely affected individuals with whole body blistering, led to the assessment of a systemic administration approach. Intravenously injected protein has become commonplace for the targeted treatment of lysosomal storage disorders and haemophilia (Desnick and Schuchman, 2012). A 60 μg dose of rC7 was intravenously injected in the tail veins of wounded immunocompromised mice or RDEB grafted models (Woodley et al., 2013). At a 2-week time

point post-injection, expression was confirmed at the wounded sites with acceleration of wound healing and functional correction of the blistering sustained for 2 months. Challenges such as the large size and likely proteolytic degradation of trimeric C7 before recruitment to the wounded sites have yet to be resolved.

Lastly, Wang *et al.* demonstrated the potential of topical application of rC7 on murine skin wounds (Wang et al., 2013). It was shown that 30 μg of protein was sufficient for the acceleration of wound closure and re-epithelialisation while showing AFs formation at the DEJ for up to 2 months. Moreover, the introduced rC7 resulted in a decrease of fibrogenic TGF-β2 expression and recruitment α-smooth muscle actin (α-SMA) myofibroblasts and an increase in antifibrogenic TGF-β3 expression, resulting in reduced scar formation. Due to the inability of rC7 to penetrate intact skin, this approach could only be usefull for deep SCC-type wounds.

Although protein therapy may have a significant beneficial outcome in patients with the added benefit of being applicable to all recipients regardless of the *COL7A1* mutation, challenges such as the short-lived expression, preparation of sufficient quantities of GMP-grade rC7 and potential risks developing an adverse immune response to the protein still remain. Nevertheless, a clinical trial is expected to initiate recruiting RDEB patients for the intradermal injection of rC7. A separate trial by Shire, aiming to deliver rC7 intravenously based on the encouraging murine data was about to commence, but has been put on hold due to severe adverse effects and toxicity encountered during testing in larger animal models (no details are available as of yet).

1.6.3 Cell therapies for RDEB

1.6.3.1 Epidermal grafting and intradermal administration of allogeneic cells

The initial response to managing RDEB came in the form of cell therapy, employing techniques used for the treatment of burns' patients. This involved skin grafting procedures using either allogeneic (Eisenberg and Llewelyn, 1998, McGrath et al., 1993) or autologous (Verplancke et al., 1997, Wollina et al., 2001) cultured keratinocyte skin sheets. The majority of the cases though resulted in poor graft take and a high incidence of skin infections.

Although keratinocytes, being the main contributors of C7 expression would appear to be the ideal cell type to be used for treatment, their challenging culturing requirements, finite expansion capacity and the requirement for superficial application demonstrate the limits of their clinical use for RDEB. The focus has therefore shifted towards the use of dermal fibroblasts also known to contribute to C7 deposition at the DEJ. Moreover, their robustness in terms of ease of propagation and immunomodulatory capacities, allowing for use of allogeneic

cells without the risk of an adverse host immune response, make them a more suitable candidate (Haniffa et al., 2007).

The hypothesis of ameliorating RDEB-associated skin blistering by delivery of allogeneic fibroblasts was primarily assessed in a hypomorphic mouse model established in the Bruckner-Tuderman lab truly recapitulating the disease phenotype while expressing C7 at 10% of normal levels (Fritsch et al., 2008). An intradermal injection of WT mouse fibroblasts resulted in incorporation of C7 at the DEJ which peaked at 7 days post-injection raising the levels of C7 to 25%-30% and was sustained throughout a 21-day observation period. A follow-up study from the same group was able to report long-term persistence of protein expression of >3 months although the cells displayed a gradual apoptotic tendency within the first month while only causing mild transitory inflammation (Kern et al., 2009). As the donor cells were derived from an EGFP+ transgenic mouse, fibroblasts could be traced confirming their clearance after 28 days. Moreover, their results confirmed that the C7 expression observed was predominantly secreted by the injected fibroblasts and not due to paracrine signaling.

Subsequent studies in man by Wong *et al.,* 2008, demonstrated the potential of this application, as expression of C7 at the DEJ with subsequent improvement of dermal-epidermal blistering at the site of injection was achieved and remained stable for 3 months in most cases and 9 months in a single case with no observed clinopathological inflammatory response (Nagy et al., 2011). Fluorescent *in situ* hybridisation (FISH) for the detection of donor Y-positive cells in a female recipient demonstrated the clearance of the fibroblasts 2 weeks following intradermal injection. The limitation of this study was the requirement for the presence of some level of expression at the DEJ before therapy as it was ineffective in patients completely lacking C7. The positive effect seen was reported to be a result of upregulation of patients' endogenous C7 stimulated by the allogeneic fibroblast injection giving rise to rudimentary AFs, although sufficient to provide amelioration of the blistering tendency of the select individuals (Wong et al., 2008). It was proposed that either an initial burst of C7 from the introduced fibroblasts or a paracrine effect exerted on the patients' keratinocytes stimulating production of mutant protein may have contributed to the partial improvement seen. Indeed, this stimulation of endogenous C7 expression by patients' own cells has recently been associated with a heparin EGF-like growth factor induced by fibroblast injections, which in turn leads to an increase in expression of the AF forming protein predominantly by the keratinocytes (Nagy et al., 2011).

The potential lack of major contribution to AF formation from the injected fibroblasts was further supported by a phase II double-blind randomised controlled trial demonstrating an equal increase in wound healing and *COL7A1* mRNA expression following intradermal injections of both allogeneic fibroblasts and a 2% albumin suspension solution (Venugopal et al., 2013).

1.6.3.2 Bone marrow transplantation of allogeneic stem cells

As RDEB is a systemic disease with patients suffering from total body epithelial and esophageal blistering, joint contractures and limb deformities, topical therapies may be considered insufficient in providing a cure. For this purpose a large amount of interest is currently focused on developing a systemic treatment. Bone marrow transplantation of allogeneic healthy donor stem cells can potentially provide a long-lasting curative effect, however limitations such as the invasiveness of the operation calling for myeloablative conditioning and stringency of HLA tissue typing have to be accounted for. Reports have confirmed the feasibility and success of this approach for congenital immunodeficiencies such as X-linked severe combined immunodeficiency disorder and X-linked adrenoleukodystrophy amongst others, which have considerably progressed the field (Cartier et al., 2009, Gaspar et al., 2011).

Proof of principle studies carried out in a *Col7a1*$^{-/-}$ knockout RDEB mouse model, demonstrated the potential of a systemic therapy through the infusion of allogeneic BM cells (Tolar et al., 2009). An enriched population of mouse allogeneic heamatopoietic stem cells positive for the signaling lymphocytic activation molecule (SLAM) CD150^{+} and negative for CD48^{-} when delivered intravenously in newborn *Col7a1*$^{-/-}$ knockout irradiated mice resulted in amelioration of blistering and a prolonged life span by a number of weeks in 15% of the animals. These effects were only seen following a high dose of $8x10^{6}$ cells and solely with the enriched cell population. Interestingly, administration of allogeneic mesenchymal, epidermal stem cell or transient amplifying cells alone were not sufficient for the alteration of the course of the disease.

This is in contrast to the findings of Fujita *et al.*, 2010, where mesenchymal stem cells (MSCs) were shown to migrate to the wounded skin and secrete type XVII collagen or differentiate into keratinocytes for the correction of JEB although did not provide a long-term effect (Fujita et al., 2010). In addition, MSCs were shown to differentiate into type III collagen-producing fibroblasts as well as myofibroblasts following stimulation by IL-10 and IL-16 amongst others (Alexeev et al., 2011). Locally transplanted allogeneic MSCs into an RDEB *Col7a1*$^{-/-}$ mouse model demonstrated migration to the wounded skin and secretion of functional C7 following fibroblastic transition attributed to the environmental cues provided by the recipient dermal fibroblasts and ECM (Alexeev et al., 2011).

A similar result was achieved in man where two RDEB patients were intradermally injected with unrelated adult allogeneic MSCs with significant improvement in wound healing after a 12-week period with reulceration shortly after, probably due to MSC exhaustion (Conget et al., 2010). The encouraging *in vivo* mouse data presented by Tolar *et al.*, 2009, led to the first RDEB patient total bone marrow transplantation (BMT) studies (Wagner et al., 2010).

Allogeneic unfiltered marrow or umbilical-cord blood stem cells from an HLA-matched donor were infused into seven children patients following a myeloablative preconditioning regimen. An amelioration in blistering and partial restoration of C7 at the DEJ was observed within the first 100 days which was more noticeable in patients expressing a low amount of mutant rudimentary C7, suggesting a baseline expression may be necessary. Patients demonstrated a 20% donor chimerism on average in the skin identified as $CD45^+$ haematopoietic and $CD45^-$ $CD31^-$ non-haematopoietic cells.

Allogeneic BMT transplantation being a highly invasive and risky procedure is associated with a high incidence of failure due to graft rejection, graft versus host disease (GVHD) and complications during myeloablation. This was highlighted during this study with the death of two patients from the aforementioned causes. An approach capable of circumventing both allograft rejection and radiation related toxicity is embryonic-BMT (E-BMT). It has been shown that during the first trimester of human gestation the foetus can accept HLA-mismatched allogeneic antigens without the need for myeloablation. In the context of RDEB, Chino *et al.,* 2008, demonstrated the infusion of allogeneic GFP-expressing bone marrow cells (BMCs) into the embryonic circulation via the vitelline vein of RDEB mice resulted in their migration and differentiation into bone marrow derived fibroblasts (BMDFs) following appropriate matrix stimulation from the injured skin (Chino et al., 2008).

One of the contributing factors thought to trigger recruitment of both allogeneic infused and autologous BM-derived cells to injured skin was discovered recently to be the high mobility group box 1 (HMGB1) protein (Tamai et al., 2011). It has been linked to the maintenance of tissue homeostasis during wounding and acceleration of healing through recruitment of BM-derived epidermal progenitors while protecting surrounding uninjured tissue by immunosuppression. Specifically, $Lin^-/PDGFR\alpha^+$ BM cells shown to be non-hematopoietic but of mesenchymal lineage are the key cells induced. HMGB1, although ubiquitously expressed, was found at high concentrations in the hypoxic environment of RDEB epidermal blisters. Topical administration of recombinant HMGB1 was shown to enhance mobilisation of the BMCs to skin wounds. E-BMT was associated with partial amelioration of the disease phenotype while survival was prolonged to 3 weeks post birth due to the small proportion of donor chimerism in the esophageal region impeding with solid feeding. E-BMT was further revealed to introduce immune tolerance to *de novo* expressed proteins, in this case GFP, signifying the potential of this approach for RDEB which would consecutively allow for protein and cell therapies to be used after birth without the risk of autoantibody production to C7 (Chino et al., 2008).

The preferred scenario would comprise of autologous gene corrected foetal BMCs delivered to the affected embryo *in utero* which could lead to a one-off cure. The newest development in the field though has been the use of induced pluripotent stem cells (iPSCs) for the treatment of RDEB. The power of this strategy lies in the ability to derive autologous pluripotent stem cells from patient fibroblasts or keratinocytes offering an inexhaustible supply of dermal, bone marrow or other progenitor cells for downstream local or systemic therapeutic applications (Tolar et al., 2011, Itoh et al., 2013).

Recent studies have demonstrated their capacity in treating RDEB through the delivery of autologous corrected *Col7a1*$^{-/-}$ mouse model iPSCs (Wenzel et al., 2014), or the use of gene editing tools such as transcription activator-like effector nucleases (TALENs) and adeno-associated virus (AAV) AAV-DJ for the correction of RDEB patient derived iPSCs for grafting onto immunodeficient mice (Osborn et al., 2013, Sebastiano et al., 2014). As an alternative to gene editing, iPSCs can also be derived from the rare spontaneously-corrected patient cells which have undergone "natural gene therapy" known as revertant mosaicism as carried out by Umegaki *et al.,* 2014, for JEB providing an unlimited supply of autologous skin cells (Umegaki-Arao et al., 2014).

1.6.4 Gene therapies for RDEB

Circumventing limitations of allogeneic cell rejection and HLA mismatch following topical or systemic therapies can be achieved through the correction of patients' own cells. This is typically carried out by vector-mediated introduction of a healthy copy of the affected gene into the desired cell population for subsequent administration to the individual.

1.6.4.1 Phage mediated gene therapy

An efficient non-viral method of delivering foreign genetic material to target cells is by bacteriophage (Clark and March, 2006). Such a system based on the φC31 bacteriophage was developed for the delivery of *COL7A1* (Ortiz-Urda et al., 2002). This was proposed to circumvent transient expression and low transfection efficiency in keratinocytes experienced with plasmid-based approaches and the transgene capacity limitations of viral vectors. Primary RDEB epidermal keratinocytes were co-transfected with a stably integrating transfer vector containing a specific 285 bp *attb* sequence and encoding *COL7A1* cDNA driven by a CMV promoter and a φC31-integrase expression plasmid. Integration into the host genome is favoured at "pseudo-*attP* sites". Following blasticidin selection for enrichment of the transfected cell population, protein analysis of both *in vitro* and *ex vivo* corrected human skin

equivalents grafted onto immunodeficient mice displayed restoration of adhesion at the DEJ with AFs formation.

The same approach was applied to RDEB patient fibroblasts aiming for correction of a more robust cell type (Ortiz-Urda et al., 2003). This resulted in a highly C7-expressing population which demonstrated restoration of dermal-epidermal cohesion in a xenograft mouse model for a duration of 4 months with a very slight but noticeable spread of correction past the injection site. This study has also demonstrated the advantage of autologous gene therapy over allogeneic cell therapy by showing that endogenous C7 expression levels secreted by normal fibroblasts can fail to deliver sufficient protein to the BMZ, whereas overexpression following vector based correction can significantly enhance that (Ortiz-Urda et al., 2003).

1.6.4.2 γ-retroviral mediated gene therapy

Viral-based gene therapy strategies for the delivery of a WT *COL7A1* gene into RDEB human patients' cells have predominantly involved the use of conventional γ-retroviral vectors as gene delivery vehicles.

Work carried out on a RDEB canine model demonstrated the use of two different retroviral vector backbones, pLZRS and pMSCV encoding full length 8.8 kb human *COL7A1* cDNA driven by a Moloney murine leukaemia virus (MoMLV) promoter for the successful transduction of both human and canine RDEB keratinocytes (Baldeschi et al., 2003, Gache et al., 2004). Their use in skin equivalents revealed reversion of RDEB cell properties including proliferation, adhesion and migration, to those of WT cells. Overexpression of C7 in the retrovirally-transduced RDEB keratinocytes was estimated to be in the magnitude of 50 times that of WT cells (Gache et al., 2004). Efficiency was higher with the pMSCV vector thought to target a high proportion of epithelial progenitor cells due to the broad host range of the amphotropic MLV envelope.

Gache *et al.* further highlighted the importance of this in a subsequent study where retroviral correction of keratinocytes obtained from a spontaneous RDEB canine model for the generation of epithelial skin sheets, showed persistent C7 protein expression for 2 years post-grafting in one of the animals (Gache et al., 2011). On the contrary, in a second animal expression disappeared after a 2-month period. This was attributed to the inefficient targeting of highly clonogenic keratinocyte stem cells, key in providing the auto-renewal capacity of the grafted tissue. The limitation of keratinocyte-based therapy is accentuated through this work as in a continuous tissue-healing environment, such as in RDEB, depletion of epidermal stem cell pools renders targeting of these populations highly infrequent (Gache et al., 2011).

Successful keratinocyte-based therapies, such as the one led by Mavilio *et al*. though has also shown the potential of this approach (Mavilio et al., 2006). Following correction of approximately 100% of keratinocytes obtained from JEB patients' palm biopsies using a *LAMB3*-encoding MLV retroviral vector, cells were developed into skin sheets for grafting on patients' legs. Epidermal regeneration was detected as early as 8 days post-transplantation and still maintained after 1 year. The long-term persistence of the graft was explained by the self-renewing capacity of vector targeted epidermal stem cells, although transit amplifying progenitor cells were undetected after the first month due to epidermal turnover.

To overcome limitations associated with the restricted 7-8 kb transgene capacity of retroviral vectors unable to efficiently accommodate the full-length 9 kb cDNA of *COL7A1*, a recombinant *COL7A1* minigene containing intact NC1 and NC2 domains and a portion of the central domain was used for virus production (Chen et al., 2000). When cloned into a γ-retroviral construct, it was able to efficiently transduce RDEB keratinocytes resulting in expression of a 230 kDa protein (700 kDa trimer) resistant to proteolytic degradation while retaining functionality showing increased proliferation, reduced cell motility and cell-substratum adhesion. However, removing portion of the triple helical domain containing the 39 a.a. hinge region may compromise the flexibility of the fibrils. An alternative approach for reduction of *COL7A1* cDNA size while maintaining functionality can be achieved through *trans*-splicing (Murauer et al., 2011). In place of the 9.2 kb cDNA, a 3.3 kb transgene was incorporated into a retroviral vector encoding for exons 65 to 118 a.a. with a 3' pre-*trans*-splicing molecule in exon 64. Correction was achieved *in vitro* in patient cells with a mutation in exon 106 with no signs of truncated C7 produced.

Moreover, the use of the strong γ-retroviral long terminal repeats (LTRs) to drive transgene expression have been associated with proto-oncogenic risks as described previously (Hacein-Bey-Abina et al., 2008). An internal promoter can be used in their place, which not only enhances the vector biosafety, but can also confer tissue specific regulated expression. Titeux *et al.* demonstrated the use of self-inactivating (SIN) retroviral vectors encoding the full-length *COL7A1* cDNA driven by either an endogenous *COL7A1* promoter or the housekeeping elongation factor (EF1α) (Titeux et al., 2010). Transduction efficiency was estimated to be in the range of 30-80% following both primary keratinocyte and fibroblast transduction at a high multiplicity of infection (MOI). Although restoration of C7 was observed in both *in vitro* and *ex vivo* skin equivalent studies this was the first study to report the secretion of truncated C7 as assessed at the protein level. These shorter forms of C7 do not appear to hinder AFs formation to the extent that dermal-epidermal adhesion is compromised although it may be associated with

a drop in efficiency. Rearrangement was predicted to occur at the proviral stage in transduced cells during the retrotranscription process.

Nevertheless, phase I clinical trials have now commenced for RDEB gene therapy using γ-retroviruses for the correction of autologous patient keratinocytes and fibroblasts. Notable studies include those led by Marinkovich M.P. and Lane A. in Stanford, US, and Hovnanian A. in Toulouse, France. Two trials using the pLZRSE-COL7A1 γ-retroviral vector assessed in a preclinical study for the *ex vivo* correction of keratinocytes (Siprashvili et al., 2010), are now underway proposing the grafting of gene-corrected autologous keratinocyte sheets (LEAES) (NCT01263379), or intradermal injection of gene-corrected autologous fibroblasts (FCX-007), however, the latter has been held up until additional toxicology data has been generated. Similarly, based on preclinical data using a SIN-γ-retroviral vector (Titeux et al., 2010), is about to be launched in Europe in 2016 for the delivery of *COL7A1*-corrected keratinocyte and fibroblast grafts (Genegraft).

1.6.4.3 Lentiviral mediated gene therapy

The use of retroviral vectors in humans has raised concerns due to recognised adverse effects such as reversion to a virulent state or activation of oncogenes (Hacein-Bey-Abina et al., 2008, Hacein-Bey-Abina et al., 2003, Howe et al., 2008, Ott et al., 2006). To diminish the risk of recombination occurring as a result of viral incorporation, 3rd generation replication defective SIN lentiviral vector constructs have been designed based on the human immunodeficiency virus (HIV-1) stripped of all virulence factors (vpu, vpr, nef, vif) and Tat. Lentiviral vectors offer a range of advantages over their retroviral counterparts. These include i) reduced genotoxic potential secured by the integration in gene rich regions as opposed to nearby transcription sites, which can lead to insertional mutagenesis by the transactivation of proto-oncogenes as suggested by integration mapping (Bushman et al., 2005, Mitchell et al., 2004, Montini et al., 2009) ii) the ability to produce concentrated virus with high titers by centrifugation and hence increased transduction efficiency; iii) the stability and sustained expression of the carrying transgene with negligible, if any, immune response; iv) larger insert capacity of 9 kb as opposed to 7-8 kb in retroviral vectors (Chen et al., 2002, Naldini, 1998), and v) potential to infect both dividing and non-dividing cells (Kuhn et al., 2002, Naldini et al., 1996a, Sakoda et al., 1999).

Furthermore, aiming to improve the safety profile of viral delivery as well as efficiency, a SIN-lentiviral vector encoding full-length human *COL7A1* cDNA was generated (Chen et al., 2002). The chosen modified murine leukaemia retroviral (MND) promoter driving the transgene

resulted in reduction of methylation and increase in expression. Viral transduction was shown to restore C7 expression in both RDEB keratinocytes and fibroblasts (Chen et al., 2002). Correction was sustained for 5 months *in vitro* with reversion of the RDEB phenotype and 2 months *in vivo* with deposition of C7 and formation of AFs at the DEJ of skin equivalent grafted mice. Subsequent follow-up studies confirmed restoration of dermal-epidermal adhesion to be feasible either by a combination of gene corrected RDEB keratinocytes and fibroblasts or when corrected keratinocytes were grafted alone. On the other hand, gene corrected fibroblasts alone were demonstrated to express stable and sufficient enough levels to reconstitute dermal-epidermal adhesion and functional correction following skin equivalent grafting in mice (Woodley et al., 2003).

Furthermore, intradermal injection of gene-corrected RDEB fibroblasts in healthy nude mice showed expression of human C7 at the BMZ. For intradermal administration of fibroblasts to be clinically meaningful, multiple injections would have to be carried out considering the limited diffusion radius of the cells. Alternatively, fibroblasts could be delivered systemically by intravenous injection (Woodley et al., 2007b). Lentivirally-corrected fibroblasts appeared to promote wound healing after homing to the skin wounds in a murine model. Recruitment of the fibroblasts from the circulation was shown to only occur when the skin was injured suggesting the involvement of factors such as HMGB1.

In a slightly different approach aimed at circumventing difficulties encountered with *ex vivo* gene correction, such as the harvesting and culturing of patient cells before gene modification, verification and subsequent transplantation, Woodley *et al.* explored the potential of using direct *in vivo* viral vector delivery to patient skin (Woodley et al., 2004b). As epidermal keratinocytes do not undergo continuous active division unless under epithelial remodelling following wounding, infection by retroviral vectors would not be possible. Instead, the minimal lentiviral vector previously used to correct both keratinocytes and fibroblasts *in vitro* was injected intradermally into RDEB skin equivalent immunodeficient mouse models. A single injection demonstrated sustained expression and reversion of blistering at the DEJ for at least 2 months. An exciting finding by these authors was the successful transduction and C7 expression of endothelial cells amongst dermal fibroblasts. This may open new avenues for the intravenous delivery of lentiviral vectors. Interestingly, there was no lentiviral integration detected in epidermal keratinocytes, presumed to be due to the depth of the injection into the underlying dermis, limiting diffusion of the vector through the BMZ and into epidermal progenitors.

1.6.5 Alternative therapeutic options

A number of recurrent mutations are found in exonic regions 73, 74 and 80 which carry multiple Gly-X-Y collagenous repeats. It has been proposed that targeted knockout of sequences within that region would not interfere with functional C7 production (Turczynski et al., 2012). An exon-skipping strategy was therefore developed using antisense oligonucleotides complementary to the *COL7A1* genomic sequence. The pre-mRNA exposed to the antisense oligonucleotides prevents normal splicing, in turn leading to the skipping of the dysfunctional exon in the mature mRNA. It has been suggested that in a clinical setting, antisense oligonucleotides can be administered *in vivo* intradermally, intravenously, intramuscularly or even topically. This strategy though will most likely only be feasible for those select exons, as skipping of sequence in non-collagenous domains would undoubtedly have a deleterious effect on the functionality of C7. An improvement to exon-skipping has recently been brought to light involving a novel premature termination codon (PTC) readthrough strategy (Cogan et al., 2014). Aminoglycosides such as geneticin, gentamicin and paromomycin when transiently delivered in an expression vector can mediate readthough of nonsense mutations and restore C7 expression.

1.7 Lentiviral gene therapy

Gene therapy can be termed as the process by which a therapeutic gene is introduced into a cellular target for the treatment of a medical disorder. This may involve the delivery of a portion or an entire gene for the replacement, modification or inactivation of the affected endogenous gene. In some instances the desired outcome may encompass the addition of *de novo* DNA sequence to a cell target for the institution of supplementary function by novel protein expression. An example of this can be seen in the breakthrough work currently underway for the expression of chimeric antigen receptors (CARs) on the surface of T-cells to combat malignant B-cells (Pule et al., 2003).

Following extensive research and elucidation of the molecular basis of a number of genetic disorders, the potential of gene therapy was realised giving rise to its development as a prospective therapeutic tool. With work dating back to the early 70s for the treatment of hyperargininemia in three patients using a therapeutic transgene carrying papilloma viral vector formulated the first human gene therapy trial (Friedmann and Roblin, 1972, Terheggen et al., 1975). Although no significant clinical benefit was demonstrated in contrary to the successful *in vivo* animal studies, this paved the way towards the development of improved transgene delivery systems. This resulted in the progression to using γ-retroviral vectors as the transgene vehicle, harnessing their ability to stably integrate into the host genome. A series of proof-of-

principle studies in the early 90s using γ-retroviral vectors demonstrated their efficacy in transducing HSCs (Deisseroth et al., 1994, Brenner, 1993, Emmons et al., 1997), which led to the first approved clinical trial. This involved the reestablishment of adenosine deaminase (ADA) protein expression in CD34+ cells of severe combined immunodeficiency (SCID) patients using a γ-retroviral vector (Bordignon et al., 1993). Although no detrimental side effects were reported following therapy, the levels of ADA showed only a marginal increase which rapidly dissipated.

This was succeeded by a large multicenter study involving twenty children patients suffering from interleukin receptor γ-chain (γc) deficient SCID-X1 (Hacein-Bey et al., 1996, Gaspar et al., 2004). A clinically significant result leading to restoration of immunological function with increase in T, B and NK cells was achieved by *ex vivo* delivery of the therapeutic γc gene into autologous bone marrow-derived CD34+ cells via a mouse leukaemia (MLV) retroviral vector (Cavazzana-Calvo et al., 2000).

After a 3 to 6 year period post-treatment, serious adverse effects, namely splenomegaly and more importantly uncontrolled exponential clonal proliferation of mature T cells, associated with the vector were reported in five cases in both trials. This was later shown to have been caused by insertional mutagenesis proximal to the *LMO-2* proto-oncogene promoter within chromosome 11 (Hacein-Bey-Abina et al., 2003, Howe et al., 2008). Despite this, the relative success of these studies boosted the field of gene therapy, which initiated the recruitment of a number of patients for subsequent clinical trials. An example of these included the use of γ-retroviral vectors as a means of restoring $gp91^{phox}$ expression in *CYBB* gene deficient X-linked chronic granulomatous disease patients (X-CGD) (Moreno-Carranza et al., 2009) and was also successfully described as a method of conferring highly targeted anti-tumour activity achieved through the vector-mediated modification of autologous patient T-cells to express the α and β chains of the anti-MART-1 TCR obtained from a metastatic melanoma patient having undergone almost complete regression following adoptive cell transfer (Morgan et al., 2006).

The outcomes of these studies were highly encouraging and demonstrated the potential of this therapeutic approach. Stable proviral integration into the host genome though was highly controversial at the time while still remaining a major concern in terms of biosafety as highlighted by the unanticipated events during the early gene therapy trials. This emphasised the need for a safer system with comparable efficiency giving rise to lentiviral vectors.

The configuration of the vectors used in the aforementioned trials was initially based on oncoretroviruses of the *Retroviridae* family and most commonly on Moloney Leukaemia Virus (MLV). These γ-retroviral vectors have now been superseded by safer alternatives of the same

retroviral family based instead on a lentiviral backbone. Both vectors have a very similar backbone encoding the same structural, integration and envelope genes with the more complex lentiviruses carrying additional genes for the regulation of viral replication, assembly and infection (Dufait et al., 2012).

1.8 HIV lifecycle

1.8.1 Viral attachment

These viruses belong to the family of enveloped single-stranded (SS) RNA viruses with chromosomal integration being an integral part of their life cycle **(Figure 1.7)**. In their mature state as a virion they carry two copies of positive strand RNA in addition to enzymes principle for the initiation of reverse transcription and integration. A viral core is formed encapsidated by two distinct protein shells, and enveloped by host cell lipid membrane incorporating viral glycoproteins conferring selective tropism. The viral life cycle commences with the detection of specific cellular surface receptors now known to be predominantly CD4 on a subset of mature T lymphocytes and macrophages. Two distinct co-receptors were later identified required for viral entry into the host cell. Both belonging to the family of G protein coupled chemokine receptors, CXCR4 was typically found to be expressed on the surface of the majority of haematopoietic progenitor cells and largely on T cells while the human chemokine CCR5 was predominantly specific to macrophages (Dragic et al., 1996). The preference for co-receptor is used to define the host-cell specificity of the virus, which can be X4 or R5 tropic, and in some cases "dual/mixed" (Feng et al., 1996).

1.8.2 Viral entry

Host-cell attachment by the virion is succeeded by a complex process termed fusion, whereby the viral core is released into the cytoplasm and the particle is uncoated for the initiation of reverse transcription. This is mediated by the subunit components of the envelope complex, collectively known as glycoprotein 160 (gp160), consisting of trimeric forms of surface gp120 non-covalently bonded to transmembrane gp41 forming an envelope spike. Association of gp120 to both CD4 receptor and either of the co-receptors institutes a conformational change in the envelope spike bringing viral and host-cell membranes in close proximity resulting in fusion (Weiss et al., 1996).

1.8.3 Reverse transcription

Following entry and disassembly of the viral core proteins into the host-cell cytoplasm the reverse transcription complex (RTC) arises, which moderates the synthesis of viral dsDNA from the ssRNA genome forming the hallmark of retroviruses **(Figure 1.8)**. Reverse transcriptase carries out two distinct enzymatic functions, with the N-terminal portion involved in RNA or DNA dependent DNA polymerisation, while the C-terminal portion confers RNase H activity to mediate cleavage of RNA when in an RNA-DNA duplex conformation with the exception of the polypurine tracts (PPTs) being resistant to degradation (Fuentes et al., 1995).

For the initiation of reverse transcription, a host-derived lysine transfer RNA ($tRNA^{Lys3}$) is employed as a primer complementary to the 5' end of the viral RNA primer binding site (PBS) for synthesis of minus strand DNA (Kovaleski et al., 2006). Reverse transcription takes place in a 3'-5' direction with synthesis of the DNA minus strand commencing with the R-U5 region while the viral RNA template undergoes degradation by RNase H activity with the exception of the PPT (Fuentes et al., 1995). This is proceeded by transfer of the R-U5 DNA-tRNA hybrid molecule to the 3' end of the template mediated by the homology of the 5' and 3' R regions. Synthesis starts from the conserved PPT sequence, serving as a primer for the synthesis of the initial portion of the complementary DNA plus strand. The process is carried out by RNA dependent DNA polymerase, starting with synthesis of the U3-R-U5 region and including a PBS. Subsequent degradation of the tRNA results in hybridisation of the two complementary DNA PBSs which triggers the bidirectional completion of both DNA strands by DNA dependent DNA polymerase (Shaharabany and Hizi, 1991). This results in a complete viral dsDNA genome, carrying a U3-R-U5 sequence on both 5' and 3' ends termed LTR, capable of host integration following nuclear import.

1.8.4 Nuclear import

One of the defining features of lentiviruses making them so efficient at host-cell infection lies in their ability to enter the nucleus of not only dividing but also non-dividing cells unlike their γ-retroviral counterparts such as MLV which can only pass the nuclear envelope during mitosis. The process is facilitated by the pre-integration complex (PIC), formed after the complete degradation of RNA following reverse transcription by the RTC (Miller et al., 1997). Owing to the large size of the PIC preventing entry via diffusion, a combination of viral elements, namely capsid (CA), central polypurine tract (cPPT), integrase (IN), matrix (MA) and Vpr which carry nuclear localisation signals (NLS) have been shown to interact with host importin and nucleoporin proteins facilitating nuclear import (Bukrinsky et al., 1993).

1.8.5 Proviral integration

Following entry of the PIC into the host-cell nucleus, the viral genome undergoes a two-step chemical processing reaction by the catalytic activity of IN. The initial step, having commenced during the earlier stage of reverse transcription termed 3' processing, involves the binding of IN to each LTR end of the viral dsDNA and cleavage of two nucleotides resulting in 3' hydroxyl groups. When in the nucleus, the PIC can interact with chromosomal DNA to engage in viral DNA-strand transfer mediated by IN. Targeted cleavage of the chromosomal DNA is performed by IN resulting in 5' overhangs that following nucleophilic attack by the 3' hydroxyl groups resolve by ligation of viral and host DNA by endogenous cell-repair machinery (Kessl et al., 2009).

Lentiviruses like HIV-1 display a preference in their integration pattern for active genes(Mitchell et al., 2004, Schroder et al., 2002) as opposed to γ-retroviruses which highly favour integration at approximately 5 kb of either side of transcriptional start sites (Wu et al., 2003). This suggests a difference in the process of target site selection between retroviruses accounted for by sequence recognition, engagement with the PIC machinery, and response to transcriptional activity (Vandegraaff and Engelman, 2007). For HIV-1, cellular cofactor cellular lens epithelium-derived growth factor (LEDGF)/p75 has been demonstrated to facilitate the targeting of the virus to gene rich regions by direct binding of IN and chromatin (Maertens et al., 2004).

1.8.6 Transcription

The integrated dsDNA viral genome can at this stage be termed provirus and utilises host machinery such as RNA polymerase II (RNA pol II) for the production of viral transcripts. Transcription initiates at the strong promoter region of U3-R junction located at the 5' LTR and terminates when it recognises the polyA signal at the 3' LTR. A number of transcription factor binding sites have additionally been located in the LTR, facilitating interactions with factors Specific protein (Sp) and nuclear factor κB (NFκB), further modulating transcription (Jones et al., 1986, Nabel and Baltimore, 1987). Synthesis of viral proteins Tat and Vpr act in turn as modulators and enhancers of viral transcription.

1.8.7 Nuclear export

Unlike cellular pre-mRNA where complete splicing of introns has to take place before processing and nuclear export of mature mRNA (Legrain and Rosbash, 1989), in the case of

HIV-1, a mixture of fully spliced and partially spliced viral mRNA can enter the cytoplasm (Cullen, 1992). This process is facilitated by the RNA-binding Rev protein encoded for by fully spliced mRNA also encoding regulatory factors Tat, Nef, Vpr and Vpu. Structural components required for assembly of the virion such as Gag, Pol, and Env, are sequestered to the cytoplasm at later stages of the replication cycle in response to elevated concentrations of translated Rev which is imported into the nucleus (Blissenbach et al., 2010). The presence of a Rev response element (RRE) in all fully and partially spliced mRNAs permits Rev to coordinate spliceosome assembly and nuclear translocation (Feinberg et al., 1986). The transcripts are then exported via the host-cell chromosome maintenance region 1 (Crm1) pathway serving as templates for translation (Malim and Cullen, 1993).

1.8.8 Translation viral assembly and budding

Following translation by host ribosomal subunits, viral assembly is almost exclusively executed by Gag. Proteolytic cleavage of the Gag p55 precursor by *pol* encoded viral protease gives rise to mature Gag protein subdomains Matrix (MA), Capsid (CA), Nucleocapsid (NC) and p6 (Gottlinger et al., 1989). During translation, the N terminus of Gag undergoes myristoylation, triggering the transporting and anchoring of Gag to the cell membrane through the action of MA which is also involved in the coating of the inner surface and stabilisation of the virion (Bryant and Ratner, 1990). CA protein p24 in turn facilitates the protein-protein interactions leading to the assembly of the immature conical shell containing the viral core.

Recognition of the HIV-1 packaging signal (Ψ), composed of a distinct 4-hairpin secondary structure, is mediated by the NC protein leading to the incorporation of two strands of capped and polyadenylated full-length RNA genome into the budding virion along with the remaining viral proteins and two copies of host $tRNA^{Lys3}$. p6 in turn is responsible for the incorporation of Vpr into the virion via interactions with p55 Gag (Paxton et al., 1993).

Env glycoprotein gp160 is transported to the cell membrane independently where it is inserted into the virus particle forming an integral part of the HIV-1 life cycle. The involvement of p6 is seen again during the final stages where it recruits cellular factors for the budding of the virion and the "pinching" off of the particle from the host cell. A series of structural and conformational rearrangements of the viral proteins signifies maturation of the viral bud into an infectious particle (Briggs and Krausslich, 2011).

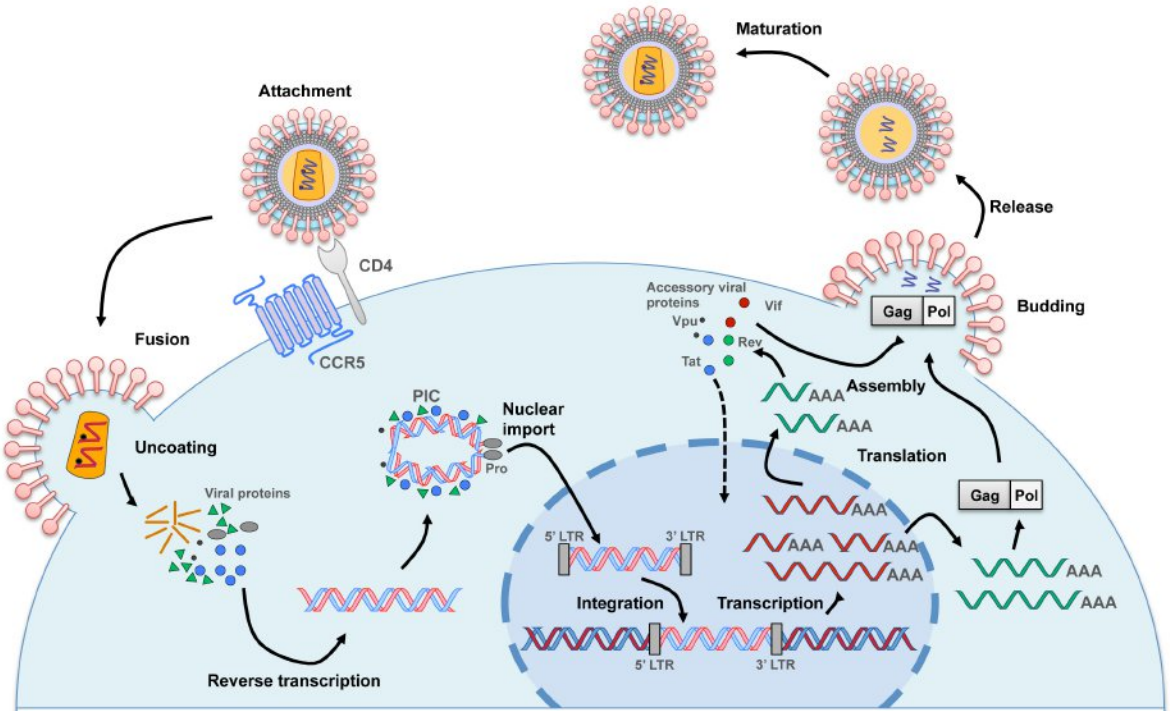

Figure 1.7 HIV-1 lifecycle in host mammalian cell.
Attachment of HIV-1 virus to cell surface of T-cell followed by fusion of host and viral membranes and release of viral proteins into the host cell cytoplasm. Using host machinery and viral reverse transcriptase, the two strands of viral RNA are reverse transcribed into dsDNA. The PIC facilitates nuclear import where following the binding of integrase to the 5' and 3' LTR the viral dsDNA integrates into host chromosomal DNA. Using host machinery, a mixture of fully spliced and partially spliced viral transcripts are generated and enter the cytoplasm. Fully spliced mRNA encodes regulatory factors Tat, Nef, Vpr and Vpu which can enter the cytoplasm. Translation is mediated by host ribosomal units and viral assembly is orchestrated by viral Gag. The synthesized viral proteins and two strands of capped and polyadenylated full-length viral RNA are enveloped by host cell membrane in which gp160 is inserted. Following budding of the immature virus, p6 facilitates the pinching off of the viral particle and release from the host cell. Structural and conformational rearrangements of the viral proteins result in maturation of the viral particle. LTR: long terminal repeat; PIC: pre-integration complex; gag, pro, pol: HIV structural polyproteins; Tat, Rev, Nef, Vpr, Vif, Vpu: HIV regulatory elements.

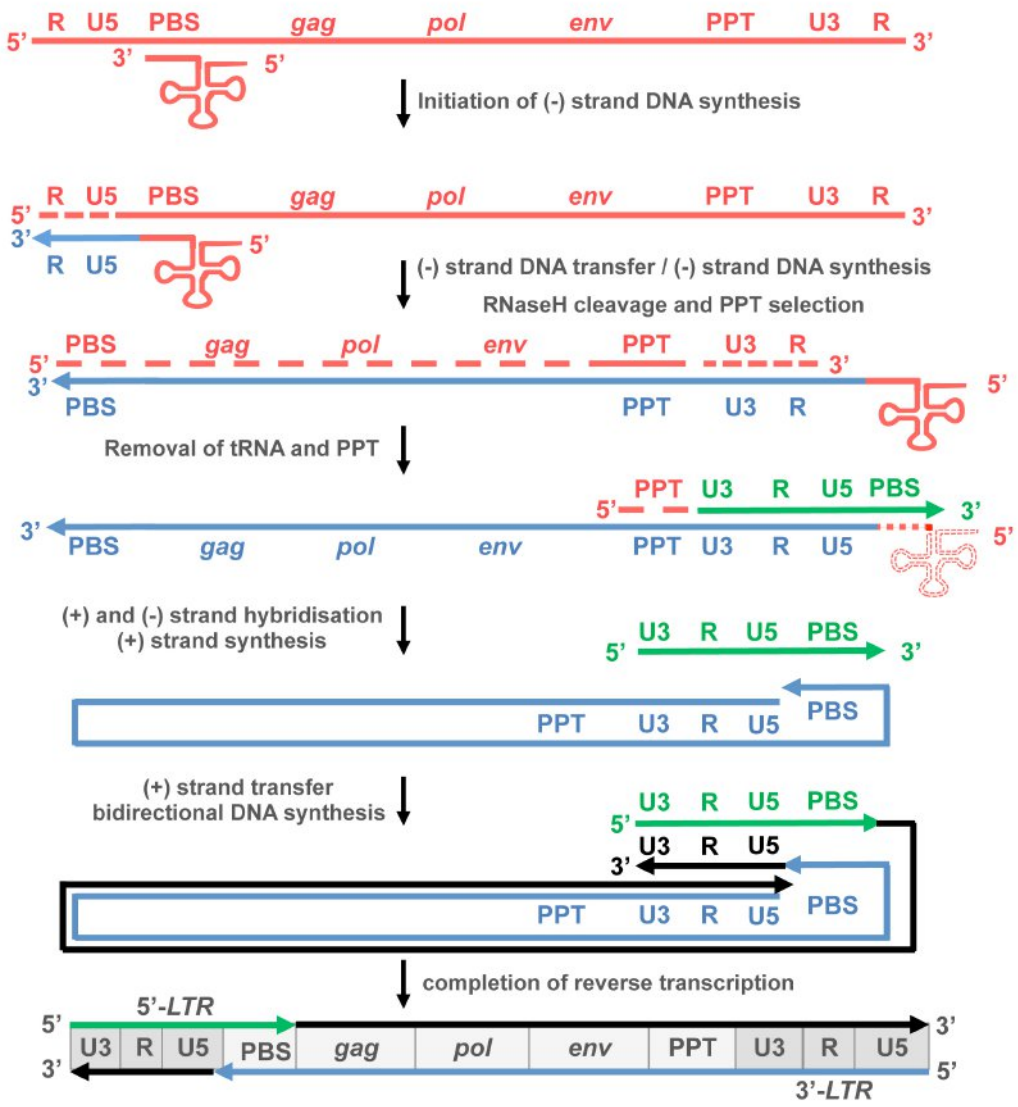

Figure 1.8 Reverse transcription of HIV-1.
Host-derived lysine transfer RNA ($tRNA^{Lys3}$) anneals to the 5' end of the viral RNA PBS for synthesis of minus (-) DNA strand. Reverse transcription takes place in a 3'-5' direction with synthesis of DNA (-) strand commencing with the R-U5 region. Viral RNA template degraded by RNase H activity with the exception of the PPT. Transfer of the R-U5 DNA-tRNA hybrid molecule to the 3' end of the template by the homology of the 5' and 3' R regions. Synthesis of plus (+) strand starts from the conserved PPT sequence and initiates with synthesis of U3-R-U5 region including a PBS, followed by degradation of the tRNA. Hybridisation of the two complementary DNA PBSs triggers the bidirectional completion of both DNA strands. A complete viral dsDNA genome is generated, carrying a U3-R-U5 sequence on both 5' and 3' ends termed LTR. *gag, pol, env*: HIV-1 structural genes; LTR: long terminal repeat; PBS: primer binding site; PPT: polypurine tract; tRNA: transfer RNA; U3 or U5: untranslated 3' or 5' region;

1.9 Development of lentiviral vectors

The insertional mutagenesis reported in the SCID-X1 trials with an estimated 1 in 10^5 chance of random integration into transcriptionally active genes coupled with the presence of a potential

100-1000 proto-oncogenes in the human genome (Hacein-Bey-Abina et al., 2003) prompted the optimisation of the vector. This came in the form of a SIN lentiviral vector based on HIV-1, which allowed to combat a number of the caveats exposed with γ-retroviral vectors (Naldini et al., 1996b). One of the benefits of lentiviral vectors over their γ-retroviral counterparts can be primarily seen in their integration profile with a preference for gene-rich regions as opposed to transcriptional start sites, promoter and regulatory regions. Modification of endogenous retroviral promoters within the LTR region known for their ability to drive expression of genes at over 100 kb downstream (Hacein-Bey-Abina et al., 2003) was a key step in reducing potential transcriptional activation of oncogenes.

The basic principle for the generation of lentiviral vectors involves the use of a packaging cell, typically human embryonic kidney (HEK) 293T cells, to assemble the vector following 3-plasmid co-transfection with a packaging plasmid, a transfer plasmid and an envelope plasmid (Naldini et al., 1996a). Since its initial development, the current vector system has undergone a series of modifications aiming to improve its safety profile, classed as generations. The major alterations were made in the packaging plasmid as the first generation lentiviral vector contained all structural *gag*, *pol*, regulatory *tat*, *rev* and accessory *vif*, *vpr*, *vpu* and *nef* viral genes with the exception of *env*.

Advances in the field later revealed that a number of these genes had no detrimental effect on infectivity or vector yield resulting in their removal and giving rise to the second generation. Accessory genes *vif*, *vpr*, *vpu* and *nef* were therefore removed, attenuating the packaging system, majorly benefiting vector safety by significantly reducing the risks of recombination which could potentially result in a functional virulent particle (Zufferey et al., 1998). Aiming to broaden the host-cell tropism of HIV-1, the envelope is frequently substituted with that of vesicular stomatitis virus (VSV) in a process termed pseudotyping. VSV glycoproteins (VSV-G) interact with a ubiquitously expressed cell surface marker gp96 enabling viral entry in a wide host range (Burns et al., 1993). Similarly, use of envelope glycoproteins from Rabies virus and Venezuelan Equine Encephalitis virus envelopes have been reported to confer neuronal tropism, essential for the treatment of neurodegenerative disorders (Trabalza et al., 2013).

Currently in use, is the 3rd generation system further reducing safety concerns of RCL formation by employing a split-genome packaging plasmid whereby the *rev* gene is provided in trans to *gag* and *pol*. This method allows for the sustained yet restricted to the packaging cell expression of Rev (Dull et al., 1998). Additionally, a series of modifications were made to the transfer plasmid making it self-inactivating, by disrupting promoter function of the 5' LTR which is replaced with a *tat*-independent constitutive promoter while still ensuring sufficient expression (Dull et al., 1998). This was made possible by adapting the 3' LTR U3 enhancer/promoter

region by deletion of 133 bp of the TATA box and binding sites required for the sequestration of transcription factors. During reverse transcription the 3'LTR deletion is transferred and acquired by the 5'LTR rendering the integrated provirus transcriptionally inactive (Miyoshi et al., 1998).

As a means of enhancing gene expression and viral titres, a post transcriptional regulatory element derived from woodchuck hepatitis virus (WPRE) shown to have promoter activity, was also added to the vector (Schambach et al., 2005, Zufferey et al., 1999). Owing to the inactivation of the viral LTR in the SIN vectors, transgene expression requires the use of an internal promoter, the choice of which is application dependent and typically selected with cell and tissue specificity in mind. Commonly used promoters which have already been approved for clinical trials can be of either viral or human origin, such as Spleen focus-forming virus (SFFV) and Cytomegalovirus (CMV), or phosphoglycerate kinase (PGK) and EF1α, respectively, allowing for stable transgene expression in both progenitor and differentiated cells. These promoters vary considerably in their strength of expression with cellular EF-1α known to drive the strongest transgene expression while viral CMV the weakest. Interestingly, when assesed in differentiated cell populations, the opposite was observed suggesting promoter selection can be optimised to the intended target cell (Hong et al., 2007). The PGK promoter, although not necessarily the strongest in terms of transgene expression, is highy desirable as it can drive robust and long-term expression and, importantly, has been reported to be active in most cell types and lineages (Qin et al., 2010).

Although the use of lentiviral vectors has been traditionally described for the stable integration of a transgene to achieve long-term permanent correction, sustained transient gene expression can also be attained independent of proviral integration. This was demonstrated with the development of non-integrating lentiviral vectors (NILV) also known as integration-deficient lentiviral vectors (IDLVs). Modification of the pol portion of the gag-pol polyprotein encoding the IN enzyme via a 64 bp deletion (Δ64V) of the catalytic domain, abolishes proviral integration with a 4-log unit drop in infectious titre and therefore background integration over WT virus yet generating the same levels of viral DNA (Leavitt et al., 1996). The non-integrated proviral forms persist as circular vector episomes which can support transgene expression (Matrai et al., 2011). This not only offers the advantage of a transient effect that can be diluted out in proliferating cells but can provide stable expression without the risks of chromosomal integration in quiescent cells. Examples of applications necessitating transient expression include the delivery of gene editing machinery such as sequence specific nucleases which are typically required for a "hit-and-run" approach. NILVs can be described as one of the safest

viral-mediated gene-transfer systems albeit the low levels of background integrations reported (Leavitt et al., 1996).

1.10 Zinc Finger Nucleases as a highly targeted gene-editing tool

Zinc finger nucleases (ZFNs) comprise one of the largest families of eukaryotic DNA binding motifs coupled to a nuclease domain capable of introducing double-stranded breaks (DSBs) in targeted regions of the genome. This provides researchers with a valuable genome editing tool for the modelling of genetic diseases both *in vitro* and *in vivo*. Their potential as a clinical application has further been realised by their use as a gene correction tool. DSBs are known to promote homologous recombination (HR) which can be exploited by the provision of homologous healthy donor sequence.

1.10.1 Zinc finger protein structure and their development

Zinc finger proteins (ZFP) generally refer to relatively small protein structural motifs that coordinate zinc ions through the interaction of histidine and cysteine residues and can bind DNA. Six classes of ZFPs have been discovered and characterised according to the protein domain and backbone shape into respective fold group. By far the most common of the ZF domains conferring DNA binding in eukaryotes and the more specifically the human genome is based on the Cys_2-His_2 conformation also known as the Cys_2-His_2–like fold group. Crystallographic studies performed at 1.6 Å resolution (Elrod-Erickson et al., 1996, Pavletich and Pabo, 1991), have revealed the precise structure of the Zif268-DNA complex variant, a mammalian transcription factor encoded by the *EGR1* gene in humans, revealing its simple, modular structure (Elrod-Erickson et al., 1998).

Each individual finger comprises of approximately 30 amino acids in a short two-stranded antiparallel β sheet and single α helix conserved ββα configuration (Elrod-Erickson et al., 1998). A small hydrophobic core retains the helix and sheets together along with a zinc ion coordinated by the conserved β sheet region cysteines and α helix histidines (Elrod-Erickson et al., 1998). A proportion of the amino acids at the N-terminal portion of the α helix typically interact with a three base pair subsite, usually guanine-rich (GCG/TGG/GCG), in the major groove of the double helix with variable selectivity (Elrod-Erickson et al., 1998).

It has been elucidated that the sequence specificity of the ZFPs relies chiefly on base contacts with amino acids located at the start of the ZF α helix at positions 1, 2, 3, and 6 with residues 1, 3, and 6 directly contacting the 3', central and 5' DNA base. This has formed the basis for generating a multitude of ZFPs with a broad range of sequence specificities by altering the four key amino acids while maintaining the remaining ones as a consensus backbone (Pavletich and Pabo, 1991, Kim and Berg, 1996, Desjarlais and Berg, 1993, Shi and Berg, 1995, Elrod-Erickson et al., 1998). This permits for the modular assembly of variable ZFP structural motifs against custom sequences making it a highly attractive framework. A highly conserved linker sequence was later used for the construction of synthetic ZFPs recognising sequences of DNA triplets, 9-18 bp in length (Liu et al., 1997) **(Figure 1.9)**.

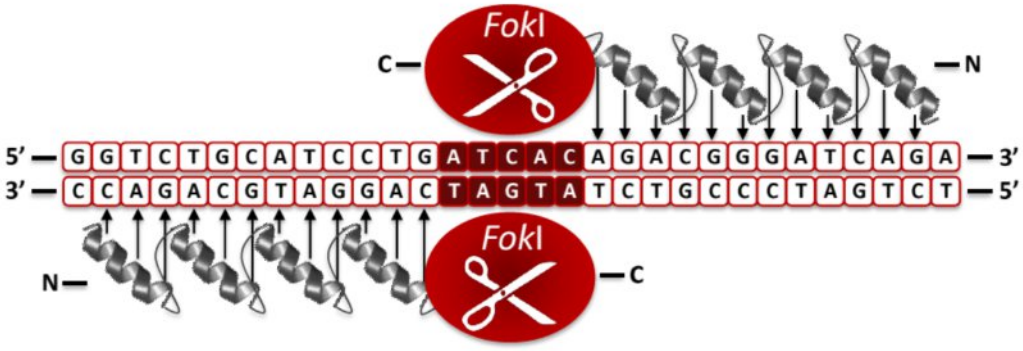

Figure 1.9 Zinc-finger nuclease structure.
Zinc-finger protein (ZFP) modules recognising nucleotide triplets are linked together up to a maximum of six constituting a ZF arm recognising a total of 18 bp of genomic DNA sequence. A ZF arm is synthesized for each strand of the genomic region to be targeted with an intervening 5 bp spacer region. The assembled ZFPs are coupled to a FokI endonuclease on their C-terminus end, modified to confer cleavage only upon formation of a heterodimer. Zinc-finger nucleases are delivered as a pair in order to create double-stranded breaks (DSBs) in a predetermined region of the genome.

Improvements have been made in the methods of assembly of multiple zinc fingers as not all combinations are as efficient at targeting the specified chromosomal DNA sequence. Techniques such as the "modular assembly" approach whereby a preselected library of ZF modules based on rational design has enabled the generation of ZFPs against all 64 possible nucleotide triplets (Beerli and Barbas, 2002, Segal et al., 1999, Kim et al., 2010, Sander et al., 2011, Gupta et al., 2012, Joung and Sander, 2013). Oligomerised pool engineering (OPEN) has been a further development in the selection of ZF arrays based on randomised libraries which unlike the "modular assembly" takes into account interactions between neighbouring ZFs in a context-dependent manner (Maeder et al., 2008). Although kits for the in-house production of ZFP modules are available, their construction remains challenging with commercially available ones remaining the preferred choice. Companies such as Sangamo Biosciences (Richmond, CA,

USA) in partnership with Sigma-Aldrich (St. Louis, MO, USA) have developed a proprietary platform for the construction and validation of ZFPs (CompoZr™) using a combination of the aforementioned approaches, offering a vast database of available custom designed modules (Gaj et al., 2013).

1.10.2 Zinc Finger Nuclease complexes for induction of DNA breaks

The main purpose for the rapid advancement in the field is due to the capacity to couple a variety of effector domains to the zinc finger modules conferring nuclease, recombinase, transposase, and activator or repressor activity. The establishment of the currently used zinc finger nuclease (ZFN) platform was achieved by the fusion of the *Fok*I cleavage domain, a type IIS restriction enzyme derived from *Flavobacterium okeanokoites*, to the carboxyl terminus of the modular ZFP monomers. *Fok*I requires dimerisation for it to cleave dsDNA with the advantage of increasing specificity at the target site by involving two inverted ZFNs spanning a maximum of 36 nucleotides. A high frequency of off-target cleavage and therefore cytotoxicity was reported due to the formation of homodimers. This led to the artificial modification of the WT *Fok*I domain to solely cut DNA upon the formation of obligate heterodimers within a 5-7bp spacer region, increasing the safety profile of ZFNs (Miller et al., 2007, Szczepek et al., 2007). Creating targeted chromosomal disruptions which result in precise endogenous gene knockouts, is an invaluable strategy permitting the modelling of diseases *in vitro* and generation of animal models and determining how genotype influences phenotype.

ZFN-induced double stranded breaks are lethal to the cell and are therefore repaired by either of two mechanisms by the endogenous cell machinery; primarily by non-homologous end joining (NHEJ) and at a lower frequency by HR. NHEJ is a mutagenic process resulting by the simple ligation of the DSB, inevitably introducing insertions/deletions (indels) in the sequence and disrupting the function of the gene. Assuming the availability of an unaffected allele, homology-directed repair (HDR) takes place correcting the DSB and hence the functionality of the gene. Induction of a DSB by ZFNs has been reported to significantly increase the frequency of HDR (Moehle et al., 2007) and occurs preferentially during the S/G2 phase (Genovese et al., 2014). This process has been harnessed predominantly for the repair of point mutations but also for the site-directed integration of therapeutic genes by the provision of a recombinant donor template sequence bearing locus-specific homology arms **(Figure 1.10)**.

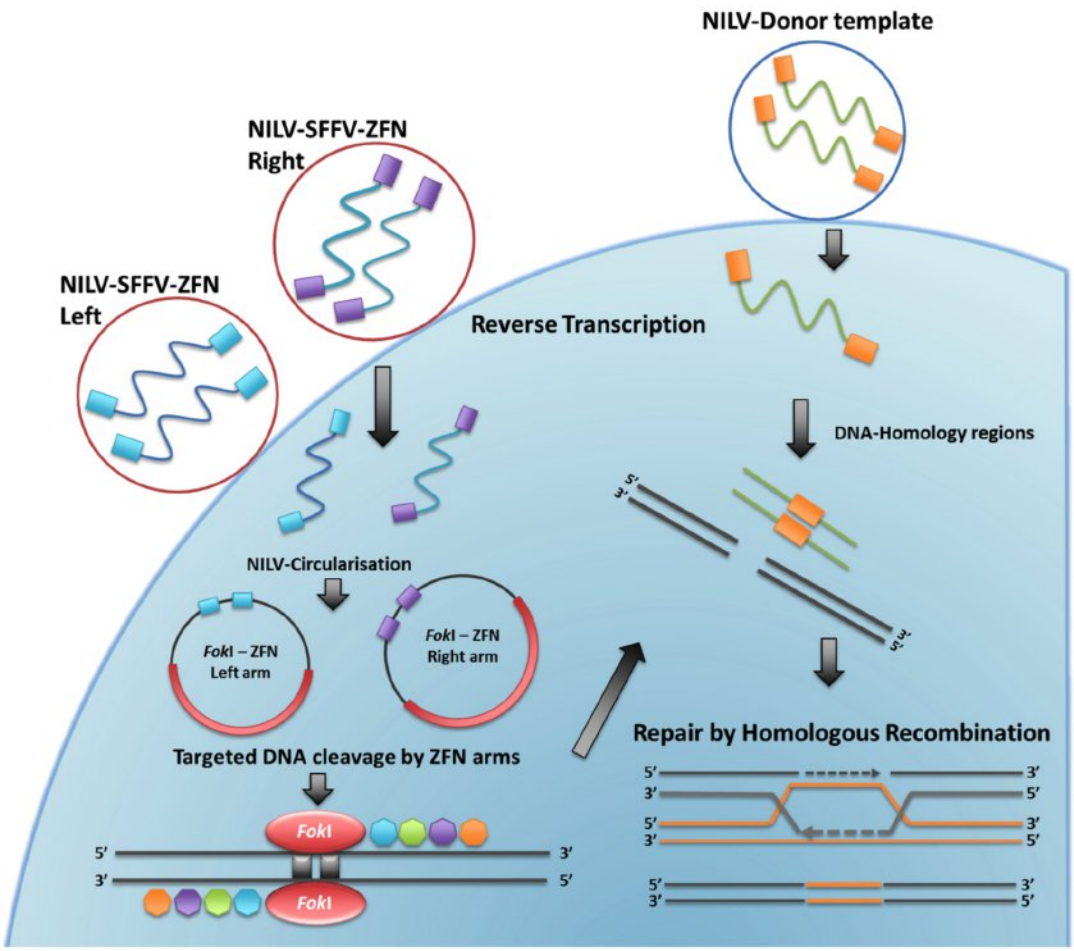

Figure 1.10 Homologous directed repair after delivery of donor template to ZFN treated mammalian cells.

Co-delivery of three non-integrating lentiviral vectors (NILVs), two of which encode the left and right portion of the zinc-finger FokI complex under the control of a spleen focus-forming virus (SFFV) promoter and a third one carrying a dsDNA sequence to be used as a donor template. After viral entry into the cell and uncoating ZFNs and donor template are reverse transcribed to cDNA which in the case of the ZFNs sequence will be translated into active ZFNs which locate the target site and cleave genomic DNA upon heterodimerisation of their FokI portions. The cell will repair the double-stranded break (DSB) predominantly by non-homologous end joining (NHEJ) but upon availability of template sequence it will stimulate the homologous recombination (HR) pathway and seal the break via homologous directed repair (HDR).

1.10.3 ZFNs and their use in the clinic

The potential of ZFN-induced genome engineering has gained momentum over the past decade and has been demonstrated in a range of model organisms, namely plants, insects, roundworms and humans (Urnov et al., 2010). Additionally, both *ex vivo* and *in vivo* genome editing tactics by the delivery of ZFNs have been reported as a treatment option against haemophilia B in mice and HIV in humans (Tebas et al., 2014, Li et al., 2011). The haemophilia study involved the *in*

vivo delivery of ZFNs targeting intron 1 of human factor IX gene via an AAV8 vector accompanied by a donor vector to stimulate HDR in a humanised mouse model for haemophilia B. The authors successfully demonstrated that at week 10, a population of cells in the range of 1-3% had undergone HDR and the circulating levels of human factor IX were directly correlated averaging around 2-3% (Li et al., 2011).

Genome editing tools have made a substantial breakthrough in search of a treatment for HIV-1 with clinical trials led by Sangamo Biosciences currently underway (NCT00842634 and NCT02388594). The miraculous clearance of the viral load in the HIV-positive "Berlin patient" who underwent allogeneic hematopoietic stem and progenitor cell (HSPC) transplantation from a donor homozygous for the *CCR5Δ32* mutation (Hutter et al., 2009, Hutter and Thiel, 2011) has propelled research forward in generating targeted *CCR5* gene knockout cells, a key co-receptor for CCR5 tropic HIV-1 entry into T-cells. A chimeric adenoviral vector Ad5/F35, with selective tropism to cells of the haematopoietic lineage, expressing ZFNs targeting a coding region upstream of the known *CCR5Δ32* mutation was established and employed for the modification of primary CD4(+) T cells (Maier et al., 2013, Perez et al., 2008). Preclinical studies in a NOD/Shi-scid/IL-2Rγ^{null} (NSG) mouse model of HIV-1 infection showed the efficient reduction of HIV-1 viral load after engraftment with the ZFN-modified CD4(+) T cells (Perez et al., 2008). A follow-up study revealed the progression of the vector to clinical scale for the *ex vivo* stable modification of autologous primary human T cells in a cohort of twelve patients with no adverse effects reported (NCT00842634) (Perez et al., 2008). Parallel studies by Sangamo BioSciences are now entering the phase II clinical trial stages (NCT01252641 and NCT01044654). The ZFN construct used by Perez *et al*. and Maier *et al.* is also being tested in parallel for delivery to CD34+ HPSCs by nucleofection aiming to overcome potential host immunogenic responses associated with adenoviral vectors, with results showing high levels of *CCR5* disruption when transplanted into NSG mice (Holt et al., 2010).

1.10.4 ZFNs for the in vitro modelling and treatment of genetic diseases

ZFNs have also been employed for the correction of a number of diseases in a preclinical *in vitro* setting with measurable success. Some of these studies have included work on X-linked severe combined immunodeficiency disorder (X-SCID) by plasmid delivery of IL2Rγ specific ZFNs (Urnov et al., 2005) and improving T-cell immunotherapy by the targeted knockout of the endogenous αβ T-cell receptor (TCR) using ZFNs delivered by either the *Sleeping Beauty* (SB) transposon system (Torikai et al., 2012) or by NILV (Provasi et al., 2012) and subsequent expression of tumour specific TCRs for the development of an allogeneic adoptive T cell therapy.

More recently, there has been a move towards the correction of patient-derived iPSCs as a regenerative medicine approach, for their obvious advantages of unlimited proliferation, multilineage differentiation and potential for autologous transplantation. Their use has been reported in sickle cell anaemia with plasmid-mediated ZFN transfer against mutated β-globin alleles (Zou et al., 2011a, Sebastiano et al., 2011); α_1-antitrypsin deficiency by the *PiggyBac* delivery of ZFNs and donor for the biallelic correction of the A1AT gene and subsequent differentiation into liver cells (Yusa et al., 2011); and X-CGD via NILV-ZFN site-specific HR targeting of a $gp91^{phox}$ minigene to the "safe harbour" AAVS1 locus (Zou et al., 2011b). Advances have also been made in the modelling and understanding of mutations associated with Down's syndrome (Jiang et al., 2013) and Parkinson's disease (Soldner et al., 2011) by ZFN-mediated gene knockout.

1.10.5 Modes of delivery of ZFN to mammalian cells

1.10.5.1 DNA plasmid/mRNA

As seen from the studies mentioned previously, the route and mode of ZFN delivery has been extensively variable. Therefore, one of the key areas of interest in the field still remains the search for an improved method of delivery (Genovese et al., 2014). Typically the custom ZFNs are delivered to target cells by transient cationic lipid-based transfection or electroporation in the form of plasmid DNA or mRNA, with the advantage of the latter being rapid expression and prevention of undesirable nuclease integration. The permissiveness of certain cell types to such delivery methods, which are also often associated with high toxicity in primary cell types, added to the prolonged and uncontrolled cDNA expression leading to potential off-target cutting further illuminates the caveats of this approach. A shift has been made towards the use of viral vectors as an alternative delivery approach (Lombardo et al., 2007).

1.10.5.2 Adeno-Associated Viruses (AAV)

Viral vectors based on both adenoviruses and AAV, commonly used in gene therapy trials, have recently made an appearance in the gene editing field. The transgene capacity of up to 4.2 kb in AAV vectors is sufficient for the packaging of both ZFN monomers while large enough to also accommodate a donor construct, making it an attractive delivery platform for both *in vitro* and *in vivo* application. Ellis *et al.* proved the efficiency of such a system by incorporating a donor substrate alongside both ZFN arms separated by a 2A cleavage domain in a recombinant AAV (rAAV) type 6 serotype. The obvious advantage is the minimisation of delivered viral particles to the cell which have been shown to cause significant toxicity. Additionally, delivery of all

three constructs as a single vector was demonstrated to substantially increase gene targeting and correction efficiency, most likely due to the minimisation of vector transduction competition (Ellis et al., 2013).

1.10.5.3 Non-integrating Lentiviral Vectors (NILV)

NILVs based on HIV-1 are favourable as a ZFN delivery platform due to their capacity to induce a permanent and heritable genome modification following HDR. Contrary to the widely used integrating lentiviral system, NILVs remain as linear or circular DNA strands in an episomal state; fundamental for the "hit-and-run" effect desired from ZFNs. That enables them to circumvent the potentially deleterious clinical consequences of transgene integration into the host chromosome. Although these vectors have been designed to entirely ablate host genomic integration, reports in the literature have revealed a low frequency of illegitimate background integrase-independent insertions (Banasik and McCray, 2010), which could potentially compromise their use in the clinic. Although the levels are practically negligible, it has been suggested that they can be further reduced by the deletion of the cPPT in the vector (Kantor et al., 2011). For successful targeted sequence cleavage both ZFN monomers have to be delivered in equal proportion. As with AAV, various groups have attempted the delivery of both ZFNs in a single vector with relative success (Joglekar et al., 2013, Yi et al., 2014, Lombardo et al., 2007). However, the process of reverse transcription resulted in recombination events in tandem repeat regions of the closely positioned ZFN monomers leading to significantly diminished nuclease activity. Codon optimisation has now been employed to address the issue (Joglekar et al., 2013).

As previously noted, the ability to target primary cells has been the main limitation of plasmid transfection. Pseudotyping, thereby offering an interchangeable viral envelope to the vector, which can confer cell specific tropism, is a powerful tool unique to this platform. Typically VSV-G is used with the added advantage of its broad host cell tropism and stability during viral concentration steps by ultracentrifugation, but others such as the native HIV-1 envelope has been used for the efficient and selective transduction of unstimulated CD4+T cells and subsequent disruption of *CCR5* (Yi et al., 2014). NILVs can therefore be used as a delivery vehicle for practically any cell type of any lineage, both dividing and non-dividing. The drawbacks of using viral vectors predominantly revolve around their challenging manipulation and complex production, although they still remain a safe and highly efficient mode of delivery to otherwise non-permissive cell types.

1.10.5.4 ZFN proteins

The most recent development aiming to enhance nuclease delivery has been the use of purified recombinant ZFN proteins which can easily permeate cell membranes due to the ZFP domains carrying a net positive charge, and induce targeted gene disruption. The main limitations associated with internalisation of highly charged proteins are the requirement of a relatively high starting protein concentration and that entry into the cell is likely to occur in a non-specific manner. Fusing targeting ligands such as transferrin to the ZFN proteins has been shown to significantly enhance the targeted delivery of the nucleases and at lower concentrations (Chen et al., 2013). Added benefits include their almost immediate effect, yet short half-life of approximately 4 hr within the host cell, thereby reducing potential integrations and off-target cleavage. Additionally, this method overcomes cell-type dependency and proves a safer option as the host cells are not exposed to any foreign genetic material. Encouraging data has been published on the delivery of ZFN in protein form for the targeting of the *CCR5* gene (Gaj et al., 2012).

1.10.6 Emergence of newer systems

A plethora of gene editing tools have been developed since the realisation of ZFNs' potential, namely meganucleases, TALENs and clustered regularly interspaced short palindromic repeats (CRISPR). All function in a similar manner comprising of a DNA binding motif associated with a nuclease. Each comes with their advantages and limitations, as do ZFNs, but none of the systems has been coined as the definitive one yet. The major drawbacks with ZFNs have been their challenging assembly in a lab setting, the stringency in the selection of compatible ZFP modules with a suggested functional obtainable ZFN pair per ~100 bp DNA sequence (Kim et al., 2009) and their reported off-target cleavage (Gabriel et al., 2011). In an attempt to combat off-target effects, ZFN nickases have been generated carrying a mutation in one of the *Fok*I subunits only allowing for a single-strand break (SSB) to occur therefore increasing their safety profile although inevitably lowering the efficiency of HDR (Kim et al., 2012, Wang et al., 2012, Ramirez et al., 2012).

TALENs derived from the *Xanthomonas* spp. bacterium similar to ZFNs can bind and cleave genomic sequence via a *Fok*I endonuclease domain coupled at their carboxyl termini responsible for DSB generation. Each DNA binding domain is composed of 33 - 35 tandem amino acid repeats forming the scaffold with amino acid repeats at positions 12 and 13 known as repeat variable diresidues (RVDs) governing the single nucleotide specificity (Kim and Kim, 2014). Approximately 20 such binding domains are required for targeted recognition of

genomic sequence. The off-target effects tend to be much lower with TALENs, primarily due to their design being such that each TALEN is specific for one nucleotide as opposed to the ZFN specific triplet. This therefore allows for a greater design flexibility and can be directed towards anywhere within the genome thereby permitting the selection of unique target sequences. Furthermore, in comparison to ZFNs they are slightly less challenging in terms of production within the lab and can be designed at a lower cost. Their overall size though, approximately three times that of ZFNs, and their highly repetitive nature restricts their delivery and can lead to rearrangement events when cloned into a NILV platform due to reverse transcriptase mediated template switching (Holkers et al., 2013).

CRISPRs make up a novel group of genome editing tools belonging to a separate family to ZFNs and TALENs. Originating from bacteria, the CRISPR system is directly involved in the acquired immunity against pathogenic viral and plasmid DNA by fragmenting it and incorporating it in the form of "spacers" into short genomic loci. Of the three CRISPR/Cas systems, type II is the most widely used for genome editing and functions by processing the DNA fragments into short CRISPR RNA (crRNA) which act as guides for the targeting of specific sequences and anneal to transactivating crRNAs (tracrRNA) which in turn sequester Cas proteins mediating DNA cleavage (Jinek et al., 2012). A requirement for the recruitment of Cas9 is a conserved dinucleotide-containing protospacer adjacent motif (PAM) sequence, typically (NGG) for *Streptococcus pyogenes* derived Cas9, upstream of the crRNA-binding region. Synthetic crRNA/tracrRNA combined structures have been designed and coined short-guide RNA (sgRNA). These typically 20 bp sequences can be designed against virtually any portion of the genome with target sites averaging one per 8 bp accounting for a PAM sequence availability, and delivered in conjunction with Cas9 as a single plasmid or vector (Jinek et al., 2012). As with ZFNs and TALENs they can induce a DSB at the target site, which can be used for disease modelling by introduction of indels through NHEJ, or HDR upon the provision of a donor template sequence.

1.11 Project aims

Although several therapeutic approaches are currently in development to combat RDEB, there is no successful treatment that can provide a cure for the affected individuals. This study proposes a method for genetically correcting patients' cells to restore the functionality of the DEJ. Possible target cells include keratinocytes, fibroblasts, mesenchymal cells and bone marrow stem cells. I plan to use a state-of-the-art lentiviral vector as a delivery system, to introduce a full-length codon optimised *COL7A1* gene into autologous RDEB patient cells the hypothesis being that *ex vivo* gene corrected cells can then be re-infused into the patient either by skin grafting, intradermal injection or systemically. Using a 3rd generation *COL7A1* expressing lentiviral vector, I aim to assess its efficiency in restoring C7 expression and function in both RDEB primary keratinocyte and fibroblast primary cells and cell lines initially *in vitro* **(Figure 1.11)**. To obtain an accurate estimation of the corrective potential of the vector, *in vivo* studies will be carried out which entails the development of a suitable RDEB animal model.

A secondary approach I wish to investigate alongside gene addition is the use of a targeted gene editing strategy to help overcome limitations associated with the large size of the transgene approaching the upper limit of vector capacity. By designing highly specific nucleases against a distinct region of a gene permits its targeted knockout by NHEJ or correction of the endogenous sequence by HDR. For this approach I aim to use ZFNs as the genome-editing tool of choice delivered via a NILV system thereby improving efficiency of delivery of genetic material to primary skin cells otherwise non-permissible to normal transfection. Harnessing both processes of the endogenous cell repair machinery following ZFN-mediated DSBs, will primarily allow for the *in vitro* modelling of RDEB through generation of monoallelic and biallelic knockouts, while further enable the quantification of HDR upon provision of an exogenous donor repair template. To our knowledge this is the first study to assess the disruption and subsequent restoration of the human *COL7A1* gene using ZFN gene-editing machinery. Besides providing us with a repeatable method of obtaining an unlimited supply of RDEB cell lines with specific mutations, it could potentially result in a personalised clinical treatment by autologous, site-specific correction of a wide range of missense, nonsense and splice site mutations via healthy donor template delivery **(Figure 1.11)**.

Hypothesis

i) Delivery of a full length *COL7A1* transgene to primary RDEB cells by lentiviral vector will restore C7 protein expression and reinstate functionality to the diseased cells.
ii) Grafting lentivirally corrected primary RDEB cells into a human:murine chimeric skin graft model will lead to AF formation at the DEJ and ameliorate the disease phenotype.
iii) *In vitro* RDEB cell models can be generated by the NHEJ activity of ZFNs targeting *COL7A1* delivered to keratinocytes by NILVs. Co-delivery of a homologous donor template can mediate site-specific repair of genomic disruptions by HDR.

Objectives

i) Develop a gene addition strategy based on a lentiviral vector platform for the restoration of C7 expression and function to autologous human RDEB patient cells.
ii) Develop a human:murine chimeric RDEB skin graft model to investigate the *in vivo* restorative potential of *ex vivo* lentivirally corrected RDEB cells.
iii) Design a state-of-the-art gene editing strategy for the site-specific manipulation of the endogenous *COL7A1* genomic sequence aiming to generate targeted DSBs and consequently correction of individual patient mutations.

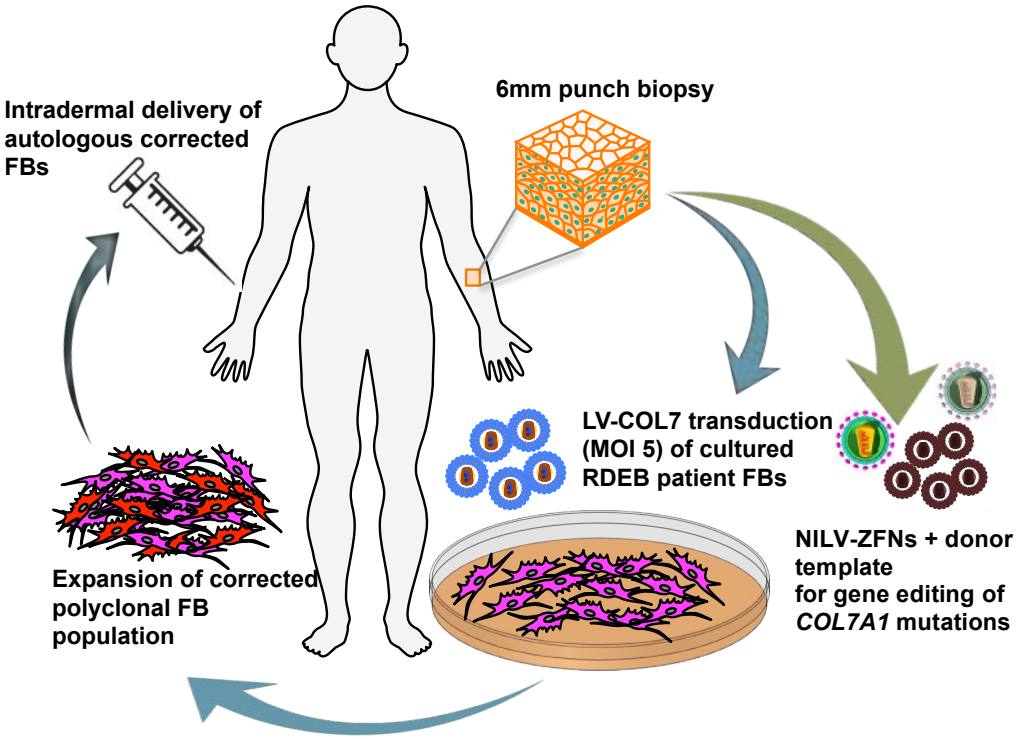

Figure 1.11 Gene modification strategies for the correction of autologous RDEB cells.
Autologous RDEB patient keratinocytes or fibroblasts isolated from 6 mm biopsy for correction by: i) gene addition using LV-COL7 vector for delivery of a full-length WT *COL7A1* transgene or ii) by targeted gene editing of *COL7A1* mutations using site-specific nucleases co-delivered with a homologous donor repair template.

Chapter 2 Materials and Methods

2.1 Materials

2.1.1 Reagents

DNA

10X TAE: 400 mM Tris-acetate and 10 mM EDTA	(Thermofisher, Waltham, MA USA)
1Kb Plus DNA ladder	(Thermofisher)
Branched PEI - Polyethylenimine (PEI)	(Sigma-Aldrich, Dorset, UK)
Deoxynucleotide (dNTPs)	(NEB, Ipswich, MA, USA)
Gel Loading Dye, Purple (6X)	(NEB)
Lipofectamine® 2000	(Thermofisher)
Platinum® Quantitative PCR SuperMix-UDG with ROX	(Thermofisher)
Sodium acetate (3M) pH 5.5	(Sigma-Aldrich)
Taq DNA Polymerase	(Roche, Welwyn Garden City, UK)
UtlraPure™ Agarose	(Thermofisher)

Protein analysis

Amersham Full-Range Rainbow Markers	(GE LifeSciences, Buckinghamshire, UK)
Amersham Hybond-P PVDF Membrane	(GE LifeSciences)
Ammonium persulfate (APS)	(Sigma-Aldrich)
cOmplete Protease Inhibitor Cocktail Tablets	(Roche)
Dithiothreitol (DTT)	(Thermofisher)
Phenylmethanesulfonyl fluoride (PMSF)	(Sigma-Aldrich)
Ponceau S Solution	(Santa Cruz, Dallas, TX, USA)
Sodium Dodecyl Sulphate (SDS)	(Sigma-Aldrich)
Triton™ X-100	(Sigma-Aldrich)
Trizma Base	(Sigma-Aldrich)
Whatman 3MM chromatography paper	(Sigma-Aldrich)
30% Acrylamide/Bis (37.5:1) solution	(Bio-Rad, Hertfordshire, UK)

Cell culture

Ascorbic acid	(Sigma-Aldrich)
Dimethyl sulfoxide (DMSO)	(Sigma-Aldrich)
Dulbeco's Modified Eagle Medium (DMEM)	(Thermofisher)
DMEM: Nutrient Mixture F-12 (DMEM/F12)	(Thermofisher)

Foetal Calf Serum (FCS)	(Seralab, West Sussex, UK)
Mitomycin C	(Sigma-Aldrich)
NB Collagenase and Neutral Protease	(SERVA, Heidelberg, Germany)
Opti-MEM®	(Thermofisher)
Penicillin Streptomycin (Pen Strep)	(Thermofisher)
Phosphate-buffered saline (PBS)	(Thermofisher)
Trypan Blue solution 0.4%	(Thermofisher)
Trypsin-EDTA (0.05%), phenol red	(Thermofisher)
Trypsin-EDTA (0.25%), phenol red	(Thermofisher)

Mouse studies / Immunofluorescence

Antifade 1,4-diazabicyclo-[2.2.2]octane (DABCO)	(Sigma-Aldrich)
Antisedan 5 mg/ml	(Pfizer, Surrey, UK)
DAPI 5mg/ml	(Sigma-Aldrich)
Dormitor 1 mg/ml	(Olenco)
DPX mountant	(Sigma-Aldrich)
Eosin Y 1% solution	(Sigma-Aldrich)
Haematoxylin Solution, Gill No.1	(Sigma-Aldrich)
Mowiol 4-88	(Merk Millipore, Hertfordshire, UK)
Paraformaldehyde 16% Solution	(VWR, Leicestershire, UK)
Pig plasma in Sodium Citrate unfiltered, 500ml	(Seralab)
ProLong Gold Antifade Mountant	(Thermofisher)
Thrombin from human plasma	(Sigma-Aldrich)
Tissue-Tek® O.C.T.™ Compound	(Sakura, Alphen aan den Rijn The Netherlands)
Vetalar V 100 mg/ml	(Pfizer)
Vetergesic 0.3 mg/ml	(Alstoe, York, UK)

Bacterial Culture

Ampicillin	(Sigma-Aldrich)
JM109 Competent Cells	(Promega, Manheim, Germany)
Kanamycin	(Sigma-Aldrich)
LB medium (capsules)	(MP Bio, Santa Ana, CA, USA)
LB-Agar Medium (capsules)	(MP Bio)
One shot Stbl3 Chemically Competent *E. coli*	(Thermofisher)
S.O.C. Medium	(Q-BioGene, Carlsbad, CA, USA)

2.1.3 Kits

BigDye® Terminator V3.1 Cycle Sequencing Kit	(Thermofisher)
Bio-Rad protein assay	(Bio-Rad)
ECLplus™	(GE Healthcare, Hatfield, UK)
Mix-n-Stain™	(Biotium, Cambridge Biosciences, Cambridge, UK)
Oris™ Cell Migration Assay	(Platypus Technologies, Madison WI, USA)
ProteoExtract®	(Merk Millipore)
QIAamp DNA Mini Kit	(QIAGEN, Manchester, UK)
QIAprep Spin Miniprep; Maxiprep; Gigaprep Kit	(QIAGEN)
QIAquick Gel Extraction Kit	(QIAGEN)
QIAquick PCR Purification Kit	(QIAGEN)
QuikChange II XL Site-Directed Mutagenesis Kit	(Agilent Technologies, Cheshire, UK)
Surveyor Mutation Detection assay	(Transgenomic, Omaha, NE, USA)
pCR®4-TOPO®	(Thermofisher)
ZR-96 Quick-gDNA™	(Zymo Research, Cambridge Biosciences, Cambridge, UK)

2.1.4 Buffers

0.5M Tris/HCL buffer, pH 6.8: 6.07 g Trizma Base (MW 121.44) was dissolved in 80 ml dH_2O and adjusted to pH 8.8 with 5 N HCL (~2 ml) and made up to 100 ml. The buffer was stored at RT.

1.5M Tris/HCL buffer, pH 8.8: 18.21 g Trizma Base (MW 121.44) was dissolved in 80 ml dH_2O and adjusted to pH 8.8 with 5 N HCL (~3 ml) and made up to 100 ml. The buffer was stored at RT.

10% ammonium persulfate (APS): 0.1 g APS was dissolved in 1 ml dH_2O and kept for up to a week at RT.

10% sodium dodecyl sulphate (SDS): 1 g SDS was dissolved in 100 ml dH_2O. The buffer was stored at RT.

10X running buffer: 0.25 M Tris, (MW 121.44) 30.3 g; 1.92 M Glycine, (MW 75.07) 144 g; 1% SDS, 10 g. Make up to 1 litre with dH_2O. Diluted with dH_2O to 1X for use. The buffer was stored at RT.

10X wash buffer: 0.5% Tween-20 in 10X PBS. Diluted with dH_2O to 1X for use. The buffer was stored at RT.

5X Sample buffer: 10% SDS, 1g; 30% Glycerol, 3 ml; 10% β-mercaptoethanol, 1 ml; 0.001% bromophenol blue, 1 mg. Made up to 10 ml with 0.5M Tris/HCL, pH 6.8, aliquoted and stored at -20°C.

Blocking solution: 5% dried skimmed milk (Marvel) in 1X wash buffer.

Diluent 1: 3% BSA in 1X wash buffer.

Diluent 2: 3% dried skimmed milk (Marvel) in 1X wash buffer

Eosin working solution: 1 part of eosin stock solution + 3 parts of 80% ethanol + 0.5 ml glacial acetic acid was mixed in 100 ml of dH_2O.

LB medium: 20 capsules per 1 L of dH_2O, autoclaved at 121°C for 15 min. Typical content per 1 L: 10 g Tryptone, 5 g Yeast Extract, 10 g NaCl.

LB-agar medium: 40 capsules per 1 L of dH_2O, autoclaved at 121°C for 15 min. Typical content per 1 L: 10 g Tryptone, 5 g Yeast Extract, 10 g NaCl, 15 g Agar.

Lysis buffer base: 50 mM Tris/HCL, pH 8.0, (MW 121.4); 150 mM NaCl, (MW 58.44), 5 mM EDTA (Ethylenediaminetetraacetic acid, MW 380.2)

Lysis buffer: 50 mM Tris/HCL, pH 8.0, (MW 121.4); 150 mM NaCl, (MW 58.44), 5 mM EDTA (Ethylenediaminetetraacetic acid, MW 380.2), 1:25 dilution of stock cocktail protease inhibitor (cOmplete cocktail tablets); 1 mM PMSF

Mowiol mountant: 6 ml glycerol and 2.4 g (10%) of Mowiol 4-88 and 6 ml water were combined and mixed in a 50 ml falcon tube by vortexing and placed on a roller for 2 hrs. 12 ml of 200 mM Tris-HCL at pH 8.5, was added to the falcon tube and was incubated at 50°C for ~3 hrs with occasional mixing. The solution was passed through a 0.45 μm sterile filter and stored in 2 ml aliquots at -20°C. Prior to use, antifade 1,4-diazabicyclo-[2.2.2]octane at 2.5% (w/v) concentration (DABCO) was added to the Mowiol mountant and allowed to dissolve for 30 min at RT to prevent photobleaching. Mowiol with antifade was kept at 4°C for up to a week.

PEI transfection reagent: For preparation of 10 mM PEI, 50 ml of PBS was adjusted to pH 4.5 using HCL. 10.3 g of polyethylenimine was weighed into a 50 ml falcon tube and 31 ml of PBS pH 4.5 was added. The solution was placed in a 75°C water bath and vortexed every 10 min until completely dissolved. The PEI was aliquoted and stored at -80°C.

Rainbow ECL full-range Molecular Weight Markers: Stock Rainbow molecular weight markers were aliquoted at 10 μl per vial and stored at -20°C.

Separating gel: (all volumes calculated for production of x2 6% 10 ml gels) dH_20, 5.35 ml; 1.5M Tris/HCL pH 8.8, 2.5 ml; 30% Acrylamide/Bis, 2 ml; 10% SDS, 0.1 ml; 10% APS, 0.075 ml; TEMED, 0.0075 ml.

S.O.C (Super Optimal Broth): liquid medium was prepared by adding 31 g of powder per 1 L of dH_2O and autoclaved at 121°C for 15 min. The final composition per L: 20 g Tryptone, 5 g Yeast Extract, 0.5 g NaCl, 5 g $MgSO_4.7H_2O$, 20 mM Glucose.

Stacking gel: dH_20, 3.05 ml; 0.5M Tris/HCL pH 6.8, 1.25 ml; 30% Acrylamide/Bis, 0.65 ml; 10% SDS, 0.05 ml; 10% APS, 0.0375 ml; TEMED, 0.0075 ml.

Stripping buffer: 2% SDS and 100 mM of β-mercaptoethanol in 62.6 mM Tris-HCL, pH 6.7 (stock β-mercaptoethanol at 14.3 M, add 70 µl of stock β-mercaptoethanol into 10 ml stripping buffer base).

Transfer buffer: 0.025 M Trizma Base (MW 1221.33), 6 g; 0.019M Glycine (MW 75.07), 29.6 g; 20% methanol, 400 ml. Dissolve in 2 L dH_2O

Trituration buffer: (For 700ml) 100 mM $CaCl_2$ (10.29 g) + 70 mM $MgCl_26H20$ (9.96 g) + 40 mM Sodium Acetate anhydrous (2.3 g). The pH was adjusted to pH 5.5 and the buffer was passed through a 0.45 µm sterile filter.

2.1.5 Culture media

Complete media (DMEM/10% FCS): DMEM; 10% FCS; 1% Pen/Strep.

Keratinocyte media: 3 parts of DMEM medium to 1 part of HAM/F12 medium; 10% FCS; 1% Pen/Strep.

Complete keratinocyte media: 3 parts of DMEM medium to 1 part of HAM/F12 medium; 10% FCS; 1% Pen/Strep; 1% RM+.

RM+: Hydrocortisone 0.4 g/ml; Choleratoxin 10^{-10} M; Transferrin 5 g/ml; Lyothyronine $2x10^{-11}$ M; Adenine $1.8x10^{-4}$ M; Insulin 5 g/ml; EGF 10 ng/ml.

N.B. Lyothyronine was initially dissolved in 1 part of HCL and 2 parts of ethanol; Adenine was dissolved in NaOH pH 9; Insulin was dissolved in 0.05 M HCL.

2.1.6 Antibodies

Table 2.1 List of primary antibodies used in this study.

Antibodies	Target/ lineage specificity	Dilution	Supplier
Keratin 10	Suprabasal keratinocytes	1:10	In-house
Desmoglein I	Cell-cell junctions Human specific	1:100	Fitzgerald Industries
mAb-C7-LH7.2	C7 protein Human specific	1:500	Sigma-Aldrich
mAb-C7-LH7.2	C7 protein Human specific	1:25 Flow	Santa Cruz
Calbio-C7-pAb	C7 protein Human/Mouse specific	1:200 IF 1:500 WB	Calbiochem
Chen-C7	C7 protein Human/Mouse specific	1:2,000 IF 1:2,500 WB	Prof. M. Chen
Purified C7-pAb	C7 protein Human specific	1:1,250	Abnova
C7-1002.3	C7 protein Human specific	1:100	Accurate Chemical
C7-C12207	C7 protein Human/Mouse specific	1:200	Assay Biotechnologies
C7-SAB4500390	C7 protein Human/Mouse specific	1:200	Sigma-Aldrich
C7-sc20774	C7 protein Human/Mouse specific	1:100	Santa Cruz
C7-sc8928	C7 protein Human/Mouse specific	1:100	Santa Cruz
Keratin 14	Basal and suprabasal Human/Mouse keratinocytes	1:1,000	Covance
MTCO2	Mitochondrial Complex IV subunit II Human specific	1:250	Abcam
Involucrin	Suprabasal keratinocytes	1:15,000	Sigma-Aldrich
Vinculin	Loading control	1:250,000	Sigma-Aldrich

Table 2.2 List of secondary antibodies used in this study.

Antibodies	Conjugate	Dilution	Supplier
Goat Anti-Mouse (IgG)	AlexaFluor 488	1:500	Invitrogen
Goat Anti-Mouse (IgG)	AlexaFluor 568	1:500	Invitrogen
Goat Anti-Rabbit (IgG)	Alexa Fluor 568	1:500	Invitrogen
Anti-Mouse (IgG)	Biotin	1:100	Sigma-Aldrich
Streptavidin	AlexaFluor 488	1:200	Thermo Fisher
Anti-Mouse (IgG)	HRP	1:3,000	GE Healthcare
Anti-Rabbit RG-96 IgG	HRP	1:7,000	Sigma-Aldrich
Goat Anti-Mouse	Cy3	1:500	Abcam
Goat Anti-Rabbit	Cy3	1:500	Abcam

2.1.7 Mammalian and murine cells

Table 2.3 List of WT mammalian and murine cells.

Cell ID	Cell Type	Immortalisation
HEK-293T	Human Embryonic Kidney Cell (Line)	SV40 large T antigen
NTERT	Human Keratinocyte (Line)	Human telomerase reverse transcriptase (hTERT)
HaCaT	Human Keratinocyte (Line)	Spontaneously transformed
NIKS	Human Keratinocyte (Line)	Spontaneously transformed
WT KC	Human Keratinocyte (Primary)	-
WT FB	Human Fibroblast (Primary)	-
3T3-SWISS	Mouse Fibroblast (Line)	Spontaneously transformed

Table 2.4 List of RDEB human patient and murine model cells.

Patient ID	Mutation c.DNA level	Mutation Protein level	Exon/ Intron	Type of Variant	Variant effect	EB type / subtype
RDEB EBKC cell line	(+/-) c.1732C>T	p.Arg578X (p.R578X)	13	Base substitution	nonsense (stop codon)	RDEB
	(+/-) c.2716C>T	p.Gln906X (p.Q906X)	21	Base substitution	nonsense (stop codon)	RDEB
RDEB patient (CK)	(+/+) c.425A>G	p.Lys142Arg (p.K142R)	3	Base substitution	missense, splicing change	RDEB
RDEB patient (EB8)	(+/-) c.1732C>T	p.Arg578X (p.R578X)	13	Base substitution	nonsense (stop codon)	RDEB
	(+/-) c.2710+2T>C (IVS20+2T>C)	-	Intron 20	Base substitution	splicing change	NHS-RDEB
RDEB patient (BT)	(+/-) c.5798G>A	p.Arg1933Gln (p.R1933G)	70	Base substitution	missense or in-frame deletion	RDEB
	(+/-) c.8440C>T	p.Arg2814X (p.R2814X)	114	Base substitution	nonsense (stop codon)	RDEB-O

2.1.8 Mouse Strains

NMRI-Foxn1^{nu} were obtained from Charles River.

NSG, or NOD scid gamma (NOD.Cg-Prkdc^{scid} Il2rg^{tm1Wjl}/SzJ) were obtained from the Institute of Child Health, UCL.

2.1.9 Primers

Table 2.5 List of PCR, qPCR and SDM primers used.

Primer name	Primer sequence
HIV packaging signal Psi forward	CAGGACTCGGCTTGCTGAAG
HIV packaging signal Psi reverse	TCCCCCGCTTAATACTGACG
HIV packaging signal Psi probe	FAM-CGCACGGCAAGAGGCGAGG-TAMRA
Human albumin forward	GCTGCTATCTCTTGTGGGCTGT
Human albumin reverse	ACTCATGGGAGCTGCTGGTTC
Human albumin probe	VIC- CCTGTCATGCCCACACAAATCTCTCC-TAMRA
SDM ex4 COL7A1 template primer Left forward	GCACCTGTCCCAGGTGTGTATTCTGATCACAG ACGGG
SDM ex4 COL7A1 template primer Left reverse	CCCGTCTGTGATCAGAATACACACCTGGGACA GGTGC
SDM ex4 COL7A1 template primer Right forward	TGTGTATTCTGATCACAGATGGCAAATCGCAG GACCTGGTGGACACAG
SDM ex4 COL7A1 template primer Right reverse	CTGTGTCCACCAGGTCCTGCGATTTGCCATCTG TGATCAGAATACACA
M13 forward	GTAAAACGACGGCCAG
M13 reverse	CAGGAAACAGCTATGAC
LV-ZFN arm forward	GACCCTGCGCCTTATTTG
LV-ZFN arm reverse	CCACATAGCGTAAAAGGAGC
COL7A1 ex4 template forward	AATTCTCCATGTGGCTGACC
COL7A1 ex4 template forward	AATTCTCCATGTGGCTGACC

2.1.10 Parental plasmids

pMD2.G: CMV driven Vesicular Stomatitis Virus envelope glycoprotein (VSV-G) expressing plasmid (Addgene).

pCMVR8.74: 2nd generation gag-pol-tat-rev expressing lentiviral packaging plasmid driven by CMV promoter (Addgene).

pCMV-dR8.74 D64V: 2nd generation integrase mutant gag-pol-tat-rev expressing lentiviral packaging plasmid driven by CMV promoter for generation of non-integrating lentiviral vectors (NILV) (Addgene).

pRSV-Rev: 3rd generation REV expressing lentiviral plasmid driven by RSV promoter (Addgene). Requires co-transfection with pMDLg/pRRE.

pMDLg/pRRE: 3rd generation gag-pol expressing lentiviral packaging plasmid driven by CMV promoter (Addgene). Requires co-transfection with pRSV-Rev.

pCCL-LV-SPINK5: 3rd generation HIV-1 SIN lentiviral transfer plasmid with SPINK5 transgene flanked by BamHI restriction enzyme recognition sites expressed from constitutive PGK promoter. Native HIV-1 U3 region in the 5' LTR replaced with Tat independent CMV promoter.

coCOL7A1: Codon optimised *COL7A1* cDNA for the removal of cryptic splice acceptor/donor sites, reduction of repetitive codon usage, addition of a Kozak consensus sequence for the initiation of translation and addition of flanking BamHI restriction enzyme recognition sites subcloned into cloning plasmid (GeneArt).

pRRL-PGK-GFP 3rd generation HIV-1 SIN lentiviral transfer plasmid with GFP transgene expressed from constitutive PGK promoter. Native HIV-1 U3 region in the 5' LTR replaced with Tat independent RSV promoter.

PZFN1: CompoZr™ Knockout Zinc Finger Nucleases targeting exon 4 of *COL7A1* left arm (Sigma-Aldrich)

PZFN2: CompoZr™ Knockout Zinc Finger Nucleases targeting exon 4 of *COL7A1* right arm (Sigma-Aldrich)

pHR'SIN.cPPT-SW: SIN 2nd generation lentiviral backbone including a MCS flanked by a SFFV promoter upstream and Woodchuck hepatitis virus post-transcriptional regulatory element (WPRE) downstream.

COL7A1 in2-ex7 donor template: A portion of the *COL7A1* cDNA sequence spanning intron 2 – exon 7 was synthesised including a 5' EcoRI and 3' XhoI restriction site. 2 base substitutions in intron 4 were introduced giving rise to a KpnI restriction digestion site to allow for distinction from endogenous *COL7A1* sequence. The sequence was synthesised and provided in a cloning vector by GeneArt.

2.1.11 Generated plasmids

pCCL-PGK-COL7A1: The pCCL-LV-COL7 3rd generation lentiviral vector with the U3 region in the 5' LTR replaced with a CMV promoter was generated by releasing the SPINK5 transgene from the parental pCCL-LV-SPINK5 promoter using BamHI restriction enzymes and retaining the PGK promoter and subcloning the codon optimised *COL7A1* transgene (GeneArt) with BamHI compatible ends.

NILV-ZFN left: Parental DNA plasmid PZFN1 was first digested with EcoRI and Klenow fragment to fill in 5' overhangs and create a blunt end and then with XhoI leaving a sticky end. The digested ZFN-FokI portion was gel extracted and purified. The parental pHR'SIN.cPPT-SW vector was linearised at the multiple cloning site with BamHI followed by 5' overhang filling using Klenow fragment and with XhoI leaving a compatible sticky end with the ZFN-FokI insert. Ligation was performed at a 1:3 backbone:insert ratio and colonies were verified by Sanger sequencing using LV-ZFN arm forward and reverse primers. (Provided by Dr. D. Almarza).

NILV-ZFN right: Performed as described with NILV-ZFN left but using PZFN1. Colonies were verified by Sanger sequencing using LV-ZFN arm forward and reverse primers. (Provided by Dr. D. Almarza).

NILV-OriginalTemp: Performed as described with NILV-ZFN left but using COL7A1 in2-ex7 donor template and subcloned into the modified pHR'SIN.cPPT-W vector lacking the SFFV promoter. Colonies were verified by Sanger sequencing using COL7A1 ex4 template forward and reverse primers. (Provided by Dr. D. Almarza).

NILV-SDMTemp: The NILV-OriginalTemp was modified by site directed mutagenesis for the introduction of 3 silent mutations in the left ZFN binding region using SDM ex4 COL7A1 template primer Left forward and reverse primers and an additional 4 silent mutations in the right ZFN binding region using SDM ex4 COL7A1 template primer Right forward and reverse primers to prevent unwanted template cleavage. Colonies were verified by Sanger sequencing using COL7A1 ex4 template forward and reverse primers.

2.1.12 E. coli bacterial competent cell strains

***Stbl3* genotype:**

F$^-$*mcr*B *mrrhsd*S20(r_B^-, m_B^-) *rec*A13 *sup*E44 *ara*-14 *gal*K2 *lac*Y1 *pro*A2 *rps*L20(Str^R)*xyl*-5 λ^- *leumtl*-1

JM109 genotype:

endA1, recA1, gyrA96, thi, hsdR17 (rk –, mk +), relA1, supE44, Δ(lac-proAB), [F´, traD36, proAB, laqIq ZΔM15]

2.2 Methods

2.2.1 Growth of E. coli bacterial cells

Escherichia coli (*E. coli*) competent *Stbl3* or *JM109* cells were grown in LB broth in a bacterial cell shaker set to 37°C and shaking at 250 rpm. *E. coli* cells transformed with plasmids containing an antibiotic resistance gene were cultured in LB broth containing either ampicillin (50 µg/ml) or kanamycin (100 µg/ml). *E. coli* colonies were selected by growing transformed competent cells on LB agar plates containing either ampicillin (50 µg/ml) or kanamycin (100 µg/ml) in a 37°C incubator. Transformed competent cells were stored in LB broth containing 15% (v/v) glycerol at -80°C.

2.2.2 Preparation of JM109 competent cells

A glycerol stock of JM109 cells was used to inoculate 10 ml LB broth and cultured in a bacterial shaker at 37°C, 250 rpm for 24 hrs. The culture was transferred to 500 ml LB broth and cultured for ~3 hrs until OD_{600} reached 0.45 - 0.55 nm measured on a spectrometer. At that point the flask of cells was placed in ice water and chilled for 2 hrs and the cells were then collected by centrifugation 2,500 *g* for 20 min at 4°C. The bacterial cell pellet was resuspended in 20 ml of ice-cold trituration buffer, then further diluted to 500 ml in the same buffer and incubated on ice for 45 min. The cells were collected by centrifugation at 1,800 *g* for 10 min and the pellet was resuspended in 40.6 ml ice cold trituration buffer. 80% autoclaved glycerol was added drop wise with gentle swirling to a final concentration of 15% (9.37 ml for total of 50 ml culture). The cells were aliquoted (200 µl) in 1.5 ml Eppendorf® tubes and chilled on dry ice. The cells were stored at -80°C until further use.

2.2.3 Bacterial transformation

200µl of chemically competent *E. coli Stbl3* cells (Invitrogen) or *E. coli* JM109 cells (in-house) were kept on ice, 10-50 ng of plasmid DNA was added and cells were incubated on ice for 30 min. Cells were then heat shocked at 42°C for 45 seconds and put directly on ice for 2 min. S.O.C (Super Optimal Broth, Q-BioGene) media was added and the cells incubated at 37°C for 1 hr with shaking at 250 rpm. Cells were centrifuged at 3,000 *g* for 2 min and resuspended in 500 µl LB with antibiotics. 100 µl was then streaked onto LB agar plates containing the appropriate antibiotic, ampicillin (50 µg/ml) or kanamycin (100 µg/ml) and incubated at 37°C overnight. Individual bacterial colonies were selected and grown for 8 hr in 3 ml LB broth with the appropriate antibiotic at 37°C agitated at 250 rpm. A small volume was stored long term in 8% glycerol at -80°C.

2.2.4 Isolation of primary keratinocytes and fibroblasts from skin biopsies

A 6 mm RDEB skin biopsy was obtained with authorisation from the National Research Ethics Services, Westminster (07/H0802/104) and with written informed consent from patients. Excess connective tissue was removed using a sterile blade and the sample was incubated in neutral protease NB (1 unit/ml) (SERVA Electrophoresis GmbH, Germany) at 37°C for 3 hrs until the epidermis peeled off. The epidermis was fragmented and incubated in a falcon tube containing 0.25% trypsin in EDTA at 37°C for 3 – 4 hrs with agitation every 30 min. The suspension containing the digested tissue was neutralised with DMEM/10% FCS and vigorously vortexed to obtain a single cell suspension and filtered through a sterile cell strainer (100 µM) into a falcon tube. The resulting suspension was then centrifuged at 850 *g* for 10 min and the cell pellet was resuspended in complete keratinocyte media and cultured at 37°C in a 10% CO_2 incubator with the addition of irradiated 3T3 cells ($1x10^6$ cells/25 cm^2). The remaining dermis was fragmented and treated with collagenase NB6 (SERVA Electrophoresis GmbH) (0.45 units/ml). The resulting cell suspension was seeded into a T25 flask and cultured at 37°C in a 5% CO_2 incubator.

2.2.5 Irradiation of mouse 3T3 cells

3T3 murine fibroblast cells were irradiated at a dose of 600 Grays (Gy) or 60 rads (1 Gy = 100 rads) using an irradiator containing a ^{137}Caesium source. The irradiation time was calculated using a reducing factor of 15%, i.e. the water-based dose x 15%. 60 Gy should take 27 min + 2 seconds. Accounting for the 15 % reducing factor, the final time was 23 min and 30 seconds (1410 seconds).

2.2.6 Culture of mammalian cell lines

HEK-293T cells were routinely cultured using DMEM/10% FCS at 37°C in a 5% CO_2 incubator and passaged when reaching confluence by washing once with 1X PBS and detaching the cells using 0.05% trypsin in EDTA. The trypsin was neutralised with DMEM/10% FCS and cells were collected by centrifugation at 400 *g* for 5 min. The cells were resuspended in the appropriate volume of DMEM/10% FCS, counted and seeded accordingly.

2.2.7 Culture of human keratinocytes

Primary human keratinocytes (passage p0) were cultured with complete keratinocyte media in T25 flasks with the addition of $1x10^6/25$ cm^2 irradiated 3T3 cells providing a supporting feeder layer for the colonies to grow. Media was changed every 2-3 days and additional 3T3 cells were added every 3-4 days. When the keratinocytes reached 70 – 80% confluency, cells were passaged to prevent stratification. Flasks were washed once with 1X PBS and 1 ml of 0.25% trypsin in EDTA was added. Flasks were primarily incubated for 3 min at RT for the detachment of the 3T3 feeder layer, washed again with 1X PBS and inoculated with a further 3 ml of trypsin. Flasks were incubated at 37°C until keratinocytes were completely detached. The trypsin was neutralised with complete keratinocyte media and the suspension was centrifuged at 400 *g* for 5 min for the collection of the cells. The pellet was resuspended and counted before re-plating at a density of $5x10^5/25$ cm^2 in a new flask with fresh feeder cells added. Human keratinocyte cell lines were cultured as described above but with the omission of the 3T3 feeder layer. Keratinocytes were cultured at 37°C in a 10% CO_2 incubator.

2.2.8 Culture of human fibroblasts

Primary human fibroblasts were routinely cultured using DMEM/10% FCS at 37°C in a 5% CO_2 incubator and passaged using 0.25% trypsin in EDTA when reaching confluence.

2.2.9 Freezing and recovery of cells

All cells were suspended in either DMEM 10%/FCS or complete keratinocyte media, counted and collected by centrifugation. The cell pellets were resuspended in the appropriate volume of cold freezing media containing 90% FCS + 10% Dimethyl Sulphoxide ($DMSO_4$) to obtain a final concentration of $2x10^6$ cells/ml and 1 ml volumes were transferred to individual cryovials. These were wrapped in 3 layers of paper tissue and stored for 24 hrs at -80°C and then

transferred to a LN_2 tank for long-term storage. Cells were recovered from LN_2 by thawing the cryovials in a 37°C water bath for ~1 min before transferring the 1 ml volume to a 50 ml falcon tube containing pre-warmed DMEM 10%/FCS. The suspension was centrifuged at 400 *g* for 5 min and the pellet was resuspended in 5 ml of the appropriate media, cells were counted and plated accordingly.

2.2.10 Restriction endonuclease DNA digestion

PCR products from genomic DNA or plasmid DNA were digested in a final volume of 20 µl containing 1X buffer (NEB), 0.1mg/ml BSA according to the requirement of each enzyme and 1 or 2 restriction enzymes (<10% final volume) assuming buffer compatibility. The reaction was incubated for 2 hrs at 37°C. In cases where the buffer system was incompatible between the 2 restriction enzymes, a QIAquick PCR Purification step intervened.

2.2.11 Filling in of 5' DNA overhangs

Blunt-end cloning steps requiring filling of 5' DNA overhangs were generated by using the 5'-3' polymerase activity of the DNA polymerase I Large (Klenow) fragment. The restriction digestion reaction from the previous step generating the 5' overhangs was heat inactivated or PCR purified and 1 unit (U) of enzyme per microgram of DNA and 200 µM of dNTPs were added to a final volume of 30 µl. The reaction was incubated at 25°C for 15 min, followed by heat inactivation of the enzyme at 75°C for 20 min.

2.2.12 Exonuclease removal of 3' DNA overhangs

Blunt-end cloning steps requiring removal of 3' DNA overhangs were generated by using the 3'-5' exonuclease activity of the DNA polymerase I Large (Klenow) fragment. The restriction digestion reaction from the previous step was heat inactivated or PCR purified and 1 unit (U) of enzyme per microgram of DNA was added to a final volume of 30 µl. The reaction was incubated at 25°C for 15 min, followed by heat inactivation of the enzyme at 75°C for 20 min.

2.2.13 Dephosphorylation of 5' DNA termini

DNA plasmids were incubated with 1 U of calf intestinal alkaline phosphatase (CIAP) (Promega) and 1X CIAP buffer in a final volume of 30 µl prior to ligation to prevent re-ligation

of linearised cloning vehicle DNA by removing phosphate groups from both 5´-termini. The reaction was incubated for 30 min at 37°C.

2.2.14 Agarose gel electrophoresis

0.7% - 2% UltraPure agarose was dissolved by heating in 1X TAE and allowed to cool before adding 0.5 µg/ml ethidium bromide. The agarose was cast in gel trays and allowed to set. DNA samples were loaded with the addition of a 6X purple loading dye and a 1 kb Plus DNA ladder was run alongside as a size reference. Electrophoresis was carried out at 80 – 120 V and gels were visualised under ultraviolet light using a UviDoc gel documentation system.

2.2.15 Agarose gel purification of digested DNA fragments

Digested DNA fragments were separated by gel electrophoresis on a 0.7% - 1.5% 1X TAE agarose gel containing ethidium bromide and exposed to UV light using a UviDoc gel system. The desired DNA fragments were excised using a sterile scalpel and gel slices of up to 400 mg were purified using the QIAquick Gel Extraction Kit according to the manufacturer's instructions and eluted in 35 – 50 µl of dH_2O.

2.2.16 Ligation of digested DNA fragments

Digested plasmid backbone (100 – 200 ng) was ligated to insert DNA at a 1:1 – 1:5 molar ratio with 1:3 typically resulting in the majority of clones using 4 U T4 DNA ligase and 1X T4 DNA ligase buffer with ATP (NEB) in a total volume of 20 µl. Ligations were performed at 16°C overnight and the ligated product was transformed into competent *E. coli* Stbl3 or JM109 cells without exceeding >10% of the total transformation volume.

2.2.17 Introduction of silent mutations by site directed mutagenesis

SDM of the donor template (10.2 kb) required HPLC purified primers of the region to be modified used at a quantity of 125 ng. This equated to 10.2 pmole of the 37 bp SDM ex4 COL7A1 template Left forward and reverse primers. A PCR reaction was set up using 1X *Pfu* PCR buffer, 10 ng template DNA, 125 ng of each left or right primer set, 200 µM dNTPs, 3 µl quick solution and 1 µl *Pfu* Turbo (2.5 U) polymerase in a final volume of 50 µl. The PCR cycle was set to 1 cycle at 95°C for 1 min, 18 cycles of 95°C for 50 seconds, 60°C for 50 seconds 68°C for 10 min 20 seconds, 1 cycle of 68°C for 7 min and the reaction was cooled to 37°C on

ice. 1 µl of DpnI (10 U) was added to digest non-nicked parental circular plasmid by incubating for 1 hr at 37°C. Mutated molecules were transformed into competent *E. coli* for nick repair. Successfully mutated sequences were confirmed by Sanger sequencing using COL7A1 ex4 template forward and reverse primers. The second set of silent mutations was introduced by repeating the assay on the mutated clone DNA using 7.9 pmole of the 48 bp SDM ex4 COL7A1 template Right forward and reverse primers.

2.2.18 Genomic DNA extraction

Individual cell pellets from ~$1x10^5$ cells were lysed with the addition of proteinase K and lysis buffer diluted in PBS at 56°C for 10 min and DNA was precipitated with 100% ethanol. DNA was collected using silica resin columns (QIAGEN DNA mini kit) according to the manufacturer's instructions and eluted in 30 µl of dH_2O. Clones grown in 96-well plates were extracted by directly lysing clones in the 96-well plate and extracting genomic DNA using the ZR-96 *Quick-g-DNA* kit.

2.2.19 TOPO-TA cloning

PCR products from the ZFN COL7A1 ex4 template amplicons were purified using the QIAquickPCR purification kit and ligated into the pCR®4-TOPO®. 4 µl of product was combined with 1 µl salt solution and 1 µl pCR®4-TOPO® vector in a final volume of 6 µl and incubated at RT for 5 min. 2 µl of the reaction were transformed into competent cells and grown on ampicillin selection LB agar plates. 6-8 colonies were picked the following day for DNA extraction and Sanger sequencing using the M13 forward and reverse primers.

2.2.20 96-well sequencing reaction and DNA precipitation

For the detection of genomic disruptions in NILV-ZFN transduced keratinocytes a PCR was carried out in a 96-well plate by adding 2 µl BigDye® Terminator V3.1 Ready Reaction Mix, 2 µl of 2.5X sequencing buffer, 4 µl of DNA template and either 2 µl 1.5 µM Fwd SDM or Rev SDM primer in a 10 µl reaction. The amplification cycles were 96°C for 1 min, followed by 25 cycles of rapid thermal ramp (1°C/second) to 96°C; 96°C for 10 seconds; rapid thermal ramp to 50°C; 50°C for 5 seconds; rapid thermal ramp to 60°C; 60°C for 4 min; rapid thermal ramp to 4°C and hold.

Following the BigDye® Terminator V3.1 Cycle Sequencing reaction, the PCR product was precipitated in a 96-well plate by centrifuging the plate at 250 *g* for 1 min followed by the addition of 1 µl 125 mM EDTA, 1 µl 3M sodium acetate and 25 µl 100% ethanol. The plate was centrifuged at 250 *g* for 1 min at 4°C and incubated at RT for 15 min. The plate was then centrifuged at 850 *g* for 30 min at 4°C and the supernatant was removed by inverting the plate and centrifuging at 250 *g* for 1 min on paper towels. 35 µl of 70% ethanol was added to the plate and centrifuged at 1,900 *g* for 15 min at 4°C. Supernatant was removed as before and the plate was air dried for 10 min. The plate was covered with a plate seal and stored at -20 before dispatching for sequencing.

2.2.21 Cell sorting by limiting dilution and FACS

Keratinocyte clones were manually diluted to obtain single colonies by diluting the bulk population to 0.85 cells/100 µl of complete keratinocyte media and seeding in multiple 96-well plates. Alternatively, automated cell sorting was carried out using a BD FACSARIA III (BD Biosciences) using FACSDiva software with cells collected in conditioned media.

2.2.22 Plasmid DNA preparation

E.coli transformed cells expressing the plasmid of choice were gown in 200 – 400 ml volumes for large-scale plasmid DNA preparation. Extraction was performed using Maxi-Prep or Giga-Prep kits (QIAGEN) carried out to the manufacturer's guidelines. DNA concentration in the eluent was measured using a Nano-Drop spectrophotometer. The measurements were taken with a 0.2 mm path length at a wavelength of 269 nm (A_{260}). Confirmation of plasmids was carried out by restriction digestion of unique restriction sites (NEB) and subjected to 0.7 - 2% agarose gel electrophoresis at 100V.

2.2.23 Lentiviral vector production

HEK-293T cells were seeded at a density of 2.0 – 2.3x10^7 per T175 cm^2 flask (12 flasks) for small scale productions and grown overnight to obtain an ~80% confluency the following day. For a single T175 cm^2 flask, a mixture of DNA plasmids was prepared by combining 25 µg of transfer plasmid (pCCL-PGK-COL7A1/pRRL-PGK-GFP), 32.5 µg of gag-pro-pol packaging plasmid pCMV-dR8.74 (for integrating lentivirus) or 32.5 µg of pCMV-dR8.74 D64V (for non-integrating lentivirus), 17.5 µg of envelope plasmid (pMDG.2) and 25 µg pRSV-Rev (for 3rd generation lentivirus) in 5 ml of Opti-MEM and passed through a 0.22 µm filter. 2 µM PEI (1 µl

of the prepared stock solution) was added to 5 ml of Opti-MEM and passed through a 0.22 µm filter. For large scale productions, cells were seeded at a density of $130x10^6$ cells/5-layer flask and transfected with 180 µg of transfer plasmid (pCCL-PGK-COL7A1/pRRL-PGK-GFP), 90 µg of gag-pro-pol packaging plasmid (pMDLg/pRRE), 55 µg of envelope plasmid (pMDG.2) and 45 µg pRSV-Rev in 25 ml of Opti-MEM and added to 25 ml of Opti-MEM containing 5 µl of PEI. The DNA plasmid and PEI mix were combined and incubated for 20 min at RT to form a DNA-PEI complex. The flasks were washed once with Opti-MEM and the complex was added (10 ml/230 ml) and topped up with an additional 2 ml of plain Opti-MEM. The cells were incubated with the transfection mix for 4 hrs in a 37°C 5% CO2 incubator. The transfection mix was then replaced with 20 ml/250 ml complete DMEM/10% FCS. 24 hrs later the media was replaced with 17 ml/250 ml complete DMEM/10% FCS. 48 hrs later the media was harvested and centrifuged at 3,300 *g* for 10 min to precipitate cell debris before passing through a 0.22 µm sterile filter. For small scale productions, the filtrate was loaded in polyalomer tubes and concentrated by ultracentrifugation in a Sorvall Discovery SE or a Beckman Coulter LE-80 for 2 hrs at 100,000 *g*. The final viral pellets were resuspended in plain reduced serum Opti-MEM and left on ice for 30 min before aliquoting and storing at −80°C until further use. Second harvest was performed at 72 hrs. For large scale productions, the first harvest was concentrated by overnight spin at 7,500 *g* and the supernatant was discarded and the volume of the second harvest was added to the flasks and centrifuged for a further 6 hrs at 8,500 *g* on an Avanti J-26S Series high speed centrifuge (Beckman Coulter). The final viral pellets were resuspended in plain reduced serum Opti-MEM and left on ice for 30 min before aliquoting and storing at −80°C until further use.

2.2.24 Vector titration

HEK-293Ts were seeded at a density of $1x10^5$ cells/well of a 24-wel plate and allowed to attach overnight. 24 hrs later, concentrated viral stocks were serially diluted 5-fold and used to transduce cells in a minimal culture volume of 300 µl DMEM/10% FCS. The volume was topped up to 1 ml DMEM/10% FCS 6 hrs later and incubated for 72 hrs. The cells were then harvested and analysed for vector expression by flow cytometry and qPCR. Viral titre was calculated off dilutions resulting in 1-10% of transgene expression to ensure 1 viral copy per cell. The titre was calculated using the formula [Titre (TU/ml) = (vector expression/100)*1000*number of cells seeded / volume of virus added].

2.2.25 Viral vector transduction of keratinocytes and fibroblasts

Primary fibroblasts cultured in DMEM/10% FCS and seeded in 24-well plates or primary keratinocytes and keratinocyte cell lines seeded in T25 flasks with lethally irradiated 3T3 cells and grown in complete keratinocyte media were transduced 24 hrs later by one or two rounds of exposure to LV-GFP or LV-COL7 vectors at MOI 1-50. Viral and culture volumes were adjusted to ensure viral volume accounted for ≤10% of the total culture volume. Virus supernatant was added to the wells/flasks in minimum volume (300 µl in 24-well / 1.5 ml in 6-well / 3 ml in T25) and topped up to optimal culturing volume after 6 hrs and kept on cells overnight. The culture media was replaced with fresh media the following day. Cells were propagated by subculturing in larger format culture plates/flasks. NTERT keratinocyte cell line was seeded at $2x10^5$ cells/well of a 6-well plate and transduced with NILV-ZFN left, NILV-ZFN right (MOI of 100 for each) and NILV-template (MOI of 200) in 1.5 ml complete keratinocyte media and topped up to 3.5 ml after 6 hrs. Medium was changed and cells propagated the following day.

2.2.26 Flow cytometry for detection of GFP

Transduced or transfected cells expressing GFP were harvested and collected by centrifugation at 400 *g* for 5 min in FACS tubes. The cells were washed once with 2% FCS/PBS and pelleted. The supernatant was aspirated and 400 µl of 2% FCS/PBS was added. The proportion of green fluorescent protein (GFP) positive cells and GFP intensity were detected by flow cytometry using a CyAn™ ADP Analyzer (Beckman Coulter, High Wycombe, UK). Forward and side scatter were used to exclude debris and aggregates and eGFP fluorescence was measured by filter 530/30 nm. In all cases, 10,000 eGFP+ cells were collected. Transduced cells were identified by eGFP fluorescence. Data were collected using Summit 4.4 (Beckman Coulter). Analysis was performed using FlowJo v7.6.5 (TreeStar, Stanford University, San Francisco, CA).

2.2.27 Flow cytometry for detection of C7

Primary keratinocytes and fibroblasts derived from subjects with RDEB were transduced with clinical grade LV-COL7 encoding lentiviral vector. Briefly, $1x10^5$ cells were seeded in 24-well plates and transduction was carried out at MOI 5 with LV-COL7. For expression analysis, cells were fixed in Fix & Perm® Medium A (Life Technologies, Paisley, UK) for 20 min at RT in the dark. The cells were then washed with 2-3 % FCS/PBS, in 2 ml, twice; spun down at 550 *g* for 4 min at RT. The cell pellets were resuspended in Fix & Perm® Medium B with mAb-C7-LH7.2

antibody at a 1:25 dilution (Santa Cruz Biotechnologies, Heidelberg, Germany), and incubated at 4°C overnight in the dark. The cells were washed with 2 %FCS/PBS, twice and pelleted at 16,600 *g* for 4 min. The cell pellets were resuspended in Fix & Perm® Medium B with Alexa 488 goat or rabbit anti-mouse 2^{ry} antibody at a 1:200 dilution, and incubated at RT for 1 hr 30 min in the dark. The cells were washed with 2% FCS/PBS twice, resuspended in 0.5 ml 2% FCS/PBS and analysed using flow cytometry.

2.2.28 Quantitative PCR (qPCR)

For the detection of integrated proviral copies in lentivirally transduced cells, genomic DNA was extracted with QIAamp DNA mini kit. The qPCR reaction was set up using 100 ng DNA template, 0.9 µM of each Psi and Albumin forward and reverse primers (Eurofins, MWG), 0.2 µM fluorescently labelled probes (Applied Biosystems) and 1X Platinum Quantitative PCR SuperMix-UDG w/ROX in a 25 µl reaction volume. The reaction was run for 1 cycle at 50°C for 2 min, 1 cycle at 95°C for 10 min, 40 cycles at 95°C for 15 seconds and 60°C for 1 min on a ABI Prism 7000 sequence detection system (Applied Biosystems) Integrated copy number was calculated with the aid of standard curves generated using serially diluted plasmid encoding both viral packaging Psi and endogenous housekeeping Albumin sequences.

2.2.29 p24 ELISA

The HIV-1 p24 levels measured in pg/ml in viral supernatants harvested after lentiviral production were analysed by ELISA to assess the physical HIV-1 titre of the NILVs. Samples were diluted 1:100,000 and 1:1,000,000 times in Opti-MEM and the ELISA was performed according to manufacturer's instructions. Briefly, the viral supernatants were diluted and then lysed before adding to pre-coated with anti-p24 antibody wells in duplicate. An internal kit standard curve was prepared by serially diluting p24 antigen and loaded in duplicate alongside samples. The plate was sealed and incubated in a 37ºC incubator overnight. The plate was washed and incubated with a biotin conjugated anti-p24 antibody for 1 hr at 37ºC. The plate was then washed and incubated with streptavidin-peroxidase solution for 30 min at RT after which stop solution was added the absorbance was read at 450 nm using a FLUOstar OPTIMA (BMG Labtech, Offenburg, Germany) and the concentration of p24 calculated in relation to the p24 antigen standards. A physical titre was derived using the following conversion factor: i: ($2x10^3$ molecules) x ($24x10^3$ Da of p24 per Physical Particle (PP)) = $48x10^6$ ii: $48x10^6$ /Avogadro's constant = ($48x10^6$) / ($6x10^{23}$) = $8x10^{-17}$ g of p24 per PP iii. There is approximately 1 PP per $1x10^{-16}$ g of p24 iv.$1x10^4$ PP per pg of p24 v. 100 Transducing Units (TU) per 1000 PP.

2.2.30 Detection of mismatches by nuclease S CEL-I assay

Clones treated with NILV-ZFNs and NILV-template were amplified for detection of mismatches by Nuclease S (CEL-I enzyme) + Enhancer. An initial PCR reaction containing 1X PCR buffer, 200 µM dNTPs, 0.5 µM of each forward and reverse ZFN primers, 0.5 U Taq polymerase (Roche) and 200 ng of extracted genomic DNA in a final volume of 50 µl was performed by heating to 95°C for 5 min, followed by 30 cycles of 95°C for 30 seconds, 64°C for 30 seconds and 72°C for 30 seconds, 1 cycle of 72°C for 5 min and kept at 4°C. 10 µl of the PCR reaction from each sample was subjected to a hybridisation reaction by heating to 95°C for 10 min and then gradually cooling to 85°C at -2°C/second, then 85°C to 25°C at -0.1°C/second and kept at 4°C. For the detection of sequence mismatches the SURVEYOR Nuclease S reaction was performed by adding 1 µl of enhancer, 1 µl of 0.15 M Mg_2Cl and 1 µl of Nuclease S enzyme to the 10 µl PCR reaction and incubated at 42°C for 60 min. Internal kit positive and negative controls (Ctrl C and Ctrl G) were carried out alongside. The reaction was run on a 1.5% agarose gel and bands corresponding to the expected sizes of uncleaved product (372 bp) or (445 bp) and cleaved product (211, 161 bp) or (245, 200 bp) according to the PCR primer sets used were detected.

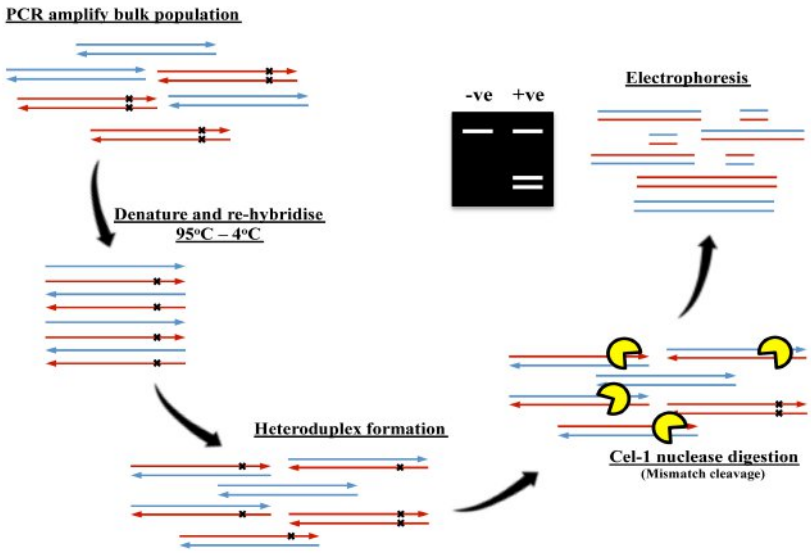

Figure 2.1 Schematic of the Surveyor nuclease CEL-I assay for the detection of ZFN activity.
The region of interest to which the ZFN arms bind and cleave is PCR amplified in the bulk cell population expected to carry mismatches in some alleles. The single or double-stranded breaks (SSB/DSB) in the genome are repaired by the NHEJ introducing indels into the sequence (depicted by black x). Heteroduplex formation is carried out by the denaturing and re-annealing step from 95°C – 4°C between mutated and WT amplicons. Cleavage then occurs by digestion with the CEL-I mismatch detecting endonuclease assay resulting in fragments of three varying lengths. The ratio of cleaved to uncleaved product seen by gel electrophoresis can be used as a rough measure of the ZFN-mediated cleavage efficiency.

2.2.31 High-throughput next generation sequencing

DNA extracted from polyclonal NTERT population transduced with NILV-ZFNs was analysed by NGS using COL7A1 ex4 template forward and COL7A1 ex4 template reverse primers. These were coupled to flanking NGS-adapter sequences using the NEBNext Multiplex Oligos for Illumina kit (NEB) as per the manufactirer's instructions. Sample sequencing was carried out on an Illumina MiSeq genome sequencer (Illumina, San Diego, CA, US). Set up and data analysis was performed by Dr. C. Deakin.

2.2.32 In situ immunofluorescence staining

Both LV-COL7 transduced and untransduced primary RDEB fibroblasts (minimum $1x10^5$ cells/per coverslip in 24-well plate) were fixed in 4% neutral buffered formalin, washed once with 1X PBS and permeabilised with 0.1% Triton X-100 in PBS. Cells were incubated with blocking solution (1% BSA in PBS) for 20 min at RT, and then incubated overnight at 4°C with 30 µl mAb-C7-LH7.2 or Calbio-C7-pAb primary antibodies. A piece of Parafilm® was placed on top of each coverslip to prevent it from drying out. After washing, cells were incubated with goat anti-mouse or goat anti-rabbit AlexaFluor-568, or Cy3 conjugated 2^{ry} antibodies and DAPI (4',6-Diamidino-2-Phenylindole). The slides were mounted on superfrost polylysine coated slides (VWR) with Mowiol or Prolong gold. Micrographs were imaged using a Leica DMLB upright microscope (Leica Microsystems CMS GmbH, Wetzlar, Germany) and a Leica SP2 laser confocal microscope (Leica, Milton Keynes, UK) and processed using Image J (Wayne Rasband (NIH)) and Inkscape 0.48.

2.2.33 SDS-PAGE immunoblotting

Transduced and untransduced cell pellets, or cultured media supernatant from cells grown for 48 hr in the absence of serum and supplemented with 50 µg/ml ascorbic acid, and concentrated using ProteoExtract® Protein Precipitation kit according to the manufacturer's guidelines (Merck Millipore, Hertfordshire, UK), were resuspended in cell lysis buffer. Samples were lysed by pipetting the cells up and down repeatedly until the cell pellet dissolved completely, and then incubated for 20 min on ice. The samples were then centrifuged at 12,400 *g* for 10 min to pellet the insoluble cell debris at 4°C. The total protein concentration in the supernatant was determined using a Bio-Rad protein assay kit (BIO-RAD, Hertfordshire, UK). Briefly, 4 µl of sample supernatant was diluted 1:50, 1:100 and 1:500 times in lysis buffer base and loaded in a 96-well flat-bottomed plate. A standard curve was formulated using 40 µg/ml of BSA serially diluted 2-fold to 2.5 µg/ml. BCA reagent was added at a 1:5 concentration to all samples and

absorbance was at an OD 595 nm. Samples from cell lysate were normalised and further diluted in 5X sample buffer and 3 µl fresh DTT (1 M) was added to a final sample volume of 35 µl and were heated at 95°C for 3 min and then kept on ice. A 6% sodium dodecyl sulphate polyacrylamide separating SDS-PAGE gel was made with a stacking gel above containing the comb. Samples were loaded and subjected to electrophoresis at 100 V in 1X running buffer. After electrophoresis, proteins were transferred to polyvinylidene fluoride membranes (PVDF) in ice-cold 1X transfer buffer at 120 V. The membrane was then washed in 1X washing buffer and blocked in 5% milk in 1X washing buffer for 1 hr at RT with shaking. The membrane was washed once and incubated with anti-C7 antibody (overnight) or anti-vinculin mAb (cl.V284, Sigma-Aldrich, Dorset, UK) (1 hr at RT) in diluent 1 with shaking. The membranes were then washed three times and further incubated with mouse anti-rabbit secondary antibody conjugated with HRP 1:7,000 or secondary HRP conjugated anti-mouse 1:3000 in diluent 2 and signals were detected using the ECLplus system. For re-probing, the membrane was stripped in 1X stripping buffer at 58°C for 30 min with agitation and then washed three times with 1X washing buffer. The blots were developed and fixed manually on x-ray film. Total protein amounts in the samples from concentrated culture medium supernatants loaded on the SDS-PAGE were checked by Ponceau S (Sigma-Aldrich, Dorset, UK) staining of the PVDF membrane following protein transfer.

2.2.34 In vitro wound healing scratch assay

Keratinocytes were seeded at a density of $1.2x10^6$ cells per well of a 6-well plate and incubated overnight at 37°C with complete keratinocyte media. 22 hrs later the media was aspirated and the cells were treated with mitomycin C (10 µg/ml) in DMEM/10% FCS for 2 hrs at 37°C. Following the incubation period, a straight vertical scratch from top to bottom and a horizontal scratch from left to right were made in the well using a P200 pipette tip held at a 90° angle. The well was washed 3 times with 1X PBS to remove the detached cells and 3.5 ml of complete keratinocyte media was added to each well. A hole was made on the lid of the plate with a sterile needle to allow for the CO_2 supply to be connected. The plate was placed on a mechanical stage in a 37°C chamber with supply of 5% CO_2 and the field was imaged using a Zeiss Axiovert time-lapse microscope (Zeiss, Germany) at 3 different locations of the vertical and horizontal scratch using a 4X objective. Images were captured every 15 min for a total of 35 hrs. The data was processed using Volocity 6.1.1 software (PerkinElmer, Coventry, UK). The extent of scratch closure was quantified by measuring the area of the scratch occupied at each time point of the migration assay, using a custom thresholding macro (Dr. Vernay B.) on ImageJ (Wayne Rasband (NIH)) and expressed as percentage change. The area under the curve

(AUC) was calculated for each triplicate of each sample and analysed by one-way ANOVA. Multiple comparisons were statistically analysed by Tukey's post-test.

2.2.35 In vitro two-dimensional migration assay

The assay was performed as described previously (Syed et al., 2012, Syed et al., 2013) with some modifications. Briefly, an Oris 96-well black plate (Oris migration assay kit, Cambridge Bioscience, Cambridge, UK) was used and Oris cell seeding stoppers were inserted according to the manufacturer's instructions. LV-COL7 transduced and untransduced RDEB primary fibroblasts were seeded at a density of $2.5x10^4$ cells/well in each well of an Oris 96-well migration assay plates using serum-free DMEM. The plate was then incubated overnight at 37°C and 5% CO_2. The next day, the cell seeding stoppers were removed and the cells were treated with mitomycin C (10 μg/ml) in DMEM/10% FCS for 2 hrs at 37°C. The wells were washed in 1X PBS and 100 ml of fresh medium was added and the plate was further incubated and the cells were allowed to migrate for ~72 hrs in the migration zone. Micrographs were captured using 4X magnification of an inverted microscope (Olympus, Japan). Cells in the migration zone were counted using ImageJ (Rasband, W.S., ImageJ, US National Institutes of Health, USA. http://imagej.nih.gov/ij/) from four independent replicates. Data was analysed by one-way ANOVA. Multiple comparisons were statistically analysed by Tukey's post-test.

2.2.36 Bioengineered skin equivalent preparation and grafting on immunodeficient mice

A fibrin matrix populated with live fibroblasts was used as the dermal component of the bioengineered skin. The methods for preparing and grafting bioengineered skin in nude mice have been previously described (Larcher et al., 2007). In brief, 1 ml of fibrinogen solution (from cryoprecipitate from porcine plasma) was added to 5.5 ml of DMEM/10% FCS containing $7.5x10^5$ human dermal fibroblasts. Immediately afterwards, 0.5 ml 0.025 mmol/l $CaCl_2$ with 11 U of bovine thrombin was added. Finally, the mixture was poured in two 35 mm wells (in 6-well culture plates) and allowed to solidify at 37 °C for 1 hr and then supplemented with 3 ml complete keratinocyte medium overnight. The procedure was repeated a number of times depending on the final number of wells or grafts to be prepared. Human keratinocytes (1.2×10^6 cells per well) were then seeded on the fibrin matrix and left submerged in complete keratinocyte medium for 72 hrs to form the epidermal layer of the bioengineered skin. When confluent, bioengineered skins were manually detached from tissue culture wells and grafted onto immunodeficient mice. All animal procedures were approved by the local ethical

committee and performed in accordance with the United Kingdom Animals Scientific Procedures Act (1986). Grafting was performed under sterile conditions using 6-week-old female nude (NMRI-Foxn1^{nu} (outbred) (Charles River) or 6-week-old male or female NOD.Cg-Prkdc^{scid} Il2rg^{tm1Wjl}/SzJ mice (NSG, Institute of Child Health, UCL). In brief, mice were aseptically cleansed and anaesthetised according to ASPA regulations and full thickness 35 mm diameter circular wounds were then created on the dorsum of the mice. Bioengineered equivalents were detached from the 6-well culture plate and placed orthotopically on the wound. The mouse skin removed to generate the wound was de-vitalised by three repeated cycles of freezing and thawing and used as a biological bandage and fixed with sutures to protect and hold the skin substitute in place during the take process. Dead mouse skin was sloughed off, generally within 15–20 days after grafting, and regenerated human skin became visible. 8-weeks after grafting, mice were given an overdose of anaesthesia and analgesics, and either the complete graft including mouse skin bordering regions for the LV-COL7 studies or 3 mm punch biopsies for the TALEN studies were taken, snap frozen in LN_2, embedded in OCT and cryosectioned at 7 μm for histological and immunohistochemical examinations. A central portion of the human graft was placed in TEM fixative for ultrastructural imaging.

2.2.37 Immunofluorescent and histological staining of bioengineered grafted tissue

Immunofluorescence staining was performed on frozen graft tissue sections following 10 min fixation with ice-cold 50% acetone/ 50% methanol (7 μm thickness). Sections were blocked for 1 hr at RT with 3% FCS in 1X PBS before incubation with primary antibodies (Table 1) mAb-C7-LH7.2, anti-desmoglein-1, anti-involucrin, anti-keratin 10, anti-MTCO2 diluted in 1X PBS overnight at 4^{o}C. 24 hrs later the slides were washed three times with 1X PBS and incubated with secondary antibodies Alexa Fluor goat anti-mouse 488 (Invitrogen, UK), goat anti-rabbit Cy3 (Life Technologies, Paisley, UK), strep 488 diluted in 3% BSA/PBS was followed for 1 hr at RT. Sections were stained with DAPI (5mg/ml) and sealed with coverslips using mowiol (Calbiochem, Nottingham, UK) or ProLong Gold antifade agent (Life Technologies, Paisley, UK) mounting reagents. Sections were also stained by haematoxylin and eosin (H&E) histochemical technique. Briefly, slides were re-hydrated in a series of 3 x 2 min incubations in 100% and 70% ethanol and water followed by a 10 min incubation in haematoxylin (Sigma-Aldrich). The slides were rinsed in hot tap water and differentiated by one dip in acid ethanol (2% HCL in 70% ethanol) and rinsed in water. The slides were stained with 1% eosin (Sigma-Aldrich) for 2 min and dehydrated in 3 x 2 min incubations in 70% and 100% ethanol. The slides were cleared by 2 x 5 min incubations in xylene before mounting with DPX. Staining was visualised and imaged using a Leica DMLB upright microscope (Leica Microsystems CMS

GmbH, Wetzlar, Germany) and a Zeiss Axiophot 2 (Zeiss, Oberkochen, Germany) and processed using Image-Pro 6.2 (MediaCybernetics, Rockville, MD, USA) or on an Olympus upright BX51 RT slider Diagnostic Spot microscope (Olympus, Tokyo, Japan) and analysed using Spot advanced 4.6 and processed using Image J (Wayne Rasband (NIH)) and Inkscape 0.48. Confocal imaging was carried out on a Zeiss LSM 510 Meta laser confocal microscope (Zeiss, Oberkochen, Germany). Post processing was carried out using ImageJ.

2.2.38 Preparation of skin grafts for transmission electron microscopy (TEM)

For TEM, the central piece (approximately 3 x 3mm^2) of each skin graft was dissected out, and fixed with half strength Karnovsky's fixative (2% (v/v) paraformaldehyde, 2.5% (v/v) glutaraldehyde in 0.1 M phosphate buffer (pH 7.4)) for 3-5 hrs at RT and kept at 4°C until further processing. After the initial fixation, tissue samples were rinsed several times in PBS and post-fixed with 1.3% osmium tetroxide in double distilled water for 2 hrs at RT. Samples were then washed, *en bloc* stained with 2% uranyl acetate in 50% ethanol and dehydrated in a graded series of ethanols. Tissue samples were further equilibrated with propylene oxide before infiltration with TAAB epoxy resin, embedded and polymerised at 70°C for 24 hrs. Ultrathin sections (70-90 nm) were prepared using a Reichert-Jung Ultracut E ultramicrotome (Eeichert-Jung, Vienna, Austria), mounted on 150 mesh copper grids (Gilder, Grantham, UK), contrasted using uranyl acetate and lead citrate and examined on a FEI Tecnai 12 (FEI Co., Hillsboro, Oregon, USA) transmission microscope operated at 120 kV. Sample processing and embedding was performed by L. Glover. Images were acquired with an AMT 16000M camera (Advanced Microscopy Techniques, Corp., Woburn, MA, USA). Morphological examination and anchoring fibril scoring of the TEM slides was blinded and performed by Dr. J.R. McMillan ultrastructural microscopy specialist.

2.2.39 Statistical analysis

Keratinocyte migration assays data was analysed by calculating the area under the curve (AUC) accounting for % scratch closure against time for each of the replicates of every sample. The AUCs were compared against the group by one-way ANOVA and multiple comparison analysis of the means was performed by Tukey's post-test. Fibroblast migration values measured by cell bodies at the end-point were analysed by one-way ANOVA and compared by Tukey's post-test. Error bars on flow cytometry data from LV-COL7 trnasduced keratinocytes and fibroblasts represent standard deviation (SD) amongst triplicates. All statistical analysis was performed on GraphPad Prism v.6.

Chapter 3 Restoration of C7 expression in RDEB cells using *COL7A1* expressing lentiviral vector

Experimental therapies for the management of RDEB through restoration of C7 protein expression have included protein replacement, cell and gene therapy and bone marrow transplantation, previously demonstrated to reinstate functionality in epithelial cells and ameliorate blistering. One of the hurdles faced in these studies has however, been the transient expression of C7 and the immunological risks of delivering allogeneic cells or recombinant protein.

In this study, I investigated the use of an autologous gene therapy strategy for the correction of RDEB patient cells. This approach involved delivery of a full-length functional copy of *COL7A1* to both RDEB patient primary keratinocytes and fibroblasts using the HIV-1 based lentiviral vector. Viral transfer presents the most efficient method of gene delivery to primary cells, allowing for safe and permanent integration of large transgenes in both dividing and non-dividing cells. Based on this, a full-length codon optimised *COL7A1* cDNA (8.9 kb) sequence was designed and incorporated into a 3rd generation HIV-1 lentiviral vector backbone. The employed lentiviral platform has been approved for use in clinical trials for other diseases including the skin disease Netherton syndrome (NCT01545323).

For the evaluation of the capacity of the *COL7A1* expressing vector in transducing RDEB cells, primary patient keratinocytes and fibroblasts isolated from RDEB skin lacking functional C7 expression were transduced and examined for vector integration using molecular techniques. It was next assessed whether introduction of a functional copy of the *COL7A1* gene could ultimately lead to the restoration of C7 expression in both RDEB cell types. This was examined by *in situ* immunofluorescence staining analysis and immunoblotting for the detection of vector-derived full-length C7 protein expression. Furthermore, as a means of detecting an associated functional improvement in gene-corrected cells, an *in vitro* wound healing assay allowing for the monitoring of C7 dependent cell migration was employed.

3.1 HIV-1 lentiviral vector carrying codon-optimised *COL7A1* transgene under the control of internal PGK promoter

The development of the RDEB gene therapy strategy employed in this study involved the use of a 3rd generation self-inactivating (SIN) HIV-1 lentiviral vector. A large deletion in the 3'LTR of the viral genome ensures only a single round of reverse transcription, leading to transcriptional inactivation of the provirus after its incorporation into the host cell rendering it replication incompetent. Furthermore, replacement of the native HIV-1 5'LTR with a chimeric Cytomegalovirus (CMV) or Rous sarcoma virus (RSV) enhancer/promoter to drive transcription in turn results in independence from the powerful transcriptional activator *tat* crucial in the replication of HIV-1. The two 3rd generation transfer plasmids available, pCCL (CMV) and pRRL (RSV) therefore allowed for packaging using both 2nd generation gag-pro-pol (pCMVR8.74) and 3rd generation *tat* mutated gag-pro-pol (pMDLg/pRRE) plasmids (Dull et al., 1998).

The SIN lentiviral vector was generated by co-transfection of the *COL7A1* transgene bearing transfer plasmid, the HIV-1 packaging plasmids and a viral envelope. Although a portion of the preliminary *in vitro* studies was carried out using 2nd generation SIN HIV-1 packaging plasmids where *rev* is provided *in cis* with *gag-pro-pol* as a single plasmid the platform was then switched to the safer 3rd generation SIN lentiviral packaging system where a further split in the packaging system allows for *rev* to be delivered *in trans* (RSV-Rev). This was employed to reduce the risk of recombination events and RCL formation. Packaging *gag-pro-pol* and regulator of virion expression *rev* genes were provided in trans as separate plasmids driven by a CMV promoter. The rev responsive element (RRE) maintained in the *gag-pro-pol* ensures its expression is *rev* dependent. The envelope plasmid of choice used to pseudotype the vector was from the Vesicular Stomatitis virus glycoprotein (VSV-G) (pMD2.G), selected for its broad host-cell tropism permitting the infection of a wide range of host cell types **(Figure 3.1)**. For the construction of the transfer plasmid, a full-length *COL7A1* cDNA was codon optimised by the replacement of inhibitory sites, cryptic splice sites, poly(A) sites and RNA instability motifs and introduction of a Kozak sequence to increase translational initiation (Fath et al., 2011).

The newly designed codon-optimised *COL7A1* transgene sequence was synthesised and subcloned into a 3rd generation lentiviral transfer plasmid pCCL-PGK-COL7A1 by GeneArt. The human phosphoglycerate kinase (PGK) promoter, a relatively strong endogenous housekeeping promoter known to outperform CMV in transcriptional activity, was selected to drive stable and constitutive expression of *COL7A1* in almost all cell types including fibroblasts (FB), keratinocytes (KC), haematopoietic, mesenchymal cells or iPSCs. A cPPT region was

incorporated in the pCCL-PGK-COL7A1 transfer plasmid as an initiation signal of reverse transcription and facilitation of nuclear import of HIV-1 cDNA through a central DNA flap as was a WPRE element shown to increase titre and expression of intronless transgenes via increased nuclear export. These sites were flanked by modified HIV-1 LTRs ΔU3-R-U5 enhancer/promoter regions at both 5' and 3' ends of the provirus **(Figure 3.1)**. Sequence fidelity of the synthesised plasmid was confirmed by direct Sanger sequencing of the whole construct. Restriction enzymes BamHI and NotI were also used to confirm plasmid size and transgene orientation **(Figure 3.2)**.

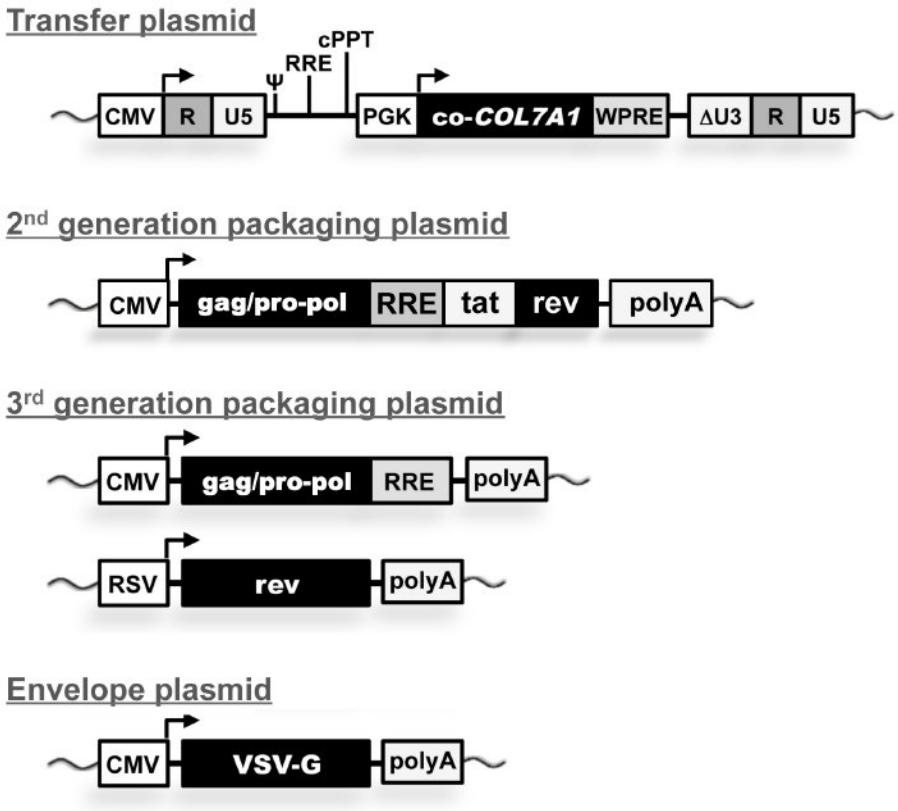

Figure 3.1 2nd and 3rd generation SIN lentiviral packaging plasmids.
Provirus map: pCCL transfer plasmid backbone; CMV: cytomegalovirus; psi (ψ) encapsidation signal; LTR: Long Terminal Repeat 5' or 3' HIV R: HIV R region; HIV delta U3: self-inactivating (SIN) ΔU3 region with a deletion; RRE: Rev responsive element; cPPT cts: central polypurine tract – central terminal sequence; PGK, Phosphoglycerate kinase promoter; *COL7A1*: human collagen VII gene (cDNA); WPRE: mutated woodchuck hepatitis virus posttranscriptional regulatory element; gag/pro-pol: HIV structural polyproteins; tat & rev: essential HIV regulatory element; polyA: polyadenylation tail; RSV: Rous sarcoma virus; VSV-G: Vesicular stomatitis virus glycoprotein.

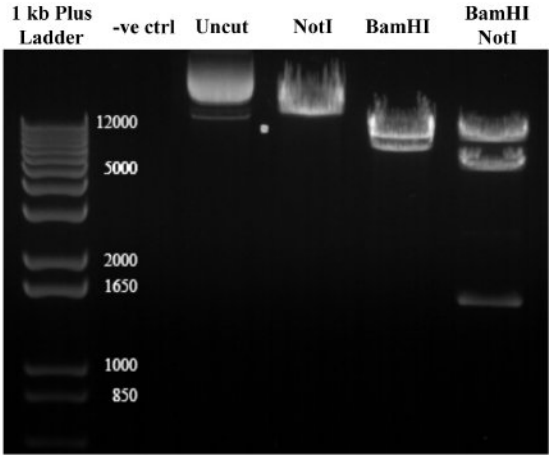

Figure 3.2 Confirmation of LV-COL7 plasmid by restriction digestion analysis.
pCCL-PGK-COL7A1 plasmid was digested with NotI and BamHI and checked on a 1.5% agarose gel. Undigested 15,926 bp band shown in first lane with second supercoiled band below. NotI single digestion linearises the pCCL-PGK-COL7A1 plasmid. BamHI digestion gives rise to two fragments 8,856 bp and 7,070 bp. Double digestion with NotI and BamHI shows the predicted three bands at sizes 8,856 bp, 5,544 bp and 1526 bp.

3.2 Production of PGK-COL7A1 expressing lentiviral vector

Production of SIN-lentiviral vectors was performed by transfecting human embryonic kidney (HEK) 293T cells with either the pCCL-PGK-COL7A1 transfer plasmid or the control pRRL-PGK-GFP transfer plasmid. Both transfer plasmids were co-transfected with the HIV-1 packaging plasmids encoding vector components pCMVR8.74 or pMDLg/pRRE, RSV-Rev and the pMD2.G using the cationic polymers polyethylenimine (PEI) for lentiviral production of LV-COL7 and LV-GFP **(Figure 3.3 A)**. Small scale (12 x 175 cm flasks) and large-scale (6 x 5-layer flasks) productions were performed to obtain sufficient volumes of viral stocks. Ultracentrifugation of viral supernatants (340-fold for small-scale or 1000-fold for large-scale) was implemented for the concentration of the viral preparations (see Methods 2.2.23).

The viral titres for both concentrated LV-COL7 and LV-GFP vector preparations were evaluated by real-time quantitative PCR (qPCR) and flow cytometry following transduction of HEK-293Ts with serial dilutions of each virus. C7 expression based titres for LV-COL7 ranged from $1x10^6$ to $5x10^7$ TU/ml with an average of $5x10^6$ TU/ml and $8x10^7$ to $5x10^8$ TU/ml with an average of $3x10^8$ TU/ml for LV-GFP **(Table 3.1)**. Physical titres calculated by measuring HIV-1 p24 in the viral supernatants were in the range of ~$7x10^8$ IP/ml for LV-COL7 and ~$5x10^8$ IP/ml for LV-GFP. There was a notable reduction in functional titres attained with the LV-COL7 vector compared to those of the LV-GFP vector, most likely due to the large *COL7A1* transgene size approaching the maximal insert capacity of the vector backbone, encumbering

packaging into fully functional virions as supported by the similar p24 levels to LV-PGK. In an attempt to improve viral titres, the commercial transfection reagent Lipofectamine 2000 was used and compared against PEI. The results showed no obvious differences in the resulting titres between the two reagents **(Table 3.1).**

Table 3.1 Titration by qPCR of LV-GFP and LV-COL7 vectors produced using two different transfection reagents.

Virus Production		
Transfection reagent	GFP TU/ml	COL7A1 TU/ml
PEI	8.12×10^7	6.98×10^5
PEI	5×10^8	3.97×10^6
Lipofectamine 2000	5.36×10^8	4×10^6
PEI	1.16×10^8	1.64×10^6
PEI	-	6×10^7

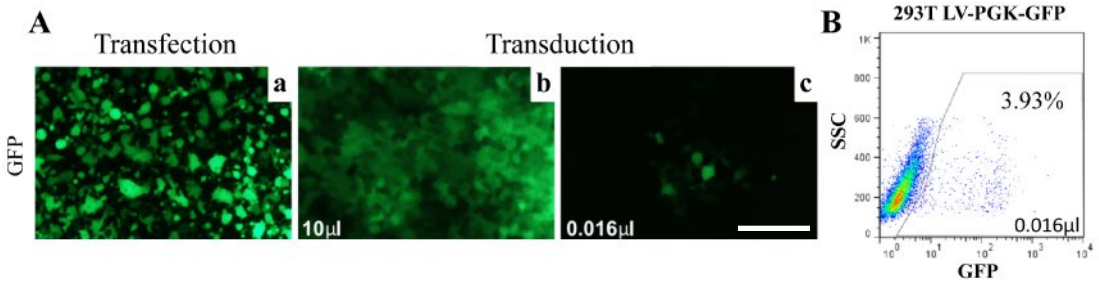

Figure 3.3 Transfection and transduction efficiency of LV-GFP vector in HEK-293T cells.
HEK-293T cells were transiently co-transfected with 3rd generation pRRL-PGK-GFP or pCCL-PGK-COL7A1 transfer plasmids and 2nd or 3rd generation accessory, packaging and envelope plasmids to produce pseudo-viruses. **(A)** Representative images of pRRL-PGK-GFP expression 2 days post transfection (n=5) **(a)**. Representative images of transduction of HEK-293T cells (n=5) with concentrated LV-GFP pseudo-virus at 5-fold decreasing concentrations **(b & c)**. The images are representations of a single experiment performed repeatedly and reproducibly. (**B**) LV-GFP infected HEK-293T cells were harvested and transduction efficiency and titre were assessed by measuring the percentage of GFP positive cells using flow cytometry. For accurate titre calculation values in the range of 2%-10% were used. Scale bar = 100 µm.

3.3 Transduction efficiency of LV-COL7 vector in primary RDEB keratinocytes and fibroblasts

Primary keratinocytes isolated from the RDEB patient (CK) were transduced with LV-COL7 vector at a multiplicity of infection (MOI) of 5. The viral transduction efficiency and transgene integration were assessed by pro-viral copy number (VCN) per cell using qPCR and further confirmed for C7 protein expression by flow cytometry. At 3 days post transduction the average VCNs per cell were in the range of 0.09-0.24. The percentage of C7 expressing cells measured at 2 weeks post transduction was 18% **(Figure 3.4 A, B)**. The reason for assessing C7 following a 2-week culturing period was to dilute out plasmid DNA contamination during viral preparation. Transduced cells demonstrated a higher intensity of C7 expression over endogenous WT levels as seen by their corresponding mean fluorescence intensity (MFI) values **(Figure 3.4 B)**. The transduced cells were maintained in culture and propagated for up to 2 months with no significant decrease of C7 expression.

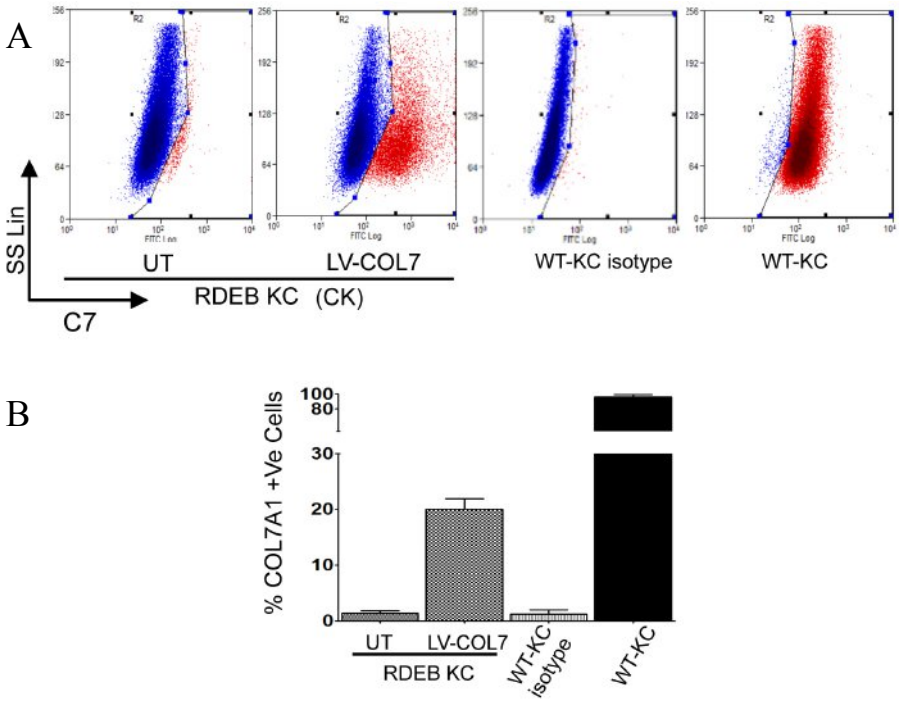

Figure 3.4 Flow cytometry analysis of LV-COL7 transduced primary RDEB keratinocytes for confirmation of C7 expression.
RDEB (CK) keratinocytes transduced in three separate wells with LV-COL7 vector were stained for intracellular C7 expression 2 weeks post viral exposure. Untransduced (UT) RDEB and wild-type (WT) keratinocytes cultured alongside in triplicate representing experimental controls were run in parallel. **(A)** Flow cytometry shows positive C7 expression in LV-COL7 transduced RDEB (CK) and WT keratinocytes, but not in the UT cells. Isotype staining confirms specificity of secondary antibody. **(B)** Triplicate values of flow cytometry data were plotted against each other. Error bars represent SD amongst triplicates.

It has previously been reported that although both keratinocytes and fibroblasts secrete C7 protein, approximately 90-97% of the protein is secreted by the keratinocytes with fibroblasts only accounting for 3-10% of total C7 production (Woodley et al., 2003). However, the slower turnover, relatively long life span *in vitro* and easier *ex vivo* manipulation of primary fibroblasts compared to the challenging to culture primary keratinocytes which differentiate after the first few passages, make fibroblasts a more suitable candidate for gene therapy applications. Studies on allogeneic fibroblasts have reported successful delivery by both intradermal and intravenous routes highlighting their versatility (Woodley et al., 2004b, Woodley et al., 2007b, Wong et al., 2008).

In this study, primary fibroblasts were isolated from 2 RDEB patients' skin biopsies (CK and EB8) (see Methods 2.2.4) and transduced with LV-COL7 at an MOI of 5. Intracellular C7 expression was measured by flow cytometry 2 weeks post transduction with average efficiencies in the two patients' cells calculated to be in the range of 9.3% - 12.8% with untransduced RDEB patient samples representing the negative control **(Figure 3.5 A, B)**. In addition, transduced cells exhibited a higher level of C7 expression than that of endogenous C7 in healthy donor cells as seen by the MFI values due to the constitutive nature of the PGK promoter **(Figure 3.5 C)**. Transgene integration was further confirmed by qPCR 2 weeks post transduction with a VCN/cell of 0.12-0.14.

These data demonstrate that despite the relatively low titres of the LV-COL7 vector, a modest fraction of primary RDEB keratinocytes and fibroblasts were transduced, resulting in genomic integration of the codon optimised *COL7A1* transgene and C7 protein expression.

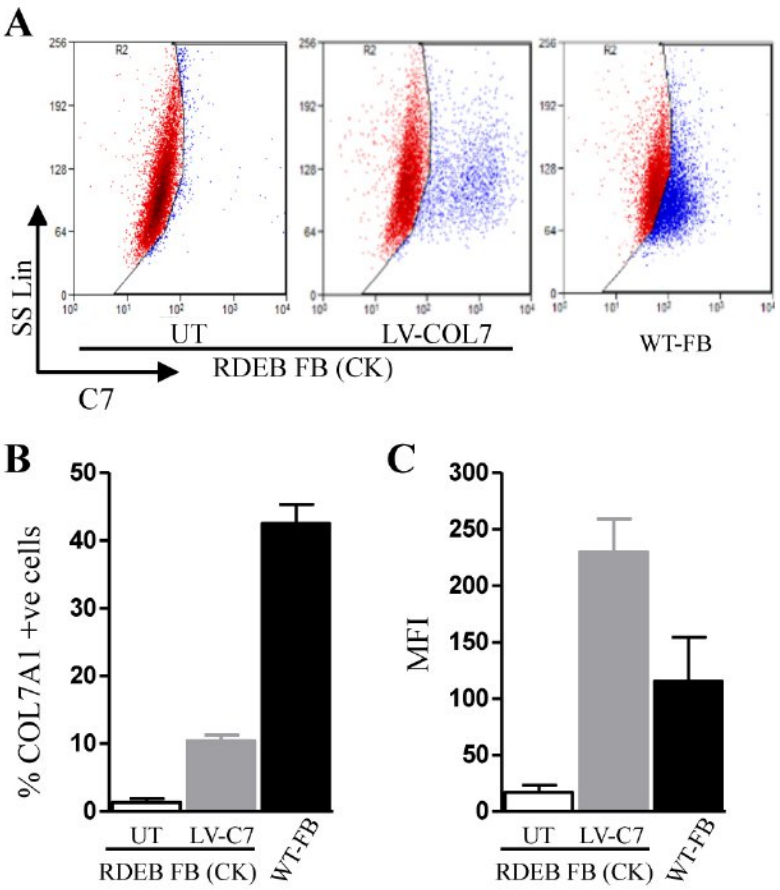

Figure 3.5 Intracellular C7 expression in LV-COL7 transduced RDEB fibroblasts.
RDEB patient (CK) and (EB8) fibroblasts transduced in triplicate with LV-COL7 vector were stained for intracellular C7 expression 2 weeks post viral exposure. **(A)** Flow cytometry showing C7 expression in LV-COL7 transduced RDEB (CK) and wild-type (WT) fibroblasts. No signal detected in untransduced (UT) sample. RDEB (CK) samples were transduced in triplicate wells. WT or UT samples were cultured alongside in triplicate wells. **(B)** Corresponding percentages of average C7 expression from flow cytometry analysis of LV-COL7 transduced RDEB (CK) fibroblasts versus WT and RDEB UT samples and corresponding mean fluorescence intensity (MFI) **(C)**. LV-COL7 transduction of RDEB patient fibroblasts shows transgene expression by positive staining of C7 protein. Error bars represent SD of triplicate sets of the two patient samples.

It has been reported that transduced cells can exhibit distinct morphological alteration such as elongation of the cell bodies and increased protrusions (Chen et al., 2002). In addition, use of a high MOI may potentially be toxic to the cells. To examine this, the cell proliferation rate calculated by total cell-counts was assessed on RDEB fibroblasts transduced with increasing concentrations of LV-COL7 vector at MOIs ranging from 1 to 50 **(Figure 3.6)**. RDEB fibroblasts were seeded at a density of $1x10^5$ cells 24 hrs prior to transduction with six different MOIs (1, 2, 10, 20, 25 & 50) and the cells were counted after 6 days. The results showed a modest increase of cell proliferation at lower MOIs of 1 and 2, while a slight decrease in cell

viability was observed above an MOI of 10. This effect was exacerbated at higher MOIs of 20 and 25 with a 3-fold drop and at an MOI of 50 with a 13-fold drop in the number of viable cells suggesting an increased level of vector-mediated cytotoxicity at high MOIs. To balance the

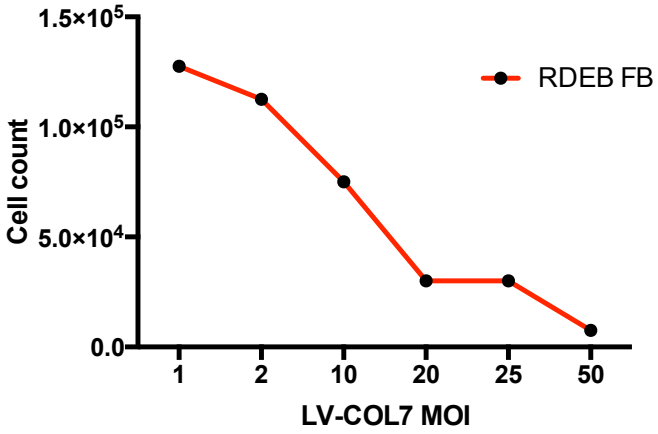

transduction efficiency and cytotoxicity, MOIs of 5 and 10 were used for further studies.

Figure 3.6 Cell proliferation and viability following escalated dose of LV-COL7 transduction
RDEB fibroblasts (FB) were seeded and transduced with a range of MOIs of LV-COL7 virus (1-50) to evaluate cell viability after 6 days of culture. A significant decrease in the total number of viable cells was observed upon increase of MOI in RDEB fibroblasts, indicating vector related cytotoxicity. The values depicted in the graft represent data from a single experiment.

3.4 Restoration of C7 protein expression in RDEB keratinocytes and fibroblasts transduced with LV-COL7 vector

3.4.1 Confirmation of C7 expression in gene modified RDEB cells by in situ immunofluorescence staining

The LV-COL7 mediated restoration of C7 expression in the transduced RDEB keratinocytes and fibroblasts was examined by *in situ* immunofluorescence staining using a specific anti-human C7 antibody (see Methods 2.2.32)

This was initially evaluated in an RDEB EBKC keratinocyte cell line (RDEB EBKC) 3 days post LV-COL7 or LV-GFP transduction with untransduced RDEB EBKCs used as a negative control. Healthy donor cells or RDEB EBKCs either untransduced or LV-COL7 transduced, were seeded on coverslips and stained for C7 using the mouse mAb anti-C7 antibody (mAb-C7-LH7.2). Positive staining was visualised in the LV-COL7 transduced RDEB EBKC and the control healthy donor population, whereas there was complete absence of C7 expression in

untransduced cells, suggesting vector-mediated restoration of C7 expression in RDEB keratinocytes. The LV-COL7 transduced cells exhibited intense cytoplasmic staining throughout the intracellular space at a much higher level than that of endogenous C7 expression seen in healthy donor keratinocytes (**Figure 3.7 a-c**). RDEB EBKC cells transduced with the LV-GFP vector were used in parallel as a control and showed strong expression of GFP protein **(Figure 3.7 d)**.

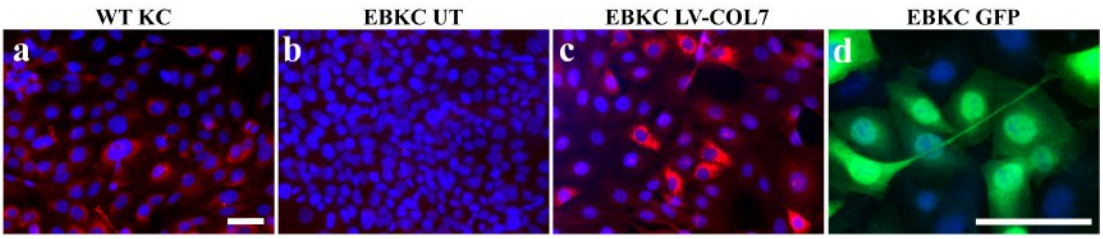

Figure 3.7 Restoration of C7 protein expression in RDEB keratinocytes transduced with LV-COL7
An untransduced (UT) RDEB EBKC cell line was transduced with LV-COL7 at an MOI of 5. At 3 days post transduction, cells were reseeded on coverslips. The cells were fixed and stained with C7 antibody *in situ*. The results showed C7 expression (red) in WT untransduced cells **(a)** and LV-COL7 transduced RDEB EBKCs **(c)**. In contrast, there was no C7 expression in UT EBKC **(b)**. RDEB EBKC cells transduced with LV-GFP were used as a transduction control **(d)**. Nuclei were counterstained with DAPI (blue). The images depicted are from representative fields of the stained coverslips allowing for qualitative assessment of protein expression. Scale bars = 25 μm.

In a similar fashion, LV-COL7 transduced RDEB patient (CK) and (EB8) fibroblasts (see materials Table 2.4) were also evaluated for vector-mediated C7 expression by *in situ* immunofluorescence staining. The cells transduced with LV-GFP vector were run in parallel representing the negative control. The results revealed pronounced LV-COL7 derived C7 protein expression in both RDEB (EB8) and (CK) fibroblasts demonstrated by intense cytoplasmic staining. The detected expression levels surpassed those of endogenous C7 expression in normal donor cells indicating transgene overexpression by the PGK promoter. Untransduced RDEB fibroblasts showed a complete absence of C7 expression **(Figure 3.8)**.

Collectively, the results showed restoration of C7 protein expression in an RDEB keratinocyte cell line and two separate RDEB primary fibroblast samples following transduction with the LV-COL7 vector with expression levels superseding those of normal donor cells.

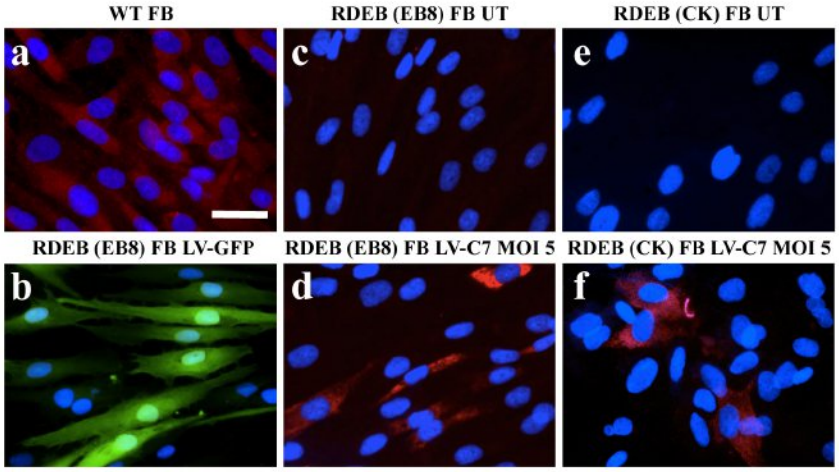

Figure 3.8 Restoration of C7 protein expression in primary RDEB fibroblasts transduced with LV-COL7.
In situ immunofluorescence staining for C7 expression (red) and nuclear stain DAPI (blue) of either healthy primary (WT) **(a)**, RDEB patient (CK) or (EB8) untransduced (UT) **(c, e)** or LV-COL7 transduced fibroblasts **(d, f)**. Control transductions performed using LV-GFP encoding vector **(b)**. C7 expression is restored after LV-COL7 transduction at MOI 5 showing intense cytoplasmic staining. These are representative fields of the stained areas from triplicate coverslips. Scale bar = 50 μm.

3.4.2 Confirmation of C7 protein production in gene modified RDEB cells by Western blot

To further confirm whether the C7 protein expressed by the LV-COL7 transduced RDEB keratinocytes and fibroblasts was formed and secreted as full-length C7, cell lysates and culture media from the transduced RDEB cells were subjected to SDS-PAGE under reducing conditions for separation of C7 in its monomeric form. The full-length C7 monomer of 290 kDa was further detected by Western blot analysis (see Methods 2.2.33).

3.4.2.1 Antibody specificity against full-length C7 protein

Three polyclonal antibodies detecting C7, two of which were sourced commercially (Calbio-C7-pAb and purified C7-pAb) and one kindly provided by Prof. M. Chen (C7-Chen) were tested for their specificity. Cell lysates from normal donor keratinocytes (WT) and untransduced (UT) RDEB EBKCs were used to evaluate the specificity, and examine possible background staining and non-specific banding. All three antibodies were shown to specifically detect full-length C7 at 290 kDa in WT cells, with no corresponding band could be visible in UT RDEB EBKCs **(Figure 3.9)**. However, the Calbio-C7-pAb antibody displayed besides the C7 290 kDa band, a high frequency of additional larger and smaller non-specific bands on the immunoblot.

The purified C7-pAb on the other hand, showed greatly reduced non-specific banding when compared to the Calbio—C7-pAb, with the major additional band appearing at ~150 kDa in all samples **(Figure 3.9)**. The C7-Chen antibody was an affinity-purified polyclonal antibody against the NC-1 domain of C7 and when assessed by Western blot, showed a clear highly specific band at 290 kDa in WT keratinocytes. However, upon high protein loading, a small number of faint bands were also visible with the most distinct one at 150 kDa similar to the Calbio-C7-pAb and purified C7-pAb. The untransduced RDEB EBKC sample though revealed a complete absence of any bands **(Figure 3.9)**. Background staining in all three antibodies was relatively low and did not interfere the results. Based on these findings, unless otherwise specified, the C7-Chen antibody was used for further studies.

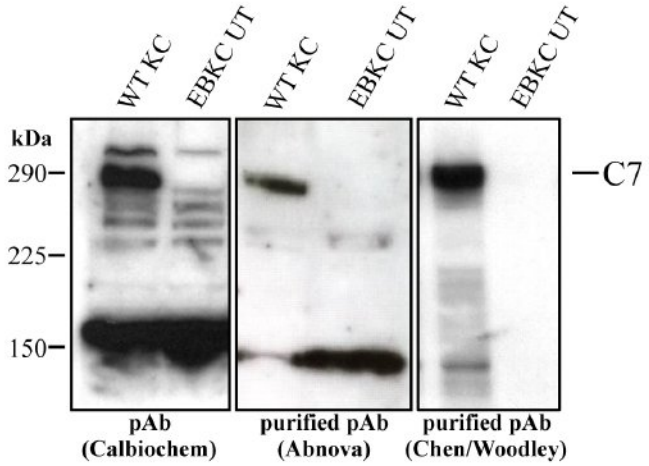

Figure 3.9 Antibody assessment for detection of C7 expression in WT and RDEB keratinocytes.
Cell pellets from WT or RDEB EBKC keratinocytes were harvested and lysed under reducing conditions and subjected to 6% SDS-PAGE. Blots were probed with either of three antibodies; Calbio-C7-pAb (Calbiochem); purified C7-pAb (Abnova); or Chen-C7 (Chen/Woodley) for detection of C7 expression at 290 kDa. All three antibodies recognised the full length C7, with the Chen-C7 showing the highest specificity for the protein and least amount of non-specific banding. These blots are representations of a single experiment.

3.4.2.2 Expression of full-length C7 in LV-COL7 transduced RDEB keratinocytes

LV-COL7-mediated restoration of C7 was initially assessed in the RDEB EBKC keratinocyte cell line for evaluation of C7 expression and durability. Western blot analysis of cell lysates of LV-COL7 transduced RDEB EBKCs revealed full-length C7 protein detected at 290 kDa, expressed at similar levels to those of endogenous C7 in WT cells. The corresponding band was entirely absent in untransduced RDEB EBKCs, indicating protein restoration in LV-COL7-transduced cells **(Figure 3.10 left panel)**. Expression in the transduced RDEB EBKCs appeared

to remain stable over a 22-day period during which time the cells underwent 7 passages. As C7 is a secreted protein, culture media was also harvested from LV-COL7-transduced RDEB EBKCs 13 days post-transduction. The cells were cultured in the absence of serum but with the supplementation of ascorbic acid for a 48-hour period prior to harvesting the media, previously shown to promote C7 secretion (Titeux et al., 2010). Culture media from untransduced RDEB EBKCs and a normal keratinocyte cell line (NIKS) were used as controls. The media samples were concentrated by protein precipitation prior to running on Western blot under reducing conditions. Strong full-length C7 expression was detected in the media samples of both LV-COL7-transduced and NIKS cells **(Figure 3.10 right panel)**. Protein loading per well was normalised by Bradford assay allowing for the addition of equal protein amounts of each sample. In addition, the consistently appearing non-specific ~150 kDa band when staining with all anti-C7 antibodies was used as an internal indicator of sample loading in cases where staining of endogenous housekeeping protein was not available.

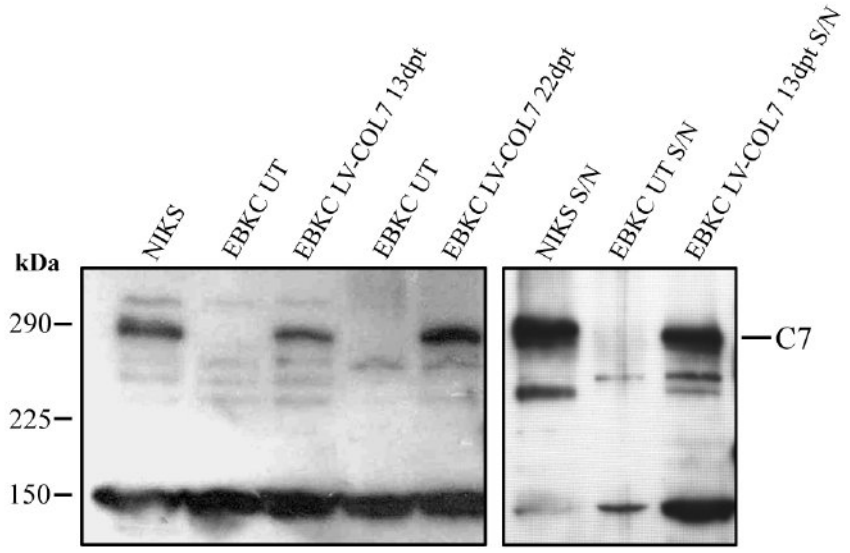

Figure 3.10 Expression of C7 in cell lysate and culture media of RDEB keratinocyte line post LV-COL7 transduction.

RDEB EBKC keratinocyte cell line was transduced with LV-COL7 and assessed for C7 expression over time in cell lysate and culture media supernatant (S/N) by Western blot on 6% SDS-PAGE. (**Left**) C7 expression detected at 290 kDa in cell lysates show of WT keratinocyte cell-line (NIKS) and RDEB EBKC LV-COL7 keratinocytes at days 13 and 22 days post transduction (dpt). There was no C7 seen in RDEB EBKC untransduced (UT) cells. **(Right)** culture media S/N after ascorbic acid supplementation (50 μg/ml) and serum starvation for 48 hrs show C7 expression at 290 kDa only in NIKS and RDEB EBKC LV-COL7. Protein loading was normalised by Bradford assay. The results show long-term C7 expression in LV-COL7 transduced RDEB EBKC cell lysates and supernatants. Immunoblot was stained with Calbio-C7-pAb.

Following the assessment of the keratinocyte cell line, primary RDEB patient (BT) keratinocytes were next evaluated for C7 expression by Western blot **(Figure 3.11 left)**. The results revealed strong C7 expression in the LV-COL7-transduced RDEB (BT) keratinocytes with a similar band intensity level to that of normal donor keratinocytes. As a transduction control, LV-COL7-transduced RDEB EBKCs were used alongside **(Figure 3.11 left)**. However, the RDEB (BT) untransduced keratinocytes also showed strong expression of a protein band at 290 kDa band which corresponded to C7 **(Figure 3.11)**. As this patient according to the genotype data carries two heterozygous mutations, with one causing an amino acid change in exon 70 (p.Arg1933Gln) and the other a PTC in exon 114 (p.Arg2814X) it is therefore possible that full-length C7 is expressed from one allele and detected by the C7-Chen antibody specific to the early NC-1 domain of C7. Furthermore the late stage mutation in the other allele resulting in truncation of a few amino acids may also be detected as there would be a minimal difference in overall protein size. Subsequent *in vivo* experiments using untransduced patient (BT) cells were carried out to confirm the functionality of the C7 protein detected through formation of AFs. Primary fibroblast cell lysate of the same RDEB patient (BT) was run alongside to detect whether a similar phenomenon occurred **(Figure 3.11 right)**. The immunoblot showed the presence of a faint band at 290 kDa corresponding to C7, albeit at much lower levels to that seen in normal donor fibroblasts or RDEB (BT) keratinocytes suggesting detection of the endogenous mutant C7.

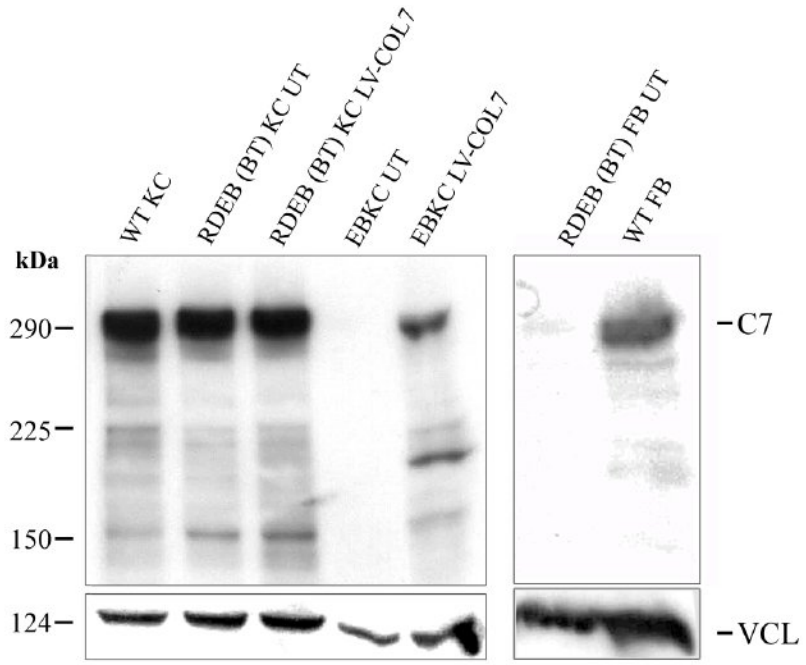

Figure 3.11 C7 expression in primary RDEB patient (BT) keratinocytes and fibroblasts.
Primary keratinocyte (KC) and fibroblast (FB) cell lysates from RDEB patient (BT) either untransduced (UT) or LV-COL7 transduced were assessed for C7 expression by Western blot on 6% SDS-PAGE. **(Left)** There was C7 protein detected at 290 kDa in the positive primary normal donor keratinocyte control WT KCs and LV-COL7 transduced RDEB EBKC but not in the untransduced (UT) RDEB EBKC negative control. Strong expression of full-length C7 was detected in both UT and LV-COL7 transduced primary patient (BT) keratinocytes. **(Right)** A faint band corresponding to C7 at 290 kDa was seen in UT RDEB patient (BT) fibroblasts, compared to the strong expression detected in primary WT positive control fibroblasts. Protein loading was normalised by Bradford assay. Vinculin (VCL) was used as an internal loading control. These are representative blot images of duplicate experiments.

3.4.2.3 LV-COL7 mediated C7 restoration in gene modified primary RDEB fibroblasts

The expression of full-length C7 was next evaluated in LV-COL7-transduced primary RDEB patient (CK and EB8) fibroblast cell lysates and culture media by Western blot with the untransduced cells used as negative controls. The results confirmed expression of full-length C7 at 290 kDa in both transduced patient cells transduced with an MOI of 5 or 10 of LV-COL7 with protein levels similar to those of normal donor endogenous C7.

There was no significant difference in C7 expression upon doubling of the MOI. Apart from the major full size C7 protein band, there were multiple smaller protein bands detected on the immunoblot, likely the result of increased protein loading. No detectable bands were observed in untransduced cell lysates **(Figure 3.12 A)**. Secreted full-length C7 expression was also assessed in media harvested from the culturing of cells. The results confirmed the presence of C7 protein secreted from the LV-COL7-transduced RDEB (CK) fibroblasts although it appeared

as three similarly sized bands slightly smaller than 290 kDa possibly caused due to degradation during sample processing **(Figure 3.12 B)**.

The results therefore confirmed that the C7 expression seen by *in situ* immunofluorescence staining corresponded to full-length 290 kDa C7 as detected by Western blot analysis of both primary RDEB keratinocytes and fibroblasts transduced with LV-COL7.

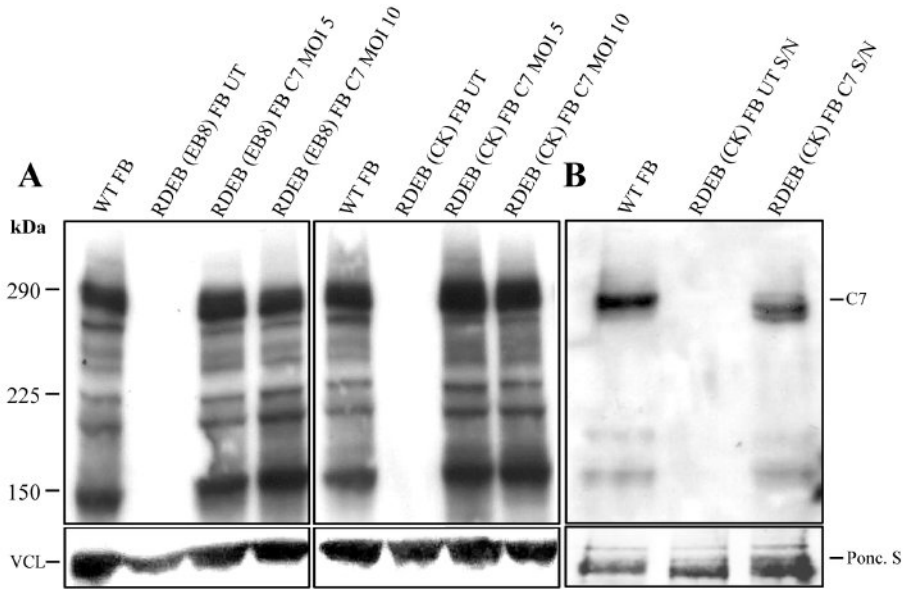

Figure 3.12 Restoration of protein expression in RDEB patient (EB8) & (CK) fibroblasts following LV-COL7 transduction.
Primary RDEB patient fibroblasts from patients (EB8) and (CK) were transduced with LV-COL7 at MOI 5 or 10 and assessed for C7 expression 2 weeks post transduction by Western blot of cell lysates and culture media supernatant (S/N) run on a 6% SDS-PAGE. **(A)** Reconstitution of C7 expression visualised at 290 kDa in both LV-COL7 transduced patient (EB8) and (CK) fibroblasts and both MOIs as well as in positive control normal donor primary WT fibroblasts. Complete absence of C7 expression in both RDEB patient (EB8) & (CK) untransduced samples. Loading was normalised by Bradford assay and vinculin used as internal loading control. **(B)** Detection of extracellular C7 expression in S/N of LV-COL7 transduced RDEB (CK) and WT fibroblasts. No protein band seen in RDEB (CK) UT S/N sample. Protein loading was normalized by Bradford assay and membrane counterstained in Ponceau S stain as loading control. The results demonstrate restoration of C7 expression in primary patient fibroblasts transduced with LV-COL7. These are representative blot images of duplicate experiments.

Due to the relatively low viral titres of LV-COL7 (~$5x10^6$ TU/ml), large volumes of the viral preparation are required for the transduction of cells with a meaningful MOI which can in turn lead to vector related cytotoxicity. Typically, the viral suspension volume did not exceed the 10% total culture volume. In an attempt to increase transduction efficiency while at the same time avoiding potential cytotoxicity, the viral dose was divided and used to transduce RDEB

patient (BT) fibroblasts at two instead of a single time point. RDEB (BT) fibroblasts were exposed to either a single or a double round of infection with LV-COL7 maintaining the total MOI at 2 and propagated for a period of 62 days. Cell lysates collected at three different time points (32, 42 and 62 days) were assessed for C7 expression by Western blot and qPCR-based pro-viral copy number. Transduction efficiency calculated by VCN/cell at 3 days post-transduction was shown to be 6.19% in cells infected with two rounds of virus, compared to 3.55% after a single time point. These results were corroborated by Western blot pointing towards a slight increase of C7 expression in RDEB fibroblasts transduced with two rounds of LV-COL7 at all three collection time points over those infected with a single dose albeit at a total MOI of 2 in both cases **(Figure 3.13)**. This is most likely due to the use of a lower volume of viral supernatant on the cells, minimising possible adverse effects on proliferation and vector related cytotoxicity. Furthermore, there was no notable decrease of C7 expression in the transduced cells over the 2-month culture period suggesting stable and constitutive transgene expression mediated by the PGK promoter **(Figure 3.13)**.

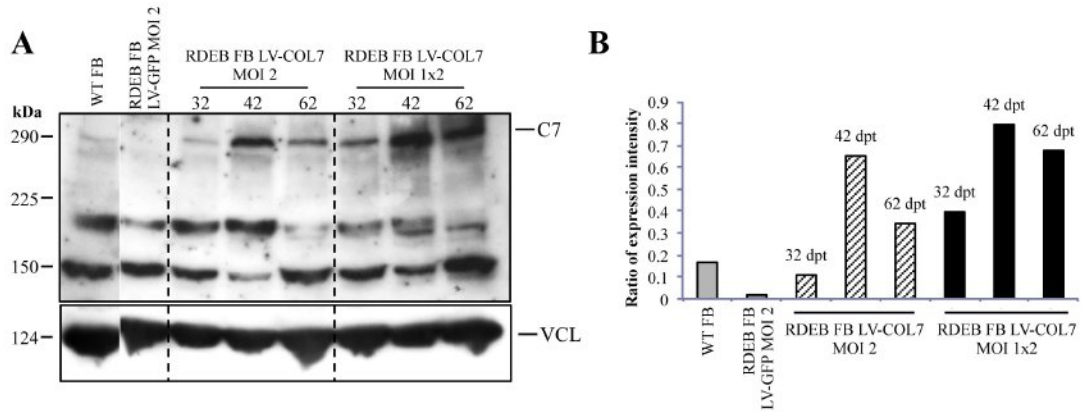

Figure 3.13 Durability of C7 expression in RDEB corrected fibroblasts *in vitro*.
Primary patient (BT) fibroblasts were transduced with a single or double round of LV-COL7 and assessed for protein expression and durability over 62 days by Western blot. **(A)** C7 protein band detected at 290 kDa of normal donor primary WT and RDEB (BT) fibroblast cell lysates harvested at 32, 42 and 62 days post transduction (dpt) with LV-COL7 at single (MOI 2) or double (MOI 1x2) round of transduction. No expression seen in LV-GFP (MOI 2) transduced RDEB (BT) fibroblast negative control. Immunoblot was stained using Calbio-C7-pAb. Vinculin (VCL) used as internal loading control. **(B)** Densitometry of C7 bands from Western blot image using ImageJ pixel intensity analysis confirms slight increase in C7 expression when a double round of transduction is carried out over single at a total MOI of 2 in all three harvest dates. These are representative blot images of a single experiment.

3.5 Functional correction in LV-COL7 transduced RDEB keratinocytes and fibroblasts

3.5.1 Improved cell migration in RDEB keratinocytes transduced with LV-COL7

Lack of C7 expression has been associated with functional alterations such as changes in cell migration and invasion compared to normal human keratinocytes thought to be due to aberrant laminin-332 organisation altering α6β4 signaling, caused by lack of C7 protein deposition (Murauer et al., 2011, Martins et al., 2009, Nystrom et al., 2013, Woodley et al., 2008, Chen et al., 2002). *In vitro* cell migration assays offer a way to evaluate the propensity and closure speed of an artificially created wound. Several cell migration assays have been previously developed for the functional assessment of C7 loss in RDEB keratinocytes and with an adaptation of a 2D scratch assay utilised in this study (Martins et al., 2009) (see Methods 2.2.34).

Normal donor keratinocyte, untransduced or LV-COL7-transduced RDEB EBKCs were plated at a concentration of $1.2x10^6$ cells/well in a 6 well plate format and a scratch was made through the centre of the well to create a "wound" area. Cell migration and closure of the wound area was monitored by time-lapse imaging over 15 minute intervals for 35 hrs and calculated by measuring the unoccupied surface area of the well after setting a threshold on the edges of the scratch **(Figure 3.14)**. All cells were pre-treated with the DNA crosslinker mitomycin C at 10 μg/ml for 2 hrs to ensure the sole measurement of migration while eliminating the cell proliferation variable.

The migration values revealed a significant level of variation amongst the three groups ($p \leq 0.01$), with complete wound closure completed within 15-35 hrs. Multiple comparison analysis showed a significant decrease in wound closure in untransduced RDEB EBKC cells with a large portion of the scratch still remaining unoccupied after 35 hrs, compared to WT healthy keratinocytes which filled the open wound space entirely within 15 hrs ($p \leq 0.001$) **(Figure 3.14 A & B)**. A lag in migration speed compared to the WT healthy keratinocytes was noticed during the initial 5 hr period in both untreated and gene-corrected RDEB EBKC cells. However, throughout the remaining period, the LV-COL7-transduced RDEB EBKCs showed a significant acceleration in migration speed compared to the untransduced cells ($p \leq 0.05$) although with complete scratch closure only achieved at 25 hrs, it was significantly slower than WT cells ($p \leq 0.05$) **(Figure 3.14 A & B)**. The data therefore suggest a partial functional recovery in the RDEB EBKCs following LV-COL7 transduction as a result of the vector-mediated C7 expression.

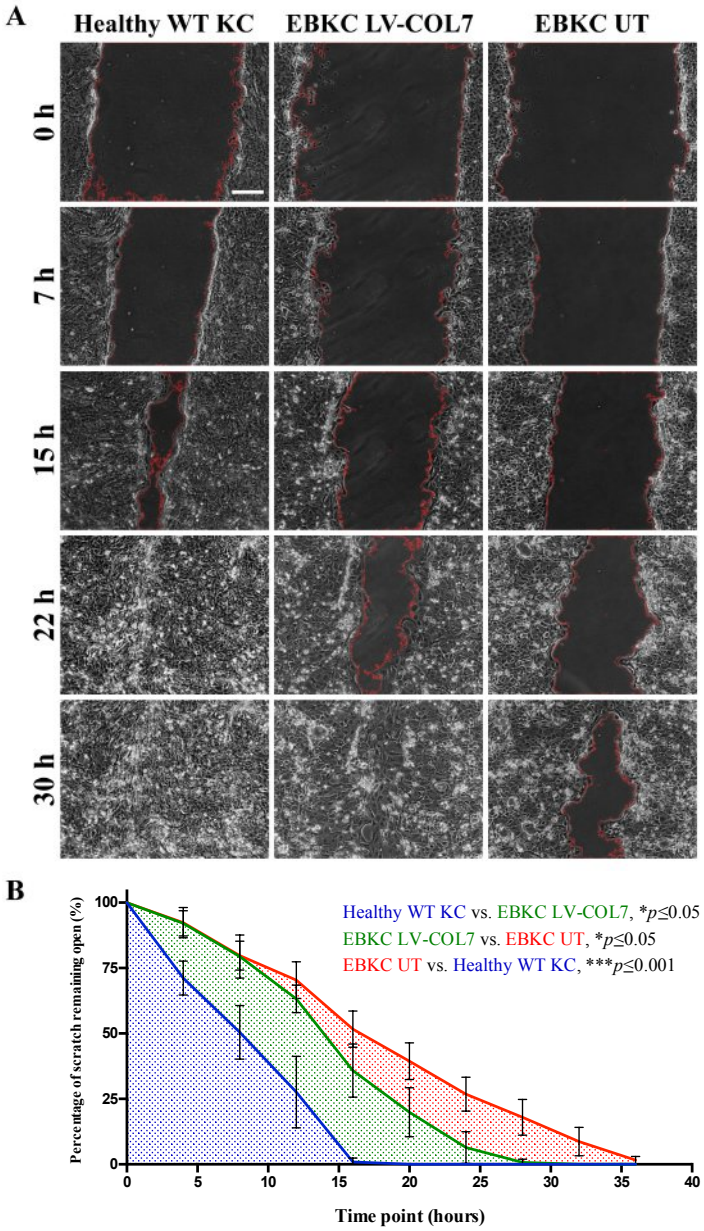

Figure 3.14 Effect on RDEB keratinocyte migration following restoration of C7 protein expression. Primary healthy WT donor, RDEB EBKC transduced with LV-COL7 and untransduced RDEB EBKC (UT) keratinocytes were seeded in a 6-well plate, treated with mitomycin C to halt proliferation and a scratch was made to compare cell migration over 35 hrs at 15-min intervals by time-lapse microscopy. **(A)**. RDEB EBKC UT cells show reduction in cell migration speed over healthy WT cells with scratch zone still open by 30 hrs. RDEB EBKCs transduced with LV-COL7 demonstrate intermediate cell migration speed with scratch closure by 25 hrs. Scale bar = 300 µm. The values of percentage closure calculated using a custom macro on ImageJ measuring proportion of empty space within the edges set by a threshold, were plotted against imaging time points over a 35 hr period (mean±SD, n=3). Statistical analysis was carried out on values collected from 5 – 35 hrs. The area under the curve (AUC) was calculated for each replicate of the 3 samples and their means were compared by one-way ANOVA and found to be significant between the groups (**$p \leq 0.01$). Tukey's post-test was used for multiple comparison analysis within the group and showed percentage of scratch closure was increased in RDEB EBKC transduced with LV-COL7 compared to UT EBKC *(*$p \leq 0.05$), although still lower than that of WT keratinocytes (*$p \leq 0.05$).

3.5.2 Normalisation of RDEB fibroblast migration following correction by LV-COL7

In vitro functional recovery was next evaluated in primary RDEB patient (CK) and (EB8) fibroblasts using the cell migration assay previously described (Syed et al., 2013) (see Methods 2.2.35). Both untransduced and LV-COL7-transduced fibroblasts were seeded at a density of $4x10^4$ cells/well in a 96-well plate containing a cell seeding stopper occupying a 2 mm area in the centre of each well. 24 hrs post seeding, the cells were treated with mitomycin C at a concentration of 10 μg/ml for 2 hrs before the stoppers were removed exposing the artificially created migration zone. The cells were continuously cultured for 72 hrs and were then fixed, counterstained with DAPI and imaged. The number of cells within the 2 mm migration zone were quantified and plotted against each other **(Figure 3.15 A & B)**.

The results demonstrated that untransduced patient (CK) fibroblasts exhibited a noticeable reduction in migration speed compared to WT healthy cells ($p \leq 0.01$) displaying a similar pattern in "wound" closure to that seen previously in the RDEB EBKC keratinocyte data. Upon transduction of the RDEB (CK) fibroblasts with LV-COL7, a significant improvement in migration speed over the untransduced sample was observed ($p \leq 0.05$) suggesting functional recovery by attaining a similar migration rate to that of in WT donor cells ($p > 0.05$).

However the migration rate of RDEB (EB8) fibroblasts revealed an inverse response RDEB (CK), with an increased migration speed of untransduced cells compared to WT donor cells ($p \leq 0.05$). Following LV-COL7 transduction though, the number of cells detected in the migration zone was reduced compared to those in the untransduced sample ($p \leq 0.05$) with normalisation of the (EB8) cell migration rate exhibiting comparable speeds to those of WT donor cells ($p > 0.05$). This points towards patient-to-patient variation with normalisation of migration speed following LV-COL7 transduction in both patients' cells.

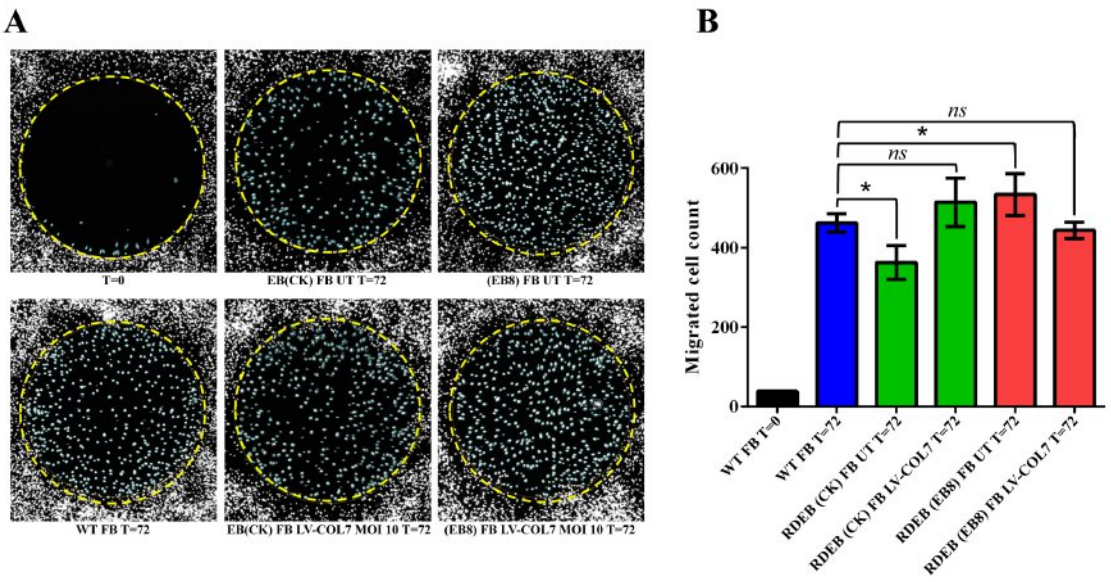

Figure 3.15 Effect of loss and restoration of C7 expression on RDEB patient (CK) and (EB8) fibroblasts.

Primary RDEB patient (CK) and (EB8) fibroblasts either untransduced or following LV-COL7 transduction were assessed for cell migration alongside normal donor fibroblasts. Cells were seeded in a 96-well plate with 2 mm stoppers and treated 24 hrs later with mitomycin C for 2 hrs halting proliferation. Stoppers were removed and cells were continuously cultured for 72 hrs and then fixed and counterstained with DAPI. The migration zone was imaged at 0 hrs (T=0) and after 72 hrs (T=72). The number of cells within the migration zone were quantified and plotted against each other. One-way ANOVA analysis comparing the RDEB (CK) group and WT fibroblasts or RDEB (EB8) group and WT fibroblasts showed significant variation in the values in both cases (**$p \leq 0.01$) and (*$p \leq 0.05$). Tukey's post-test showed a decreased migration rate in UT RDEB (CK) fibroblasts compared to WT fibroblasts ($p \leq 0.01$) but regained migration speed after cells were transduced with LV-COL7 ((A) upper panel, (B) green bars with normalisation to WT levels (ns $p > 0.05$)). Increased migration was observed in UT RDEB (EB8) fibroblasts compared to WT donor cells (*$p \leq 0.05$), which decreased back to a similar speed to that of donor cells after LV-COL7 transduction ((A) lower panel, (B) red bars (ns $p > 0.05$)).

There has been conflicting evidence published regarding the effect on migration speed following loss of C7 protein. Although a previous study (Chen et al., 2002) has reported a significant increase in *COL7A1* deficient RDEB cells measured by an *in vitro* colloidal gold assay, more recently published reports revealed an inverse effect whereby wounds generated on RDEB mouse models showed delayed re-epithelialisation and maturation of the granulation tissue (Nystrom et al., 2013). This disparity was noticed in the data generated in this study. The cause of variation amongst individual patients remains unknown. However, the results obtained from both RDEB EBKC keratinocytes and RDEB (CK) and EB8 fibroblasts clearly point towards functional improvement of the RDEB phenotype following LV-COL7 transduction confirmed by the normalisation of migration rates.

3.6 Discussion

This work has demonstrated a feasible strategy for the restoration of C7 expression and function in RDEB cells by a viral vector-mediated gene addition/replacement approach. This was achieved by the design and production of a state-of-the-art clinically-compliant 3rd generation SIN lentiviral vector based on HIV-1, stripped of virulence factors and with packaging and nuclear import accessory proteins delivered *in trans*, therefore eliminating the potential of generating replication competent lentiviruses. Within this system the codon optimised *COL7A1* cDNA transgene, was packaged and delivered to RDEB patient keratinocyte and fibroblast cells. Use of degenerate codons throughout the transgene was employed for the removal of major cryptic splice sites and minimisation of repetitive sequence predominantly found in the triple-helical collagenous coding region of *COL7A1*. This can otherwise have a deleterious effect on C7 expression through transgene rearrangement during viral packaging and aberrant splicing of the expressed protein, with a reported detection of 25-33% of abnormal C7 in retrovirally transduced RDEB keratinocytes and fibroblasts (Titeux et al., 2010).

Concentrated batches of therapeutic lentiviral vectors carrying a functional copy of *COL7A1* were produced and confirmed for their infectivity resulting in a modest titre of ~5x10^6 TU/ml. The infectivity range however was 2-log lower than that of the LV-GFP vector. The most plausible explanation for the variation between the viral titres is the increased size of the *COL7A1* transgene hampering its packaging into functional lentiviral particles having a maximal transgene capacity of 8-9 kb (Siprashvili et al., 2010, Titeux et al., 2010). This was further corroborated by p24 levels of the LV-COL7 viral preparations, demonstrating a 10-15 fold higher physical titre when compared to the functional titre obtained from titration on HEK-293Ts. This however may also be a result of sequences within the transgene resulting in aberrant splicing of primary transcripts (Moiani et al., 2012).

However, restoration of the otherwise null C7 expression was achieved following LV-COL7 transduction of the *COL7A1*-deficient patient keratinocyte and fibroblast populations using a range of MOIs of 2-10 exhibiting robust and sustained over-expression of the *de novo* full-length C7 protein. Moreover, from the immunoblots presented, there was no immediate evidence of truncated C7 protein expressed in the transduced cells suggesting the advantage of codon optimisation. Expression levels in the transduced cells superseded those of endogenous C7 of WT cells mediated by the strong constitutive activity of the PGK promoter demonstrated by both *in situ* immunofluorescence staining

and Western blot, despite transduction efficiency not exceeding ~25%, presumably owed to the low vector titre and the resilient nature of primary keratinocytes to infection. Limited by the maximum viral supernatant volume used during transduction having to fall below 10% of the total culturing volume, use of a high MOI would not be feasible as a means of compensating for the reduced titre as it is associated with a high-level of cytotoxicity. Instead, dividing the viral dose over two time points as demonstrated in primary RDEB fibroblasts, resulted in a slightly increased transduction efficiency measured by C7 expression while ensured a reduction in the viral load. Alternatively, an indirect method for the improvement in the percentage of LV-COL7 transduced cells, would be the incorporation of a selectable surface marker co-expressed with *COL7A1*. This would permit for the enrichment of gene-corrected clones thereby circumventing the requirement of a high, potentially cytotoxic MOI.

Furthermore, cell migration assays also demonstrated that following LV-COL7 transduction of RDEB cells, the impaired migration rates were normalised in both keratinocytes and fibroblasts, indicating functional recovery due to restoration C7 expression.

It is believed that the observed C7 over-expression may be sufficient in providing functional restoration in skin. Both gene-modified keratinocytes and fibroblasts were subsequently used in *in vivo* experiments delineated in the following chapter to ultimately assess whether the restoration achieved *in vitro* could achieve meaningful reversion of the RDEB phenotype.

Chapter 4 Functional evaluation of gene modified RDEB cells in *in vivo* human:murine chimeric skin graft model

Following confirmation of C7 protein expression and recovery of migration in RDEB cells transduced with LV-COL7 vector *in vitro,* the functional restoration of C7 as assessed by its ability to form AFs at the DEJ thereby ameliorating the RDEB-associated blistering and separation phenotype was examined. Previous studies have suggested that C7 expression levels as low as 10% of normal endogenous levels reported in some RDEB patients were sufficient for the formation of rudimentary AF structures conferring a certain level of attachment and blistering amelioration (Wagner et al., 2010, Fritsch et al., 2008). Added to the slow turnover of C7 protein, it could be argued that even a low proportion of corrected RDEB keratinocytes and/or fibroblast overexpressing C7, may be adequate in providing a therapeutic and long-lasting effect by restoring adhesion at the DEJ. Therefore, despite the modest LV-COL7 transduction efficiency of 18% in keratinocytes and 12% in fibroblasts, it was expected that C7 expression would be visualised *in vivo* and present with a certain degree of functional amelioration.

Although *Col7a1*$^{-/-}$ mice have previously been generated by others (Fritsch et al., 2008, Heinonen et al., 1999), these strains have a limited lifespan and are unsuitable to address whether LV-COL7-transduced human fibroblasts and keratinocytes can confer functional correction and restore dermal-epidermal integrity *in vivo*.

In this study, a pre-clinical human:murine chimeric skin graft model was used. This model was developed based on a previously described method (Larcher et al., 2007) which allows for the grafting of a bioengineered skin equivalent (SE) comprised of human keratinocytes and fibroblasts onto immunodeficient mice giving rise to full-thickness human skin. Optimisation of the model by altering the recipient mouse strain was also assessed in this study to evaluate whether this could lead to an increased grafting success rate. Rigorous assessment to confirm the human origin of the grafted tissue and the ability of the epithelial cells to progress through a normal differentiation cycle was also carried out. This method therefore allowed for the development of a robust *in vivo* RDEB disease model recapitulating the skin blistering phenotype in which the proposed autologous gene correction strategy could be tested. This was executed by replacing unmodified RDEB keratinocytes and/or fibroblasts during preparation of the bioengineered SEs with LV-COL7 gene-corrected cell combinations. The grafts were primarily assessed for the deposition of C7 at the DEJ secreted from the gene corrected cells using immunofluorescence analysis, while the functionality of C7, evaluated by its capacity to

form fully functional AFs and ultimately restore adhesion to the DEJ, was investigated by morphological and ultrastructural imaging.

4.1 Histological features of bioengineered human skin grafts

4.1.1 Identification of the human skin graft and distinction from mouse tissue using human-specific tissue markers

Prior to testing the pre-clinical RDEB mouse model, unique markers permitting the distinction between the human and mouse skin structure of the grafts were identified and tested.

Skin samples from a healthy human donor and a mouse were embedded in OCT and 7 μm thick frozen sections were obtained. Firstly, tissues were stained with haematoxylin and eosin (H&E) for the morphological examination of the skin. An easily distinguishable thicker epidermal compartment was observed in human tissue with multiple tightly organised cell layers. The lower compartment comprised of larger and more spherical basal keratinocytes formed the apical side of the basement membrane zone (BMZ) whereas differentiating keratinocytes formed the *stratum spinosum* and *granulosum* located the intermediate epidermal compartments and terminally differentiated keratinocytes made up the *stratum corneum* in the uppermost epidermal compartment lacking a nucleus and flatter in morphology **(Figure 4.1 a)**. Mouse epidermis on the contrary, appeared very thin with 2 to 3 layers of keratinocytes and a less pronounced cornified layer **(Figure 4.1 b)**. Furthermore a higher density of hair follicles could be seen in the murine epidermis compared to human skin.

Subsequently, species-specific antibodies for the detection of human mitochondrial (MTCO2) and desmosomal (Desmoglein-1) proteins were further used for identification of the human origin of the skin and distinction from mouse tissue. Immunofluorescence staining for MTCO2 revealed intense cytoplasmic staining of the entire epidermis and of dermal fibroblasts in human tissue **(Figure 4.1 c)**. In contrast, there was no such staining in the mouse epidermis, although faint signal was detected at the section edge and surrounding the hair follicles from autofluorescence from the 2^{ry} antibody **(Figure 4.1 d)**. Desmoglein-1 staining showed strong expression in the human epidermis with a membranous localisation of the staining, whereas no such staining pattern was observed in mouse tissue **(Figure 4.1 e, f)**. These results suggested the distinction between human and mouse skin can be robustly recognised using a combination of epidermal cyto-architectural staining of the epidermis by H&E, and by species-specific mitochondrial and desmosomal staining.

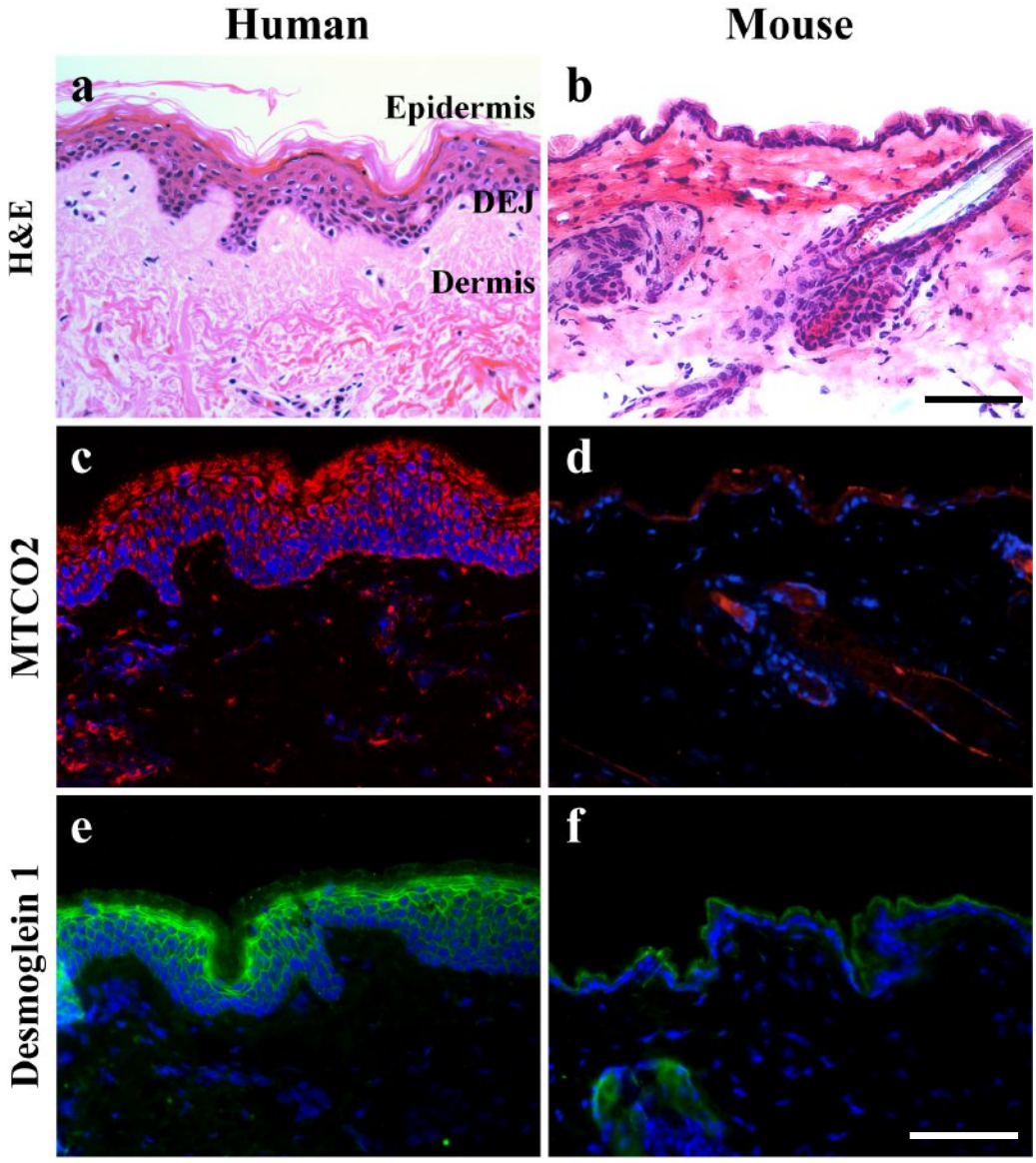

Figure 4.1 Morphological staining of skin by H&E and species-specific antibodies differentiates between human and mouse tissue.

Biopsies from healthy human **(a, c, e)** or WT mouse **(b, d, f)** were cryo-sectioned at 7 μm thickness and stained by H&E for morphological assessment and IF for human proteins: complex IV subunit II mitochondrial marker (MTCO2) and desmoglein-1. Histological staining shows distinct multilayered thick epidermis in human skin **(a)** compared to a thin epidermal layer populated by hair follicles in mouse skin **(b)**. There was positive staining for MTCO2 (red) in human epidermal keratinocytes and dermal fibroblasts **(c)**, with no staining following a similar pattern in mouse tissue **(d)**. Desmoglein-1 staining (green) showed positive signal in the *stratum granulosum* of the human epidermis **(e)**, but not in mouse tissue **(f)**. Nuclei were stained with DAPI (blue). Scale bar = 100 μm.

4.1.2 Detection of human C7 protein in bioengineered human grafts

A series of commercially available antibodies against C7 were tested in search of a highly species-specific option for the accurate determination of the human origin of C7 **(Figure 4.2)**. Both human and mouse tissue were stained with 8 separate antibodies against C7 by immunofluorescence and the results were analysed. 4 antibodies showed positive staining at the DEJ (Calbio-C7-pAb, mAb-C7-LH7.2 and C7-Chen) including SantaCruz sc8928 displaying faint staining. The Calbio-C7-pAb and C7-Chen antibodies detected both human and mouse C7 protein due to recognition of homologous epitopes and were therefore not used for the study. In contrast, mAb-C7-LH7.2 showed strong and defined staining at the DEJ of human skin with no cross-reactivity to mouse C7 **(Figure 4.2)**.

The mAb-C7-LH7.2 antibody was further tested in human and mouse tissue from separate donors and similar results were obtained showing strong signal localisation of C7 at the DEJ and with weaker punctate cytoplasmic staining of dermal fibroblasts. In contrast, no such staining was observed in mouse skin **(Figure 4.3)**. These results confirmed the mAb-C7-LH7.2 antibody specificity showing no cross-reactivity between human and mouse tissue **(Figure 4.3)**. The antibody was therefore utilised for all subsequent immunofluorescence staining for the detection of human C7 expression.

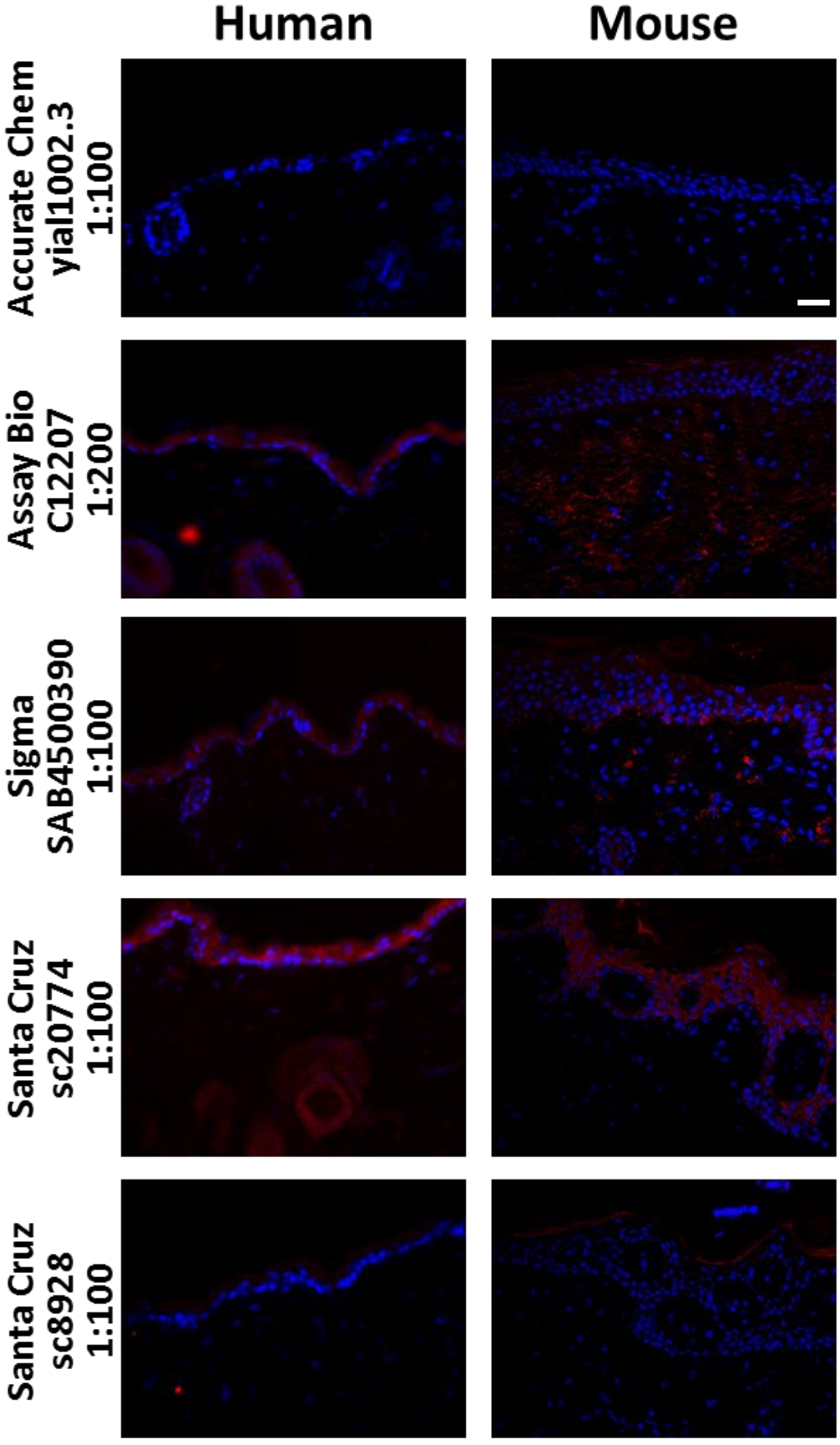
Human
Mouse
Accurate Chem
yial1002.3
1:100
Assay Bio
C12207
1:200
Sigma
SAB4500390
1:100
Santa Cruz
sc20774
1:100
Santa Cruz
sc8928
1:100

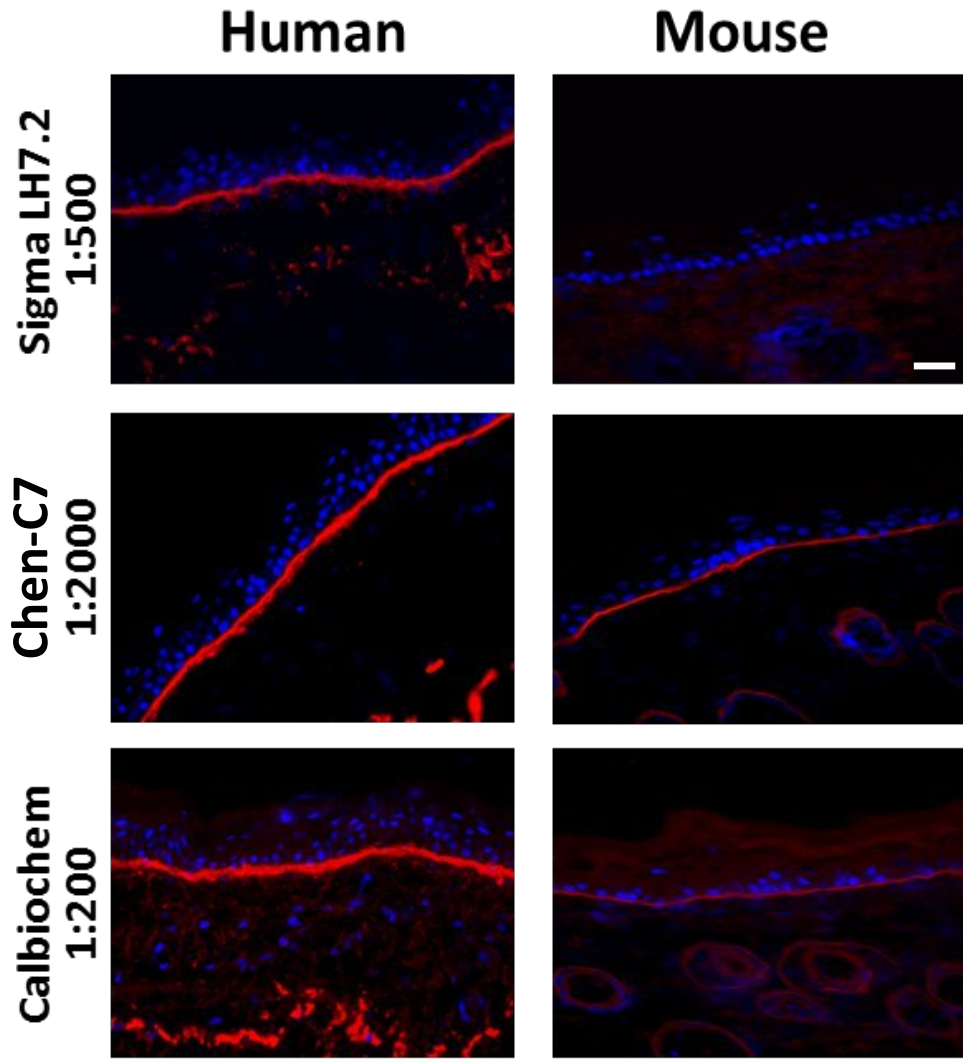

Figure 4.2 Detection of species-specific C7 expression in human and mouse tissue.
Evaluation of species-specific antibodies against C7 protein in human and mouse sample tissue using 8 antibodies, 7 were commercially sourced and 1 was from Prof. M. Chen. The top panel shows antibodies that exhibited limited or no detection of either human or mouse C7 at the DEJ (red). Background expression seen in 2nd, 3rd and 4th lanes, with diffuse staining of the epidermis. Bottom panel shows antibodies resulting in strong detection of C7 at the DEJ of human and mouse tissue. mAb-C7-LH7.2 was the only antibody to show human specific staining with no cross-reactivity to mouse C7. Scale bars = 100 μm.

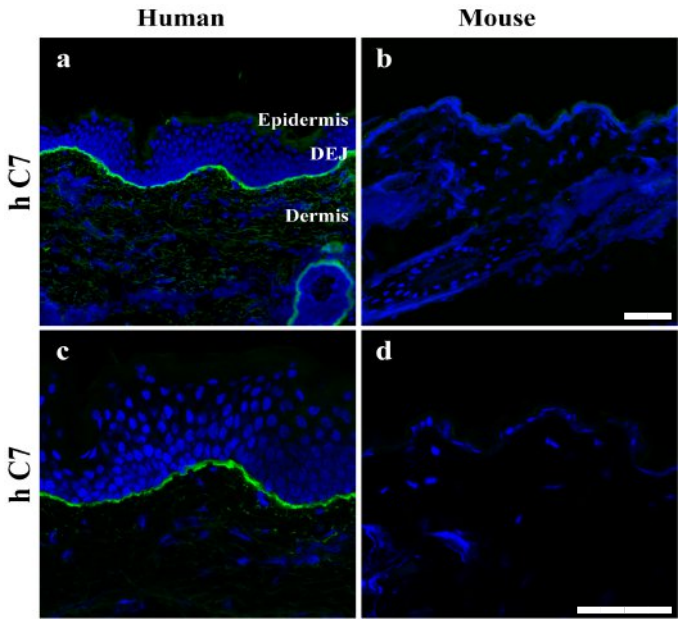

Figure 4.3 Human specific C7 recognition in skin using mAb-C7-LH7.2 immunofluorescent staining.

Healthy human donor **(left panel)** or mouse **(right panel)** 7 µm thick skin sections were stained against human C7 using mAb-C7-LH7.2 antibody and imaged at two different magnifications. Positive staining for C7 (green) is detected in human skin at the dermal-epidermal junction (DEJ) **(a, c)**. There was no staining in mouse skin, indicating no detection of mouse C7 or cross reactivity with mouse tissue **(b, d)**. Nuclei were stained with DAPI (blue). Scale bars = 100 µm.

4.1.3 Epidermal differentiation markers in human and mouse skin

To allow confirmation of the maturation of bioengineered human grafts on the human:murine chimeric mice models, verification of natural keratinocyte progression through all stages of differentiation was carried out. A panel of proliferation and differentiation markers were tested on healthy human skin, and compared to mouse skin **(Figure 4.4)**. The results showed strong expression of the early differentiation marker involucrin, localised within the *stratum granulosum* of human but not mouse tissue. **(Figure 4.4 a, b)**. Keratin intermediate filament marker, keratin 10, a protein mainly expressed in both *stratum spinosum* and *granulosum* was expressed in the uppermost suprabasal layers of the epidermis in the human skin, while mouse tissue exhibited autofluorescence at the tissue edge with a dissimilar signal localisation and expression pattern to human skin **(Figure 4.4 c, d)**. In addition, the cytoskeletal intermediate filament protein and marker of keratinocyte proliferation, keratin 14, showed strong expression in basal keratinocytes of the human skin with reduced intensity in the *stratum spinosum* and *granulosum*. Staining was also detected in the mouse epidermis and around the hair follicle **(Figure 4.4 e, f)**.

Taken together, these results indicate a clear morphological distinction and specific epidermal protein expression between human and mouse skin. The specific anti-human C7 antibody could furthermore provide robust and high quality staining, while a panel of differentiation markers was shown to successfully detect distinct keratinocyte *strata*. The above staining procedures and antibody combinations will therefore be used for distinguishing bioengineered human SEs from mouse tissue, evaluation of epidermal maturation and, ultimately, for the detection of the human origin of C7 expression.

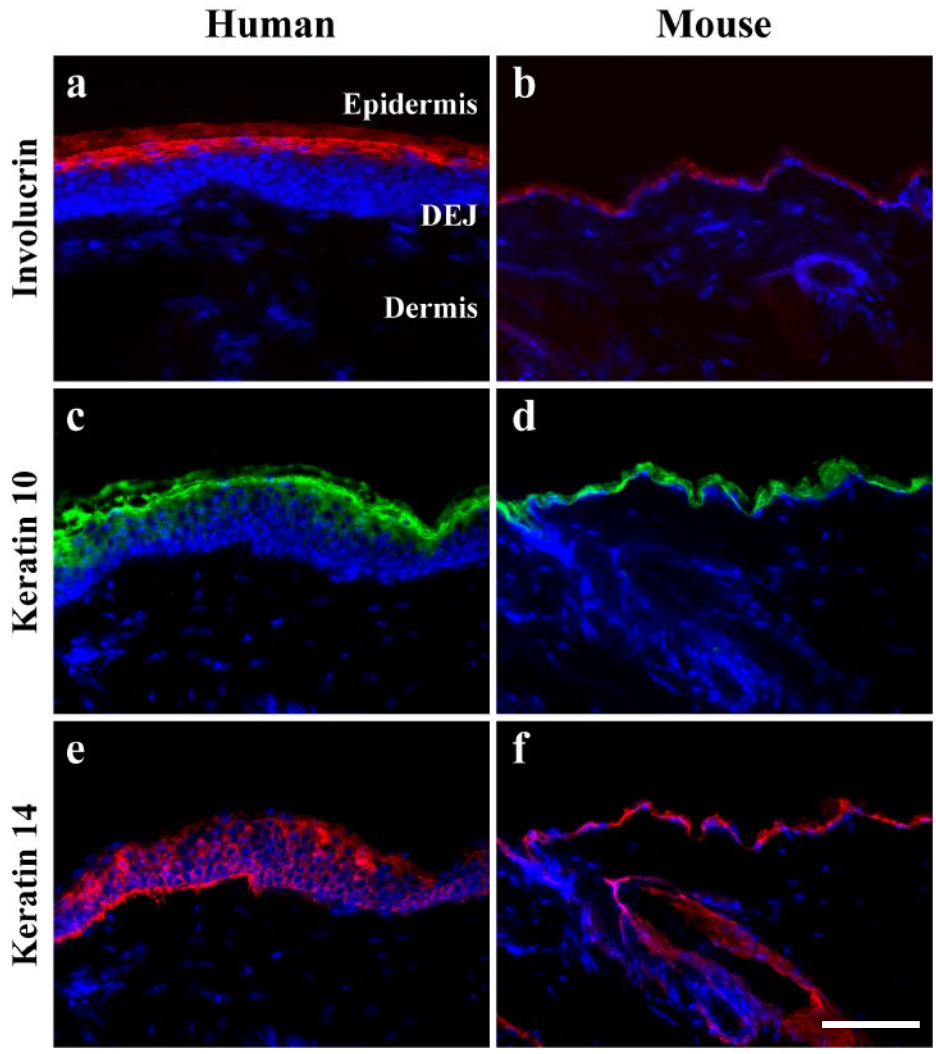

Figure 4.4 Epidermal maturation and differentiation markers in human and mouse tissue.
Healthy human donor (n=2) **(a, c, e)** and mouse (n=3) **(b, d, f)** skin tissue were sectioned at 7 µm thickness and stained with a panel of epidermal markers including early terminal differentiation marker involucrin **(a, b)** spinous layer specific keratin 10 **(c, d)** and basal cytokeratin marker keratin 14 **(e, f)**. Compartmentalised staining of all three epidermal proteins was seen in human skin while mouse skin demonstrates faint non-specific expression. Nuclei were stained with DAPI (blue). The images shown are from representative fields of multiple tissue sections. Scale bar = 100 µm.

4.2 Development of an *in vivo* pre-clinical RDEB human:murine chimeric skin graft model

4.2.1 Formation of bioengineered RDEB skin equivalents

For the *in vivo* assessment of vector-mediated functional correction, a robust RDEB mouse model recapitulating the disease characteristics was required. Since the *Col7a1*$^{-/-}$ knockout murine models available in Germany and the US are lethal, they would not be suitable for testing the gene therapy approach that we proposed. For this reason, a human:murine chimeric skin graft model using a nude NMRI-*Foxn1*^{nu} athymic mouse strain was selected to generate a pre-clinical gene therapy model for RDEB (Larcher et al., 2007). In this model, a bioengineered SE composed of normal donor or RDEB patient keratinocytes and fibroblasts either untransduced or transduced with LV-COL7 was grafted onto the dorsal back region of an immunocompromised mouse strain (see Methods 2.2.36).

Preliminary experiments were carried out to validate the model by using a combination of immortalised human keratinocytes (NIKS) (see materials Table 2.3) either untransduced or transduced with LV-GFP and primary healthy donor fibroblasts. A supporting scaffold was formulated from coagulant factors extracted from porcine plasma cryoprecipitate, $7.5x10^5$ fibroblasts and thrombin. $1.2x10^6$ keratinocytes were seeded on the surface of the semi-solid gel-like fibrin matrix the following day **(Figure 4.5 A)**. The bioengineered fibroblast and keratinocyte comprised SEs were cultured until keratinocytes reached the desired confluency and then grafted on the dorsal region of the back of the NMRI-*Foxn1*^{nu} athymic mice **(Figure 4.5 B)**. 6 weeks post-grafting, the murine dorsal region was examined under UV light for GFP expression with the results confirming the persistence of the grafted cells localised in the central portion of the grafted tissue **(Figure 4.5 C)**.

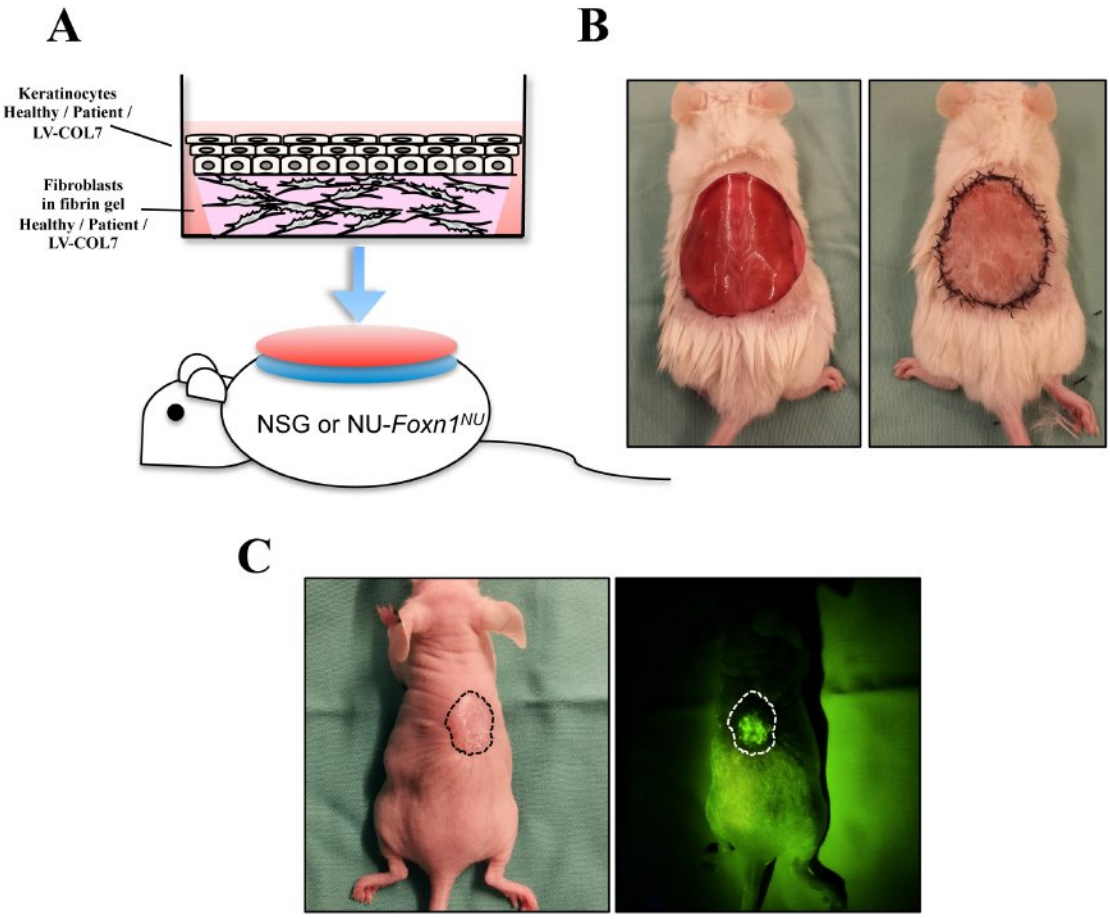

Figure 4.5 Human:murine chimeric skin graft model.
Bioengineered skin equivalents (SEs) were generated by using a fibrin scaffold containing human keratinocytes and fibroblasts and transplanted onto immunodeficient mice for formation of a full thickness human graft. **(A)** 3D fibrin gel comprised of porcine plasma cryoprecipitate, human thrombin and either normal donor or RDEB patient keratinocytes and fibroblasts untransduced or transduced with LV-COL7 or LV-GFP generated *in vitro*. **(B)** Grafting of SEs onto NMRI-*Foxn1*^{nu} athymic or NOD.Cg-*Prkdc*^{scid} *Il2rg*^{tm1Wjl}/SzJ (NSG) mice. **(C)** 6-weeks post grafting, full-thickness skin of human origin is visible. Confirmation of grafting by GFP expression of LV-GFP transduced human keratinocytes.

4.2.2 Human:murine chimeric skin graft model for the in vivo assessment of RDEB gene therapy

A pilot experiment was performed using bio-engineered skin grafts generated by using a combination of NIKS or RDEB EBKC keratinocytes either untransduced or LV-COL7 transduced, and primary or RDEB patient (BT) fibroblasts untransduced or following LV-COL7 transduction. 8-week post grafting, the grafts were harvested and cryosectioned for analysis. Immunofluorescent staining using the mAb-C7-LH7.2 antibody demonstrated C7 expression at the DEJ of the LV-COL7 transduced RDEB cell combination at comparable levels to control grafts generated from NIKS and primary fibroblasts **(Figure 4.6 d, g)**. On the contrary, there was no deposition of C7 detected at the DEJ of skin grafts generated from the combination of untransduced EBKC and RDEB fibroblasts **(Figure 4.6 a)**. H&E staining revealed a distinct thickening of the epidermis in all grafts with visible stratification and formation of a cornified layer resembling that of human skin **(Figure 4.6 c, f, i, j)**. Furthermore, the graft generated from the combination of untransduced RDEB keratinocytes and fibroblasts exhibited a blister-like morphology with subepidermal cleavage at the DEJ recapitulating the RDEB phenotype, whereas no discernible tissue cleavage or blistering could be detected in the LV-COL7 transduced RDEB or healthy donor cell **(Figure 4.6 c, f)**.

These results have demonstrated the use of a human:murine chimeric skin graft model for the *in vivo* modelling of RDEB and for the functional assessment of C7 expression in gene corrected cells.

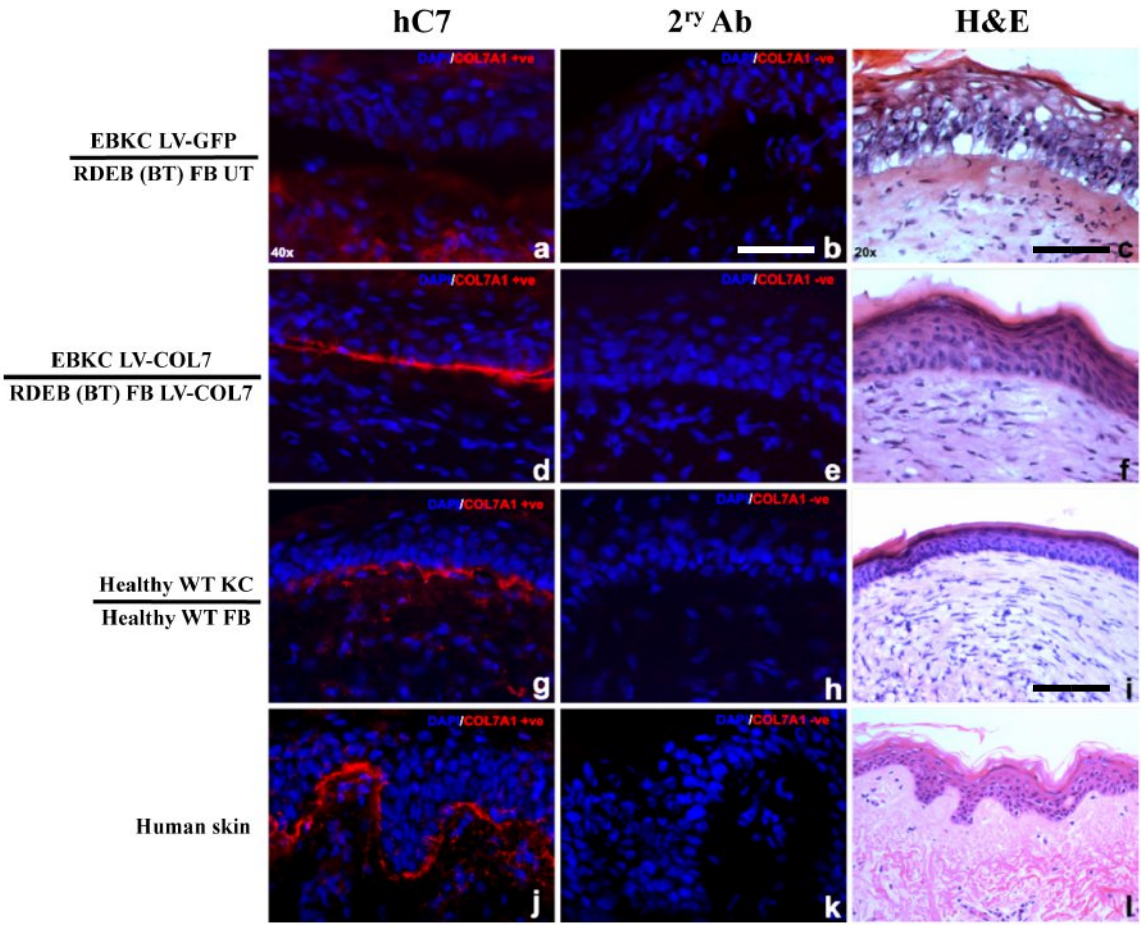

Figure 4.6 Assessment of C7 expression and graft morphology using LV-COL7 transduced keratinocytes in pre-clinical human:murine chimeric skin graft RDEB model.

Bioengineered human skin equivalents generated by the combination of healthy donor primary keratinocytes and fibroblasts (WT KC/FB) (n=2) or RDEB EBKC keratinocytes cells with or without LV-COL7 transduction (n=4) and RDEB patient (BT) fibroblasts (n=2), were grafted onto NMRI-*Foxn1*^{nu} athymic nude mice (n=8) and harvested 8 weeks post grafting. H&E staining shows thick epidermis with attachment of DEJ in LV-COL7 transduced RDEB keratinocyte graft **(f)** and WT KC/FB graft **(i)** while a distinct blistering phenotype was seen in the untransduced (UT) RDEB cell combination **(c)**. Immunofluroscence staining using mAb-C7-LH7.2 antibody shows positive C7 expression (red) at the DEJ of grafts generated from LV-COL7 transduced RDEB EBKC and patient (BT) fibroblasts **(d)** and WT KC/FB combination **(g)**, with a similar staining pattern to that of human skin control **(j)**. No expression of C7 was seen at the DEJ of graft generated from the UT RDEB cell combination **(a)**. Images of 2^{ry} antibody control staining revealed no background staining **(b, e, h, k)**. Scale bars = 100 μm.

A major hurdle encountered in this study was the relatively high occurrence of graft rejection in the NMRI-*Foxn1*^{nu} mouse strain with up to 50% of the bioengineered SEs failing to engraft (personal communication with Dr. F. Larcher confirmed similar observations) (of the 12 NMRI-*Foxn1*^{nu}mice grafted 7 mice showed graft rejection). This may be due to the presence of circulating B-cells in this strain. Therefore, the NOD.Cg-*Prkdc*^{scid} *Il2rg*^{tm1Wjl}/SzJ (NSG) mouse strain was selected (Shultz et al., 2005). A loss-of-function mutation in the *Prkdc* gene causes a knockdown of the T cell receptor (TCR) and the B cell immunoglobulin gene (IG), preventing their development and maturation, resulting in the *scid* phenotype. In addition, a null mutation in *IL2rg* inhibiting the production of a number of interleukins including IL-15, results in a disruption of signalling with NK cells, preventing their development. Using the NSG strain as the recipient of the bioengineered SEs showed an increase of grafting success rate to 80% (15 out of 17 NSG grafted mice had human skin graft growing). Therefore, the NSG-based human:murine chimeric skin graft model was utilised for all subsequent *in vivo* work.

4.3 Functional recovery of C7 in RDEB skin grafts genetically corrected by LV-COL7

4.3.1 Restoration of C7 expression in graft generated by LV-COL7 corrected RDEB patient fibroblasts

Primary cells obtained from either healthy donors or RDEB patients with or without LV-COL7 transduction were used for evaluation of the efficacy of the gene therapy strategy in the *in vivo* human:murine skin graft model.

Firstly, to test whether gene corrected RDEB fibroblasts alone would be sufficient for the functional recovery of C7 in RDEB skin, indicated by the formation of robust AFs, primary fibroblasts from RDEB patient (CK) were transduced with LV-COL7 at an MOI of 10. Both untransduced RDEB patient (CK) fibroblasts or LV-COL7 transduced patient (CK) fibroblasts were formulated into bioengineered SEs as previously described with the combination of primary untransduced RDEB (CK) keratinocytes. Control SEs were prepared alongside using a combination of primary healthy donor keratinocytes and fibroblasts. The bioengineered SEs were then grafted onto 6 to 8-week old NSG mice (total number of 8) in duplicate for healthy donor and RDEB untransduced control groups and quadruplicate for the LV-COL7 transduced group. 2-3 weeks post grafting, the devitalised mouse skin used as a biological bandage had sloughed off and revealed a noticeably thicker epidermis resembling that of human skin. 8-

weeks post grafting, the grafts were harvested with attention to preserve portion of the bordering mouse tissue and snap frozen for cryosectioning.

Graft morphology was evaluated by staining frozen sections of each graft with H&E. The results revealed a distinct border between mouse and human tissue **(Figure 4.7 a-c)**. The skin grafts examined from each group showed a noticeably thicker epidermis than that of the bordering mouse tissue, comprising of 10-12 keratinocyte cell layers, while there was also a thickened cornified layer and absence of hair follicles in the human grafts. Staining of the grafts with a panel of human specific antibodies **(**described in section **4.1.1)** further corroborated these findings. Clear boundaries of where mouse and engineered human skin grafts fused were easily distinguished in all grafts. Blistering, visualised as sub-epidermal tissue separation was apparent in the graft generated from non-gene corrected cells, whereas intact adhesion of the DEJ was seen in healthy donor and LV-COL7 gene corrected grafts **(Figure 4.7 b)**. Immunofluorescence staining with human specific antibodies desmoglein-1 and MTCO2 showed positive staining restricted to the human graft with no signal detected in the bordering mouse tissue **(Figure 4.7 g-i, j-l)**. The staining patterns of both MTCO2 and desmoglein-1 were comparable to those observed in the previous section **(4.1.3)**, with cytoplasmic staining of keratinocytes and fibroblasts for MTCO2 and suprabasal membranous epidermal staining for desmoglein-1.

7 out of the 8 grafted mice presented with full-thickness skin of human origin confirmed by desmoglein-1 and MTCO2 expression. The single case that failed however, displayed positive staining of MTCO2 in a portion of the fibroblasts in the dermis. This suggested that on this occasion, mouse keratinocytes may have migrated into the wound during the graft take process and replaced the human keratinocytes, resulting in a mixed cell population in the graft with human fibroblasts in the dermis and mouse keratinocytes in the epidermis.

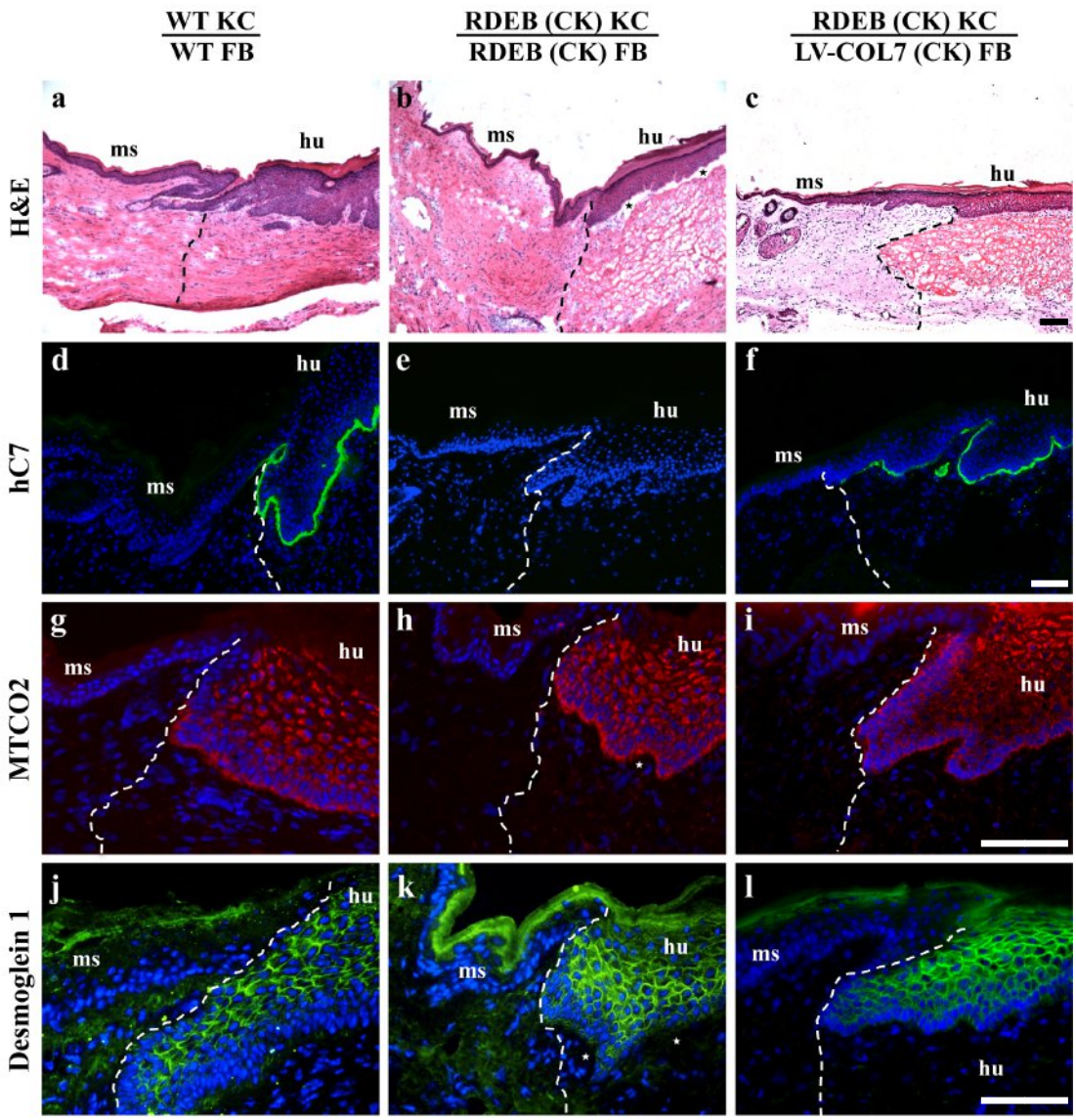

Figure 4.7 Confirmation of bioengineered human SEs grafted on NSG mice by H&E and human specific antibody staining.

Harvested grafts were stained for H&E and human specific desmosomal and mitochondrial markers desmoglein-1 and MTCO2. H&E staining shows a defined border (dotted line) between mouse (ms) and bioengineered human (hu) skin **(a-c)** with thickened epidermis and loss of hair follicles **(b)**. Human specific anti-C7 antibody (green) is expressed in healthy and gene corrected graft **(d, f)** but not in the untransduced graft **(e)**. MTCO2 (red) stained both epidermis and dermis in all grafts but not in the mouse portion of the tissue **(g-i)**. Desmoglein-1 (green) shows a defined epidermal human/mouse tissue border in all grafts **(j-l)**. Splitting at the DEJ of the untransduced graft is depicted (stars). Nuclei were stained with DAPI (blue). Scale bars = 100 μm.

Examination of the H&E stained morphology of the DEJ under low-magnification, revealed visible tissue cleavage in the graft generated using untransduced RDEB cells **(Figure 4.7 b)**. On the contrary, this phenotype was not observed in the grafts generated using healthy or transduced fibroblasts **(Figure 4.7 c)**. To determine whether this was a LV-COL7 mediated effect, suggesting the secretion and deposition of functional C7 at the DEJ, grafts were stained

with mAb-C7-LH7.2 antibody. The results showed an overexpression of C7 protein throughout the DEJ of the graft generated using LV-COL7 transduced RDEB fibroblasts similar to that in healthy donor cell graft **(Figure 4.8 a&d, c&f)**. The intensity of C7 expression allowed for its detection in fibroblasts in the dermis as cytoplasmic staining seen predominantly in the transduced graft and to a lesser extent in the healthy control graft. The epidermis appeared securely attached to the underlying dermis with no visible indication of separation or blistering. In contrast, the graft generated using the untransduced RDEB cell combination showed no discernible C7 expression at the DEJ, with sub-epidermal tissue separation from the dermis, closely resembling RDEB patient skin **(Figure 4.8 b&e)**.

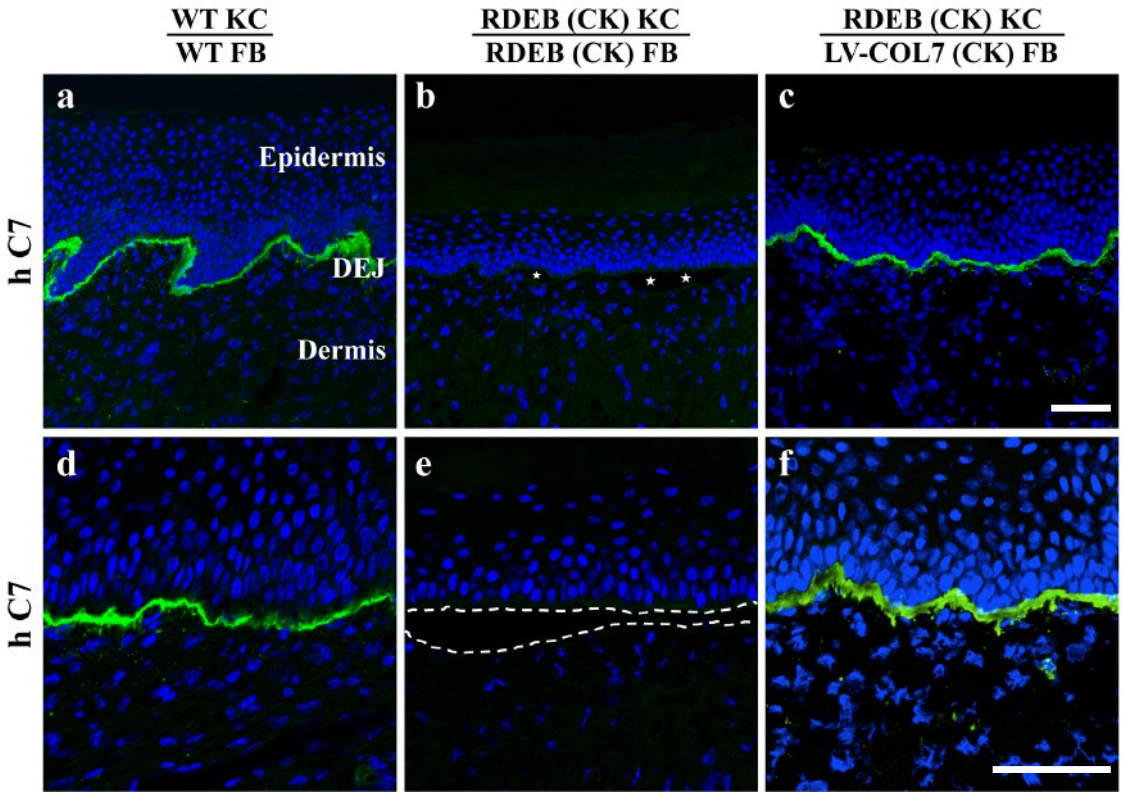

Figure 4.8 Restoration of C7 expression at the DEJ of the transduced graft mediated by LV-COL7 gene correction of RDEB patient fibroblasts.
Harvested grafts were cryosectioned and stained for human C7 at the DEJ. The morphology showed a blistering phenotype (asterisks) with dermal-epidermal cleavage (dotted line) in the graft generated with untransduced RDEB patient keratinocytes and fibroblasts **(b, e)**, whereas, there was no such phenotype in grafts generated by healthy donor **(a, d)**, or LV-COL7 transduced RDEB fibroblasts containing grafts **(c, f)**. Immunofluorescence staining using human specific anti-C7 antibody (green) shows strong C7 expression at the DEJ of healthy donor **(a, d)** and LV-COL7 transduced graft **(c, f)**. In contrast, no C7 expression is seen in untransduced graft. These results indicate the restoration of C7 expression in the grafts with COL7 gene corrected cells. The disappearance of the blistering phenotype in the gene corrected graft suggested the re-establishment of dermal-epidermal adhesion after C7 restoration. Nuclei were stained with DAPI (blue). Scale bars = 100 μm.

The grafts were also examined for epidermal proliferation and differentiation markers involucrin, keratin 10 and keratin 14 **(Figure 4.9)**. A fully developed epidermis staining positive for all three markers in grafts generated using healthy donor, RDEB patient untransduced or LV-COL7 transduced fibroblasts suggested normal differentiation and maturation of the grafts 8 weeks post grafting **(Figure 4.9 d-f, g-i, j-l)**. Although all grafts, irrespective of the cell combinations, showed a differentiated and matured epidermis, extensive tissue separation and blister formation between basal keratinocytes and the underlying dermis was clearly observed in the untransduced RDEB graft. These data clearly indicate that LV-COL7 transduction of the fibroblasts alone can lead to restoration of C7 expression and amelioration of tissue cleavage at the DEJ.

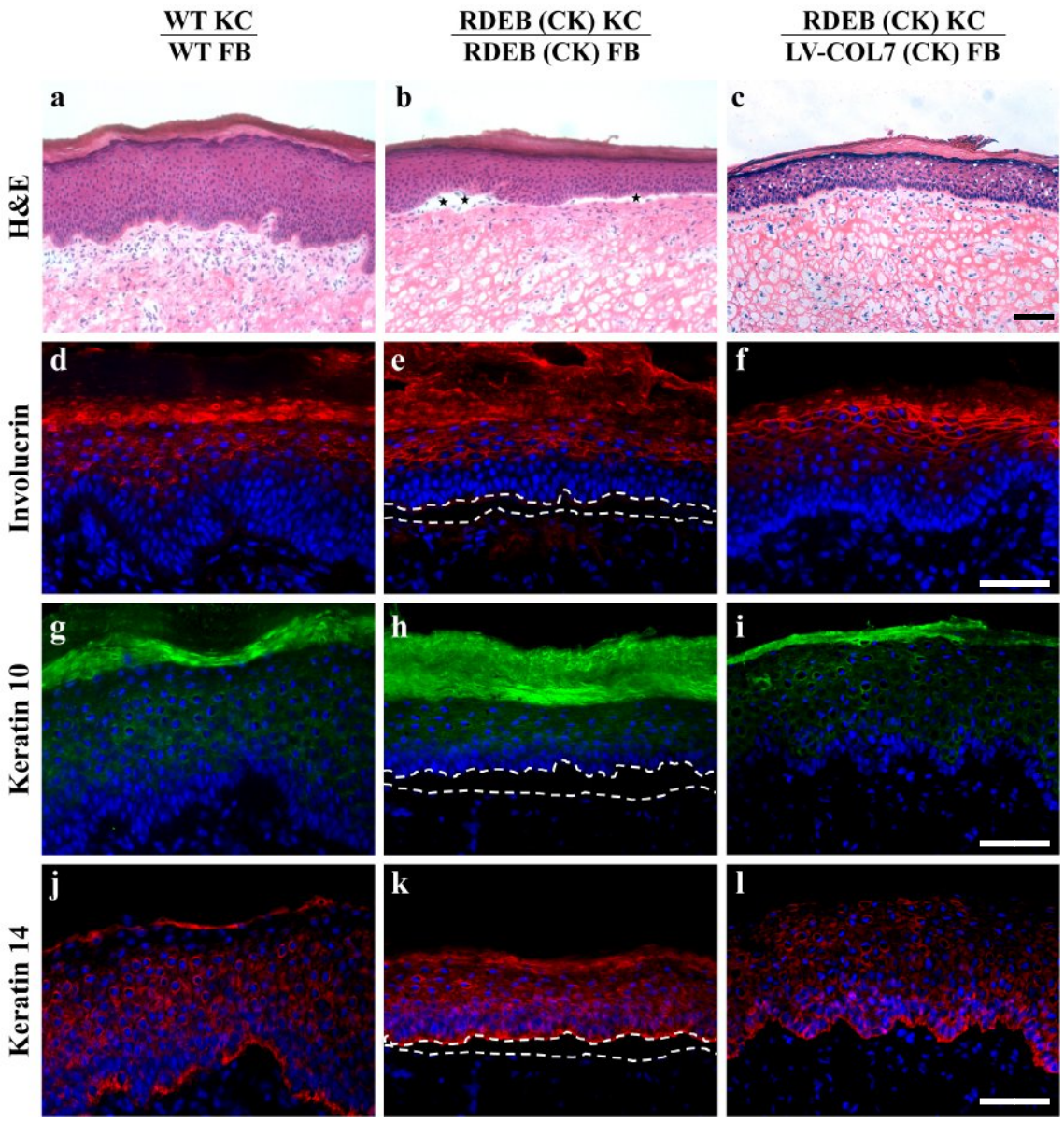

Figure 4.9 Expression of epidermal maturation and differentiation markers in grafts generated from primary RDEB patient (CK) keratinocytes and fibroblasts.

Differentiation and maturation of the harvested grafts were assessed by H&E and with epidermal protein specific antibodies against involucrin and keratins 10 and 14 proteins. No tissue cleavage seen in LV-COL7 fibroblast transduced graft suggesting vector-mediated restoration of adhesion **(b)**. Positive and negative controls represented by healthy donor graft **(a)** and untransduced RDEB graft **(c)**. Staining of grafts with involucrin (red) **(d-f)** and keratin 10 (green) **(g-i)** as markers of keratinocyte differentiation and keratin 14 (red) **(j-l)** as a keratinocyte proliferation marker. All grafts were positively stained for these markers indicating maturation of the harvested grafts. Tissue separation/cleavage in RDEB untransduced combination depicted by dotted lines at DEJ. Nuclei were stained with DAPI (blue). Scale bars = 100 μm.

4.3.2 Assessment of C7 function in an in vivo human:murine skin graft model

It was previously described (Section 3.4.2.2), that RDEB (BT) keratinocytes showed full-length C7 expression by Western blot. It was speculated that detection of the 290 kDa protein band corresponding to C7 by the Chen-C7 antibody, was due to the amino acid substitution mutation in one allele, or the late stage truncation of the other allele potentially resulting in expression of the full-length C7 protein although rendered non-functional. To confirm this, bioengineered SEs were generated using RDEB keratinocytes and fibroblasts from patients (BT) and (EB8) transduced with LV-COL7 at an MOI of 5 and 10, respectively, and grafted onto NSG mice (n=2) to measure the combined effect on the level of C7 expression and functional restoration to the DEJ following gene correction in both cell types. Untransduced RDEB patient (BT) keratinocytes and fibroblasts were used in parallel as negative control (n=1). The skin grafts were harvested after 8 weeks and examined.

It was immediately noticed during sample processing that the epidermis in the untransduced negative control graft separated from the underlying dermis without exerting any external force, whereas not such phenomenon occurred with the LV-COL7 gene corrected graft. This observation indicated that the full-length endogenous C7 expression of patient BT cells did not appear to confer a functional effect in the adhesion of the DEJ.

The graft morphology and expression of human specific protein markers were also examined. The results demonstrated a thickened epidermis and distinct dermal morphology lacking mouse hair follicles in the human grafts **(Figure 4.10 a&b)**. A distinct boundary between mouse and human skin confirmed by positive staining of MTCO2, desmoglein-1 and human C7 solely within the human grafts was also detected **(Figure 4.10 c-h)**. Morphological H&E staining also revealed RDEB-like severe splitting of the DEJ in the graft generated using untransduced cells confirming the lack of functional adhesion conferred by the patient cells **(Figure 4.10 a&b)**.

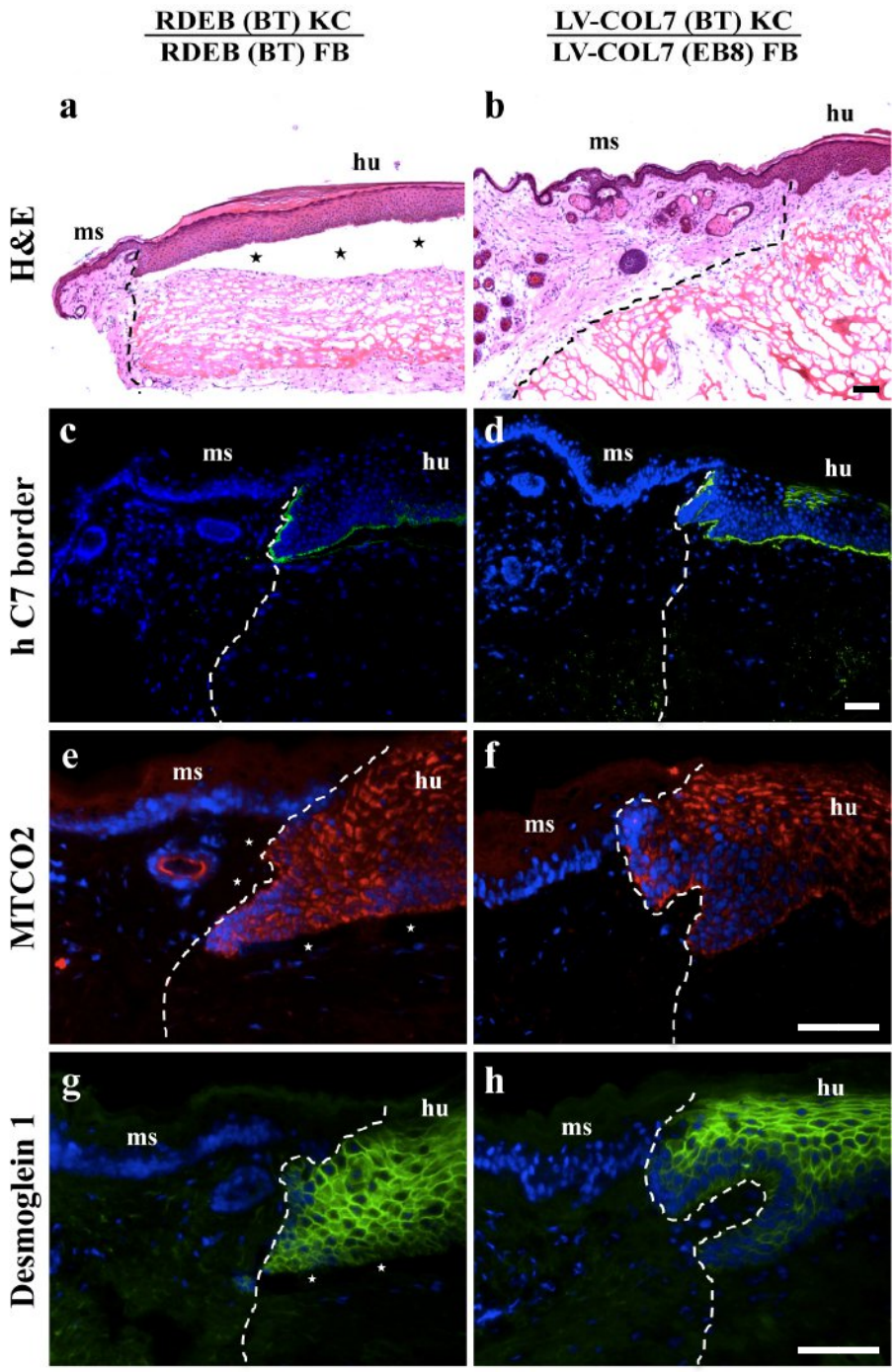

Figure 4.10 Verification of human origin of bioengineered SEs grafted on NSG mice by morphological and species specific staining.

Grafts were stained with antibodies against human specific mitochondrial (MTCO2) and desmosomal (desmoglein-1) markers or H&E across the human:murine tissue junction. H&E staining of grafts generated from either untransduced **(a)** or LV-COL7 transduced fibroblast RDEB patient cells **(b)** showed defined border (dotted line) between mouse (ms) and bioengineered human (hu) skin. Blistering at the DEJ of untransduced graft **(a)** is depicted (stars). Human specific anti-C7 antibody (green) showing expression in transduced graft **(d)** with weak expression in untransduced graft **(c)**. No cross-reactivity seen beyond border into mouse tissue. MTCO2 (red) stained positive in human region of epidermis and dermis in both grafts **(e, f)**. Defined epidermal human/mouse tissue border detected by human specific desmoglein-1 (green) **(g, h)**. Nuclei were stained with DAPI (blue). Scale bars = 100 μm.

Human-specific C7 expression was further evaluated using the mAb-C7-LH7.2 antibody, which revealed strong C7 protein expression in the gene corrected graft with intense staining in basal keratinocytes at the DEJ region and in a portion of the dermal fibroblasts **(Figure 4.11 b)**. Positive C7 staining was also observed along the BMZ of the untransduced graft with no signal detected in the dermis, consistent with previous Western blot results showing C7 expression in patient BT keratinocytes **(Figure 4.11 a)**. From the results combined demonstrating severe sub-epidermal tissue separation but positive C7 expression at the DEJ of the untransduced graft, it can be concluded that the endogenous C7 protein in the RDEB patient (BT) keratinocytes was in fact non-functional. Restoration of tissue separation following LV-COL7 transduction of the cells in the gene corrected graft further illustrated the efficacy of the *in vivo* model for the functional assessment of C7.

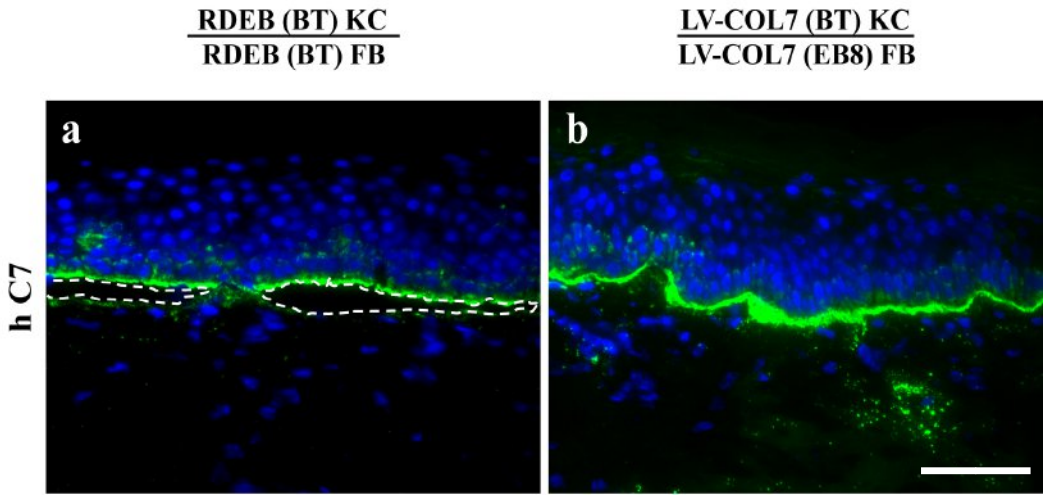

Figure 4.11 Restoration of C7 expression in graft generated by the combination of LV-COL7 transduced keratinocytes and fibroblasts.
Grafts comprised of RDEB cells either untransduced or transduced with LV-COL7 were examined for the expression of human C7. The morphology shows a blistering phenotype with dermal-epidermal cleavage (dotted line) in the untransduced graft **(a)**, whereas secure attachment of DEJ is seen in grafts generated with LV-COL7 transduced RDEB cells **(b)**. Immunofluorescence staining using human specific anti-C7 antibody (mAb-C7-LH7.2) (green) shows strong C7 expression at the DEJ of transduced LV-COL7 graft **(b)**. Weaker C7 expression is visible in untransduced graft although non-functional as confirmed by severe dermal-epidermal separation. The results indicate the restoration of C7 following LV-COL7 gene correction of both RDEB keratinocytes and fibroblasts and amelioration of tissue cleavage. Nuclei were stained with DAPI (blue). Scale bar = 100 μm.

The grafts were further stained with epidermal protein markers to assess epidermal maturation in the grafted tissue. Keratinocyte differentiation was confirmed by positive staining of keratin 10 **(Figure 4.12 e&f)** and involucrin **(Figure 4.12 c&d)** in the suprabasal and cornified layers. Keratin 14 was predominantly expressed by the basal keratinocytes with diffuse staining in suprabasal layers **(Figure 4.12 g&h)**. The positive staining of all three epidermal markers, and

the organised layering and well-formed *stratum corneum* seen by H&E **(Figure 4.12 a&b),** suggested that the human grafts underwent proliferation and maturation during the 8-week period on the NSG mice.

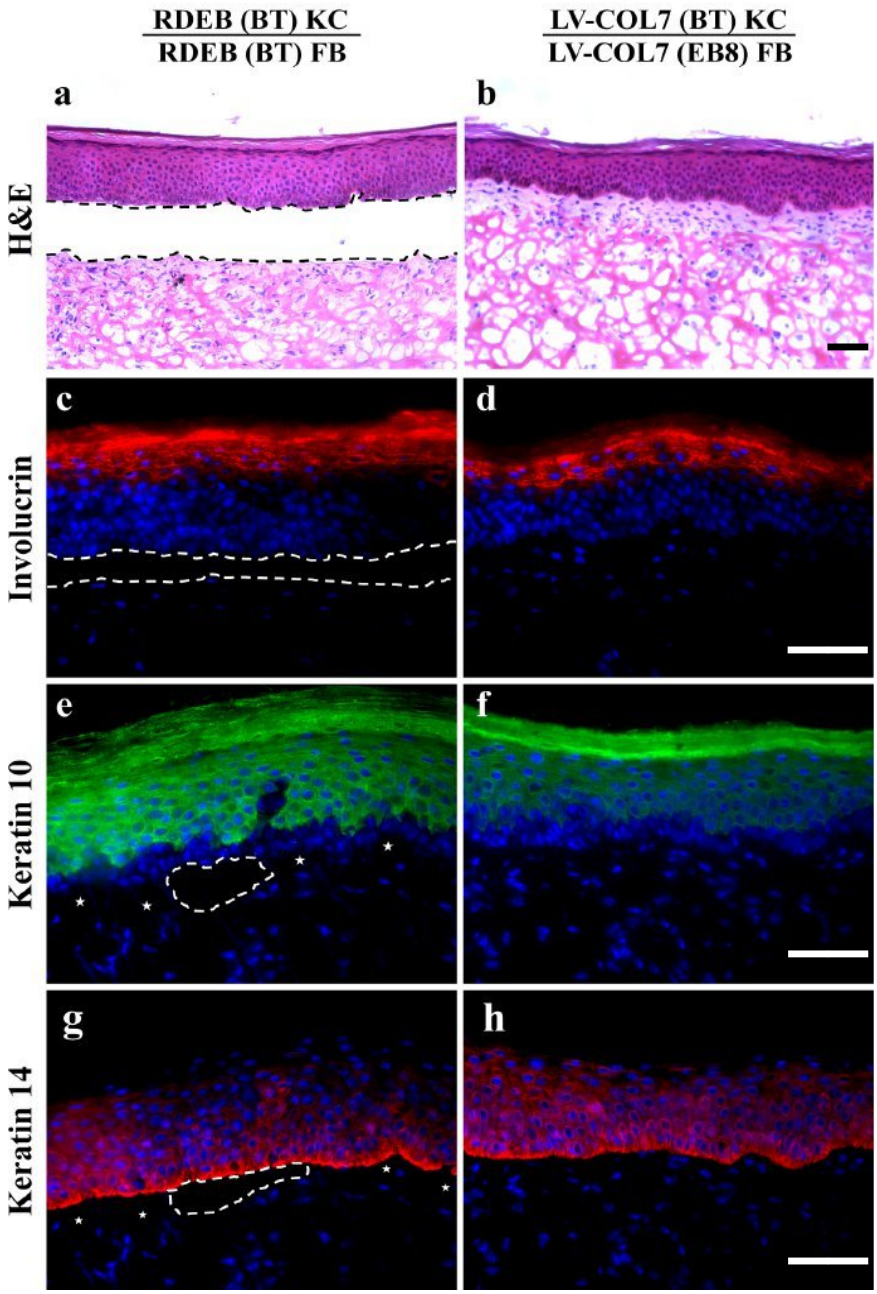

Figure 4.12 Expression of maturation and differentiation markers in patient (BT) & (EB8) bioengineered skin grafts.

Grafts were stained for H&E and epidermal differentiation and maturation markers involucrin and keratins 10 and 14. The non-gene corrected graft generated from untransduced RDEB patient (BT) cells **(a)** shows tissue splitting at the DEJ (stars/dotted line), whereas no tissue separation is seen in the LV-COL7 transduced graft **(b)**. Epidermal differentiation confirmed by involucrin (red) **(c, d)**, keratin 10 (green) **(e, f)** and keratin 14 (red) **(g, h)** in both grafts suggesting epidermal proliferation and maturation occurred. Nuclei were stained with DAPI (blue). Scale bars = 100 μm.

4.4 Anchoring fibril formation in gene corrected grafts confirmed by transmission electron microscopy

4.4.1 Amelioration of tissue cleavage through functional C7 anchoring fibril formation in graft generated from LV-COL7 gene corrected fibroblasts

Immunofluorescent staining of the harvested graft generated from the combination of untransduced RDEB patient keratinocytes and LV-COL7 transduced RDEB patient fibroblasts showed the restoration of C7 expression at the DEJ. To evaluate whether this vector-mediated C7 expression could form functional AFs, the skin graft was further examined at the ultrastructural level by transmission electron microscopy (TEM).

Fixed and resin embedded graft tissue was processed into ultrathin 100 nm thickness sections and examined by TEM (see Methods 2.2.38). Low magnification micrographs were initially acquired to allow for the visualisation of the basal keratinocytes and underlying fibroblasts **(Figure 4.13)**. At first glance, extensive tissue cleavage was observed in the graft generated from untransduced RDEB patient keratinocytes and fibroblasts, which appeared to have been restored following gene correction of the RDEB patient fibroblasts alone.

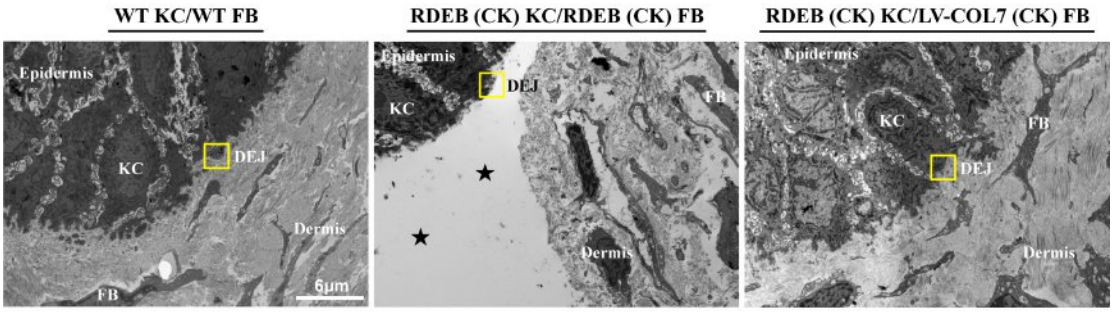

Figure 4.13 Ultrastructural morphology of grafts generated from RDEB patient (CK) cells imaged by TEM.
Morphological assessment of graft DEJ was performed by low power magnification (x1,200) TEM. Extensive *sublamina densa* split (stars) in graft generated from untransduced RDEB patient (CK) keratinocytes and fibroblasts with separation between epidermis and underlying dermis **(middle)**. No blistering or separation was visible in LV-COL7 transduced RDEB (CK) fibroblast graft **(right)** or healthy donor graft **(left)**, highlighting vector-mediated restoration of adhesion. Dermal-epidermal junction (DEJ); Fibroblasts (FB); Keratinocytes (KC); Melanosome (MN); yellow squares depict area of DEJ imaged at high magnification in figure 4.14. Scale bar = 6µm.

Upon closer inspection of a select portion of the DEJ at high magnification, an abundance of rope-like structures throughout the DEJ of the LV-COL7 fibroblast transduced graft could be clearly seen, which were, according to their location and morphology, confirmed to be type VII collagen AFs **(Figure 4.14 C)**. The healthy control graft exhibited a similar AF structure with normal cross-banding and with the NC-2 domain extending 200 nm into the dermis looping around dermal type I and III collagen fibres **(Figure 4.14 A)**. In both gene corrected and healthy grafts, the AF morphology could be described as thick, looped and arching and in some areas of the gene corrected graft, their numbers appeared increased over those seen in the healthy control. The NC-1 domain of C7 was closely associated with the hemidesmosomes of the basal keratinocytes, which appeared to be large in size, well-formed with sub-basal dense plates. The AFs in most cases could be seen extending from the DEJ down to the papillary dermis and looping round dermal collagens bundles before re-attaching to the DEJ.

In instances where the whole AF could not be seen, it was most likely due to the oblique sectioning of the specimen, suggesting the continuation of the fibril may be on a different plane of view. There was a an abundance of plasmalemmal vesicles within the finger-like protrusions of the basal keratinocytes in close proximity to the BMZ assisting in the deposition of mature C7 protein to the DEJ. More importantly, in both healthy control and gene corrected grafts there was no indication of blistering or tissue cleavage at the DEJ. Instead, there was a robust *lamina densa* throughout and dense AF distribution, demonstrating functional correction at the DEJ and restoration of dermal-epidermal adhesion in the gene corrected graft.

In contrast, the graft comprised of untransduced RDEB patient keratinocytes and fibroblasts resulted in a severe blistering phenotype **(Figure 4.14 B)**. There was an extensive *sublamina densa* split with complete separation of the epidermis from the underlying dermis. The hemidesmosomes appeared reduced in number, slightly smaller and in some cases appeared to be internalised. There were no clear discernible AFs attached at the DEJ, which is in line with the lack of type VII collagen expression observed by immunofluorescence (Section 4.3.1). This graft appeared to truly recapitulate the RDEB disease phenotype with loss of AFs leading to tissue separation at the DEJ. Visualisation of the keratinocytes in a number of areas within all three healthy, uncorrected and gene corrected grafts suggested a possible migratory phenotype, a sign of a wounded environment, i.e. keratinocyte protrusions extending deep within the dermis as a way of increasing the surface area of attachment. Additionally, an elevated amount of plasmalemmal vesicles and slightly reduced number of hemidesmosomes also suggested reorganisation of the wound-bed taking place. Increased activity was also apparent within the dermis, with instances of *lamina densa* reduplication and with a somewhat disorganised type I and III dermal microfilbril bundle arrangement.

WT KC/WT FB

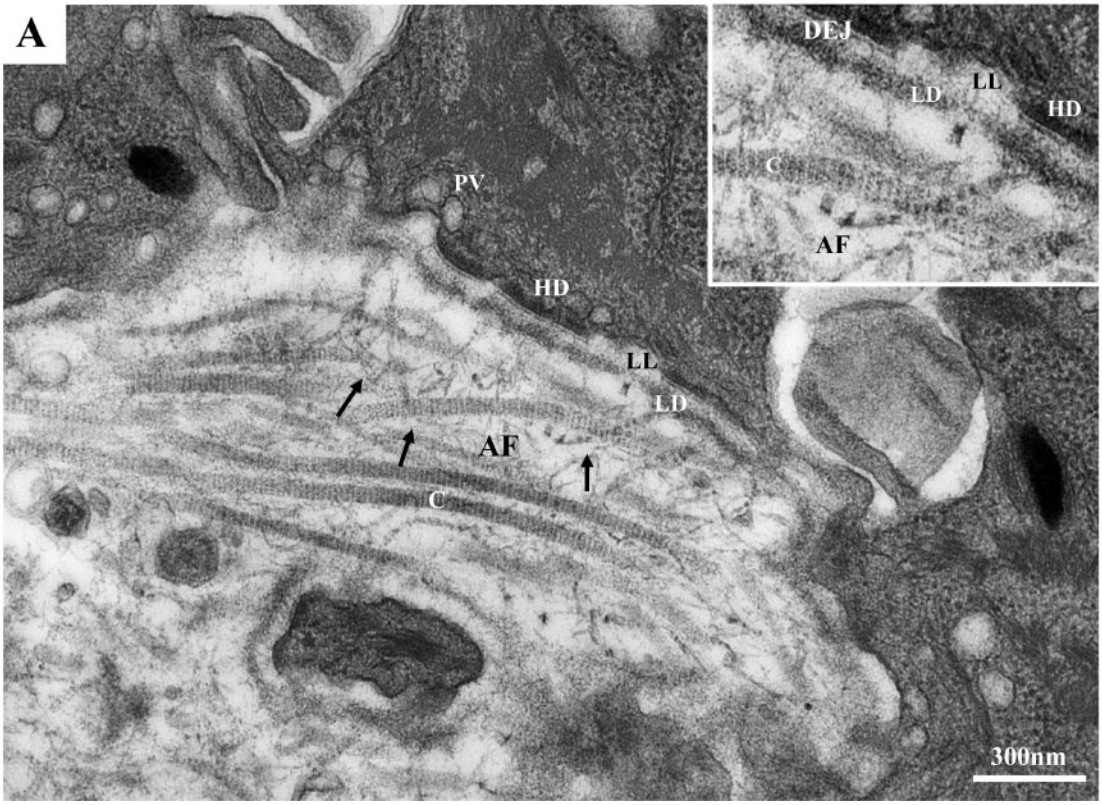

RDEB (CK) KC/RDEB (CK) FB

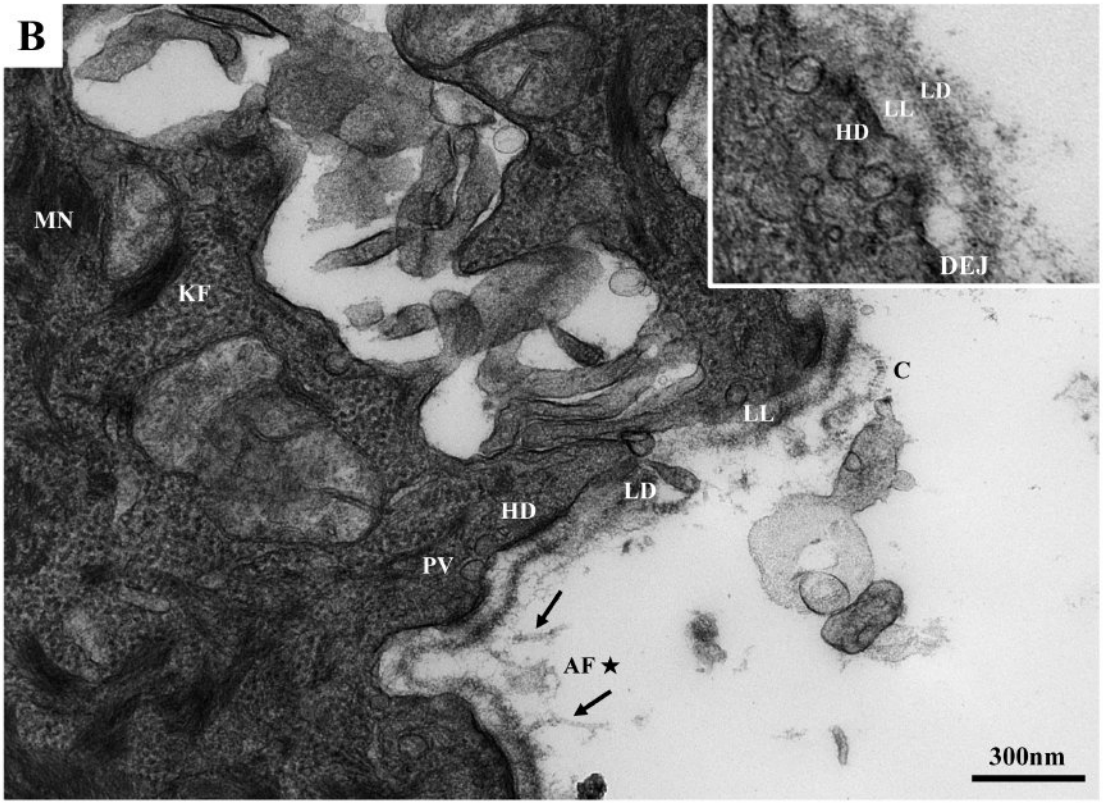

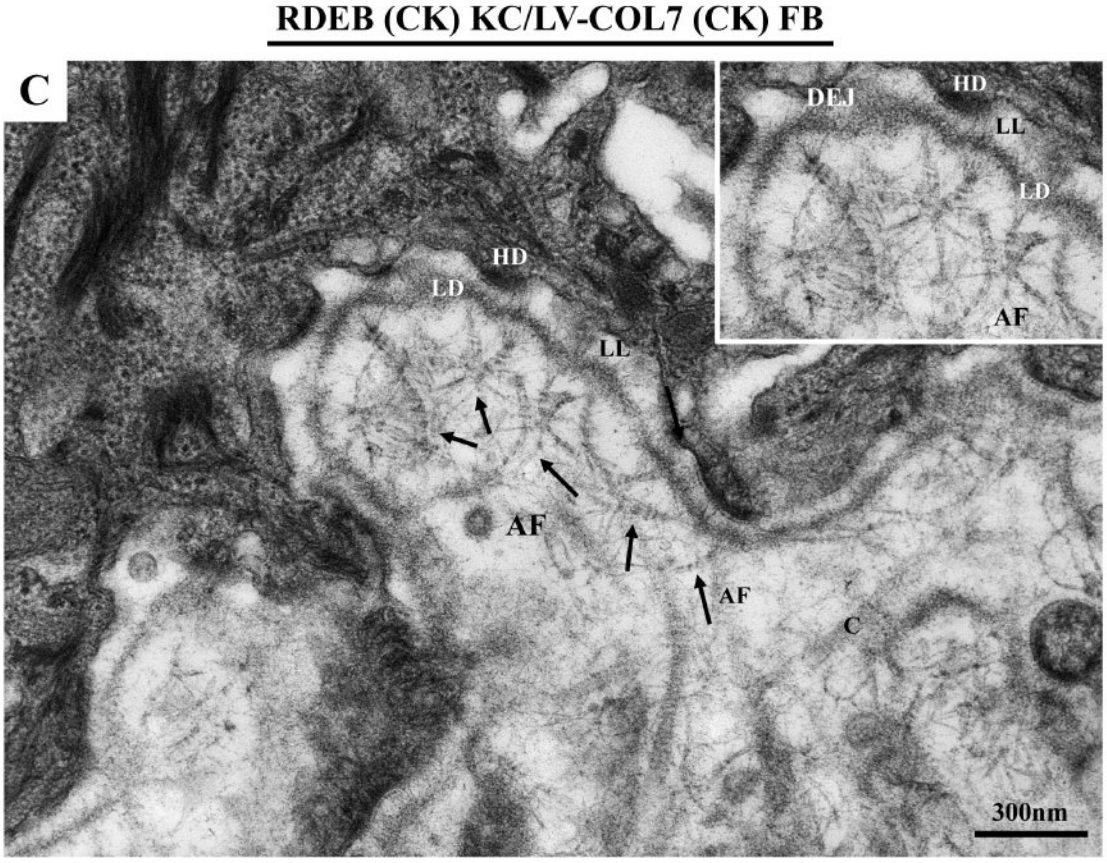

Figure 4.14 Functional correction of DEJ through LV-COL7 mediated restoration of type VII collagen anchoring fibrils in gene corrected fibroblast graft.

Grafts were examined for anchoring fibril (AF) formation at the DEJ by high-powered TEM. Healthy donor graft **(A)**, showed intact DEJ with numerous large hemidesmosomes. Thick, cross-banded type VII AFs (arrows) extend ~200 nm into the dermis looping round type I and III collagen. High proportion of C7 protein depositing plasmalemmal vesicles were visible. Untransduced graft generated from RDEB patient (CK) keratinocytes and fibroblasts **(B)** showed extensive tissue cleavage at the DEJ with *lamina densa* reduplication. Complete absence of type VII collagen fibrils resulting in separation of epidermis from underlying dermis. Gene corrected graft generated from LV-COL7 transduced RDEB (CK) fibroblasts and untransduced RDEB (CK) keratinocytes **(C)** showed restoration of dermal-epidermal adhesion by formation of several thick, looping, arching and cross-banded type VII collagen AFs at the DEJ. Anchoring fibril (AF), collagen type I and III (C), dermal–epidermal junction (DEJ), hemidesmosome (HD), keratin filament (KF), *lamina densa* (LD), *lamina lucida* (LL), melanin (MN), plasmalemmal vesicle (PV). Images taken at x13,000 and x30,000 magnification. Scale bar =300nm.

4.4.2 Anchoring fibril formation in graft generated using a combination of LV-COL7 transduced RDEB keratinocytes and fibroblasts

Grafts generated using RDEB patient (BT) and (EB8) keratinocyte and fibroblast combinations, with or without LV-COL7 transduction were processed and examined by TEM. At the ultrastructural level, the gene corrected graft showed strong attachment at the DEJ with no visible blistering or tissue separation under low magnification **(Figure 4.15)**. The epidermis appeared to be well formed with large hemidesmosomes at the basal keratinocyte layer and an increased amount of plasmalemmal vesicles. Within the dermis there appeared to be slight collagen remodelling, characteristic of wound-bed healing. At the DEJ there was solid *lamina densa* formation with distinguishable AFs extending from the hemidesmosomes and looping through the dermis anchoring round type I and III collagen fibres. Their morphology could be characterised as cross-banded, looping and arching although were reduced in number and slightly thinner compared to the AFs restored in the previous fibroblast transduced CK patient combination **(Figure 4.16 B)**. In the graft generated from untransduced RDEB patient (BT) cells there was relative undulation of the DEJ and a high proportion of hemidesmosomes although a large *sublamina densa* split was immediately apparent **(Figure 4.16 A)**. It is arguable whether AFs could be detected in the field of view although if any, they can only be described as short, rudimentary, very thin, rarely arching and wispy. More importantly, these AFs did not appear to confer sufficient anchoring in order to prevent tissue separation and blistering at the DEJ.

These results provided strong evidence of functional restoration of the RDEB phenotype upon correction of patient cells with LV-COL7. The vector-mediated C7 expression observed following immunofluorescent staining of grafts was directly linked to a functional correction through *de novo* formation of AFs securing the DEJ. The quality and abundance of the AFs detected was equal or in some cases exceeded that of healthy donor cell controls thought to be due to transgene overexpression. Grafting of corrected fibroblasts alone did not appear to perform inferiorly to using a combination of both corrected fibroblasts and keratinocytes. Although this may be due to patient variation it can be speculated that correction of fibroblasts alone being the more robust cell-type are sufficient for functional correction of the DEJ and phenotypic reversion of RDEB aberrations.

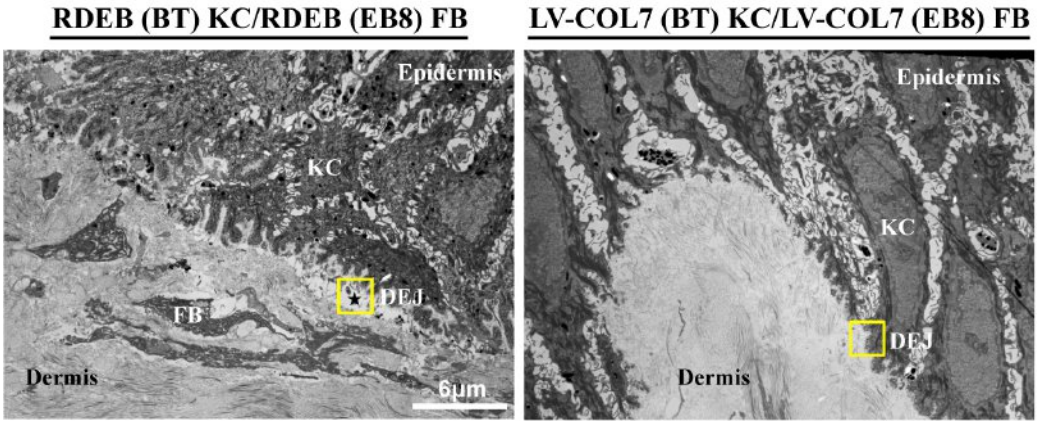

Figure 4.15 Ultrastructural morphology of grafts generated from patient (BT) and (EB8) cell combination imaged by TEM.

Morphological assessment of structural integrity of DEJ in grafts generated from either untransduced or LV-COL7 transduced RDEB patient (BT) and (EB8) keratinocytes and fibroblasts by low power TEM (x1,200). *Sublamina densa* split (star) in untransduced RDEB graft showing separation between epidermis and underlying dermis **(left)**. No blistering or separation visible in graft generated from both RDEB keratinocytes and fibroblasts transduced with LV-COL7 **(right),** highlighting vector-mediated restoration of adhesion. Dermal-epidermal junction (DEJ); Fibroblasts (FB); Keratinocytes (KC); yellow squares depict area of DEJ imaged at high magnification in figure 4.16. Scale bar = 6µm.

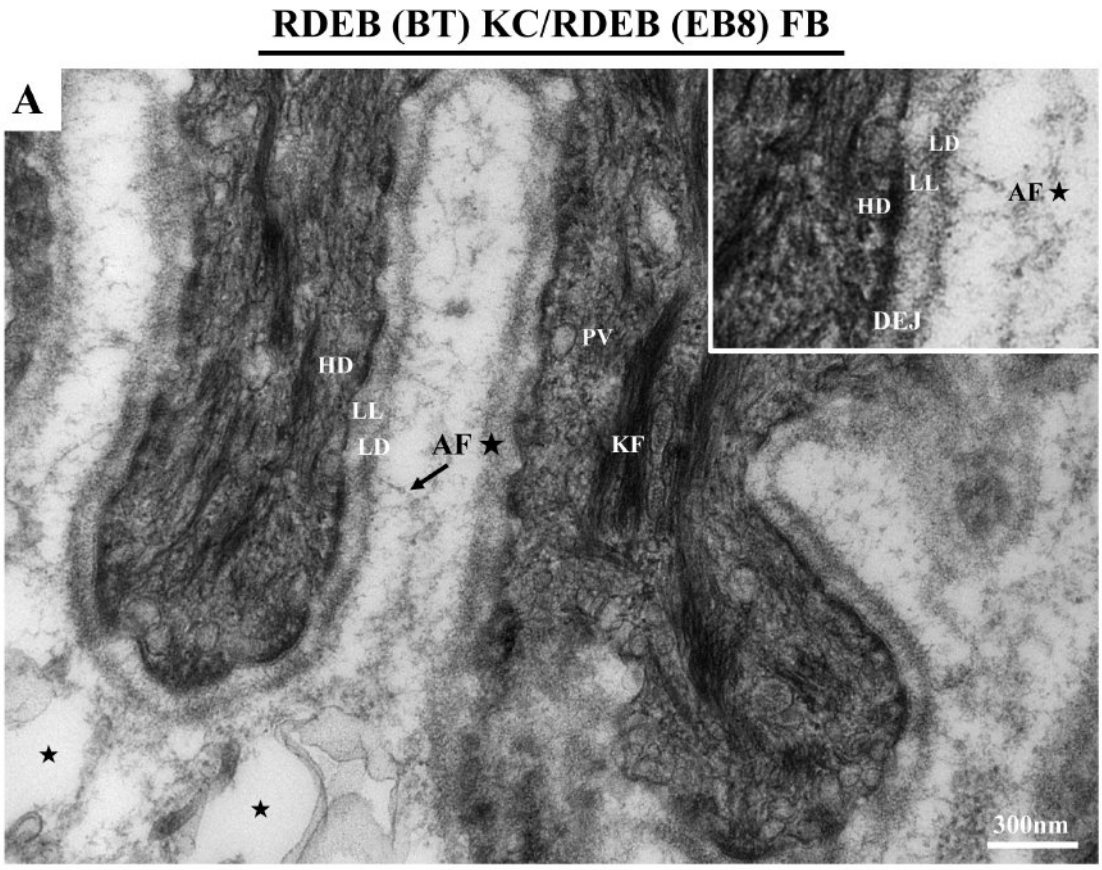

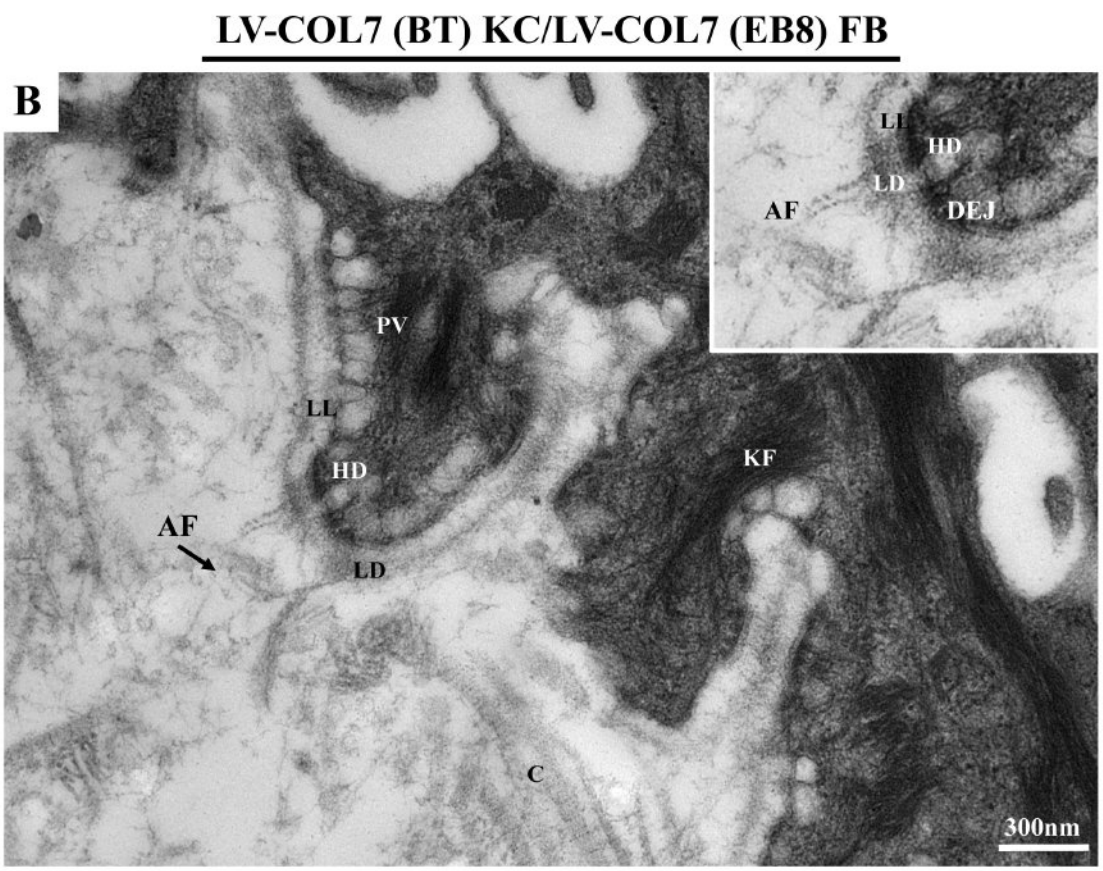

Figure 4.16 Restoration of anchoring fibril formation following LV-COL7 mediated correction of RDEB patient keratinocytes and fibroblasts.

Grafts were examined by high-powered TEM for detection of type VII collagen anchoring fibrils (AFs) following transduction of RDEB patient (BT) keratinocytes and (EB8) fibroblasts with LV-COL7.The graft generated from untransduced RDEB patient cells **(A)** showed blistering (stars) at the DEJ. Possible rudimentary AFs present, although conferring no visible functional effect. Undulation of keratinocyte protrusions suggesting wounded migratory phenotype. The gene corrected graft combination **(B)** showed restoration of dermal-epidermal adhesion. Looping, arching and cross-banded type VII collagen AFs extending ~200 nm into the dermis looping round type I and III collagen visible providing attachment at the DEJ. High proportion of C7 protein depositing plasmalemmal vesicles seen above *lamina lucida*. Anchoring fibril (AF), collagen type I and III (C), dermal–epidermal junction (DEJ), hemidesmosome (HD), keratin filament (KF), *lamina densa* (LD), *lamina lucida* (LL), melanin (MN), plasmalemmal vesicle (PV). Images taken at x13,000 and x30,000 magnification. Scale bar =300nm.

4.5 Discussion

A chimeric human:murine RDEB skin graft mouse model was established for the investigation of C7 expression and functional correction of the RDEB phenotype mediated by LV-COL7 in an *in vivo* setting. Although the two published RDEB murine models can truly recapitulate the disease phenotype with lack of C7 expression and with neonates developing large haemorrhagic subepidermal blisters on the trunk and extremities, life expectancy is limited to approximately 1 week due to the severity of their phenotype (Heinonen et al., 1999, Fritsch et al., 2008). In search of a more robust alternative, the technique developed by Larcher *et al.* was investigated and successfully utilised for the culture of bioengineered human grafts on immunodeficient murine hosts allowing for the generation of the chimeric human:murine RDEB models.

Following initial experimentation with the proposed NMRI-*Foxn1*^{nu} hairless mouse strain facilitating the process of grafting, a high incidence of graft rejection was encountered possibly to be due to residual functionality of NK and B-cells. Instead, replacement of the NMRI-*Foxn1*^{nu} with the NSG mouse strain resulted in a marked increase in the grafting success rate. The NSG strain lacks T-cells, B-cells, and NK cells and such profound cellular and humoral immunodeficiency has proven an excellent model of studies requiring human cell engraftment (Shultz et al., 2005).

The model robustly replicated the disease phenotype with full thickness human skin displaying tissue cleavage and blistering at the DEJ. Lack of C7 protein expression by immunofluorescence directly translated to absence of AFs at the ultrastructural level and hence disruption of BMZ integrity. To assess whether the phenotype could be reversed using the LV-COL7 therapeutic vector, both RDEB primary patient keratinocyte and fibroblast cells were transduced *ex vivo* and confirmed to express C7 *in vitro* prior to formulating into a skin equivalent matrix. Eight weeks post grafting onto immunocompromised NSG mice and obtaining full thickness human skin tissue, confirmed through the meticulous detection of human specific protein, samples were processed revealing restoration of C7 expression and deposition of protein at the DEJ. Use of a validated anti-human C7 specific antibody exhibiting no cross-reactivity in mouse, ratified the human, and hence LV-COL7 derived origin of the detected C7.

In line with the *in vitro* protein assays showing overexpression of C7 albeit the modest overall transduction efficiency, corrected grafts similarly exhibited intense expression of secreted C7 with cytoplasmic staining visible even in individual gene-corrected fibroblasts. Although the therapeutic potential of the LV-COL7 vector was immediately realised in the corrected grafts by

histological staining indicating phenotypic reversion of the associated disease characteristics, functional correction was further affirmed following detection of type VII collagen AFs.

TEM examination clearly depicted thick rope-like AFs populating the DEJ which abrogated the blistering phenotype and restored adhesion of the epidermis to the underlying dermis. Importantly, this was confirmed in both conditions in which either a combination of gene-corrected keratinocytes and fibroblasts, or gene-corrected fibroblasts alone were used for grafting. However, the observed overexpression of C7, suggested that gene correction of a single C7 contributing skin cell type, in this case fibroblasts, is capable of conferring a sufficient level of functional correction. On the contrary, endogenous C7 expression levels of allogeneic healthy donor fibroblasts alone may not have been adequate in providing sufficient anchoring as they only contribute for approximately 10% of total C7 secretion in skin.

Keratinocytes, being the major contributors of C7 to the DEJ in healthy skin, are not anticipated to confer as long a lasting therapeutic benefit as fibroblasts if grafted alone. The ~47 day turnover from basal, to the terminally differentiated keratinocytes of the cornified layer (Iizuka, 1994), implies that unless a modest portion of stem cell keratinocytes were to be gene-corrected during LV-COL7 exposure, the transduced cells would rapidly be replaced by uncorrected ones. This effect would in fact be further accelerated due to C7 expression restricted to the basal keratinocytes (Ryynanen et al., 1992). Moreover, the extensive damage of the wound bed in blistered regions of RDEB patient skin would most likely hinder the graft “take” process if applied as skin sheets. Furthermore, transport of C7 protein secreted from the keratinocytes through the basement membrane and into the dermal compartment would be delayed and incomplete (Ryynanen et al., 1992). Bioengineered grafts comprised of LV-COL7 transduced RDEB keratinocytes alone were therefore not assessed for their therapeutic ability.

However, the potential of keratinocytes can not be denied, as demonstrated in a study where a retroviral vector was used to deliver dog C7 protein to canine RDEB cells (Gache et al., 2011). The corrected cells were grafted on the RDEB dogs in the form of epithelial sheet and showed persistence of expression for up to 2 years with ectopic expression of C7 also seen in the suprabasal layer. Further investigation revealed that the sustained expression was due to the transduction of highly clonogenic cells.

Fibroblasts on the other hand, circumvent a number of the drawbacks associated with keratinocytes, chiefly being the slower turnover *in vivo* ensuring sustained expression over a prolonged post engraftment period. This further suggests that fibroblasts remain within originally transplanted locations secreting C7 into the extracellular space which is in turn sequestered by BMZ proteins and contributes to AF formation (Chen et al., 1999, Chen et al.,

1997). In addition, the ease of their *in vitro* manipulation, allowing for up to 30 cell passages with no specialised culturing requirements enables their propagation to attain large cell numbers without undergoing growth arrest and differentiation (Krueger, 2000).

In line with reports having previously shown restoration of C7 expression and improvement in DEJ of murine RDEB models using gene corrected keratinocytes (Murauer et al., 2011, Gache et al., 2004), fibroblasts (Woodley et al., 2003, Woodley et al., 2007b, Ortiz-Urda et al., 2003, Goto et al., 2006) or a combination of the two (Titeux et al., 2010, Chen et al., 2002), I was also able to provide definitive evidence of functional AF formation from RDEB cells corrected using a clinical grade LV-COL7 vector highlighting the therapeutic potential of an autologous gene therapy approach.

Chapter 5 Genome editing as a tool for establishing an *in vitro* RDEB model and correcting mutations in *COL7A1*

Over 600 mutations including missense, nonsense, splicing, small insertions or deletions in *COL7A1* have been reported to cause RDEB (Varki et al., 2007). Current gene therapy strategies rely on the addition of a full-length, WT copy of *COL7A1* cDNA into RDEB patients' cells carrying mutations in the *COL7A1* gene. A gene addition approach carries complications such as the large size of the *COL7A1* gene, spanning 8.9 kb in its cDNA form making packaging into current viral vectors systems and subsequent delivery to target cells a challenging task (Chen et al., 2000, Chen et al., 2002, Titeux et al., 2010). The potential of a targeted gene editing approach, whereby individual mutations can be corrected for the restoration of endogenous C7 expression instead of introducing an exogenous full-length copy of *COL7A1* cDNA sequence is very appealing.

To date, there has only been a single report on the use of gene editing by TALEN technology, as a tool for the *in vitro* correction of a homozygous PTC mutation in RDEB fibroblasts (Osborn et al., 2013). The results of the study prove the feasibility of a site-specific genome editing approach for the correction of *COL7A1* mutations. In addition, as one aspect of gene editing involves the introduction of monoallelic or biallelic mutations, it allows for the targeted disruption of WT *COL7A1*. In this way, RDEB cell models can be generated enabling the functional characterisation of the disease thereby bypassing the challenge of obtaining and culturing precious primary RDEB patient cells. Ultimately, genome editing enables the exploration of an alternative strategy for the correction of *COL7A1* in autologous RDEB cells and restoration of endogenous C7 expression beyond traditional viral-mediated gene addition.

In this chapter, a ZFN-mediated genome editing approach was developed for RDEB. The efficiency of site-specific targeting of *COL7A1* using ZFNs was primarily investigated using a WT keratinocyte cell line. Considering the resilient nature of keratinocytes to infection, the ZFN platform was packaged into a lentiviral platform and used to transduce the target cells. To ensure transient expression of the ZFNs within the target cell, the integrase defective HIV-1 packaging plasmid was utilised for the generation of NILVs. Cleavage efficiency following ZFN delivery using either a DNA plasmid or viral-based delivery platform was assessed and the genomic disruption and protein knockdown levels *in vitro* were examined. This aspect of gene editing resulting in site-specific genomic disruptions by non-homologous end joining (NHEJ) allowed for the *in vitro* modelling of RDEB.

This was followed by an evaluation of the corrective capacity of the ZFN system by harnessing the homologous directed repair (HDR) pathway through co-delivery of healthy donor template. This was determined through the detection of template sequence within the target cell genome by direct Sanger sequencing. Lastly, a proof of principle study assessing *in vivo* restoration of the DEJ anchoring, mediated by RDEB fibroblasts having undergone correction of *COL7A1* by TALEN gene editing was assessed in the human:murine chimeric skin graft model.

5.1 Targeted disruption of *COL7A1* by DNA plasmid-based ZFN delivery

ZFNs specific to exon 4 of human *COL7A1* were designed with the intention of targeting a cluster of known patient mutations in the proximal genomic region while preserving ZFN-induced gene disruption within 100 bp from the target mutation site for optimal efficiency (Elliott et al., 1998). The ZFNs were custom-synthesised by Sigma (CompoZr® technology) with each ZFN monomer annealing to an 18 bp sequence of exon 4; 5'-TCCCAGGTCTGCATCCTG-3' on the top strand and 5'-TCCTGGGACTTCCCGTCT-3' on the complementary strand with a 5 bp spacer sequence 5'-ATCAC-3' in between and constructs were subcloned into DNA delivery plasmids. The ZFN activity was estimated to be ~13.5% in human K562 cells as assessed by the supplier.

The ZFN activity was firstly measured in a keratinocyte cell line (HaCaT). $2.5x10^6$ cells were nucleofected with 3 μg of the ZFN DNA plasmid pair using the Amaxa™ Nucleofector™. A plasmid encoding eGFP nucleofected in parallel was used as a positive control. The ZFN activity assessed by the detection of disruptions presented as insertions/deletions (indels) in the *COL7A1* genomic sequence created by NHEJ following the delivery of ZFN DNA plasmid pair was examined by surveyor nuclease CEL-I assay (see Methods 2.2.30). CEL-I nuclease digestion of DNA extracted from the polyclonal HaCaT ZFN-nucleofected population presented with a cleaved product at (161 and 211 bp) compared to DNA from the GFP nucleofected population, suggesting disruption of the *COL7A1* DNA sequence due to NHEJ **(Figure 5.1)**. In order to confirm the ZFN cleavage efficiency, the nucleofected HaCaT population was sorted into single cells by FACS. Individual clones were propagated and sequenced across the ZFN binding region in *COL7A1*. The data revealed a single base pair deletion in 1 out of 8 clones tested.

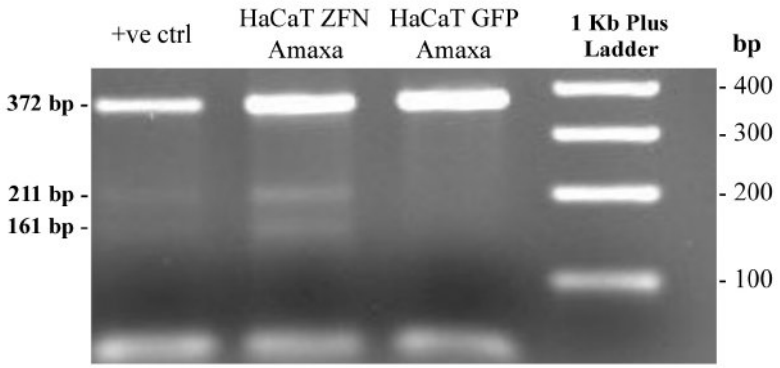

Figure 5.1 CEL-I assay for the detection of ZFN-mediated cleavage in HaCaT keratinocytes.
Exons 3-5 of *COL7A1* were amplified by PCR based heteroduplex reaction and products were examined by CEL-I assay for mismatch detection. A cleaved product was seen at 211 bp and 161 bp in HaCaT keratinocytes nucleofected with the left and right ZFN DNA plasmid (**lane 2)** and in the positive (+ve) kit control (**lane 1**), whereas there was no digested band in GFP nucleofected sample representing the negative control (**lane 3)**.

5.2 Disruption of *COL7A1* in keratinocytes by lentiviral-based ZFN delivery - generation of an *in vitro* RDEB cell model

5.2.1 Improvement of ZFN delivery efficiency by incorporation of ZFN sequences into a non-integrating lentiviral platform

Delivery of plasmid DNA to keratinocytes or stem cells through transient transfection or by electroporation remains a challenging and inefficient method as demonstrated with the ZFNs, which is sometimes associated with a significant level of cytotoxicity. Therefore, lentiviral vectors were used to improve the efficiency of ZFN delivery. Both left and right ZFN DNA sequences described in section 5.1, were separately subcloned into the 2nd generation lentiviral transfer plasmid (pHR'SIN.cPPT-SW) containing a spleen focus-forming virus (SFFV) promoter using EcoRI /BamHI blunt end sites and an XhoI sticky end site. Positive clones were confirmed by restriction enzyme digestion and DNA sequencing. Vectors were pseudotyped with VSV-G (pMD2.G) and packaged using the HIV-1-based NILV system by co-transfecting the HEK-293T host cells with the Δ64 mutated *gag/pro-pol* plasmid (pCMV-dR8.74-D64V) **(Figure 5.2)**. Left and right ZFN sequence-bearing transfer plasmids were packaged into separate NILV constructs. Viral titres were determined by quantifying the HIV-1 p24 antigen concentrations by ELISA (see Methods 2.2.29). The viral protein p24 levels (ng/ml) corresponding to a physical titre were converted to an estimated functional titre (IP/ml)

assuming a range of 10 to 100 TU per pg of p24. Viral preparations were concentrated by 340-fold and average viral titres converted from p24 protein levels were $4.17x10^{8-9}$ IP/ml for NILV-ZFN Left and $2.68x10^{8-9}$ IP/ml for NILV-ZFN Right.

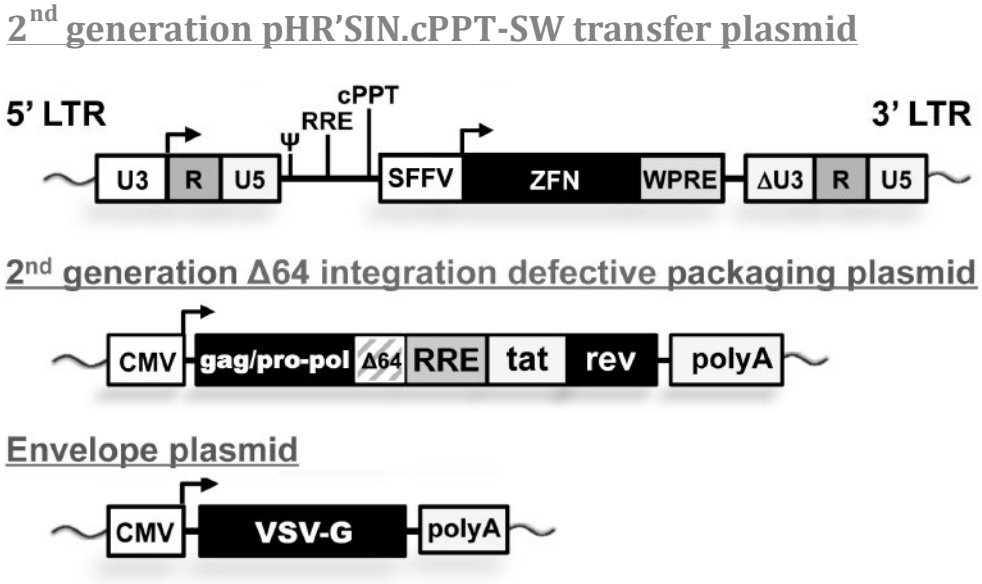

Figure 5.2 Schematic of 2nd generation NILV transfer and packaging system.
NILV-ZFN transfer, packaging and envelope plasmids. U3: untranslated 3' end; HIV1R: human immunodeficiency virus 1 reverse; U5: untranslated 5' end; ψ: psi packaging signal; RRE: rev response element; cPPT: central polypurine tract; SFFV: spleen-focus forming virus promoter; ZFN: Zinc Finger Nuclease transgene; WPRE: woodchuck hepatitis posttranscriptional regulatory element; ΔU3: deletion in untranslated 3' end; CMV: cytomegalovirus promoter; gag/pro-pol: HIV-1 structural and accessory polyproteins; Δ64: substitution of aspartic acid to valine in HIV-1 integrase; tat: HIV-1 trans-activating regulatory protein; rev: HIV-1 accessory protein; polyA: polyadenylation tail; VSV-G: vesicular stomatitis virus glycoprotein.

5.2.2 Efficiency of NHEJ-mediated cleavage in keratinocytes transduced with NILV-ZFNs

To assess the NILV-ZFN cleavage efficiency, the keratinocyte cell line, NTERT, encoding a WT copy of the *COL7A1* gene, was seeded at a density of $2x10^5$ cells/well of a 24-well plate and co-transduced with left and right NILV-ZFNs at MOIs of 20 or 100, respectively. Owing to the high viral titres, the virus volume added fell below the 10% threshold of the total cell culturing volume, and therefore, no obvious cytotoxicity or impaired cell growth was observed in transduced cells. Subsequent experiments were therefore carried out using the cells transduced with an MOI of 100.

The transduced cells were propagated for 7 days and DNA was extracted and amplified by PCR for the genomic region covering exon 4 and incorporating the ZFN cut site by PCR. PCR products were further run using the heteroduplex hybridisation program and subjected to CEL-I assay. The results revealed two additional faint bands corresponding to the expected sizes of the cleaved heteroduplex in the NILV-ZFN transduced population, suggesting ZFN-mediated cleavage and NHEJ activity in the targeted region. In contrast, no additional bands were detected in untransduced or NILV-GFP-transduced cell controls **(Figure 5.3)**.

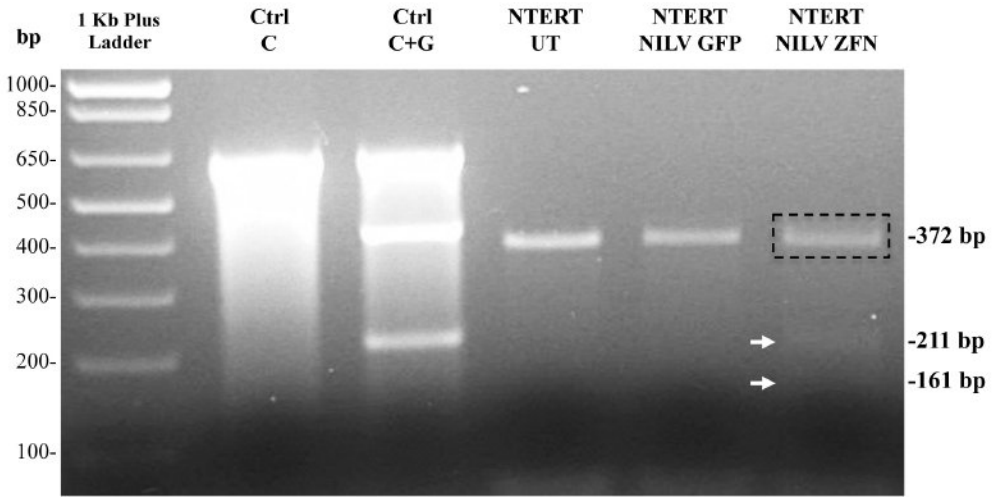

Figure 5.3 CEL-I assay confirming NHEJ in bulk population of NILV-ZFNs transduced NTERTs. Bulk populations of untransduced NILV-GFP or NILV-ZFN NTERTs were PCR amplified across the ZFN cut site region and allowed to form heteroduplexes before digesting with CEL-I nuclease. **Lanes Ctrl C** and **Ctrl C+G** show internal kit negative and positive controls respectively; **Lanes NTERT UT** and **NTERT NILV GFP** represent untransduced (UT) or NILV-GFP transduced experimental negative controls; **Lane NTERT NILV ZFN** represents bulk population of NILV-ZFN transduced NTERTs at MOI of 100. The results showed the expected digested products at 211 bp and 161 bp in the positive control and at 416 bp and 217 bp in cells transduced with NILV-ZFNs, but not in the UT or NILV-GFP transduced NTERTs.

To further investigate the mutation frequency mediated by ZFNs in the NILV-ZFN transduced NTERT cells, a set of barcoded primers specifically amplifying the region of interest within exon 4 of *COL7A1* were designed. DNA extracted from the untransduced and NILV-ZFN transduced NTERTs were PCR amplified and analysed by high throughput next generation sequencing (NGS) using an Illumina MiSeq genome sequencer (see Methods 2.2.31). Approximately $1.6x10^6$ raw reads were passed through a series of deconvoluting filtering steps allowing for the removal of ~$4x10^5$ unmatched reads with the post-filtered fraction containing solely matched reads. Sequence alignment against the endogenous *COL7A1* sequence ultimately resulted in detection of 18.3% of mismatches caused by NHEJ-mediated indels while 81.7% of the cells were unaffected. Analysis of the untransduced population resulted in a non-specific

background readout of 0.3% **(Table 5.1)**. Although not to be used as a reliable method of quantification, the obtained NGS data confirm the qualitative result of the CEL-I assay demonstrating the functionality of the NILV-ZFNs through the detection of genomic disruptions in *COL7A1*. These data further point towards an improved efficiency of ZFN delivery by NILV over plasmid DNA nucleofections.

Table 5.1 Mutation analysis by high-throughput sequencing of polyclonal NILV-ZFN transduced NTERT population.

Illumina MiSeq	**Bulk UT KC**		**Bulk NILV-ZFN KC**	
Number of raw reads	1594858	100%	1616697	100%
Number of reads after Q30 filtering	1305443	81.9%	1284425	79.4%
Number of reads after matching paired end reads	1296396	81.3%	1190989	73.7%
Total reads post-filtering	**1296396**	**100%**	**1190989**	**100%**
Total analysed reads of expected sequence	**1292303**	**99.7%**	**973503**	**81.7%**
Total analysed reads (sequences) of non-matching sequence	**4093 (81)**	**0.3%**	**217486 (722)**	**18.3%**

5.2.3 Assessment of NILV-ZFN cleavage frequency in single cell clones

To further confirm and quantify the NILV-ZFN cleavage activity seen in the polyclonal transduced NTERT population, single cells were manually sorted by limiting dilution cloning. A total of 48 single clones were expanded from the polyclonal population. DNA sequences amplified for the exon 4 region of *COL7A1* were examined for the detection of indels across the ZFN cut site by Sanger sequencing. 36 out of 48 clones were unaffected, while 10 out of 48 clones (20.8%) presented with monoallelic disruption and 2 out of 48 clones (4.2%) showed biallelic disruption at the ZFN target site **(Figure 5.4)**. Of the 10 clones exhibiting monoallelic disruption, clone cl3 & cl26 were selected, identified to have a 2 bp deletion within the ZFN cut site. Both clones, showing biallelic disruption, cl4 and cl15, were selected and when sequenced, were shown to have deletions at the ZFN cut site of 2 bp and 4 bp, respectively **(Figure 5.4)**.

CEL-I digestion was carried out on PCR hybridised heteroduplex products of the selected clones to further verify the single and double stranded breaks in *COL7A1* **(Figure 5.5)**. Both

clones (cl3 & cl26) which showed monoallelic disruption carried heterozygous mutations which resulted in the two expected shorter fragments after CEL-I-mediated mismatch cleavage. The results from cl4, which had presented with biallelic disruption, also revealed the additional smaller cleaved fragments upon CEL-I digestion suggesting it was a heterozygous mutant clone. The sequencing data confirmed cl4 had a compound heterozygous mutation, as in addition to the 2 bp deletion seen in both alleles, a single base mismatch in one allele was also detected. The biallelic disruption detected in cl15 only revealed a single undigested PCR product confirming the Sanger sequencing data, which showed a matching homozygous mutation in both alleles. The heteroduplex PCR product of cl15 was spiked by hybridisation with that of unmodified NTERT clone (cl1) carrying the WT *COL7A1* sequence which confirmed the mutation seen by the digestion of the hybridised cl15+cl1 PCR product **(Figure 5.5)**.

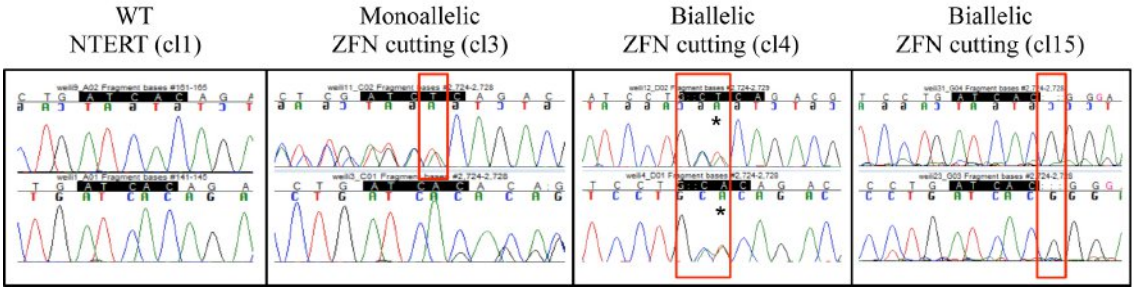

Figure 5.4 Detection of NILV-ZFN induced mutations by Sanger sequencing.
Individual NILV-ZFN treated NTERT clones were sequenced along the ZFN cut site for the detection of indels. Untransduced WT NTERT cells **(cl1)** show intact endogenous *COL7A1* sequence; NILV-ZFN transduced NTERTs show monoallelic disruption in *COL7A1* **(cl3)**; biallelic disruption with compound heterozygous mutations **(cl4)** and a homozygous mutation **(cl15)** in *COL7A1*. The sequencing results of the individual NTERT clones confirmed NHEJ mediated heterozygous and homozygous mutations following NILV-ZFN transduction. Mutations highlighted by red borders; asterisk: single-nucleotide changes.

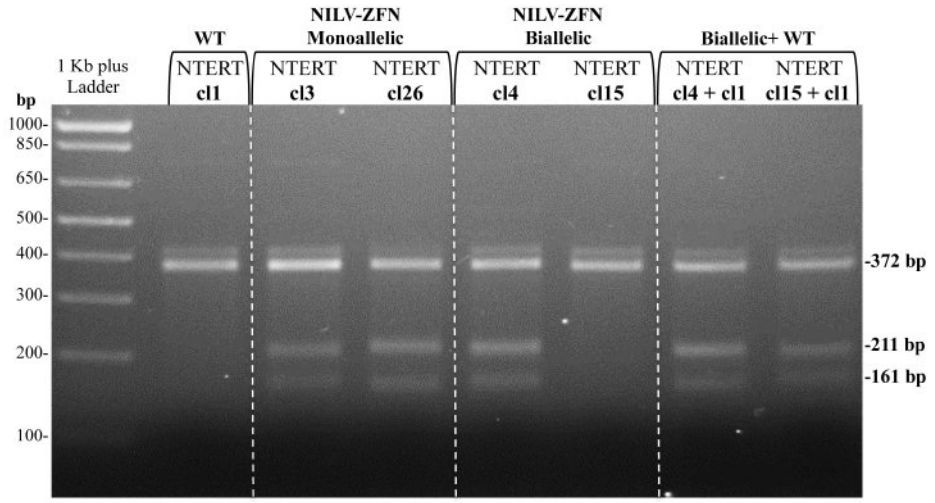

Figure 5.5 Detection of mutations in selected clones of NILV-ZFN transduced NTERTs by CEL-I nuclease assay.

NILV-ZFN treated NTERT clones detected to have undergone NHEJ were subjected to CEL-I assay for further detection of mismatches caused by indels. Wild-type (WT cl1) or NILV-ZFN transduced NTERT KC clones were PCR amplified for a region of the ZFN cut site and after heteroduplex hybridisation the product was digested with CEL-I. WT clone **(cl1)** shows single full-length product (372 bp) suggesting no mutation in the region, whereas heterozygous mutant NILV-ZFN transduced clones **(cl3)** & **(cl26)** and compound heterozygous mutant **(cl4)**, show cleaved product at 211 bp and 161 bp suggesting NHEJ-induced mismatches in the sequence. Homozygous mutant clone **(cl15)** showed no cleaved product as the incurred DSB resulted in identical deletions in both alleles. Hybridisation of cl1 with cl4 or cl15 showed appearance of cleaved product, confirming NHEJ in cl15.

5.2.4 NILV-ZFN treated NTERT clones result in significant C7 disruption

As there was no donor template provided to support homologous recombination for repair of the NILV-ZFN-induced genomic break, the mutations introduced during the error-prone NHEJ pathway are expected to result in frameshifts and PTCs in *COL7A1* with a functional impact on C7 protein expression. To examine whether C7 expression was affected following NILV-ZFN treatment, cell lysates from clones cl1, cl3, cl26, cl4 & cl15 were subjected to 6% SDS-PAGE and probed with the Chen-C7 antibody. The results showed a marked decrease of C7 protein expression in cl3 & cl26 carrying a heterozygous null mutation and complete absence of protein bands in the compound heterozygous mutant cl4 and homozygous mutant cl15 compared to WT NTERT cl1 C7 expression levels **(Figure 5.6)**. The reduction in C7 protein expression levels was corroborated by *in situ* immunofluorescence staining in clones using mAb-C7-LH7.2. The results showed an approximately 50% reduction and 100% reduction of C7 levels in monoallelic and biallelic disruption respectively **(Figure 5.7)**.

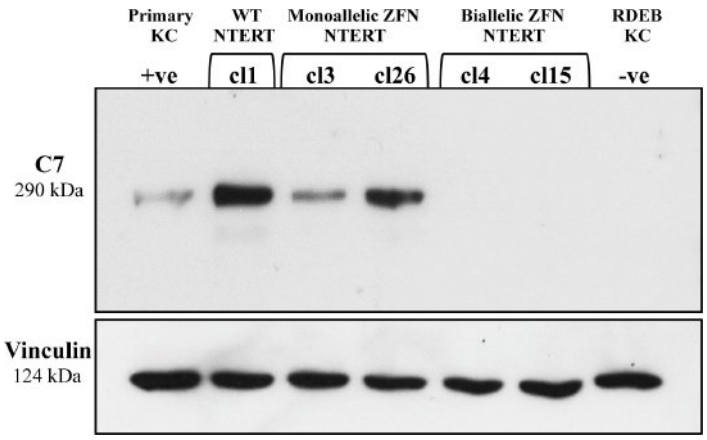

Figure 5.6 Disruption of C7 expression following NILV-ZFN.
C7 protein levels were assessed in cell lysates from NTERT clones following transduction with NILV-ZFNs by Western blot. Primary keratinocytes **(KC)** and untransduced wild-type NTERTs **(WT NTERT)** representing the positive controls show positive C7 expression at 290 kDa while RDEB EBKCs representing the negative control demonstrate complete lack of expression. NILV-ZFN transduced NTERTs with monoallelic disruption of *COL7A1* **(NTERT cl3 & cl26)** show ~50% reduction of C7 expression compared to WT NTERTs, and complete absence of C7 expression in NTERT clones **(cl4)** and **(cl5)** with biallelic disruption of *COL7A1*. Vinculin was used as a loading control.

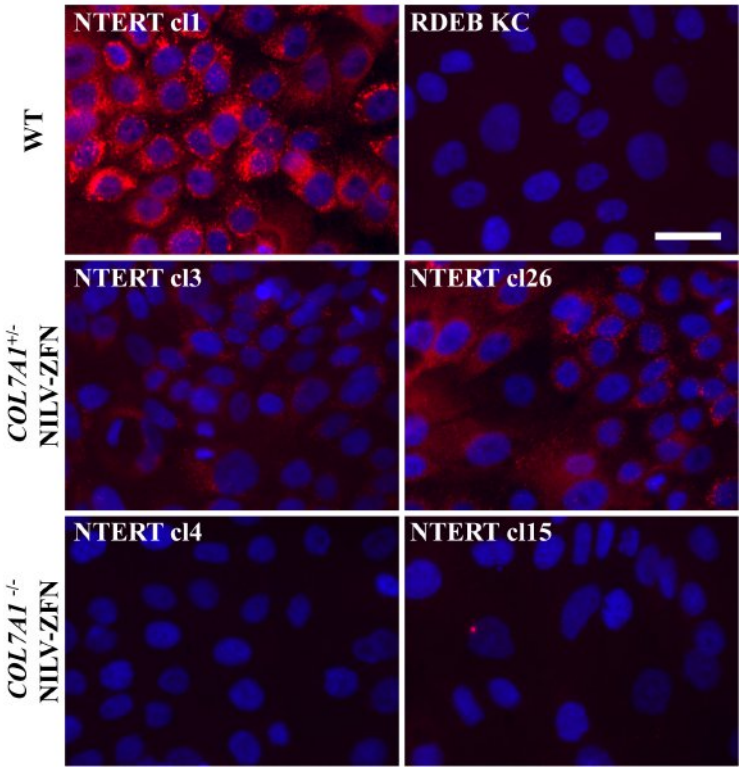

Figure 5.7 C7 expression in NTERTs following NILV-ZFN mediated disruption of *COL7A1*.
In situ immunofluorescence staining for C7 expression was performed in NTERT clones treated with NILV-ZFNs. **Top left** panel indicates wild-type (WT) NTERT positively expressing C7 (red). The **top right** panel show absence of C7 staining in RDEB EBKCs representing the negative control; the **middle** panel depicts partial C7 expression in monoallelic disrupted clones (cl3 & cl26) compared to WT NTERTs and the **lower** panel shows biallelic disrupted clones (cl4 & cl15) with abrogation of C7 protein expression. Nuclei were counterstained with DAPI (blue). Scale bar = 25 μm.

Taken together, these data demonstrated transduction of NTERTs with NILV-ZFNs targeting exon 4 of *COL7A1* could induce DSBs in the region, with a frequency of 25%. There appeared to be a direct correlation between the ZFN-induced genomic disruptions in the target gene and protein expression level, resulting in partial or complete C7 knockdown following monoallelic and biallelic disruption respectively.

5.2.5 Alteration of migration speed in cells transduced with NILV-ZFNs

The functional change in the ZFN-treated clones were examined by *in vitro* "wound-healing" scratch assay **(Figure 5.8)**. Previous studies (Section 3.5.1) have demonstrated that lack of C7 expression can affect cell migration. In order to assess whether the NILV-ZFN treated NTERTs exhibit a similar effect, monoallelic and biallelic disrupted clones were seeded in 6-well plates at a density of $1.2x10^6$ cells and treated with mitomycin C for 2 hrs to induce cell cycle arrest (see Methods 2.2.34). A scratch was made in the confluent cultures and the open 'wound' area closure time was monitored by time-lapse microscopy over a 10 hr period. Representative images from three separate time points suggest a reduced "wound" closure speed in the affected clones, cl3 and cl4, over WT cl1. The AUC of each clone was further calculated and analysed. The results when statistically compared by one-way ANOVA showed significant variation in migration values within the group ($p \leq 0.001$). Multiple comparison analysis revealed monoallelic disrupted cl3 partially expressing C7 to have a noticeable decrease in migration over WT cl1 ($p \leq 0.05$) with full scratch closure at ~9 hrs. The effect was exacerbated in biallellic disrupted cl4 NTERTs lacking C7 expression, with scratch closure time (~10 hrs) being significantly reduced to that of WT cl1 ($p \leq 0.001$). Migration speed was also found to be reduced in cl4 when compared to cl3 ($p \leq 0.01$) **(Figure 5.2 A & B)**.

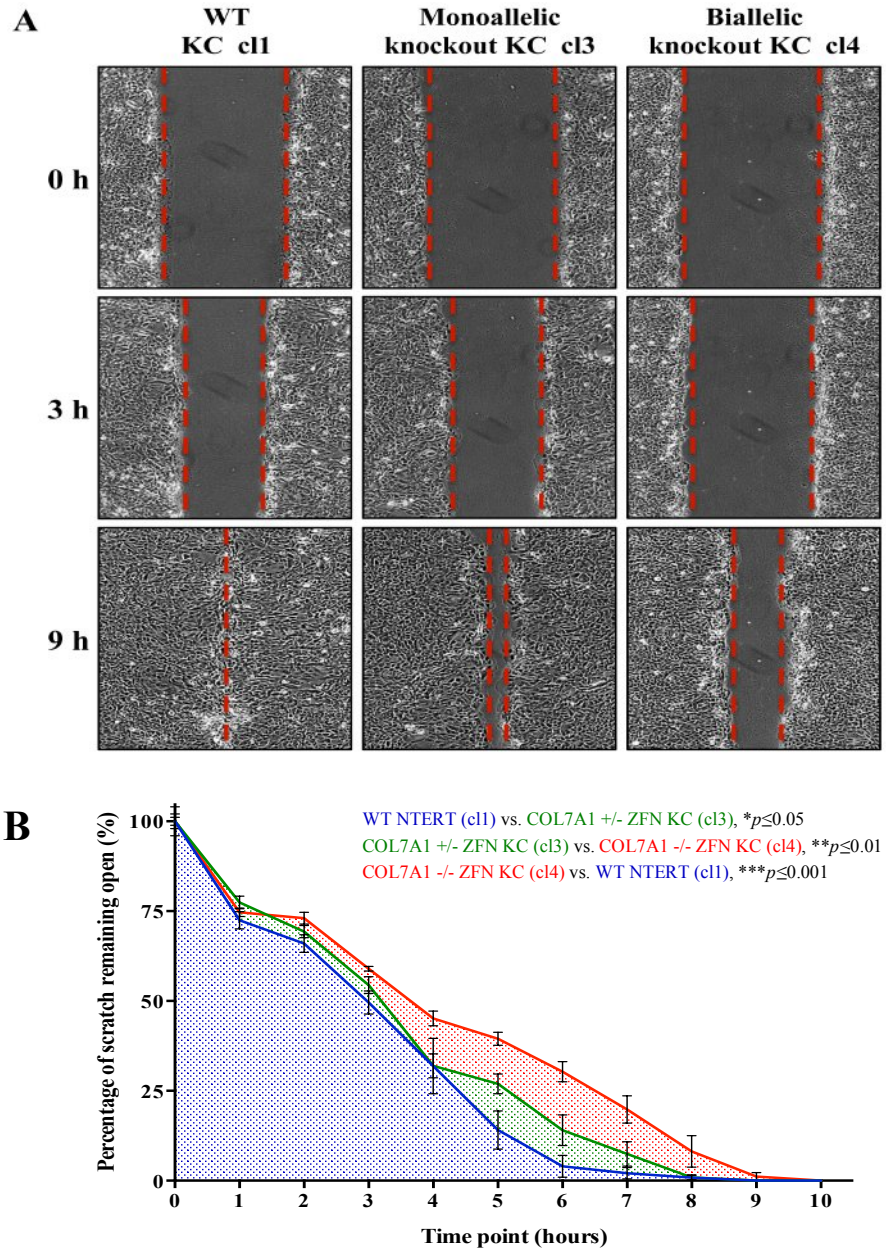

Figure 5.8 Assessment of migration in NTERT keratinocytes following NILV-ZFN transduction causing downregulation of C7.

NTERT cells with *COL7A1* knock out (cl4) or knock down (cl3) were treated with Mitomycin C and the rates of cell migration were assessed by an *in vitro* scratch assay over 10 hrs. Images were captured by time-lapse microscopy at 15 min intervals and representative images at 0, 3 and 9 hrs are shown **(A)**. WT represents NTERTs with WT COL7A1 sequence and normal C7 expression; cl3 represents NTERTs with monoallelic *COL7A1* gene disruption and partial C7 expression and cl4 represents NTERTs with biallelic *COL7A1* disruption and lack of C7 expression. The percentage of non-occupied open "wounded" areas were dynamically analysed over a 10 hr period **(B)**. Error bars were calculated based on standard error of the mean (n=3). Area under the curve (AUC) values of each replicate of each clone were calculated for each clone and analysed statistically. The results showed significant differences in migration rates amongst the 3 NTERT populations (**p<0.001, one-way ANOVA). Multiple comparison analysis by Tukey post-test was further used and results showed a decreased migration rate compared to WT NTERT cells (cl1) in both *COL7A1* knockdown (cl3) (*$p\leq0.05$) and knockout (cl4) cells (**$p\leq0.001$).

5.2.6 Restoration of C7 expression in NILV-ZFN COL7A1 knockout cells following transduction with LV-COL7

The RDEB cell model generated by NILV-ZFN mediated knockout of *COL7A1* was further tested for the RDEB lentiviral-based gene addition strategy using LV-COL7. NILV-ZFN clone 4 (cl4) carrying compound heterozygous mutations resulting in absence of C7 expression was transduced with LV-COL7 viral vector at an MOI of 1.6. The transduced cells were assessed for C7 protein expression by *in situ* immunofluorescence staining using Calbio-C7-pAb. The results revealed positive staining for C7 in the LV-COL7 vector transduced cl4 cells, but not in untransduced cl4 cells. **(Figure 5.9 B)**. The percentage of positively stained cells were counted in three individual optical images and the results showed 15.23% ± 5.7% cells to be positively expressing C7. C7 expression was further assessed by Western blot and full-length C7 was seen in cl4 cells transduced with LV-COL7, WT NTERT and cl3 clones and primary keratinocytes **(Figure 5.9 A)**. In contrast, no C7 expression could be detected in either untransduced cl4 cells or in LV-GFP control vector transduced cl4 cells. However, a very faint band at 290 kDa was noticed in both untransduced and LV-GFP transduced NILV-ZFN cl4 cells. Supported by previous examination of cl4 at genomic and protein level confirming the absence of C7 (sections 5.2.3 and 5.2.4), the weak signal seen is most likely a result of minor spillage from the neighbouring C7 positive well. The proviral copy number confirming genomic integration was also assessed by quantitative PCR and the results showed a 0.021 VCN/cell, indicating 2.1% transduction efficiency in the cl4 cells transduced with LV-COL7 at MOI 1.6.

These results, therefore suggest that NILV-ZFN generated *COL7A1* knockout cells can be utilised as an *in vitro* RDEB cell model for the *in vitro* functional assessment of the disease, while can also offer a platform for the investigation of alternative gene therapy approaches.

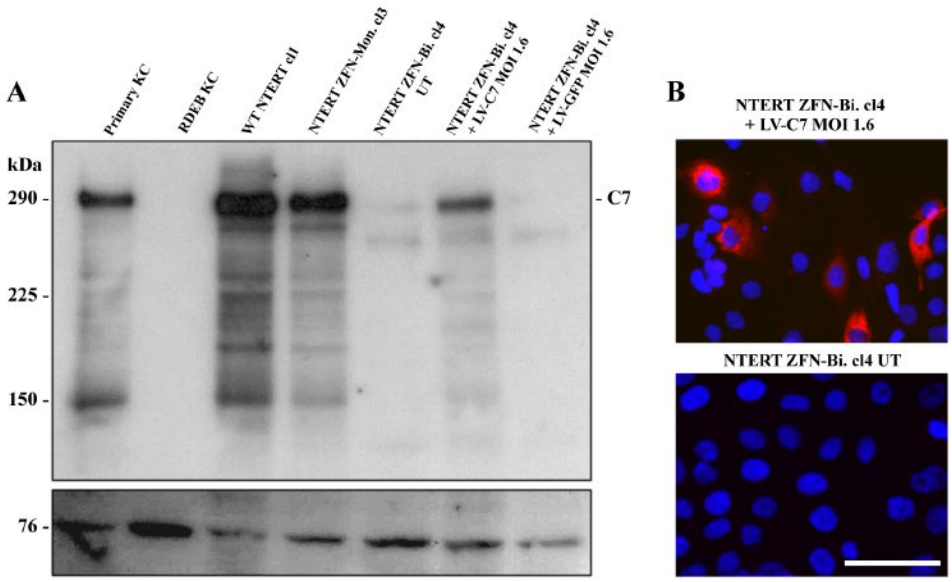

Figure 5.9 Restoration of C7 expression in NILV-ZFN cl4 cells transduced with LV-COL7.
NILV-ZFN cl4 cells carrying heterozygous biallelic mutations in *COL7A1* were transduced with LV-COL7 at an MOI of 1.6. The C7 protein expression was examined by Western blot and *in situ* immunofluorescence staining. The Western blot results representing results from a single experiment **(A)** showed restoration of a 290 kDa C7 protein in LV-COL7 transduced NILV-ZFN cl4 cells. Positive controls included primary healthy donor keratinocytes, NTERT cells expressing WT *COL7A1* (WT); NTERT cells carrying the heterozygous *COL7A1* mutation (cl3) generated by NILV-ZFNs. Negative controls included RDEB EBKC (RDEB KC UT) and NTERT cells carrying the compound heterozygous mutation in *COL7A1* (cl4), either untransduced or transduced with LV-GFP. Faint expression in untransduced cl4 was due to sample overflow from neighbouring well. Non-specific band at 76 kDa was used as internal loading control. *In situ* immunofluorescence staining **(B)** shows C7 expression (red) in NILV-ZFN *COL7A1* knockout cl4 cells transduced with LV-COL7. There was no C7 expression in untransduced NILV-ZFN cl4 cells. These images depict a single representative field of the stained area. Scale bar = 50 μm.

5.3 Gene editing in *COL7A1* by homologous recombination-mediated repair following co-delivery of NILV-ZFNs and homologous donor template

5.3.1 The design and subcloning of a homologous donor template

ZFNs when co-delivered with exogenous template sequence, present the ability to edit and correct mutations within targeted genomic regions by triggering the HDR pathway. To test this function, a homologous donor template was designed bearing a portion of the WT *COL7A1* sequence spanning exons 3 to 7 while preserving introns 2 to 7 **(Figure 5.10)**. The donor template was designed taking into consideration the optimal length of the homology arms with a

recommended span of ~400-800 bps on either side of the ZFN cleavage site acknowledging that most efficient repair occurs within the first 100 bps (Hasty et al., 1991, Thomas et al., 1986, Elliott et al., 1998, Ran et al., 2013). To enable detection of the template sequence upon integration, a KpnI restriction site was included within intron 4 of the donor template sequence to allow for confirmation of HDR. EcoRI and XhoI restriction sites were further added at the 5' and 3' ends of the donor template sequence, respectively, to allow for subcloning into the pHR'SIN.cPPT-SW lentiviral transfer plasmid **(Figure 5.10)**. The designed donor template was commercially synthesised (GeneArt) and subsequently subcloned into the modified lentiviral pHR'SIN.cPPT-W plasmid lacking an SFFV promoter (NILV-OriginalTemp). The viral preparations employed the Δ64 integrase defective packaging plasmid for production as a NILV as previously described (Section 5.2.1).

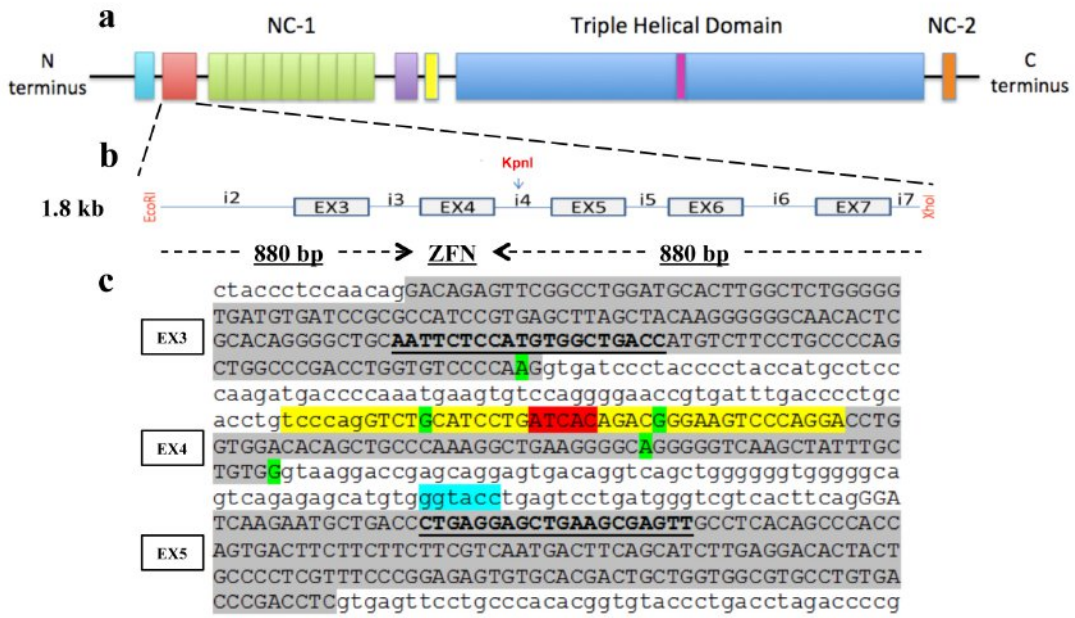

Figure 5.10 Donor template design.
The donor template was designed spanning exons 3 to 7 including introns 2 to 7 of *COL7A1*. **(a)** C7 protein monomer; **(b)** synthesised recombinant 1.8 kb donor template sequence spanning intron 2-7 with addition of KpnI digestion site; **(c)** exons 3-5 of recombinant donor template sequence indicating ZFN binding sites (yellow), ZFN cleavage site (red) and the addition of KpnI restriction site (blue). Capitals highlighted in grey: exons; lower case: introns; green: known mutations; bold underlined: PCR primer sites.

In an attempt to avoid ZFN-mediated cleavage of the donor template containing the ZFN binding sites, silent mutations were introduced in the ZFN recognition sequence of the template to protect from unwanted cutting. Site-directed mutagenesis (SDM) was performed by using complementary primers containing the desired base substitutions (see Methods 2.2.17). 7 individual silent mutations were introduced over a distance of >40 bps, with 3 nucleotide substitutions in the left and an additional 4 in the right ZFN recognition regions, in a two-step SDM reaction process using two sets of mutagenic primers. Positive colonies were checked by Sanger sequencing and the correctly modified clones showing incorporation of all 7 silent mutations were used for preparation of virus (NILV-SDMTemp). Titres of concentrated viral preparations for both NILV-OriginalTemp and NILV-SDMTemp vectors were assessed by p24 ELISA assay and converted to a biological titre (see Methods 2.2.29). The viral titre range was from $4.82x10^{7-8}$ to $2.81x10^{8-9}$ IP/ml.

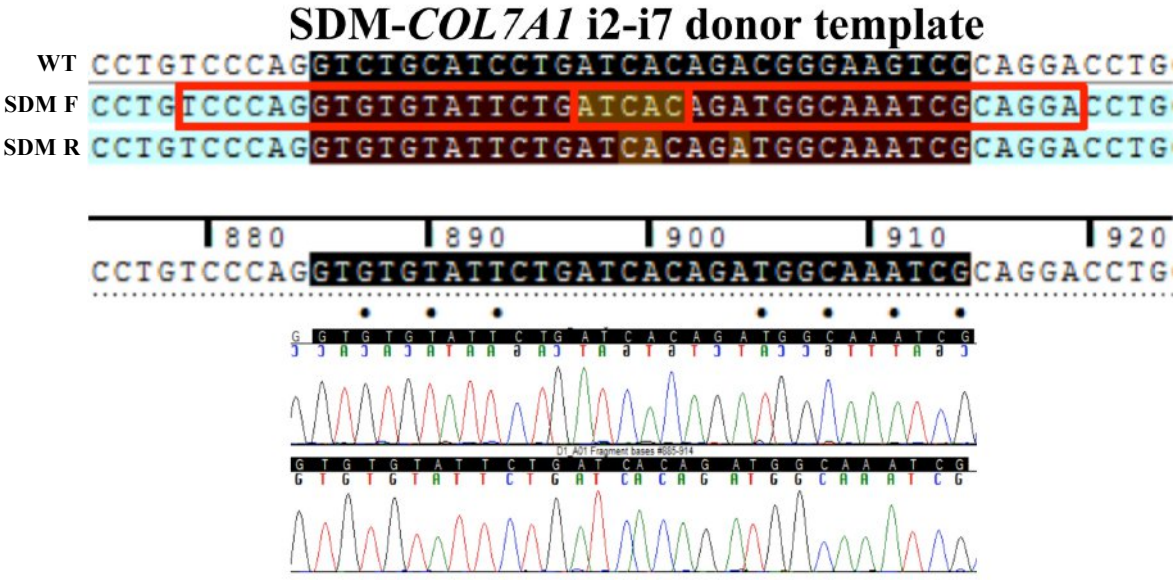

Figure 5.11 ZFN binding site modification of donor template sequence by site directed mutagenesis
Original template sequence was modified by introducing silent mutations by site directed mutagenesis (SDM) to the ZFN binding site to prevent unwanted cleavage. The sequences show a correctly modified clone with 7 introduced silent mutations in exon 4 of the donor template sequenced using forward (SDM ex4 COL7A1 template forward) and reverse primers (SDM ex4 COL7A1 template reverse) when compared against WT *COL7A1* reference sequence (WT). Marked dots indicate base substitutions, resulting in degenerate codons encoding same amino acid as the endogenous sequence.

5.3.2 Integration of donor template into "recipient" genomic DNA by HDR pathway following NILV-induced DSBs

To examine the efficiency of the donor template to integrate into recipient genomic DNA following ZFN cleavage through the process of HDR, both the NILV-OriginalTemp and NILV-SDMTemp were tested. As there was no RDEB patient keratinocytes available with a mutation spanning exon 4, NTERT cells carrying a WT copy of *COL7A1* with normal levels of endogenous C7 expression were selected for a proof-of-principle study. Although this implies that NILV-ZFN/template transduced cells successfully undergone HDR could not be detected on account of C7 expression restoration, the unique KpnI restriction site incorporated in the donor template was used to confirm template integration.

WT NTERT cells were seeded at a density of $2x10^5$ cells /well of a 24-well plate and co-transduced the following day with NILV-ZFN (Left) and NILV-ZFN (Right) at an MOI of 100 of each and with either NILV-OriginalTemp or NILV-SDMTemp at an MOI of 200. There was no noticeable toxicity observed the following day. ZFNs and donor template NILVs were co-delivered at the same time-point to ensure the template sequences were reverse transcribed and readily available by the time the ZFNs have undergone translation and mediated cleavage.

DNA extracted from the transduced cells was assessed for template integration by KpnI digestion of the PCR amplified product of the targeted genomic region. A very faint band was observed by gel electrophoresis, suggesting donor template integration in a small portion of the transduced cells **(Figure 5.12 A)**. This was confirmed in NTERTs transduced with both NILV-OriginalTemp and NILV-SMDTemp templates. The transduced cells were further propagated for about 14 days to dilute out transient expression of the NILVs and were then sorted as single cell clones by limiting dilution (see method 2.2.21). 103 clones from cells transduced with NILV-ZFNs + NILV-OriginalTemp and 85 clones from cells transduced with NILVs + NILV-SDMTemp were picked and expanded for DNA extraction. The region spanning exons 3 to 5 was amplified and sequenced for detection of the novel KpnI site and the SDM modifications. The results revealed 1 (cl13) out of 103 NILV-ZFNs + NILV-OriginalTemp clones contained the KpnI site and 1 (cl8) out of 85 NILV-ZFNs + NILV-SDMTemp transduced clones contained both the KpnI site and the SDM modifications. The template integration efficiencies were 0.97% and 1.17%, respectively. In both cases the integration of the template sequence was monoallelic. It was noticed, that the frequency of NHEJ dropped significantly compared to the values obtained by NILV-ZFN transduction alone. This may be due to viral competition during co-introduction of cells with three separate vectors, NILV-ZFN left, NILV-ZFN right and a NILV-template.

The positive clones cl13 & cl8 were further analysed by restriction digestion of KpnI. The results confirmed the presence of the expected band sizes corresponding to the digested template in both NILV-OriginalTemp and NILV-SDMTemp transduced clones **(Figure 5.12 B)**. A substantial amount of undigested product was observed in these samples compared to digestion of the positive control template plasmid. This is unlikely due to inefficient activity of the enzyme, but rather, a result of the monoallelic presence of the KpnI site in these clones.

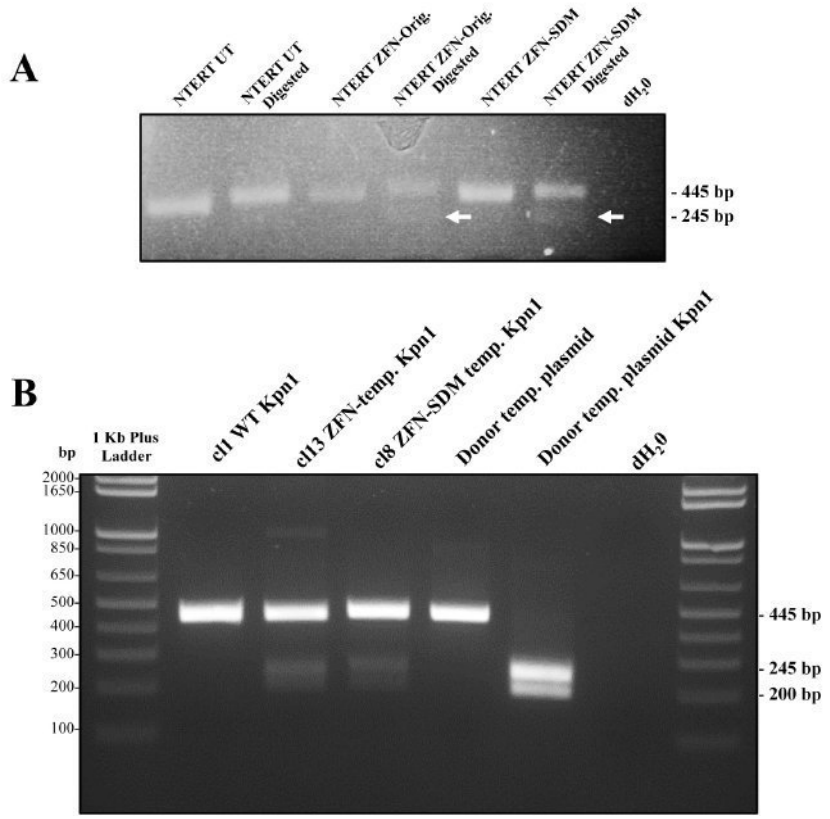

Figure 5.12 Confirmation of template integration in NILV-ZFN + NILV-template transduced NTERTs by KpnI digestion

PCR amplicons from polyclonal cells or single cloned cells transduced with NILV-ZFNs + NILV-OriginalTemp or NILV-SDMTemp were examined for template integration using KpnI digestion. **(A):** PCR products from polyclonal NTERT cells transduced with NILV-ZFNs + NILV-OriginalTemp or NILV-SDMTemp shows faint band at 245 bp corresponding to digested product, compared to untransduced NTERTs and undigested negative controls. **(B):** PCR products from single cell clones cl13 transduced with NILV-ZFNs + NILV-OriginalTemp and cl8 transduced with NILV-ZFNs + NILV-SDMTemp digested with KpnI showing digested products at 200 bp and 245 bp. Control sample included positive control pHR'SIN.cPPT-TempW template plasmid and WT NTERT clone cl1 digested with KpnI and negative control undigested pHR'SIN.cPPT-TempW template plasmid. The results showed both polyclonal cells and single cell clones contained the novel KpnI site, suggesting integration of donor template into the recipient NTERT cell genome following co-transduction with ZFN and template NILVs.

5.3.3 SDM modification in the donor template eliminates unwanted cleavage mediated by NILV-ZFNs

Sanger sequencing of exons 3-5 of the *COL7A1* sequence in cells transduced with NILV-ZFNs + NILV-OriginalTemp or NILV-SDMTemp confirmed the presence of the novel KpnI sequence in both cl13 and cl8 clones within intron 4. The introduced SDM modification sites were further detected in cl8 **(Figure 5.13)**.

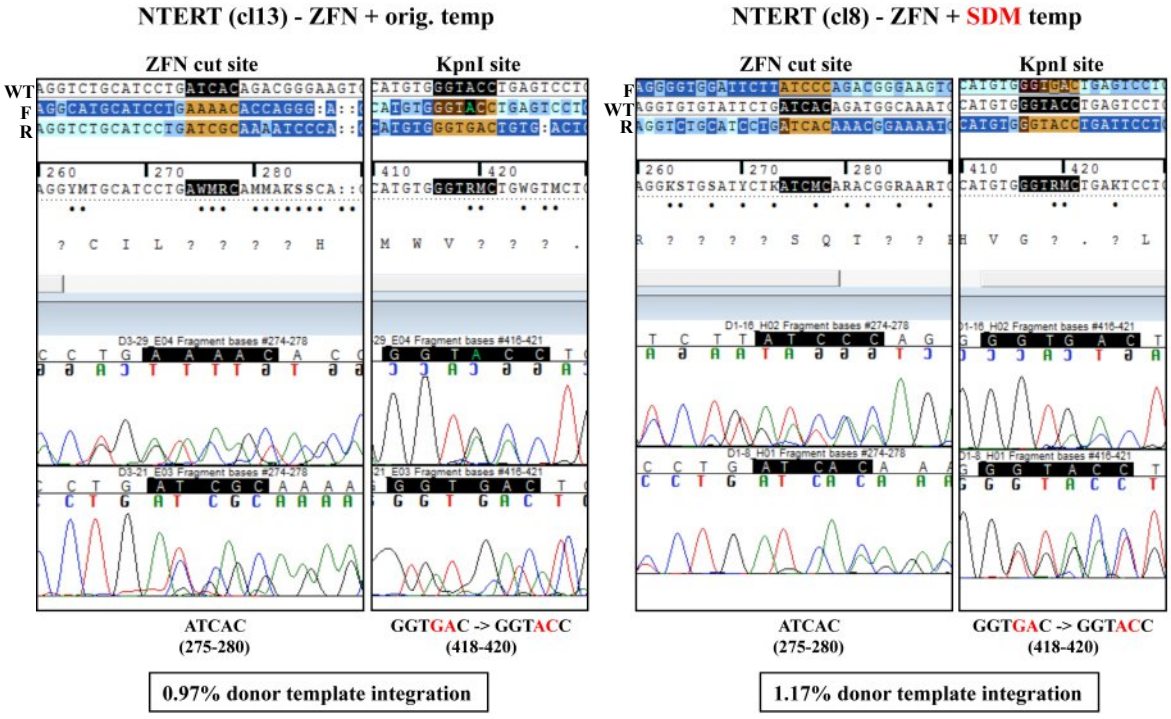

Figure 5.13 Confirmation of HDR-mediated template integration by SDM and KpnI site detection in NTERT clones using Sanger sequencing.
Amplicons of the *COL7A1* exon 3-5 genomic region using both SDM ex4 COL7A1 template-forward and reverse primers were sequenced. The results show the novel KpnI restriction site in both clones cl13 & cl8, but not in WT *COL7A1* reference sequence (WT). In addition, cl8 transduced with NILV-SDMTemp also shows incorporation of silent mutations introduced by SDM.

The PCR amplicon sequence traces indicated both clones cl13 and cl8 had monoallelic sequence variation. To further clarify the mutation sites, subcloning of the PCR amplicons into the TA vector TOPO® TA was carried out (see Methods 2.2.19). This allows for the two alleles to be individually subcloned into the vectors enabling the reliable detection of nucleotide changes in each allele. Positive clones were assessed by sequencing and results showed matched donor template sequences in NILV-ZFNs + NILV-SDMTemp transduced cl8 with incorporation of SDM modifications and the KpnI site ~145 bp upstream of the ZFN cut site in one allele

(Figure 5.14). A single base pair deletion at the ZFN cut site was detected in the other allele of cl8, but without additional donor template sequence. In clone cl13, transduced with NILV-ZFNs + NILV-OriginalTemp, one allele showed incorporation of the KpnI site, although importantly, a 7 bp deletion at the ZFN cut site and approximately 9 nucleotide substitutions, typically G>A were also detected in that same allele. In the other allele, there was a 10 bp deletion upstream of the ZFN cut site within the right ZFN binding region and no detection of additional donor template sequence **(Figure 5.14)**. The sequence variation observed in cl13 is likely to be caused by cleavage of the unmodified donor template by the NILV-ZFNs as the same phenomenon was not observed in cl8 transduced with NILV-SDMTemp. This highlights the requirement for the modification of the ZFN binding sites in the donor template sequence.

It was also noticed that during sequence analysis of both TOPO subcloned cl13 and cl8, a third allele with no sign of integrated template sequence or any additional mutations was detected. It is possible that this was a result of cross contamination from a second clone.

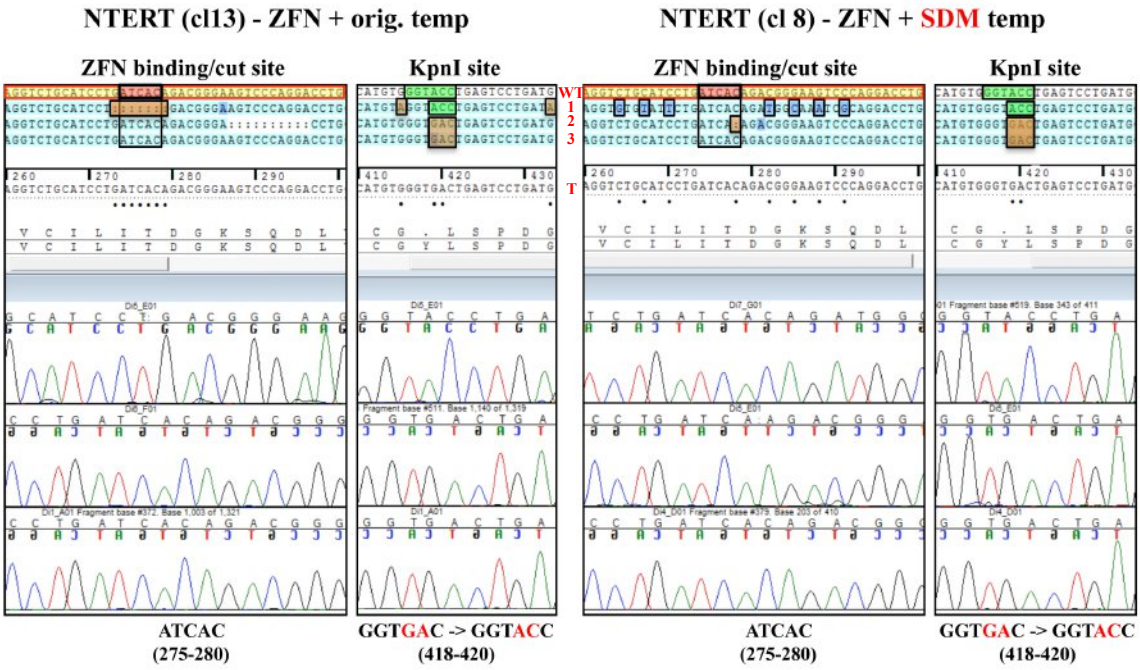

Figure 5.14 Identification of template integration sequences in NILV-ZFNs + NILV-template clones after TOPO-TA subcloning.
PCR amplicons from NILV-OriginalTemp cl13 **(left)** and NILV-SDMTemp cl8 **(right)** were subcloned into a TOPO TA vector and sequenced across exons 3-5 and aligned against WT *COL7A1* genomic sequence (WT). Results demonstrate successful monoallelic HDR in both clones with KpnI sequence and SDM silent mutations based on template sequence (T). However, a number of mutations were detected in cells transduced with NILV-ZFNs + NILV-OriginalTemp, indicating the importance of modification ZFN binding site sequence in the donor template. Yellow: ZFN binding domain; red: ZFN cut site; green: KpnI site; orange: mismatches/deletions compared to reference; blue: SDM modifications; dots: alignment mismatches; WT: WT *COL7A1* sequence; 1, 2, 3: individual alleles; T: integrated template sequence.

The results obtained from KpnI digestion experiments and single clone sequencing analysis demonstrated the successful integration of donor sequences mediated by the HDR pathway following ZFN induced genomic DSBs. Furthermore, the NILV delivery of ZFNs and template resulted in a notable improvement over plasmid DNA nucleofections. Moreover, incorporation of silent mutations in the homologous ZFN binding regions of the donor template sequence could successfully eliminate unwanted donor template cleavage by ZFNs.

5.4 Restoration of C7 expression at DEJ of *in vivo* human:murine RDEB skin graft model following *COL7A1* gene editing in RDEB fibroblasts

With a slightly enhanced targeting efficiency over ZFNs, TALENs known to have a available target binding site every ~35 bp of DNA, can be manufactured with relative ease within the laboratory and when coupled to an obligate heterodimeric *Fok1* nuclease domain can be utilised for precise genome editing. This strategy was employed for the site-specific correction of a *COL7A1* mutation in RDEB fibroblasts (Osborn et al., 2013). The authors had constructed plasmid DNA vectors containing specific TALEN sequences targeting an exon 14 PTC found in *COL7A1* of primary RDEB patient fibroblasts which were co-transfected with WT donor template for site-specific repair of the mutation. Positive clones were selected by puromycin resistance and monoallelic correction verified by sequencing of integrated template was further confirmed by Western blot and *in situ* immunofluorescence staining. The results showed restoration of C7 expression in the RDEB fibroblasts.

In support of this study, I investigated the *in vivo* functional potential of these cells in Prof. J. Tolar's lab (University of Minnesota, US). To assess whether the TALEN-corrected RDEB fibroblasts could deposit functional C7 at the DEJ and contribute towards the amelioration of subepidermal tissue cleavage, a human:murine chimeric skin graft model (see Methods 2.2.36 and Section 4.2) was used. Healthy donor, RDEB patient unmodified or TALEN-corrected fibroblasts and RDEB keratinocytes were used to generate bioengineered SEs. These were then grafted onto the dorsum of 6-week old athymic NMRI-*Foxn1*^{nu} mice and allowed to develop over an 8-week period. A 3 mm biopsy of the fully stratified human skin was harvested at week 8 post-transplant. The morphological characterisation by H&E staining and immunofluorescent analysis using a combination of human specific (mAb-C7-LH7.2) and mouse/human specific (Calbio-C7-pAb) C7 antibodies was carried out to confirm the grafting procedure **(Figure 5.15).**

The results revealed restoration of C7 expression and deposition of the protein at the DEJ of the TALEN-corrected graft, solely contributed to by the fibroblasts **(Figure 5.15 i-k)**. On the contrary, no signal was observed in the RDEB unmodified patient cell combination **(Figure 5.19 e-g)**. The healthy donor cell combination was used as a control to verify the effectiveness of the procedure showing strong human C7 deposition at the DEJ **(Figure 5.15 a-c)**. The specificity of the antibodies in detecting human C7 by mAb-C7-LH7.2 or both human and mouse C7 by Calbio-C7-pAb was confirmed in human and mouse tissue stained controls (**Figure 5.15 m-o & q-s)** and in the previous chapter (Section 4.1.2 Figure 4.2). Skin morphology was analysed by H&E staining with the results showing a distinctly thickened epidermis in all grafts closely resembling a human-like structure **(Figure 5.15 d, h, l)**. Furthermore, when focusing on the DEJ, strong dermal epidermal attachment was observed in the healthy donor combination **(Figure 5.15 d)**, whereas the epidermis appears to have completely separated from the underlying dermis in the unmodified patient sample due to tissue cleavage at the DEJ **(Figure 5.15 h).** Upon TALEN-mediated correction of the fibroblasts mediating HDR from a donor repair template, deposited C7 appears to have sufficiently restored the integrity of the BMZ therefore postulating the abundance of fully functional anchoring fibrils **(Figure 5.15 l)**.

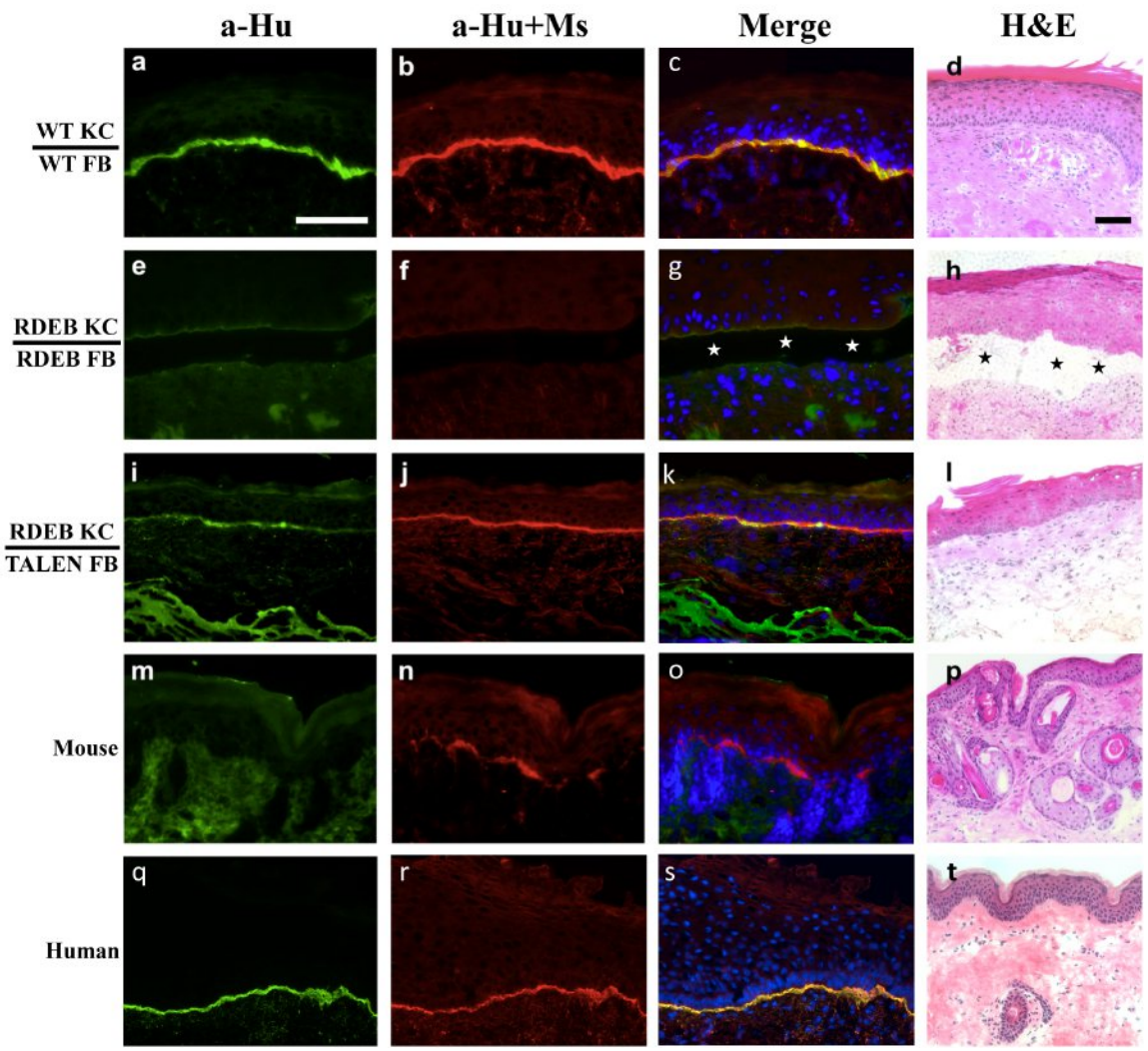

Figure 5.15 Correction of RDEB patient fibroblasts by TALENs leads to deposition of human C7 at the DEJ.

Bioengineered skin equivalents (SE) were grafted onto athymic NMRI-*Foxn1*^{nu} mice and 3 mm punch biopsies were harvested after 8 weeks for detection of human C7 by immunofluorescent staining. **(a-d)** represents SE seeded with healthy donor keratinocytes (KC) and fibroblasts (FB) (*n* = 2); **(e-h)** SE seeded with RDEB patient unmodified KC and FB (*n* = 2); **(i-l)** SE seeded with RDEB patient unmodified KC and TALEN corrected RDEB FB *(n* = 4); **(m-p)** represents control mouse skin tissue; **(q, r)** control human skin tissue. Antibodies that recognise either human only (green, α-H, mAb-C7-LH7.2) **(a, e, i ,m, q)** or both human and mouse C7 (red, α-H+M, Calbio-C7-pAb) **(b, f ,j, n, r)** were used to differentiate between human and mouse derived C7. Merged images reveal co-localisation of staining (yellow) in grafts where the C7 is of human origin **(c, k, s)**. The results depict restored C7 expression in the RDEB TALEN-corrected FB graft which was otherwise absent in unmodified RDEB grafts. H&E staining for morphological assessment of grafted tissue **(d, h, l)** against mouse **(p)** and human control skin **(t)**. Blistering and tissue separation at the DEJ is apparent in the RDEB uncorrected graft (stars) **(h)**. Scale bar = 100 μm.

5.5 Discussion

This work has highlighted the potential therapeutic use and possible improvement of available gene editing machinery for RDEB. This was shown by initially selecting a genomic target site within exon 4 of *COL7A1* to introduce a DSB using a pair of sequence specific ZFNs. Preliminary experiments delivering the ZFNs as plasmid DNA resulted in modest cleavage which was greatly increased by subcloning of the ZFN sequences into a NILV platform overcoming the notoriously hard to transfect nature of keratinocytes. Although there is a direct correlation between ZFN dose and cleavage efficiency, ZFNs delivered to target cells at high concentrations have been associated with an increased level of genotoxicity and hence cytotoxicity due to off-target effects (Bohne and Cathomen, 2008). This effect is greatly exacerbated when delivered to keratinocytes in plasmid DNA form, reported to decrease survival by 63.5% at concentrations of 1 μg/ml, while only achieving a ~7% genomic disruption efficiency (Hoher et al., 2012).

In this study, I showed ZFNs delivered by NILV led to a 25% knockdown of *COL7A1* with no noticeable detriment to target cell survival. This implies that NILV-based delivery is highly efficient and can greatly increase ZFN-mediated cleavage without negatively impacting cell survival. By harnessing the error-prone NHEJ endogenous cell repair mechanism, it allowed for the generation of *COL7A1* knockouts in both monoallelic and biallelic fashion resulting in either partial or entire loss of C7 protein expression. Functional assessment of the knockout clones by evaluation of the migration rate by an *in vitro* "wound healing" assay revealed the similarity of the knockout cells to RDEB patient cells. The first part of this study, therefore, demonstrated the successful modelling of the RDEB disease phenotype in a keratinocyte cell line for potential use in downstream applications assessing correction efficiency.

The significance of this result is highlighted by the fact that RDEB patient sample availability is scarce and the isolated primary cultures can be particularly challenging to propagate. Therefore, using the ZFN technology an infinite supply of RDEB-like cells can be generated carrying a wide range of user-defined mutations. This scenario was tested using the full *COL7A1* knockout model developed here for the assessment of C7 restoration by gene addition. Using the previously described LV-COL7 vector, C7 was successfully restored to the developed RDEB cell model in line with initial results obtained from transduction of RDEB patient primary keratinocytes.

A discrepancy was noticed in the untransduced cl4 biallelic disrupted cells, showing faint protein expression by Western blot at 290 kDa corresponding to C7. This was not believed to be true expression as the clone was extensively characterised during previous assessment at both

genomic and protein level. As the clone carried a compound heterozygous mutation it was hypothesised that one allele could potentially result in a missense mutation with full-length non-functional C7 expression. The Chen-C7 antibody detecting the NC-1 domain could therefore still detect the protein. Alternatively, the possibility of two different clones being present in the population could explain the expression. As both these scenarios would have resulted in a significantly stronger band while also would have been detected during initial assessment by three independent assays, it can be extrapolated that this was a case of technical error causing contamination from the neighbouring C7 expressing sample during loading of the SDS-PAGE.

Ultimately, a strategy for the potential correction of patient mutations and restoration of endogenous C7 expression in autologous cells using ZFNs was developed based on prompting cells to undergo repair of DSBs by homologous recombination as opposed to the error prone NHEJ. This was achieved through the provision of a 1.8 kb donor template sequence with ~880 bp of homologous arms to the WT *COL7A1* genomic sequence flanking the ZFN cut-site. At first, the use of primary RDEB patient (CK) keratinocytes with a homozygous mutation at c.425 A>G in exon 3, 99 bp from the ZFN cut site and within the optimal range of the donor template for HDR efficiency to occur was proposed. Sequencing though of endogenous *COL7A1* in the (CK) keratinocytes isolated for detection of the homozygous c.425 A>G mutation showed sequence variation with the specified mutation detected in only a single allele hampering their use for this study. Similarly, NILV-ZFN transduced cl13, cl26, cl4 and cl15, which would have allowed for the detection of C7 restoration following HDR, could not be used due to the disruption of the ZFN binding sites by the initial exposure to the NILV-ZFNs hence hampering generation of a second DSB.

Therefore this study was performed on WT NTERT cells with template integration relying upon detection of the introduced unique KpnI restriction site. An added concern when co-delivering ZFNs alongside the donor template included the potential cleavage of the template by the ZFNs as the targeted binding sites are conserved in both endogenous and template sequence (Porteus, 2006). By introducing silent mutations in the ZFN recognition sequences of the template while maintaining the peptide sequence, unwanted cleavage could be eliminated. This was shown to be the case in clones detected to have undergone template integration, with intact template sequence observed when transduced with the SDM construct. On the contrary, a substantial number of deletions and substitutions were detected at the target site when the unmodified template was provided instead. Homologous recombination by both SDM and unmodified template sequences resulting in repair of the ZFN introduced DSBs was confirmed to be monoallelic at a frequency of ~1%. This is in line with the observation that HDR occurs at a 30-fold lower frequency to NHEJ (Coluccio et al., 2013). Low levels of HDR in keratinocyte cell

lines have also been reported by others in the field with a 50% drop when applied to primary keratinocytes (Coluccio et al., 2013). Moreover, their study investigated the possibility of improving donor template delivery by adenoviral vectors, although they noticed an increase of NHEJ while NILV template delivery appeared to promote homologous recombination.

NILVs, however, have been reported to sustain a low level of background integration upon delivery (Nightingale et al., 2006, Leavitt et al., 1996). This has been estimated to be in the range of 10^{-2} to 10^{-4} times less than integrating vectors. Delivery of NILV donor template alone, has demonstrated background integration levels of <2% in permissive cell lines which upon co-delivery with NILV-ZFNs otherwise showed >35% efficiency of HDR (Lombardo et al., 2007). This effect was significantly reduced in less permissive primary cells with background integration only accounting for 0.005%. An analogous response is expected in keratinocytes considering the low efficiency of transduction.

Owing to the endogenous C7 expression in the NTERT cells treated in this study, and therefore inability to assess restoration at the protein level as with RDEB cells, an accurate measurement of off-target integration was not possible. Moreover, with ZFNs and template delivered as three separate NILVs, detection of potential integration events based on viral sequence would prove inaccurate. Delivery of ZFNs and template as a single construct has been hypothesised as a means of increasing the efficiency of the system (Lombardo et al., 2007).

The study presented here, has been the first to employ ZFNs for the gene editing and development of a therapeutic strategy for *COL7A1* RDEB mutations. Although the ZFN platform theoretically shows potential for the correction of patient specific point mutations the low frequency of HDR is a limiting factor. It has been suggested that target cells may be more prone to undergo homologous recombination in the S/G2 phase, which should be considered as a way of improving the frequency of repair (Mohrin et al., 2010).

A study being carried out in parallel by our collaborators showed confirmation of a *COL7A1* patient mutation by TALEN-mediated gene editing (Osborn et al., 2013). The repetitive sequence in the DNA binding region of TALENs hampers their incorporation into viral delivery systems resulting in rearrangements (Holkers et al., 2013). This, therefore, limits their delivery by either plasmid DNA or mRNA with the caveats being reduced efficiency and increased cytotoxicity. To increase the proportion of HDR corrected cells the template had to encode a puromycin resistance gene to allow for selection. I was given the opportunity to assess the performance of these cells *in vivo* on the chimeric human:murine skin graft model. Analogous to the observations concluded to previously (Section 4.3.1), deposition of C7 contributed from corrected fibroblasts alone was able to restore dermal-epidermal adhesion and reverse the

RDEB phenotype. What renders this study particularly promising, is that endogenous corrected C7 expressed at low levels was shown to be sufficient in providing a significant therapeutic benefit, therefore highlighting the clinical potential of autologous gene editing tools. This is a step forward in the development of a personalised therapy approach for RDEB, which can be caused by a substantial number of potentially easily targeted mutations.

Chapter 6 Discussion

This project has demonstrated a potential *ex vivo* gene therapy approach for the correction of autologous RDEB patient cells by gene addition and editing strategies. A full-length codon-optimised copy of *COL7A1* was efficiently delivered to primary RDEB cells by therapeutic lentiviral vector resulting in restoration of C7 protein expression and functional correction of dermal-epidermal adhesion in a preclinical human:murine chimeric RDEB skin graft model. In addition, gene-editing using ZFNs against *COL7A1* was implemented for the targeted knockout of the gene enabling the *in vitro* modelling of RDEB. A proof-of-concept evaluation for the site-specific repair of *COL7A1* mutations mediated by ZFN triggered HDR was also investigated.

6.1 Proposal of an autologous gene therapy for RDEB

The selected strategy in contrast to delivery of allogeneic cells aimed to overcome the limitations encountered by others, chiefly clearance of cells within a period of 2 weeks (Wong et al., 2008). *In vivo* mouse studies have previously demonstrated dose dependent functional restoration of the DEJ using healthy donor fibroblasts in RDEB skin equivalents and persistence of up to 16 weeks (Woodley et al., 2003). The study led by Wong et al. (Wong et al., 2008), forming the first clinical trial to intradermally inject allogeneic fibroblasts for RDEB demonstrated a two-fold increase in C7 expression levels at the injection site visualised by immunofluorescence. Importantly, although expression levels were sustained yet decreased over 3 months, cells were undetectable after 2 weeks.

A separate trial showed a similar result with detection of intradermally injected allogeneic fibroblasts on day 7 with clearance by day 28 (Petrof et al., 2013). These observations led the authors to investigate further, which revealed expression was in fact a result of upregulation of patients' own endogenous mutant C7, as confirmed by the rudimentary AFs seen by TEM. It has been postulated that both an initial boost of C7 from the allogeneic fibroblasts coupled with the slow turnover of the protein, and an autocrine effect exerted on recipient keratinocytes by inflammation-induced HB-EGF, may have indirectly led to increased synthesis and secretion of endogenous C7 (Wong et al., 2008, Nagy et al., 2011). Furthermore, upregulation of C7 was only displayed in patients with baseline expression of mutant protein. Allogeneic fibroblast death and eventual clearance was most likely mediated by a host immune response with reported transient increase of haematopoietic cell marker CD45, dendritic cell marker CD11c, dermal macrophage marker CD68 and IgM (Wong et al., 2008).

The limitations associated with allogeneic cell delivery therefore provide a strong rationale for the development of an autologous therapy for RDEB. This poses a more elegant strategy and is expected to offer sustained benefit without eliciting an allo-immune response. As C7 is expressed by both fibroblasts and keratinocytes in the skin, this allows for the potential correction of either cell type providing a range of options for their clinical application. Autologous keratinocytes can be corrected and cultured to produce skin sheets for superficial grafting as has been previously carried out in a JEB human trial with promising results (Mavilio et al., 2006).

A phase I clinical trial has recently commenced to investigate correction of RDEB keratinocytes using the LZRSE-Col7A1 retroviral vector and transplantation of autologous epidermal sheets in RDEB patients (LEAES) (NCT01263379). The extensive damage to the dermal wound bed in RDEB patients though hampers graft take and skin infections are commonplace (Ryynanen et al., 1992). The use of keratinocytes for the treatment of RDEB may therefore be restricted to milder abrasions or as a combination therapy. Fibroblasts on the other are a better candidate being a more robust cell type, offering easier propagation and maintenance *in vitro*. Moreover, they offer broader potential administration routes with delivery possible intradermally (Kern et al., 2009, Wong et al., 2008, Petrof et al., 2013, Woodley et al., 2003), intravenously (Woodley et al., 2007b) or in a supporting matrix for deeper wounds, typically following surgical excision of SCCs.

6.2 Overcoming the obstacles of gene transfer to epithelial cells using 3rd generation lentiviral vectors

Keratinocytes and to a lesser extent fibroblasts are known to be resilient to transfection which would allow for the introduction of foreign DNA into their nucleus. It has been proposed that the most efficient way of introducing genetic material into keratinocytes is via a virus (Deng et al., 1997, Di Nunzio et al., 2008). For that reason, a lentiviral vector delivery system was used, known to attain a high efficiency of infection in a range of cell types, for the delivery of full length *COL7A1* cDNA. The configuration selected was based on the 3rd generation pCCL SIN-lentiviral vector, currently approved and used in a number of clinical gene therapy trials for the treatment of Netherton syndrome, X-CGD, ADA and WAS (NCT01545323, NCT02234934, NCT01380990, NCT01347242).

Selection of a lentiviral system also offered a number of benefits over its γ-retroviral counterpart, the key ones including their potential to infect both dividing and non-dividing cells enabling the targeting of post-mitotic, highly differentiated cells, and their safer integration

profile with preference for gene rich regions, although have been considered to be potentially more disruptive to the host cell genome than γ-retroviruses (Maruggi et al., 2009). Furthermore and with relation to the *COL7A1* cDNA, lentiviruses can accommodate and efficiently package transgenes of up to 9 kb with retroviruses restricted to 7-8 kb. Development of this transfer plasmid was undertaken with safety in mind, stripping it of all virulence factors and replacing the otherwise strong LTR promoter, capable of activating genes several kb downstream, with a CMV promoter (Zufferey et al., 1998). The full-length 8.9 kb *COL7A1* transgene has previously been successfully incorporated into an MLV retroviral vector (Titeux et al., 2010), although their integration profile, favouring regions proximal to transcription start sites and growth controlling genes with the potential upregulation of oncogenes, is a high-risk concern (Titeux et al., 2010, Maruggi et al., 2009, Wu et al., 2003). In addition, improvement of the vector throughout the generations enabling *tat* independent transcription and delivery of accessory plasmids in *trans* greatly reduced the likelihood of RCL formation (Dull et al., 1998).

Although pseudotyping of the viral particles with foreign envelopes can be used to confer cell specific tropism, preservation of the ubiquitously targeting VSV-G envelope as was carried out for this study allows for sufficient transduction of skin cells while it also offers the advantage of withstanding concentration by ultracentrifugation (Burns et al., 1993).

Expression of the *COL7A1* transgene by a human promoter such as PGK which was selected for LV-COL7, reduces the potential methylation and hence transgene silencing. Significant fold decrease in transgene expression due to methylation induced silencing of the driving promoter has been seen when using CMV and SFFV promoters over PGK (Herbst et al., 2012). The constitutive nature of this promoter also allowed for sustained expression of the *COL7A1* transgene, which led to a desirable overexpression of C7 protein. Other groups have opted for the synthetically modified MND promoter, containing the U3 region of a modified MoMuLV LTR believed to reduce viral promoter methylation, or the stronger EF1α promoter which when tested against the endogenous *COL7A1* promoter, demonstrated a significant increase in expression levels (Chen et al., 2002, Titeux et al., 2010).

The rationale behind selecting the PGK promoter was its enhanced ability in also transducing heamatopoietic progenitor cells (Salmon et al., 2000) and mesenchymal cells (McGinley et al., 2011), making this system applicable for future direction into the systemic correction of RDEB. Although the EF1α promoter has been reported to have a slight advantage over PGK in expression levels when incorporated into a SIN configuration, addition of a WPRE sequence upstream of the 3' LTR has been shown to rescue the negative effect (Salmon et al., 2000). A further consideration for the selection of the PGK promoter over the EF1α was the size difference with PGK being 672 bp shorter, therefore allowing more space for the large *COL7A1*

transgene and hence more efficient packaging into viral particles. In the minimal SMPU-C7 vector utilised by Chen *et al.*, in order to compensate for the reduced transgene capacity of γ-retroviral vectors, the WPRE sequence had to be removed and a minimal Ψ packaging signal was used, reducing HIV-derived sequences to 774 nucleotides (Chen et al., 2002). In the LV-COL7 vector used in this study, a mutated version of WPRE (WPREmut6) was included. This retained the ability of enhanced transgene expression through an increase of nuclear and cytoplasmic mRNA levels by improving transcript termination, while abrogating synthesis of woodchuck hepatitis virus X protein (WHX), a transcriptional activator associated with liver tumor development (Zanta-Boussif et al., 2009). For the improvement of transduction efficiency, a cPPT sequence was included to facilitate nuclear translocation of the PIC.

The LV-COL7 vector when prepared using the 4-plasmid transient co-transfection protocol with the PEI cationic polymer and concentrated by ultracentrifugation, exhibited a 2-log drop in functional titres ($5x10^6$) compared to the same vector backbone containing the reporter transgene *eGFP* in place of *COL7A1*. It was suspected this was predominately caused by the increased transgene size rather than vector configuration or technique. It is however also plausible that despite removal of major cryptic splice acceptor and donor sites within the transgene, residual sites may still result in aberrant mRNA transcript formation through alternative splicing (Moiani et al., 2012). In support of the inefficient packaging of the *COL7A1* transgene into functional LVs, when p24 viral antigen levels were measured in the viral supernatants, HIV viral capsid protein concentrations were found to be similar to those of LV-GFP vector. As levels of p24 provide a measure of physical titre rather than functional titre, and the similarity seen between LV-COL7 and LV-GFP suggests an accumulation of empty vectors in the LV-COL7 preparation. These findings are in line with observations by Kumar *et al.* showing proviral length can be extended to 18 kb in VSV-G pseudotyped lentiviral vectors, suggesting no absolute packaging limit although the increase in transgene size was seen to be directly associated with a semi-logarithmic drop in titres (Kumar et al., 2001). This was linked primarily to interference with viral encapsidation and also limitations during nuclear export of proviral RNA.

However, it is also possible that the RNA genome undergoes successful packaging, but the error-prone nature of reverse transcriptase and its frequent dissociation from the template lead to mutations or disruption during viral DNA synthesis, affecting proviral integration and gene expression (Urbinati et al., 2009, Matrai et al., 2010). Furthermore, it's noteworthy to mention that reducing the length of the vector backbone has minimal effect on the increase of functional titres as does reducing the proviral integration sequence length (al Yacoub et al., 2007). In addition, alteration of transfer plasmid DNA amount or ratio to packaging plasmids similarly

had little effect. Modifications to the concentration protocol have been suggested to dramatically increase viral yield by 80% by reducing centrifugal speed to 20,000xg as opposed to the typical 100,000xg combined with the addition of a sucrose cushion (al Yacoub et al., 2007). In this study viral preparations were harvested following ultracentrifugation at 100,00xg and 340-fold concentration for optimal recovery.

6.3 Lentiviral vector caveats- in search of optimisation strategies

In this study, the overall efficiency of transgene delivery in primary RDEB keratinocytes and fibroblasts using the LV-COL7 vector measured by C7 expression, ranged between ~10-20% following single or double rounds of transduction. When directly paralleled to other studies, performance of LV-COL7 appeared to be modest. Transduction efficiencies of 95% were attained at an MOI of 25 ($7.5 \pm 0.8x10^7$ TU/ml) using an MND driven SMPU-C7 minimal lentiviral vector (Chen et al., 2002) and 30-80% when cells were transduced over two time points at an MOI of 20 ($1x10^7$ TU/ml – $5x10^8$ TU/ml) using an EF1α driven pCMS-COL7A1 retroviral vector with the supplementation of polybrene (Titeux et al., 2010). However, despite the lower titre and reduced transduction efficiency of LV-COL7, robust and sustained expression of full-length C7 was achieved, which was able to form fully functional AFs and restore adhesion at the DEJ of a chimeric human:murine skin graft model. The reasons for the lower transduction efficiency of LV-COL7, may be due to the viral vector utilised although expression levels following transduction with LV-GFP using comparable MOIs were ~90-100%. Alternatively, this could potentially be a discrepancy in the measurement of protein expression and hence transduction efficiency according to the assay and conditions used.

With the increased transgene size being the most logical explanation for the reduced transduction efficiency, a previous study attempted to manipulate the *COL7A1* cDNA sequence to create a minigene and improve the viral vector titer as originally carried out for the 14 kb DMD cDNA (Dunckley et al., 1993, Vincent et al., 1993). For the *COL7A1* minigene, 678 non-critical amino acids from the central collagenous region including the 39 amino acid hinge region were removed while preserving the triple-helical assembly of the gene (Chen et al., 2000). Although it was shown to express a shorter 230 kDa form of C7 with similar functionality to WT cells *in vitro*, it may, when assessed *in vivo,* result in a dysfunctional translated protein lacking structural integrity and flexibility, or even elicit an immunogenic response to the shorter product from the host. Furthermore, as reducing the size of the viral backbone is unlikely to result in an increase in titre and hence transduction efficiency, it was hypothesised that including a selectable marker could instead allow for enrichment of transduced cells thereby increasing the yield of gene-corrected cells.

Preliminary experiments were carried out introducing a self-cleavable CD34 epitope downstream of the *COL7A1* transgene for co-expression following transduction (data not shown). This could potentially allow for FACS based sorting of the transduced population resulting in a highly expressing heterogeneous population. However, considering the observed overexpression of C7 protein levels over endogenous C7 seen in both LV-COL7 transduced RDEB keratinocytes and fibroblasts mediated by the constitutive PGK promoter, such additional manipulation may be superfluous. Moreover, this is further supported by data suggesting expression of as low as 10% of WT C7 levels at the DEJ can confer adequate dermal-epidermal adhesion and maintain skin integrity (Fritsch et al., 2008, Wagner et al., 2010).

A crucial optimisation strategy applied to the LV-COL7 vector used in this study differentiating it from other RDEB gene therapy reports, has been the use of a codon optimised *COL7A1* transgene sequence to ensure the production of functional C7. Previous reports have documented the appearance of truncated forms of C7 following retroviral delivery of full-length *COL7A1* cDNA to both RDEB fibroblasts and keratinocytes (Titeux et al., 2010). These aberrations were further noticed at the genomic level with detection of shorter proviral forms suggesting rearrangements were most likely caused during retrotranscription. The presence of Gly-X-Y repeats in the triple helical collagenous region of *COL7A1* can trigger intramolecular template switching of the reverse transcriptase, a mechanism native to retroviruses facilitating their genetic variability in the host (Cocquet et al., 2006). It was hypothesised that codon optimisation of the transgene would abrogate those effects. The *COL7A1* transgene was therefore commercially codon optimised for the removal of cryptic splice sites, replacement of repetitive sequence using degenerate codons and was further coupled to a Kozak consensus sequence ensuring more efficient initiation of translation of full-length *COL7A1*.

Protein analysis of transduced RDEB fibroblasts and keratinocytes did not reveal truncated forms of C7 in the bulk population suggesting full-length expression. However, studies carried out in our lab showed the presence of shorter C7 protein forms at 230 kDa in ~6% of transduced keratinocyte clones (data not shown). Sequencing of the entire incorporated *COL7A1* transgene in clones expressing abnormal C7 using overlapping primers, showed deletions in all three colonies clustered around exons 31-40 within the Gly-X-Y rich triple helical domains shown to contain tandem repeats. This suggested that aberrations in *COL7A1* following LV-COL7 transduction of cells still occurred despite codon optimisation of the transgene, albeit at a significantly reduced frequency compared to reports of ~20% rearrangement when using WT endogenous *COL7A1* sequence (Titeux et al., 2010). It was speculated that codon optimisation of those specific regions could have inadvertently introduced repetitive sequences. Replacing

those defined regions with endogenous non-codon optimised sequence may help in reducing aberrant clone formation even further. In addition, a functional assessment of the aberrant clones carried out in our lab, also demonstrated that these clones performed equally to uncorrected RDEB patient cells in terms of attachment, proliferation and migration indicating that patients receiving a mixed population of transduced cells containing such clones would not suffer any detrimental effects.

In an effort to decipher the reason behind transgene rearrangement, a retrotranscription independent, non-viral, transposon based delivery platform was investigated which instead relies on a "cut and paste" mechanism of chromosomal integration upon recognition of inverted terminal repeat sequences (ITRs) at either end of the transposon by the transposase. I generated a *COL7A1* carrying *PiggyBac* (PB) transposon vector with the advantage of this platform being its unlimited cargo capacity (data not shown). Although C7 expression was successfully restored in RDEB keratinocytes after transposition of PB-PGK-COL7A1-IRES-GFP by the Super *PiggyBac* transposase, true integration events only accounted for <2% of the population following 3 weeks of culture. As this platform still appears to be in the early stages of development, it could therefore not be used to attain meaningful data on C7 rearrangement.

6.4 Determining the functional properties of *de novo* synthesised C7

Despite having confirmed the synthesis and secretion of full-length C7 expression by LV-COL7 transduced RDEB cells, the actual functionality of C7 cannot be inferred solely based on these data. For this purpose, a semi-quantitative *in vitro* functional assay simulating the process of wound healing by measuring cell migration over an artificially created scratch was employed. RDEB keratinocytes lacking C7 expression revealed a significantly reduced migration rate over WT cells. Following gene correction of the RDEB keratinocytes however, the rate of migration appeared to recover suggesting normalisation of the migratory phenotype although still remained below those of WT cells. As all cells had been pre-treated with mitomycin C, the proliferation variable was removed from the measurement. There appeared to be a lag in migration during the first 5 hrs in untransduced and LV-COL7 transduced RDEB keratinocytes, which then proceeded with the transduced sample showing significant variation and accelerated migration until complete closure of the scratch. This was speculated to be due to the moderately low transduction efficiency with <20% of cells secreting C7, perhaps being insufficient in exhibiting an immediately detectable effect. This migration pattern was further supported in the subsequent study which showed NTERT clones having undergone ZFN-mediated *COL7A1* knockdown resulted in a regression of migration speed compared to WT levels upon monoallelic disruption which was significantly augmented in biallelic disrupted clones.

Interestingly, when migration was analysed in RDEB fibroblasts, there was variation amongst the two tested untransduced patient cells demonstrating both reduced and increased migration speeds compared to WT. Importantly though, LV-COL7 transduction resulted in normalisation of the values in both cases.

This increased migration propensity has been linked to early SCC development in RDEB keratinocytes (Martins et al., 2009). The RDEB patient (EB8), whose fibroblasts exhibited increased migration has not displayed clinical evidence of SCC, however a predisposition to malignancy can not be ruled out. There have been contradicting reports concerning the effect on *in vitro* wound closure of keratinocytes in the absence of C7 expression. Originally described by Chen et al. (Chen et al., 2002), RDEB keratinocytes appear to migrate in an inverse fashion to the findings of the study presented here with WT keratinocytes having a lower migration index value. This though might instead be explained by their choice of protocol involving the treatment and coating of the cell-culture surface with type I collagen prior to seeding and performing a colloidal gold migration assay. On the other hand, the assay performed here, involves culturing keratinocytes in untreated tissue culture dishes to confluency before performing the scratch assay, therefore allowing for the secretion and deposition of endogenous extracellular matrix proteins (collagens, laminin, fibronectin).

Nystrom *et al.* similarly to the observations in my study, demonstrated from both *in vitro* and *in vivo* data a significant reduction in migration speed of *Col7a1* hypomorphic mouse keratinocytes, expressing 10% of normal C7 levels, when compared to wild type keratinocytes (Nystrom et al., 2013). This was proposed to have been mediated by a direct interaction of C7 with the laminin-332/integrin α6β4 complex known to influence directional migration of keratinocytes (Pullar et al., 2006, Sehgal et al., 2006, Tsuruta et al., 2011). It has been suggested that RDEB cells overexpress α6β4 (Nystrom et al., 2013). That, in turn, not only alters laminin-332 organisation but is also associated with an activation of E-cadherin, which tightens cell–cell contact thereby delaying migration (Hintermann et al., 2005). Hence, the reduced migration speed in the RDEB cells and the ZFN-knockout clones observed can be most likely attributed to the alteration in α6β4 signaling mediated by the knockout and lack of C7 protein deposition leading to aberrant laminin-332 organisation and E-cadherin activation.

The variability in the RDEB fibroblast migration data, as well as the disparity in the published reports illustrates the limitations of this *in vitro* assay in obtaining an accurate representation and confirmation of functional correction following treatment. Therefore it can only be stated that restoration of C7 following LV-COL7 transduction of RDEB cells results in normalisation and functional recovery of migration.

6.5 Development of a RDEB human:murine chimeric model allows for *in vivo* evaluation of gene corrected cells

Acknowledging the limitations of *in vitro* assays shown to hinder true functional evaluation of the *de novo* synthesised C7, adopting a procedure for the generation of a chimeric human:murine RDEB skin graft model previously described (Larcher et al., 2007), allowed for the examination of the functionality of the secreted C7 *in vivo*. RDEB patient keratinocyte and fibroblast cells either untransduced or having undergone gene correction by LV-COL7 were used to generate bioengineered SEs which were then grafted onto immunodeficient mice. Initial validation of the grafting method was carried out on hairless NMRI-*Foxn1*^{nu} mice as suggested by the authors of the aforementioned study, although a high rate of graft rejection (~50%) with mouse skin re-epithelialisation overtaking human graft growth was observed, presumably due to fully functional circulating B-cells in the NMRI-*Foxn1*^{nu} strain. This was circumvented by using the NSG strain, greatly increasing the grafting success rate (>80%), confirmed by the clearly defined borders between mouse and human skin. Both dermis and epidermis of the harvested tissue 8 weeks post grafting showed distinctive human specific staining confirming maturation and differentiation of the graft and formation of a multilayered stratified epidermis with apparent cornification. Importantly, the mouse model truly recapitulated the disease phenotype with lack of functional C7 expression at the DEJ which was supported by lack of AFs at the ultrastructural level resulting in severe tissue separation.

In vivo assessment of the corrective capacity of the LV-COL7 vector allowed for the demonstration of the restorative potential for both skin cell types opening a number of possible therapeutic avenues in patients. Deposition of C7 at the DEJ of gene corrected grafts resulting in amelioration of the blistering and reversion of the RDEB phenotype was seen using both a combination of gene corrected keratinocytes and fibroblasts and with fibroblasts alone. There is compelling evidence to consider autologous keratinocyte gene therapy as a treatment for RDEB. In this study keratinocytes were gene-corrected and shown to contribute to restoration of the DEJ *in vivo*. Pre-clinical data in mice that led to the (LEAES) (NCT01263379) trial demonstrated graft persistence and C7 expression with the transplanted cells undergoing up to 12 epidermal turnover cycles (Siprashvili et al., 2010). This however implies the need for efficient transduction of epidermal stem cells and keratinocyte progenitors as supported by studies in canine RDEB (Gache et al., 2011). Moreover, continuous tissue damage in EB patients leads to gradual loss of transit amplifying progenitor cells and exhaustion in epidermal stem cell pools (Mavilio et al., 2006), which would significantly reduce their availability for transduction. Grafting using gene-corrected keratinocytes alone in this study was therefore not attempted.

The exclusive effect of fibroblasts, considered to be the main contributors of therapeutic C7 in skin (Kern et al., 2009, Goto et al., 2006) was therefore explored for restoration of dermal-epidermal adhesion. There was clear evidence of complete reversion of the diseased phenotype with overexpression of C7 protein at the DEJ which following secretion into the dermal ECM is sequestered by BMZ macromolecules such as laminin-332, type IV collagen and fibronectin resulting in the generation of thick centrosymetrically banded AFs. Although C7 expression levels at the DEJ of the gene-corrected grafts were supranormal, there is evidence to suggest potential saturation of C7 binding to laminin-332 and type IV collagen BMZ components (Woodley et al., 2003). As previously shown, C7 has a high affinity for both of these BMZ proteins (Chen et al., 1999, Chen et al., 1997). As the levels of expression of both laminin-332 and type IV collagen are unaffected in RDEB patients and therefore are a limiting factor for C7 binding (Woodley et al., 2003), overexpression of C7 is unlikely to cause adverse effects.

Moreover, staining of the grafts for keratinocyte differentiation markers confirmed that C7 expression from the transduced fibroblasts did not disrupt epidermal morphology. The epidermis in gene corrected grafts similar to WT grafts showed precise localisation of keratins 10 and 14 and involucrin. The *de novo* synthesised C7 therefore appears to be functionally indistinguishable from WT C7.

6.6 Fibroblasts demonstrate desirable characteristics making them suitable therapeutic candidates.

Fibroblasts present a much more versatile and robust target cell due to their ease of handling, propagation and expansion and moreover their potential routes of administration (Goto et al., 2006). Furthermore, they provide mechanical strength through the active production of ECM constituting the structural supporting framework. Their mesenchymal origin implies that the appropriate stimulation, such as epithelial stress caused by inflammation or tissue injury, can trigger their proliferation and orchestrate the reorganisation of the wounded epithelium. More recently, they have been linked to the modulation of immune-cell behavior through the production of cytokines, chemokines and prostanoids (Flavell et al., 2008).

The slow turnover of both fibroblasts and C7 protein allows for multiple intradermal injections at sites of injury offering long term correction albeit clearance of allogeneic fibroblasts within a few weeks of injection (Kern et al., 2009, Petrof et al., 2013, Wong et al., 2008, Woodley et al., 2003). Assessment of allogeneic fibroblast injections in RDEB mice has demonstrated allogeneic derived C7 *in vivo* to have a turnover of >100 days despite clearance of the cells 28 days post injection. Cell clearance was reported to be due to proliferation arrest and eventual

apoptosis although the mild inflammation observed may have been a contributing factor (Kern et al., 2009). Examination of the harvested graft tissue by human specific staining of the chimeric human:murine RDEB model tested here, confirmed the presence of the LV-COL7 transduced primary RDEB fibroblasts after 8-weeks of *in vivo* culture suggesting increased persistence or potentially active proliferation. In addition, although biopsies were not harvested at earlier time points, staining for C7 at the DEJ at 8 weeks, revealed intense C7 expression superseding endogenous levels. Although this is in part due to the constitutive PGK promoter activity driving high levels of transgene expression, it also supports the hypothesis that the activity of the grafted cells has not been majorly compromised. A concern with fibroblast therapy is hypertrophic scar formation caused by the excessive synthesis of ECM proteins from the injected cells (Kern et al., 2009). As this is a recurrent complication in RDEB patients, markers of fibrosis such as α smooth muscle actin (α-SMA), TGF-β and tenascin-C would have to be examined following intradermal injection of the cells.

The evident limitation of such a strategy though is the small diffusion radius and inaccessibility of internally affected sites such as the erosions of the esophagus. Intradermal fibroblast administration in RDEB mice has shown cells to disperse throughout all vertical layers of the dermis at the injection site, although only exhibited slight overall lateral migration of ~10 mm (Kern et al., 2009).

Systemic delivery of fibroblasts via intravenous administration as a way to address those shortcomings has shown to promote wound healing and support phenotypic amelioration by homing to the injured site (Woodley et al., 2007b). The precise mechanism of fibroblast recruitment from the periphery is unknown although it has been speculated that factors such as HMGB1 involved in the recruitment of MSCs to wounded sites may be common amongst cells of stromal origin (Woodley et al., 2007b, Tamai et al., 2011). Such recruitment has also been described in a subset of fibroblasts termed bone marrow derived fibroblasts (BMDFs) when following transplantation of bone marrow cells into the fetal circulation of mouse embryos, fibroblast progenitors migrate to uninjured skin and aggregate around hair follicle structures (Chino et al., 2008). Upon the appropriate matrix stimulation, these progenitors can give rise to *de novo* dermal fibroblasts and facilitate wound healing. Admittedly, the tissue distribution following systemic administration of gene corrected fibroblasts might pose a concern. Woodley *et al.* demonstrated in a mouse model, that trafficking of intravenously injected human fibroblasts was confined and maintained within cutaneous sites of injury for 6 weeks, with none detected in brain, kidney, spleen, liver and heart although small foci of the lungs showed positivity with no adverse effects (Woodley et al., 2007b). It is believed that in an immune competent patient, cells migrated to unintended sites would be rapidly cleared (Woodley et al.,

2007b). An additional strategy for the use of gene corrected fibroblasts could potentially be their implementation in deeper wound remodelling. RDEB patients typically develop multiple sites of SCCs requiring surgical excision. Diseased fibroblasts such as those in RDEB have been shown to promote tumour progression, growth and metastasis by facilitating angiogenesis at the site highlighting the need for their removal (Flavell et al., 2008). A clinically bioengineered scaffold similar to Apligraf® but containing autologous gene corrected fibroblasts overlayed with an autologous epidermal sheet could therefore be used to "fill" the wound following excision of SCCs.

With the majority of these approaches only able to target the disease topically, in this study I have also explored a systemic strategy based on the encouraging results of the allogeneic BMT trial (Wagner et al., 2010). With the design of LV-COL7 optimised for the transduction of stem cell populations, murine HSCs and MSCs were harvested from RDEB *Col7a1*$^{null/null}$ or *Col7a1*$^{flNeo/flNeo}$ hypomorphic mice for *ex vivo* correction and autologous systemic transplantation (data not shown). Although C7 was restored in the transduced cells, survival of the mice was not significantly extended.

It is widely debated which stem cell population would be able to show clinical benefit in RDEB. MSCs in particular have been shown to migrate to wounded sites and contribute to tissue regeneration while also confer immunomodulatory properties (Wang et al., 2014, Fujita et al., 2010). Supporting evidence by Tamai et al. has demonstrated a subset of MSCs with a lineage-negative / platelet-derived growth factor receptor alpha-positive ($Lin^-/PDGFR\alpha^+$) marker profile can be mobilised from the bone marrow to the site of injury through the action of HMGB1, a potent inflammatory regulator and chemo-attractant involved in tissue remodelling secreted by necrotic and apoptotic cells (Tamai et al., 2011). The fate of the recruited MSCs still remains somewhat unclear with reports suggesting both the exertion of restorative paracrine effects and the transdiferentiation to non-haematopoietic collagen secreting cells of the epithelial lineage (Tamai et al., 2011, Prockop, 1997).

6.7 Personalised medicine for RDEB - genome editing as a tool for the correction of *COL7A1* mutations

With gene addition, the endogenous copy of the mutant gene remains intact with the potential of producing mutant protein. This may not always have a deleterious/negative effect. In the case of RDEB, it has been hypothesised that mutant endogenous C7 giving rise to rudimentary AFs can assemble with allogeneic introduced healthy C7, resulting in a clinically significant level of amelioration (Wagner et al., 2010). However, there may be adverse effects associated with the

combined expression of mutant and healthy protein, as the functionality of the mutant-healthy aggregates is unknown. This may interfere by diluting out the benefits of the healthy protein in a dominant negative manner. Gene manipulation executed via gene editing allows for a "seamless" method of correction without permanent integration of foreign genetic code into the host genome. Moreover, gene editing could help overcome obstacles encountered with conventional gene therapy, such as the delivery of full-length cDNA or the potential complications arising from constitutive gene expression by the LTRs or exogenous promoters that could potentially contribute to C7 mediated fibrosis (Perdoni et al., 2015).

With over 600 mutations having been reported within *COL7A1*, a number of these sites exhibit hot-spot occurrence with population variants (Cuadrado-Corrales et al., 2010, Nishie et al., 2014). Hot-spot mutations make ideal targets for correction by site-specific gene editing. For this study, the ZFN platform was selected as the gene-editing tool of choice for the targeted modification of *COL7A1*. Their recent emergence in a clinical setting for the targeted knockout of *CCR5* in autologous HIV patients' T-cells illustrates their clinical potential (NCT01252641, NCT02388594, NCT00842634).

The strategy for the correction of *COL7A1* mutations in RDEB cells using ZFNs presented here constitutes the first attempt of its kind in the field. The efficiency of ZFN delivery and nuclease activity within the target cell was examined initially in generating site-specific *COL7A1* knockout lines and subsequently in conferring targeted repair by homologous recombination. A modest degree genomic disruption was initially observed at exon 4 of *COL7A1* by plasmid DNA transfections of the ZFN arms. Plasmid DNA-based ZFN delivery to keratinocytes, besides resulting in low cleavage efficiency, is also associated with a significant level of cytotoxicity (Hoher et al., 2012). Switching from DNA plasmid transfection to a viral delivery system doubled the rate of disruption. By cloning each aspect of the ZFNs into NILVs, infection of keratinocytes was greatly improved while ensuring their expression remained transient with knockout occurring in a "hit and run" fashion. Long-term persistence of ZFNs in the cell has been associated with an increase in off-target cleavage predominantly seen when delivered as DNA. Delivery of ZFNs as proteins using cell-penetrating peptides has been presented as the safest option (Liu et al., 2015).

Delivery of the ZFNs by NILV provides an intermediate option between the two in terms of off-target effects, however, genomic regions with significant homology at the target site are still prone to cleavage. This was reported to be the case with mutations found in the *CCR2* locus following specific targeting of *CCR5* (Gabriel et al., 2011). Nevertheless, lentiviral transfer still remains the most efficient method of gene delivery to epithelial cells (Kuhn et al., 2002). Although reports have indicated the likelihood of low level background integrations with

NILVs, these are thought to occur with an incidence of 10^3 to 10^4 times less than with integrative vectors at similar frequency as with delivery of naked DNA (Nightingale et al., 2006, Leavitt et al., 1996). Both monoallelic and biallelic disruption of the gene was achieved in this study albeit the latter at a significantly lower frequency, detected by mismatches formed during the error-prone NHEJ and single strand annealing (SSA) models of repair to resolve induced DSBs. This correlated to a partial or complete reduction in C7 protein expression, respectively. Functionally, these clones appeared to recapitulate the *in vitro* characteristics of RDEB cells with a delayed wound closure speed associated with the lack of C7 deposition. LV-COL7 transduction of the generated compound heterozygous *COL7A1* mutant keratinocyte line led to the restoration of C7 expression confirming the efficiency of gene-addition and demonstrating the application of the generated *in vitro* RDEB model.

The ability to create DSBs in targeted genomic regions can be harnessed in a therapeutic setting for diseases carrying a dominant pattern of inheritance. Dominant negative mutations in *COL7A1* in ~70% of autosomal DDEB patients can lead to severe blistering at the DEJ (Pfendner and Lucky, 1993a). Gene editing for the monoallelic targeted disruption of the affected gene could therefore be a feasible treatment option. For RDEB, provision of a homologous donor template sequence would be required for the repair of the induced DSB and correction of the disease causing mutation. Designing the donor template sequence to span 6 exons of endogenous *COL7A1* was aimed at covering a wide range of mutations clustered around the cut site for site-specific correction. The length of the homologous regions was selected based on published data demonstrating the use of ≈400-800 bp on either side of the cut site resulted in greater recombination frequency than when shorter ≈50-100 bp homologous regions were used (Orlando et al., 2010). When designing nucleases and donor templates against a target sequence, the optimal distance at which correction can be mediated was also taken into consideration, shown to be within 100 bp of the cut site with a 4-fold drop in efficiency when the intended site is at a greater distance. Correction though has been demonstrated at ≈500 bp away from the cut site albeit at a frequency of below 0.1% (Elliott et al., 1998). The observed clustering of mutations around nearby exons in *COL7A1* can therefore allow for the potential increase in target sites using a single ZFN pair. Template integration was first assessed on WT NTERT cells by co-delivery of the NILV-ZFN pair alongside NILV-template. Co-delivery of ZFNs and template as NILVs was postulated to promote efficiency of HDR by 10-100 fold as donor template sequence would be available in an episomal state while the ZFNs underwent transcription and translation into effector nucleases initiating genomic DSBs (Lombardo et al., 2007). The study by Genovese *et al.*, demonstrated sufficient gene correction of the *IL2RG* gene responsible for SCID-X1 when template was delivered by NILV one day prior to ZFNs (Genovese et al., 2014). The nucleases in contrast to ours were delivered

as mRNA allowing for their rapid protein synthesis. Co-delivery of both template and ZFNs as NILVs therefore aimed to synchronise the timing of DSB generation and template availability. When direct sequencing was performed for the detection of HDR events, template sequence integration was observed in the transduced cells, however deletions and substitutions were also detected around the ZFN cut site. This was hypothesised to have been caused by NILV-ZFN mediated cleavage of the template sequence containing homologous ZFN recognition regions.

Redesign of the template by the introduction of silent mutations in both left and right ZFN binding regions, rectified this "off-target" effect. Sanger sequencing revealed monoallelic template integration in 1.17% of clones as detected by the degenerate nucleotides used for the silent mutations as well as the introduced KpnI site. These results further highlighted the ability to potentially correct mutations at least 145 bp away from the ZFN cut site. Although at a significantly reduced frequency, random genomic integration of template may occur when delivering an exogenous dsDNA sequence. To abrogate this potential adverse effect, single stranded oligonucleotides (ssODN) donors can be designed shown to increase knock in frequency, although their main limitation is their notably smaller size of a maximum of ≈100 bp, restricting the correction distance from the cut site (Chen et al., 2011, Duda et al., 2014). As suitable primary RDEB patient cells carrying an exon 4 mutation were not available at the time, functional characterisation of restored protein expression data was not possible.

Gene editing for *COL7A1* mutations has previously been reported by using TALENs, in which a homozygous PTC mutation in exon 14 in RDEB patient fibroblasts was corrected (Osborn et al., 2013). The authors achieved monoallelic gene correction by HDR in 6 of the 18 puromycin selected clones. In this study, I used one of the expanded gene-corrected clones to generate bioengineered SEs which when grafted onto a human:murine chimeric skin graft model showed strong expression of C7 at the DEJ with restoration of blistering. This result presented a clear indication of the potential of gene editing for RDEB showing restoration of endogenous C7 expression is sufficient in ameliorating the disease phenotype. However, this further highlights the limitation of gene-editing mediated repair, which occurs at a very low frequency necessitating the inclusion of a selectable marker. Although TALENs may offer certain advantages over ZFNs in terms of target availability and reduced manufacturing costs and expertise requirement, their delivery is restricted to DNA or mRNA transfection due to their highly homologous repetitive-variable domains (RVDs), resulting in rearrangement when delivered by lentiviral platform (Holkers et al., 2013). This is mediated by the intrinsic template switching mechanism of simple and complex retroviruses, which undergo obligate minus-strand to plus-strand transfer as a means of generating genotypic variability, shown to be increased in the presence of direct repeats. In addition, ZFNs having been available for over a decade,

further offer the benefit of having undergone rigorous evaluation by the scientific community exposing their possible caveats and making them a robust gene editing platform as seen by their recent introduction in clinical trials.

The low incidence of HDR still remains the major limitation in the field of gene editing further corroborated by this study's findings. This signifies the need for improved strategies that can boost the rate of homologous recombination to clinically significant levels.

The preferential time for HDR to occur is during S/G2 phase of the cell cycle (Mohrin et al., 2010), with a peak in repair at the mid-S cycle phase and a gradual decline in late S and G2 phases (Karanam et al., 2012). Methods for delaying transit through the S/G2 phase have been shown to increase HDR in HSCs by using an aryl hydrocarbon receptor antagonist StemRegenin 1 preserving stemness by stalling differentiation (Genovese et al., 2014). A similar outcome could potentially be achieved in keratinocytes by exposing cells to hypothermic conditions by incubation at 30°C following ZFN delivery. This method termed "cold shock" has primarily been reported to increase of NHEJ levels by two to tenfold over conventional culturing by increasing the amount of ZFN protein in the target cell (Doyon et al., 2010). Besides a transient growth arrest that was restored following incubation at 37°C, temporary hypothermic conditions were shown to significantly reduce off-target cleavage (Doyon et al., 2010). Based on evidence in the literature it can be speculated that an increase in the incidence of DSBs should also promote a higher level of HDR (Donoho et al., 1998, Taghian and Nickoloff, 1997). This hypothesis has now been confirmed with both ZFNs (Duda et al., 2014) and TALENs (Remy et al., 2014).

The identification and selection of HDR modified clones presents a major barrier in the success of gene editing as a potential therapy. For *in vitro* assessment a fluorescent reporter could potentially be included within the intronic sequence of the template as direct cell sorting for cytoplasmic C7 would require permeabilisation of the cells. Alternatively, a *floxed* antibiotic resistance gene allowing for cre-recombinase-mediated removal post selection could be used (Osborn et al., 2013). My study having been carried out on WT cells ruling out the possibility of selection based on restoration of protein expression, relied solely on detection of HDR by PCR methods. This involved individual screening of genomic sequence and TA subcloned sequence of hundreds of individual clones for identification of ones bearing template highlighting the pitfalls of this approach.

Despite the need for an improvement in HDR efficiency, an important factor to be considered is the limited lifespan of epithelial cells. Extended manipulation and culturing of both keratinocytes and fibroblasts *in vitro* such as during gene-editing and clonal selection can

rapidly lead to growth arrest, terminal differentiation and senescence of cells (Dickson et al., 2000). A better-suited candidate for targeting would therefore have to bypass these hurdles. Recent studies have explored the use of iPSCs for epidermolysis bullosa with encouraging results (Sebastiano et al., 2014, Osborn et al., 2013, Tolar et al., 2011, Itoh et al., 2013, Umegaki-Arao et al., 2014). Spontaneous reversions of *COL7A1* mutations described as revertant mosaicism or "natural gene therapy" are being increasingly detected in RDEB patients. Isolation of revertant patient cells presents a particularly promising application of iPSCs for an autologous cell therapy (Tolar et al., 2014). Of particular relevance was the work showing TALEN-mediated gene corrected RDEB fibroblasts being subsequently reprogrammed into iPSCs (Osborn et al., 2013). iPSCs derived from autologous human fibroblasts have now entered the first in man clinical trial led by the Riken Institute for the autologous treatment of macular degeneration based on pre-clinical safety studies carried out in mice and on human primates (Kamao et al., 2014, Kanemura et al., 2014). For inherited skin diseases like RDEB, the unlimited self-renewal capacity and hence the ability to genetically manipulate iPSCs without compromising on the passage number of the cells, coupled with the ever-growing expertise on the derivation of autologous iPSCs from primary patient fibroblasts, could open new avenues for potential treatment of the disease (Itoh et al., 2013).

In our lab, we have initiated experiments whereby iPSCs have been generated from an RDEB patient carrying a homozygous exon 3 mutation in *COL7A1* and subjected to our NILV-ZFN with NILV-template co-delivery strategy. We observed a marked increase in the rate of HDR of 12.5% with a modest proportion of biallelic corrected clones. This was verified both by PCR based methods and also by restoration of C7 expression. Work is currently underway for their reprogramming into keratinocyte cells. We suspect the increased efficiency of HDR in iPSCs to be mediated by factors such as cell cycle timing, chromatin context reported to alter the balance between NHEJ and HDR repair pathways (van Sluis and McStay, 2015), and also the higher permissiveness of iPSCs to viral transduction. Furthermore, a high proportion of corrected clones could eliminate the need for clonal selection and instead allow for administration of a heterogeneous population.

Recently, the novel CRISPR/Cas9 gene-editing technology has surfaced, demonstrating a remarkably high rate of targeted disruption. The bacterial Cas9 nuclease capable of recognising $G(N_{19})$ coupled to an NGG PAM sequence can therefore maximise the potential human genomic targets covering over ≈40% of exons. Following recognition of the PAM sequence, DNA strand separation leads to RNA binding which then proceeds distally to the end of the target sequence and triggers Cas9 catalysis (Sternberg et al., 2014). The technology has already been used in number proof-of-concept experiments (Niu et al., 2014, Schwank et al., 2013).

Nevertheless, the advantage of the increased flexibility in available target sites also poses the greatest concern of the CRISPR/Cas9 system, namely high frequency of off-target cleavage. This emphasises the importance of diligent selection of the target sequence, which can currently be conducted with the aid of genome screening bioinformatics tools for off-target site prediction. In addition, designing of sgRNAs is remarkably cost effective and user-friendly thereby allowing for rapid screening of whole sgRNA libraries. In light of this, we have constructed a number of potential sgRNAs in close proximity to our ZFN target site and have incorporated them into a widely tested lentiviral delivery platform encoding a human optimised Cas9 gene and a selectable fluorescent reporter (Sanjana et al., 2014). This will permit the side-by-side comparison with our NILV-ZFNs while also allowing us to explore alternative target sites for a wide range of mutations steering us towards a patient tailored therapy.

6.8 Concluding remarks

RDEB can undoubtedly be classed as one of the most devastating inherited genodermatosis with a detrimental quality of life and poor prognosis. Finding a cure for this disease still remains a distant thought with available treatment options solely relying on palliative care and wound management associated with an immense socioeconomic burden on the patients and their families. Pioneering work is being carried out globally investigating multifaceted therapeutic strategies for the management of RDEB with encouraging results. The accepted consensus is that obtaining a clinically significant outcome will require a combinatorial approach as a number of caveats have been exposed in present studies (Tolar and Wagner, 2015). These generally involve allogeneic cell clearance, short-lived protein expression, adverse immunogenic reactions and most importantly restriction to topical delivery. The systemic nature of the disease calls for a systemic treatment such as BMT although with RDEB patients being severely immunocompromised, this strategy can lead to the demise of individuals acquiring pathogenic infections following myeloablative treatment.

In this study, I investigated a novel strategy for the correction of autologous patient cells using a state-of-the-art clinical viral vector. This involved rigorous assessment of its efficiency *in vitro* while exposing its potential shortcomings, and ultimately functionally correcting the disease phenotype in a purpose designed RDEB human:murine chimeric skin graft model.

The positive outcome of these data formed the basis for proposal of therapeutic application in man. We have recently been granted MHRA approval for the initiation of a Phase I safety study evaluating the topical administration of autologous LV-COL7 corrected fibroblasts to RDEB patients (NCT02493816). Granted the success of this trial, we envisage a therapeutic strategy

where we can tackle the hurdle of systemic delivery and administer an autologous genetically corrected therapeutic capable of conferring total body disease amelioration. We hypothesize MSCs to offer such characteristics and have therefore initiated preliminary experiments for their assessment.

Wanting to stay at the forefront of novel and groundbreaking technologies, in this study, I also explored the rapidly growing field of gene-editing for the site-specific correction of individual patients' mutations with encouraging results. As the molecular tools available are still in their infancy we expect significant advances to be made in the simplification of their architecture, their increased efficiency and improved safety profile. Their recent admission in the clinic for the treatment of HIV has provided the field with firm grounding for what may in the imminent future become a viable patient tailored therapy.

Attempting to develop a cure for RDEB is short of a mammoth task due to the extent of the damage not only affecting the total surface of the skin, but also extending to the internal organs and skeletal integrity. Early studies have been instrumental in the understanding of the genetic causes of the disease allowing the scientific community to develop strategies for its correction. The last 15 years have seen an enormous upsurge in the field owed to the emergence of new technologies. With clinical trials now in the pipeline we believe availability of treatment options to be imminent. It is doubtful that a one-fits-all therapy will be able to combat RDEB. It is imperative that we recognise the extent to which what may be considered a minor success in the field can provide inconceivable improvement in these patients' otherwise agonising life. I feel honoured to have been part of this cause and to have hopefully contributed in the fight against this devastating disease.

References

ADACHI, E., HOPKINSON, I. & HAYASHI, T. 1997. Basement-membrane stromal relationships: interactions between collagen fibrils and the lamina densa. *Int Rev Cytol,* 173**,** 73-156.

AL YACOUB, N., ROMANOWSKA, M., HARITONOVA, N. & FOERSTER, J. 2007. Optimized production and concentration of lentiviral vectors containing large inserts. *J Gene Med,* 9**,** 579-84.

ALAM, H., SEHGAL, L., KUNDU, S. T., DALAL, S. N. & VAIDYA, M. M. 2011. Novel function of keratins 5 and 14 in proliferation and differentiation of stratified epithelial cells. *Mol Biol Cell,* 22**,** 4068-78.

ALEXEEV, V., UITTO, J. & IGOUCHEVA, O. 2011. Gene expression signatures of mouse bone marrow-derived mesenchymal stem cells in the cutaneous environment and therapeutic implications for blistering skin disorder. *Cytotherapy,* 13**,** 30-45.

AUMAILLEY, M., BRUCKNER-TUDERMAN, L., CARTER, W. G., DEUTZMANN, R., EDGAR, D., EKBLOM, P., ENGEL, J., ENGVALL, E., HOHENESTER, E., JONES, J. C., KLEINMAN, H. K., MARINKOVICH, M. P., MARTIN, G. R., MAYER, U., MENEGUZZI, G., MINER, J. H., MIYAZAKI, K., PATARROYO, M., PAULSSON, M., QUARANTA, V., SANES, J. R., SASAKI, T., SEKIGUCHI, K., SOROKIN, L. M., TALTS, J. F., TRYGGVASON, K., UITTO, J., VIRTANEN, I., VON DER MARK, K., WEWER, U. M., YAMADA, Y. & YURCHENCO, P. D. 2005. A simplified laminin nomenclature. *Matrix biology : journal of the International Society for Matrix Biology,* 24**,** 326-32.

AUMAILLEY, M. & SMYTH, N. 1998. The role of laminins in basement membrane function. *J Anat,* 193 (Pt 1)**,** 1-21.

AYMAN, T., YEREBAKAN, O., CIFTCIOGLU, M. A. & ALPSOY, E. 2002. A 13-year-old girl with recessive dystrophic epidermolysis bullosa presenting with squamous cell carcinoma. *Pediatric dermatology,* 19**,** 436-8.

BACHINGER, H. P., MORRIS, N. P., LUNSTRUM, G. P., KEENE, D. R., ROSENBAUM, L. M., COMPTON, L. A. & BURGESON, R. E. 1990. The relationship of the biophysical and biochemical characteristics of type VII collagen to the function of anchoring fibrils. *The Journal of biological chemistry,* 265**,** 10095-101.

BALDESCHI, C., GACHE, Y., RATTENHOLL, A., BOUILLE, P., DANOS, O., ORTONNE, J. P., BRUCKNER-TUDERMAN, L. & MENEGUZZI, G. 2003. Genetic correction of canine dystrophic epidermolysis bullosa mediated by retroviral vectors. *Hum Mol Genet,* 12**,** 1897-905.

BANASIK, M. B. & MCCRAY, P. B., JR. 2010. Integrase-defective lentiviral vectors: progress and applications. *Gene Ther,* 17**,** 150-7.

BEERLI, R. R. & BARBAS, C. F., 3RD 2002. Engineering polydactyl zinc-finger transcription factors. *Nat Biotechnol,* 20**,** 135-41.

BENTZ, H., MORRIS, N. P., MURRAY, L. W., SAKAI, L. Y., HOLLISTER, D. W. & BURGESON, R. E. 1983. Isolation and partial characterization of a new human

collagen with an extended triple-helical structural domain. *Proceedings of the National Academy of Sciences of the United States of America,* 80**,** 3168-72.

BLANPAIN, C. & FUCHS, E. 2009. Epidermal homeostasis: a balancing act of stem cells in the skin. *Nat Rev Mol Cell Biol,* 10**,** 207-17.

BLISSENBACH, M., GREWE, B., HOFFMANN, B., BRANDT, S. & UBERLA, K. 2010. Nuclear RNA export and packaging functions of HIV-1 Rev revisited. *J Virol,* 84**,** 6598-604.

BOHNE, J. & CATHOMEN, T. 2008. Genotoxicity in gene therapy: an account of vector integration and designer nucleases. *Curr Opin Mol Ther,* 10**,** 214-23.

BOLLING, M. C., LEMMINK, H. H., JANSEN, G. H. & JONKMAN, M. F. 2011. Mutations in KRT5 and KRT14 cause epidermolysis bullosa simplex in 75% of the patients. *The British journal of dermatology,* 164**,** 637-44.

BORDIGNON, C., MAVILIO, F., FERRARI, G., SERVIDA, P., UGAZIO, A. G., NOTARANGELO, L. D., GILBOA, E., ROSSINI, S., O'REILLY, R. J., SMITH, C. A. & ET AL. 1993. Transfer of the ADA gene into bone marrow cells and peripheral blood lymphocytes for the treatment of patients affected by ADA-deficient SCID. *Hum Gene Ther,* 4**,** 513-20.

BRENNER, M. K. 1993. Gene transfer into human hematopoietic progenitor cells: a review of current clinical protocols. *J Hematother,* 2**,** 7-17.

BRIGGS, J. A. & KRAUSSLICH, H. G. 2011. The molecular architecture of HIV. *J Mol Biol,* 410**,** 491-500.

BRUCKNER, A. L., BEDOCS, L. A., KEISER, E., TANG, J. Y., DOERNBRACK, C., ARBUCKLE, H. A., BERMAN, S., KENT, K. & BACHRACH, L. K. 2011. Correlates of low bone mass in children with generalized forms of epidermolysis bullosa. *Journal of the American Academy of Dermatology,* 65**,** 1001-9.

BRUCKNER-TUDERMAN, L. 2009. Can type VII collagen injections cure dystrophic epidermolysis bullosa? *Molecular therapy : the journal of the American Society of Gene Therapy,* 17**,** 6-7.

BRUCKNER-TUDERMAN, L. & HAS, C. 2014. Disorders of the cutaneous basement membrane zone--the paradigm of epidermolysis bullosa. *Matrix Biol,* 33**,** 29-34.

BRYANT, M. & RATNER, L. 1990. Myristoylation-dependent replication and assembly of human immunodeficiency virus 1. *Proc Natl Acad Sci U S A,* 87**,** 523-7.

BUKRINSKY, M. I., HAGGERTY, S., DEMPSEY, M. P., SHAROVA, N., ADZHUBEL, A., SPITZ, L., LEWIS, P., GOLDFARB, D., EMERMAN, M. & STEVENSON, M. 1993. A nuclear localization signal within HIV-1 matrix protein that governs infection of non-dividing cells. *Nature,* 365**,** 666-9.

BURGESON, R. E. 1993. Type VII collagen, anchoring fibrils, and epidermolysis bullosa. *The Journal of investigative dermatology,* 101**,** 252-5.

BURGESON, R. E., LUNSTRUM, G. P., ROKOSOVA, B., RIMBERG, C. S., ROSENBAUM, L. M. & KEENE, D. R. 1990. The structure and function of type VII collagen. *Annals of the New York Academy of Sciences,* 580**,** 32-43.

BURNS, J. C., FRIEDMANN, T., DRIEVER, W., BURRASCANO, M. & YEE, J. K. 1993. Vesicular stomatitis virus G glycoprotein pseudotyped retroviral vectors: concentration to very high titer and efficient gene transfer into mammalian and nonmammalian cells. *Proc Natl Acad Sci U S A,* 90**,** 8033-7.

BUSHMAN, F., LEWINSKI, M., CIUFFI, A., BARR, S., LEIPZIG, J., HANNENHALLI, S. & HOFFMANN, C. 2005. Genome-wide analysis of retroviral DNA integration. *Nature reviews. Microbiology,* 3**,** 848-58.

CARROLL, J. M., ALBERS, K. M., GARLICK, J. A., HARRINGTON, R. & TAICHMAN, L. B. 1993. Tissue- and stratum-specific expression of the human involucrin promoter in transgenic mice. *Proc Natl Acad Sci U S A,* 90**,** 10270-4.

CARTIER, N., HACEIN-BEY-ABINA, S., BARTHOLOMAE, C. C., VERES, G., SCHMIDT, M., KUTSCHERA, I., VIDAUD, M., ABEL, U., DAL-CORTIVO, L., CACCAVELLI, L., MAHLAOUI, N., KIERMER, V., MITTELSTAEDT, D., BELLESME, C., LAHLOU, N., LEFRERE, F., BLANCHE, S., AUDIT, M., PAYEN, E., LEBOULCH, P., L'HOMME, B., BOUGNERES, P., VON KALLE, C., FISCHER, A., CAVAZZANA-CALVO, M. & AUBOURG, P. 2009. Hematopoietic stem cell gene therapy with a lentiviral vector in X-linked adrenoleukodystrophy. *Science,* 326**,** 818-23.

CAVAZZANA-CALVO, M., HACEIN-BEY, S., DE SAINT BASILE, G., GROSS, F., YVON, E., NUSBAUM, P., SELZ, F., HUE, C., CERTAIN, S., CASANOVA, J. L., BOUSSO, P., DEIST, F. L. & FISCHER, A. 2000. Gene therapy of human severe combined immunodeficiency (SCID)-X1 disease. *Science,* 288**,** 669-72.

CHARLESWORTH, A., GAGNOUX-PALACIOS, L., BONDUELLE, M., ORTONNE, J. P., DE RAEVE, L. & MENEGUZZI, G. 2003. Identification of a lethal form of epidermolysis bullosa simplex associated with a homozygous genetic mutation in plectin. *The Journal of investigative dermatology,* 121**,** 1344-8.

CHEN, F., PRUETT-MILLER, S. M., HUANG, Y., GJOKA, M., DUDA, K., TAUNTON, J., COLLINGWOOD, T. N., FRODIN, M. & DAVIS, G. D. 2011. High-frequency genome editing using ssDNA oligonucleotides with zinc-finger nucleases. *Nat Methods,* 8**,** 753-5.

CHEN, M., KASAHARA, N., KEENE, D. R., CHAN, L., HOEFFLER, W. K., FINLAY, D., BARCOVA, M., CANNON, P. M., MAZUREK, C. & WOODLEY, D. T. 2002. Restoration of type VII collagen expression and function in dystrophic epidermolysis bullosa. *Nature genetics,* 32**,** 670-5.

CHEN, M., MARINKOVICH, M. P., JONES, J. C., O'TOOLE, E. A., LI, Y. Y. & WOODLEY, D. T. 1999. NC1 domain of type VII collagen binds to the beta3 chain of laminin 5 via a unique subdomain within the fibronectin-like repeats. *J Invest Dermatol,* 112**,** 177-83.

CHEN, M., MARINKOVICH, M. P., VEIS, A., CAI, X., RAO, C. N., O'TOOLE, E. A. & WOODLEY, D. T. 1997. Interactions of the amino-terminal noncollagenous (NC1) domain of type VII collagen with extracellular matrix components. A potential role in epidermal-dermal adherence in human skin. *J Biol Chem,* 272**,** 14516-22.

CHEN, M., O'TOOLE, E. A., MUELLENHOFF, M., MEDINA, E., KASAHARA, N. & WOODLEY, D. T. 2000. Development and characterization of a recombinant truncated type VII collagen "minigene". Implication for gene therapy of dystrophic epidermolysis bullosa. *J Biol Chem,* 275**,** 24429-35.

CHEN, Z., JAAFAR, L., AGYEKUM, D. G., XIAO, H., WADE, M. F., KUMARAN, R. I., SPECTOR, D. L., BAO, G., PORTEUS, M. H., DYNAN, W. S. & MEILER, S. E. 2013. Receptor-mediated delivery of engineered nucleases for genome modification. *Nucleic Acids Res,* 41**,** e182.

CHINO, T., TAMAI, K., YAMAZAKI, T., OTSURU, S., KIKUCHI, Y., NIMURA, K., ENDO, M., NAGAI, M., UITTO, J., KITAJIMA, Y. & KANEDA, Y. 2008. Bone marrow cell transfer into fetal circulation can ameliorate genetic skin diseases by providing fibroblasts to the skin and inducing immune tolerance. *Am J Pathol,* 173**,** 803-14.

CHRISTIANO, A. M., GREENSPAN, D. S., LEE, S. & UITTO, J. 1994a. Cloning of human type VII collagen. Complete primary sequence of the alpha 1(VII) chain and identification of intragenic polymorphisms. *The Journal of biological chemistry,* 269**,** 20256-62.

CHRISTIANO, A. M., HOFFMAN, G. G., CHUNG-HONET, L. C., LEE, S., CHENG, W., UITTO, J. & GREENSPAN, D. S. 1994b. Structural organization of the human type VII collagen gene (COL7A1), composed of more exons than any previously characterized gene. *Genomics,* 21**,** 169-79.

CHRISTIANO, A. M., ROSENBAUM, L. M., CHUNG-HONET, L. C., PARENTE, M. G., WOODLEY, D. T., PAN, T. C., ZHANG, R. Z., CHU, M. L., BURGESON, R. E. & UITTO, J. 1992. The large non-collagenous domain (NC-1) of type VII collagen is amino-terminal and chimeric. Homology to cartilage matrix protein, the type III domains of fibronectin and the A domains of von Willebrand factor. *Human molecular genetics,* 1**,** 475-81.

CHU, M. L., ZHANG, R. Z., PAN, T. C., STOKES, D., CONWAY, D., KUO, H. J., GLANVILLE, R., MAYER, U., MANN, K., DEUTZMANN, R. & ET AL. 1990. Mosaic structure of globular domains in the human type VI collagen alpha 3 chain: similarity to von Willebrand factor, fibronectin, actin, salivary proteins and aprotinin type protease inhibitors. *The EMBO journal,* 9**,** 385-93.

CHUNG, H. J. & UITTO, J. 2010. Type VII collagen: the anchoring fibril protein at fault in dystrophic epidermolysis bullosa. *Dermatologic clinics,* 28**,** 93-105.

CLARK, J. R. & MARCH, J. B. 2006. Bacteriophages and biotechnology: vaccines, gene therapy and antibacterials. *Trends Biotechnol,* 24**,** 212-8.

COCQUET, J., CHONG, A., ZHANG, G. & VEITIA, R. A. 2006. Reverse transcriptase template switching and false alternative transcripts. *Genomics,* 88**,** 127-31.

COGAN, J., WEINSTEIN, J., WANG, X., HOU, Y., MARTIN, S., SOUTH, A. P., WOODLEY, D. T. & CHEN, M. 2014. Aminoglycosides restore full-length type VII collagen by overcoming premature termination codons: therapeutic implications for dystrophic epidermolysis bullosa. *Mol Ther,* 22**,** 1741-52.

COLOMBO, M., BRITTINGHAM, R. J., KLEMENT, J. F., MAJSTEREK, I., BIRK, D. E., UITTO, J. & FERTALA, A. 2003. Procollagen VII self-assembly depends on site-specific interactions and is promoted by cleavage of the NC2 domain with procollagen C-proteinase. *Biochemistry,* 42**,** 11434-42.

COLUCCIO, A., MISELLI, F., LOMBARDO, A., MARCONI, A., MALAGOLI TAGLIAZUCCHI, G., GONCALVES, M. A., PINCELLI, C., MARUGGI, G., DEL

RIO, M., NALDINI, L., LARCHER, F., MAVILIO, F. & RECCHIA, A. 2013. Targeted gene addition in human epithelial stem cells by zinc-finger nuclease-mediated homologous recombination. *Mol Ther,* 21**,** 1695-704.

CONGET, P., RODRIGUEZ, F., KRAMER, S., ALLERS, C., SIMON, V., PALISSON, F., GONZALEZ, S. & YUBERO, M. J. 2010. Replenishment of type VII collagen and re-epithelialization of chronically ulcerated skin after intradermal administration of allogeneic mesenchymal stromal cells in two patients with recessive dystrophic epidermolysis bullosa. *Cytotherapy,* 12**,** 429-31.

COULOMBE, P. A., KOPAN, R. & FUCHS, E. 1989. Expression of keratin K14 in the epidermis and hair follicle: insights into complex programs of differentiation. *J Cell Biol,* 109**,** 2295-312.

CUADRADO-CORRALES, N., SANCHEZ-JIMENO, C., GARCIA, M., ESCAMEZ, M. J., ILLERA, N., HERNANDEZ-MARTIN, A., TRUJILLO-TIEBAS, M. J., AYUSO, C. & DEL RIO, M. 2010. A prevalent mutation with founder effect in Spanish Recessive Dystrophic Epidermolysis Bullosa families. *BMC Med Genet,* 11**,** 139.

CULLEN, B. R. 1992. Mechanism of action of regulatory proteins encoded by complex retroviruses. *Microbiol Rev,* 56**,** 375-94.

CUTTLE, L., NATAATMADJA, M., FRASER, J. F., KEMPF, M., KIMBLE, R. M. & HAYES, M. T. 2005. Collagen in the scarless fetal skin wound: detection with picrosirius-polarization. *Wound Repair Regen,* 13**,** 198-204.

DANG, N. & MURRELL, D. F. 2008. Mutation analysis and characterization of COL7A1 mutations in dystrophic epidermolysis bullosa. *Experimental dermatology,* 17**,** 553-68.

DEISSEROTH, A. B., KAVANAGH, J. & CHAMPLIN, R. 1994. Use of safety-modified retroviruses to introduce chemotherapy resistance sequences into normal hematopoietic cells for chemoprotection during the therapy of ovarian cancer: a pilot trial. *Hum Gene Ther,* 5**,** 1507-22.

DENDA, M., KOYAMA, J., NAMBA, R. & HORII, I. 1994. Stratum corneum lipid morphology and transepidermal water loss in normal skin and surfactant-induced scaly skin. *Arch Dermatol Res,* 286**,** 41-6.

DENG, H., LIN, Q. & KHAVARI, P. A. 1997. Sustainable cutaneous gene delivery. *Nat Biotechnol,* 15**,** 1388-91.

DESJARLAIS, J. R. & BERG, J. M. 1993. Use of a zinc-finger consensus sequence framework and specificity rules to design specific DNA binding proteins. *Proc Natl Acad Sci U S A,* 90**,** 2256-60.

DESNICK, R. J. & SCHUCHMAN, E. H. 2012. Enzyme replacement therapy for lysosomal diseases: lessons from 20 years of experience and remaining challenges. *Annu Rev Genomics Hum Genet,* 13**,** 307-35.

DI NUNZIO, F., MARUGGI, G., FERRARI, S., DI IORIO, E., POLETTI, V., GARCIA, M., DEL RIO, M., DE LUCA, M., LARCHER, F., PELLEGRINI, G. & MAVILIO, F. 2008. Correction of laminin-5 deficiency in human epidermal stem cells by transcriptionally targeted lentiviral vectors. *Mol Ther,* 16**,** 1977-85.

DICKSON, M. A., HAHN, W. C., INO, Y., RONFARD, V., WU, J. Y., WEINBERG, R. A., LOUIS, D. N., LI, F. P. & RHEINWALD, J. G. 2000. Human keratinocytes that express hTERT and also bypass a p16(INK4a)-enforced mechanism that limits life span become immortal yet retain normal growth and differentiation characteristics. *Mol Cell Biol,* 20**,** 1436-47.

DONOHO, G., JASIN, M. & BERG, P. 1998. Analysis of gene targeting and intrachromosomal homologous recombination stimulated by genomic double-strand breaks in mouse embryonic stem cells. *Mol Cell Biol,* 18**,** 4070-8.

DOYON, Y., CHOI, V. M., XIA, D. F., VO, T. D., GREGORY, P. D. & HOLMES, M. C. 2010. Transient cold shock enhances zinc-finger nuclease-mediated gene disruption. *Nat Methods,* 7**,** 459-60.

DRAGIC, T., LITWIN, V., ALLAWAY, G. P., MARTIN, S. R., HUANG, Y., NAGASHIMA, K. A., CAYANAN, C., MADDON, P. J., KOUP, R. A., MOORE, J. P. & PAXTON, W. A. 1996. HIV-1 entry into CD4+ cells is mediated by the chemokine receptor CC-CKR-5. *Nature,* 381**,** 667-73.

DUDA, K., LONOWSKI, L. A., KOFOED-NIELSEN, M., IBARRA, A., DELAY, C. M., KANG, Q., YANG, Z., PRUETT-MILLER, S. M., BENNETT, E. P., WANDALL, H. H., DAVIS, G. D., HANSEN, S. H. & FRODIN, M. 2014. High-efficiency genome editing via 2A-coupled co-expression of fluorescent proteins and zinc finger nucleases or CRISPR/Cas9 nickase pairs. *Nucleic Acids Res,* 42**,** e84.

DUFAIT, I., LIECHTENSTEIN, T., LANNA, A., BRICOGNE, C., LARANGA, R., PADELLA, A., BRECKPOT, K. & ESCORS, D. 2012. Retroviral and lentiviral vectors for the induction of immunological tolerance. *Scientifica (Cairo),* 2012.

DULL, T., ZUFFEREY, R., KELLY, M., MANDEL, R. J., NGUYEN, M., TRONO, D. & NALDINI, L. 1998. A third-generation lentivirus vector with a conditional packaging system. *Journal of virology,* 72**,** 8463-71.

DUNCKLEY, M. G., WELLS, D. J., WALSH, F. S. & DICKSON, G. 1993. Direct retroviral-mediated transfer of a dystrophin minigene into mdx mouse muscle in vivo. *Hum Mol Genet,* 2**,** 717-23.

EISENBERG, M. & LLEWELYN, D. 1998. Surgical management of hands in children with recessive dystrophic epidermolysis bullosa: use of allogeneic composite cultured skin grafts. *Br J Plast Surg,* 51**,** 608-13.

ELIAS, P., AHN, S., BROWN, B., CRUMRINE, D. & FEINGOLD, K. R. 2002. Origin of the epidermal calcium gradient: regulation by barrier status and role of active vs passive mechanisms. *J Invest Dermatol,* 119**,** 1269-74.

ELLIOTT, B., RICHARDSON, C., WINDERBAUM, J., NICKOLOFF, J. A. & JASIN, M. 1998. Gene conversion tracts from double-strand break repair in mammalian cells. *Mol Cell Biol,* 18**,** 93-101.

ELLIS, B. L., HIRSCH, M. L., PORTER, S. N., SAMULSKI, R. J. & PORTEUS, M. H. 2013. Zinc-finger nuclease-mediated gene correction using single AAV vector transduction and enhancement by Food and Drug Administration-approved drugs. *Gene Ther,* 20**,** 35-42.

ELROD-ERICKSON, M., BENSON, T. E. & PABO, C. O. 1998. High-resolution structures of variant Zif268-DNA complexes: implications for understanding zinc finger-DNA recognition. *Structure,* 6**,** 451-64.

ELROD-ERICKSON, M., ROULD, M. A., NEKLUDOVA, L. & PABO, C. O. 1996. Zif268 protein-DNA complex refined at 1.6 A: a model system for understanding zinc finger-DNA interactions. *Structure,* 4**,** 1171-80.

EMMONS, R. V., DOREN, S., ZUJEWSKI, J., COTTLER-FOX, M., CARTER, C. S., HINES, K., O'SHAUGHNESSY, J. A., LEITMAN, S. F., GREENBLATT, J. J., COWAN, K. & DUNBAR, C. E. 1997. Retroviral gene transduction of adult peripheral blood or marrow-derived CD34+ cells for six hours without growth factors or on autologous stroma does not improve marking efficiency assessed in vivo. *Blood,* 89**,** 4040-6.

FATH, S., BAUER, A. P., LISS, M., SPRIESTERSBACH, A., MAERTENS, B., HAHN, P., LUDWIG, C., SCHAFER, F., GRAF, M. & WAGNER, R. 2011. Multiparameter RNA and codon optimization: a standardized tool to assess and enhance autologous mammalian gene expression. *PloS one,* 6**,** e17596.

FEINBERG, M. B., JARRETT, R. F., ALDOVINI, A., GALLO, R. C. & WONG-STAAL, F. 1986. HTLV-III expression and production involve complex regulation at the levels of splicing and translation of viral RNA. *Cell,* 46**,** 807-17.

FENG, Y., BRODER, C. C., KENNEDY, P. E. & BERGER, E. A. 1996. HIV-1 entry cofactor: functional cDNA cloning of a seven-transmembrane, G protein-coupled receptor. *Science,* 272**,** 872-7.

FINE, J.-D., BRUCKNER-TUDERMAN, L., EADY, R. A., BAUER, E. A., BAUER, J. W., HAS, C., HEAGERTY, A., HINTNER, H., HOVNANIAN, A. & JONKMAN, M. F. 2014. Inherited epidermolysis bullosa: updated recommendations on diagnosis and classification. *Journal of the American Academy of Dermatology,* 70**,** 1103-1126.

FINE, J.-D. & MELLERIO, J. E. 2009. Extracutaneous manifestations and complications of inherited epidermolysis bullosa: part I. Epithelial associated tissues. *Journal of the American Academy of Dermatology,* 61**,** 367-384.

FINE, J. D., BAUER, E. A., BRIGGAMAN, R. A., CARTER, D. M., EADY, R. A., ESTERLY, N. B., HOLBROOK, K. A., HURWITZ, S., JOHNSON, L., LIN, A. & ET AL. 1991. Revised clinical and laboratory criteria for subtypes of inherited epidermolysis bullosa. A consensus report by the Subcommittee on Diagnosis and Classification of the National Epidermolysis Bullosa Registry. *Journal of the American Academy of Dermatology,* 24**,** 119-35.

FINE, J. D., EADY, R. A., BAUER, E. A., BAUER, J. W., BRUCKNER-TUDERMAN, L., HEAGERTY, A., HINTNER, H., HOVNANIAN, A., JONKMAN, M. F., LEIGH, I., MCGRATH, J. A., MELLERIO, J. E., MURRELL, D. F., SHIMIZU, H., UITTO, J., VAHLQUIST, A., WOODLEY, D. & ZAMBRUNO, G. 2008. The classification of inherited epidermolysis bullosa (EB): Report of the Third International Consensus Meeting on Diagnosis and Classification of EB. *Journal of the American Academy of Dermatology,* 58**,** 931-50.

FINE, J. D., JOHNSON, L. B., WEINER, M., LI, K. P. & SUCHINDRAN, C. 2009. Epidermolysis bullosa and the risk of life-threatening cancers: the National EB Registry experience, 1986-2006. *Journal of the American Academy of Dermatology,* 60**,** 203-11.

FLAVELL, S. J., HOU, T. Z., LAX, S., FILER, A. D., SALMON, M. & BUCKLEY, C. D. 2008. Fibroblasts as novel therapeutic targets in chronic inflammation. *Br J Pharmacol,* 153 Suppl 1**,** S241-6.

FRIEDMANN, T. & ROBLIN, R. 1972. Gene therapy for human genetic disease? *Science,* 175**,** 949-55.

FRITSCH, A., LOECKERMANN, S., KERN, J. S., BRAUN, A., BOSL, M. R., BLEY, T. A., SCHUMANN, H., VON ELVERFELDT, D., PAUL, D., ERLACHER, M., BERENS VON RAUTENFELD, D., HAUSSER, I., FASSLER, R. & BRUCKNER-TUDERMAN, L. 2008. A hypomorphic mouse model of dystrophic epidermolysis bullosa reveals mechanisms of disease and response to fibroblast therapy. *The Journal of clinical investigation,* 118**,** 1669-79.

FUCHS, E. 1995. Keratins and the skin. *Annu Rev Cell Dev Biol,* 11**,** 123-53.

FUENTES, G. M., RODRIGUEZ-RODRIGUEZ, L., FAY, P. J. & BAMBARA, R. A. 1995. Use of an oligoribonucleotide containing the polypurine tract sequence as a primer by HIV reverse transcriptase. *J Biol Chem,* 270**,** 28169-76.

FUJITA, Y., ABE, R., INOKUMA, D., SASAKI, M., HOSHINA, D., NATSUGA, K., NISHIE, W., MCMILLAN, J. R., NAKAMURA, H., SHIMIZU, T., AKIYAMA, M., SAWAMURA, D. & SHIMIZU, H. 2010. Bone marrow transplantation restores epidermal basement membrane protein expression and rescues epidermolysis bullosa model mice. *Proceedings of the National Academy of Sciences of the United States of America,* 107**,** 14345-50.

GABRIEL, R., LOMBARDO, A., ARENS, A., MILLER, J. C., GENOVESE, P., KAEPPEL, C., NOWROUZI, A., BARTHOLOMAE, C. C., WANG, J., FRIEDMAN, G., HOLMES, M. C., GREGORY, P. D., GLIMM, H., SCHMIDT, M., NALDINI, L. & VON KALLE, C. 2011. An unbiased genome-wide analysis of zinc-finger nuclease specificity. *Nat Biotechnol,* 29**,** 816-23.

GACHE, Y., BALDESCHI, C., DEL RIO, M., GAGNOUX-PALACIOS, L., LARCHER, F., LACOUR, J. P. & MENEGUZZI, G. 2004. Construction of skin equivalents for gene therapy of recessive dystrophic epidermolysis bullosa. *Hum Gene Ther,* 15**,** 921-33.

GACHE, Y., PIN, D., GAGNOUX-PALACIOS, L., CAROZZO, C. & MENEGUZZI, G. 2011. Correction of dog dystrophic epidermolysis bullosa by transplantation of genetically modified epidermal autografts. *The Journal of investigative dermatology,* 131**,** 2069-78.

GAJ, T., GERSBACH, C. A. & BARBAS, C. F., 3RD 2013. ZFN, TALEN, and CRISPR/Cas-based methods for genome engineering. *Trends Biotechnol,* 31**,** 397-405.

GAJ, T., GUO, J., KATO, Y., SIRK, S. J. & BARBAS, C. F., 3RD 2012. Targeted gene knockout by direct delivery of zinc-finger nuclease proteins. *Nat Methods,* 9**,** 805-7.

GASPAR, H. B., COORAY, S., GILMOUR, K. C., PARSLEY, K. L., ADAMS, S., HOWE, S. J., AL GHONAIUM, A., BAYFORD, J., BROWN, L., DAVIES, E. G., KINNON, C. & THRASHER, A. J. 2011. Long-term persistence of a polyclonal T cell repertoire after gene therapy for X-linked severe combined immunodeficiency. *Science translational medicine,* 3**,** 97ra79.

GASPAR, H. B., PARSLEY, K. L., HOWE, S., KING, D., GILMOUR, K. C., SINCLAIR, J., BROUNS, G., SCHMIDT, M., VON KALLE, C., BARINGTON, T., JAKOBSEN, M.

A., CHRISTENSEN, H. O., AL GHONAIUM, A., WHITE, H. N., SMITH, J. L., LEVINSKY, R. J., ALI, R. R., KINNON, C. & THRASHER, A. J. 2004. Gene therapy of X-linked severe combined immunodeficiency by use of a pseudotyped gammaretroviral vector. *Lancet,* 364**,** 2181-7.

GENOVESE, P., SCHIROLI, G., ESCOBAR, G., DI TOMASO, T., FIRRITO, C., CALABRIA, A., MOI, D., MAZZIERI, R., BONINI, C., HOLMES, M. C., GREGORY, P. D., VAN DER BURG, M., GENTNER, B., MONTINI, E., LOMBARDO, A. & NALDINI, L. 2014. Targeted genome editing in human repopulating haematopoietic stem cells. *Nature,* 510**,** 235-40.

GOLDBERG, G. I., EISEN, A. Z. & BAUER, E. A. 1988. Tissue stress and tumor promotion. Possible relevance to epidermolysis bullosa. *Arch Dermatol,* 124**,** 737-41.

GOTO, M., SAWAMURA, D., ITO, K., ABE, M., NISHIE, W., SAKAI, K., SHIBAKI, A., AKIYAMA, M. & SHIMIZU, H. 2006. Fibroblasts show more potential as target cells than keratinocytes in COL7A1 gene therapy of dystrophic epidermolysis bullosa. *Journal of Investigative Dermatology,* 126**,** 766-772.

GOTTLINGER, H. G., SODROSKI, J. G. & HASELTINE, W. A. 1989. Role of capsid precursor processing and myristoylation in morphogenesis and infectivity of human immunodeficiency virus type 1. *Proc Natl Acad Sci U S A,* 86**,** 5781-5.

GREEN, H. 1991. Cultured cells for the treatment of disease. *Sci Am,* 265**,** 96-102.

GREENSPAN, D. S. 1993. The carboxyl-terminal half of type VII collagen, including the non-collagenous NC-2 domain and intron/exon organization of the corresponding region of the COL7A1 gene. *Human molecular genetics,* 2**,** 273-8.

GUMBINER, B. M. 1996. Cell adhesion: the molecular basis of tissue architecture and morphogenesis. *Cell,* 84**,** 345-57.

GUPTA, A., CHRISTENSEN, R. G., RAYLA, A. L., LAKSHMANAN, A., STORMO, G. D. & WOLFE, S. A. 2012. An optimized two-finger archive for ZFN-mediated gene targeting. *Nat Methods,* 9**,** 588-90.

HACEIN-BEY, H., CAVAZZANA-CALVO, M., LE DEIST, F., DAUTRY-VARSAT, A., HIVROZ, C., RIVIERE, I., DANOS, O., HEARD, J. M., SUGAMURA, K., FISCHER, A. & DE SAINT BASILE, G. 1996. gamma-c gene transfer into SCID X1 patients' B-cell lines restores normal high-affinity interleukin-2 receptor expression and function. *Blood,* 87**,** 3108-16.

HACEIN-BEY-ABINA, S., GARRIGUE, A., WANG, G. P., SOULIER, J., LIM, A., MORILLON, E., CLAPPIER, E., CACCAVELLI, L., DELABESSE, E., BELDJORD, K., ASNAFI, V., MACINTYRE, E., DAL CORTIVO, L., RADFORD, I., BROUSSE, N., SIGAUX, F., MOSHOUS, D., HAUER, J., BORKHARDT, A., BELOHRADSKY, B. H., WINTERGERST, U., VELEZ, M. C., LEIVA, L., SORENSEN, R., WULFFRAAT, N., BLANCHE, S., BUSHMAN, F. D., FISCHER, A. & CAVAZZANA-CALVO, M. 2008. Insertional oncogenesis in 4 patients after retrovirus-mediated gene therapy of SCID-X1. *The Journal of clinical investigation,* 118**,** 3132-42.

HACEIN-BEY-ABINA, S., VON KALLE, C., SCHMIDT, M., MCCORMACK, M. P., WULFFRAAT, N., LEBOULCH, P., LIM, A., OSBORNE, C. S., PAWLIUK, R., MORILLON, E., SORENSEN, R., FORSTER, A., FRASER, P., COHEN, J. I., DE

SAINT BASILE, G., ALEXANDER, I., WINTERGERST, U., FREBOURG, T., AURIAS, A., STOPPA-LYONNET, D., ROMANA, S., RADFORD-WEISS, I., GROSS, F., VALENSI, F., DELABESSE, E., MACINTYRE, E., SIGAUX, F., SOULIER, J., LEIVA, L. E., WISSLER, M., PRINZ, C., RABBITTS, T. H., LE DEIST, F., FISCHER, A. & CAVAZZANA-CALVO, M. 2003. LMO2-associated clonal T cell proliferation in two patients after gene therapy for SCID-X1. *Science,* 302**,** 415-9.

HANIFFA, M. A., WANG, X. N., HOLTICK, U., RAE, M., ISAACS, J. D., DICKINSON, A. M., HILKENS, C. M. & COLLIN, M. P. 2007. Adult human fibroblasts are potent immunoregulatory cells and functionally equivalent to mesenchymal stem cells. *J Immunol,* 179**,** 1595-604.

HAS, C., CASTIGLIA, D., DEL RIO, M., DIEZ, M. G., PICCINNI, E., KIRITSI, D., KOHLHASE, J., ITIN, P., MARTIN, L., FISCHER, J., ZAMBRUNO, G. & BRUCKNER-TUDERMAN, L. 2011. Kindler syndrome: extension of FERMT1 mutational spectrum and natural history. *Hum Mutat,* 32**,** 1204-12.

HASTY, P., RIVERA-PEREZ, J. & BRADLEY, A. 1991. The length of homology required for gene targeting in embryonic stem cells. *Mol Cell Biol,* 11**,** 5586-91.

HEINONEN, S., MANNIKKO, M., KLEMENT, J. F., WHITAKER-MENEZES, D., MURPHY, G. F. & UITTO, J. 1999. Targeted inactivation of the type VII collagen gene (Col7a1) in mice results in severe blistering phenotype: a model for recessive dystrophic epidermolysis bullosa. *Journal of cell science,* 112 (Pt 21)**,** 3641-8.

HERBST, F., BALL, C. R., TUORTO, F., NOWROUZI, A., WANG, W., ZAVIDIJ, O., DIETER, S. M., FESSLER, S., VAN DER HOEVEN, F., KLOZ, U., LYKO, F., SCHMIDT, M., VON KALLE, C. & GLIMM, H. 2012. Extensive methylation of promoter sequences silences lentiviral transgene expression during stem cell differentiation in vivo. *Mol Ther,* 20**,** 1014-21.

HINTERMANN, E., YANG, N., O'SULLIVAN, D., HIGGINS, J. M. & QUARANTA, V. 2005. Integrin alpha6beta4-erbB2 complex inhibits haptotaxis by up-regulating E-cadherin cell-cell junctions in keratinocytes. *J Biol Chem,* 280**,** 8004-15.

HOHER, T., WALLACE, L., KHAN, K., CATHOMEN, T. & REICHELT, J. 2012. Highly efficient zinc-finger nuclease-mediated disruption of an eGFP transgene in keratinocyte stem cells without impairment of stem cell properties. *Stem Cell Rev,* 8**,** 426-34.

HOLKERS, M., MAGGIO, I., LIU, J., JANSSEN, J. M., MISELLI, F., MUSSOLINO, C., RECCHIA, A., CATHOMEN, T. & GONCALVES, M. A. 2013. Differential integrity of TALE nuclease genes following adenoviral and lentiviral vector gene transfer into human cells. *Nucleic Acids Res,* 41**,** e63.

HOLT, N., WANG, J., KIM, K., FRIEDMAN, G., WANG, X., TAUPIN, V., CROOKS, G. M., KOHN, D. B., GREGORY, P. D., HOLMES, M. C. & CANNON, P. M. 2010. Human hematopoietic stem/progenitor cells modified by zinc-finger nucleases targeted to CCR5 control HIV-1 in vivo. *Nat Biotechnol,* 28**,** 839-47.

HONG, S., HWANG, D. Y., YOON, S., ISACSON, O., RAMEZANI, A., HAWLEY, R. G. & KIM, K. S. 2007. Functional analysis of various promoters in lentiviral vectors at different stages of in vitro differentiation of mouse embryonic stem cells. *Mol Ther,* 15**,** 1630-9.

HORN, H. M., PRIESTLEY, G. C., EADY, R. A. & TIDMAN, M. J. 1997. The prevalence of epidermolysis bullosa in Scotland. *Br J Dermatol,* 136**,** 560-4.

HOWE, S. J., MANSOUR, M. R., SCHWARZWAELDER, K., BARTHOLOMAE, C., HUBANK, M., KEMPSKI, H., BRUGMAN, M. H., PIKE-OVERZET, K., CHATTERS, S. J., DE RIDDER, D., GILMOUR, K. C., ADAMS, S., THORNHILL, S. I., PARSLEY, K. L., STAAL, F. J., GALE, R. E., LINCH, D. C., BAYFORD, J., BROWN, L., QUAYE, M., KINNON, C., ANCLIFF, P., WEBB, D. K., SCHMIDT, M., VON KALLE, C., GASPAR, H. B. & THRASHER, A. J. 2008. Insertional mutagenesis combined with acquired somatic mutations causes leukemogenesis following gene therapy of SCID-X1 patients. *The Journal of clinical investigation,* 118**,** 3143-50.

HSU, Y. C., LI, L. & FUCHS, E. 2014. Emerging interactions between skin stem cells and their niches. *Nat Med,* 20**,** 847-56.

HUTTER, G., NOWAK, D., MOSSNER, M., GANEPOLA, S., MUSSIG, A., ALLERS, K., SCHNEIDER, T., HOFMANN, J., KUCHERER, C., BLAU, O., BLAU, I. W., HOFMANN, W. K. & THIEL, E. 2009. Long-term control of HIV by CCR5 Delta32/Delta32 stem-cell transplantation. *N Engl J Med,* 360**,** 692-8.

HUTTER, G. & THIEL, E. 2011. Allogeneic transplantation of CCR5-deficient progenitor cells in a patient with HIV infection: an update after 3 years and the search for patient no. 2. *AIDS,* 25**,** 273-4.

IIZUKA, H. 1994. Epidermal turnover time. *J Dermatol Sci,* 8**,** 215-7.

ITO, M., LIU, Y., YANG, Z., NGUYEN, J., LIANG, F., MORRIS, R. J. & COTSARELIS, G. 2005. Stem cells in the hair follicle bulge contribute to wound repair but not to homeostasis of the epidermis. *Nat Med,* 11**,** 1351-4.

ITOH, M., UMEGAKI-ARAO, N., GUO, Z., LIU, L., HIGGINS, C. A. & CHRISTIANO, A. M. 2013. Generation of 3D skin equivalents fully reconstituted from human induced pluripotent stem cells (iPSCs). *PLoS One,* 8**,** e77673.

JIANG, J., JING, Y., COST, G. J., CHIANG, J. C., KOLPA, H. J., COTTON, A. M., CARONE, D. M., CARONE, B. R., SHIVAK, D. A., GUSCHIN, D. Y., PEARL, J. R., REBAR, E. J., BYRON, M., GREGORY, P. D., BROWN, C. J., URNOV, F. D., HALL, L. L. & LAWRENCE, J. B. 2013. Translating dosage compensation to trisomy 21. *Nature,* 500**,** 296-300.

JINEK, M., CHYLINSKI, K., FONFARA, I., HAUER, M., DOUDNA, J. A. & CHARPENTIER, E. 2012. A programmable dual-RNA-guided DNA endonuclease in adaptive bacterial immunity. *Science,* 337**,** 816-21.

JOBARD, F., BOUADJAR, B., CAUX, F., HADJ-RABIA, S., HAS, C., MATSUDA, F., WEISSENBACH, J., LATHROP, M., PRUD'HOMME, J. F. & FISCHER, J. 2003. Identification of mutations in a new gene encoding a FERM family protein with a pleckstrin homology domain in Kindler syndrome. *Hum Mol Genet,* 12**,** 925-35.

JOGLEKAR, A. V., HOLLIS, R. P., KUFTINEC, G., SENADHEERA, S., CHAN, R. & KOHN, D. B. 2013. Integrase-defective lentiviral vectors as a delivery platform for targeted modification of adenosine deaminase locus. *Mol Ther,* 21**,** 1705-17.

JONES, E. Y. & MILLER, A. 1991. Analysis of structural design features in collagen. *Journal of molecular biology,* 218**,** 209-19.

JONES, J. C., HOPKINSON, S. B. & GOLDFINGER, L. E. 1998. Structure and assembly of hemidesmosomes. *Bioessays,* 20**,** 488-94.

JONES, K. A., KADONAGA, J. T., LUCIW, P. A. & TJIAN, R. 1986. Activation of the AIDS retrovirus promoter by the cellular transcription factor, Sp1. *Science,* 232**,** 755-9.

JONES, P. H., HARPER, S. & WATT, F. M. 1995. Stem cell patterning and fate in human epidermis. *Cell,* 80**,** 83-93.

JOUNG, J. K. & SANDER, J. D. 2013. TALENs: a widely applicable technology for targeted genome editing. *Nat Rev Mol Cell Biol,* 14**,** 49-55.

KADLER, K. E., BALDOCK, C., BELLA, J. & BOOT-HANDFORD, R. P. 2007. Collagens at a glance. *Journal of cell science,* 120**,** 1955-8.

KAMAO, H., MANDAI, M., OKAMOTO, S., SAKAI, N., SUGA, A., SUGITA, S., KIRYU, J. & TAKAHASHI, M. 2014. Characterization of human induced pluripotent stem cell-derived retinal pigment epithelium cell sheets aiming for clinical application. *Stem Cell Reports,* 2**,** 205-18.

KANEMURA, H., GO, M. J., SHIKAMURA, M., NISHISHITA, N., SAKAI, N., KAMAO, H., MANDAI, M., MORINAGA, C., TAKAHASHI, M. & KAWAMATA, S. 2014. Tumorigenicity studies of induced pluripotent stem cell (iPSC)-derived retinal pigment epithelium (RPE) for the treatment of age-related macular degeneration. *PLoS One,* 9**,** e85336.

KANTOR, B., BAYER, M., MA, H., SAMULSKI, J., LI, C., MCCOWN, T. & KAFRI, T. 2011. Notable reduction in illegitimate integration mediated by a PPT-deleted, nonintegrating lentiviral vector. *Mol Ther,* 19**,** 547-56.

KARANAM, K., KAFRI, R., LOEWER, A. & LAHAV, G. 2012. Quantitative live cell imaging reveals a gradual shift between DNA repair mechanisms and a maximal use of HR in mid S phase. *Mol Cell,* 47**,** 320-9.

KERN, J. S., LOECKERMANN, S., FRITSCH, A., HAUSSER, I., ROTH, W., MAGIN, T. M., MACK, C., MÜLLER, M. L., PAUL, O. & RUTHER, P. 2009. Mechanisms of fibroblast cell therapy for dystrophic epidermolysis bullosa: high stability of collagen VII favors long-term skin integrity. *Molecular Therapy,* 17**,** 1605-1615.

KESSL, J. J., MCKEE, C. J., EIDAHL, J. O., SHKRIABAI, N., KATZ, A. & KVARATSKHELIA, M. 2009. HIV-1 Integrase-DNA Recognition Mechanisms. *Viruses,* 1**,** 713-36.

KIM, C. A. & BERG, J. M. 1996. A 2.2 A resolution crystal structure of a designed zinc finger protein bound to DNA. *Nat Struct Biol,* 3**,** 940-5.

KIM, E., KIM, S., KIM, D. H., CHOI, B. S., CHOI, I. Y. & KIM, J. S. 2012. Precision genome engineering with programmable DNA-nicking enzymes. *Genome Res,* 22**,** 1327-33.

KIM, H. & KIM, J. S. 2014. A guide to genome engineering with programmable nucleases. *Nat Rev Genet,* 15**,** 321-34.

KIM, H. J., LEE, H. J., KIM, H., CHO, S. W. & KIM, J. S. 2009. Targeted genome editing in human cells with zinc finger nucleases constructed via modular assembly. *Genome Res,* 19**,** 1279-88.

KIM, J. S., LEE, H. J. & CARROLL, D. 2010. Genome editing with modularly assembled zinc-finger nucleases. *Nat Methods,* 7**,** 91; author reply 91-2.

KIRKORIAN, A. Y., WEITZ, N. A., TLOUGAN, B. & MOREL, K. D. 2014. Evaluation of wound care options in patients with recessive dystrophic epidermolysis bullosa: a costly necessity. *Pediatr Dermatol,* 31**,** 33-7.

KIVIRIKKO, S., LI, K., CHRISTIANO, A. M. & UITTO, J. 1996. Cloning of mouse type VII collagen reveals evolutionary conservation of functional protein domains and genomic organization. *The Journal of investigative dermatology,* 106**,** 1300-6.

KÖBNER, H. 1886. Hereditäre Anlage zur Blasenbildung (Epidermolysis bullosa hereditaria). *Deutsche Medizinische Wochenschrift,* 12.

KOCH, P. J. & ROOP, D. R. 2004. The role of keratins in epidermal development and homeostasis--going beyond the obvious. *J Invest Dermatol,* 123**,** x-xi.

KOVALESKI, B. J., KENNEDY, R., HONG, M. K., DATTA, S. A., KLEIMAN, L., REIN, A. & MUSIER-FORSYTH, K. 2006. In vitro characterization of the interaction between HIV-1 Gag and human lysyl-tRNA synthetase. *J Biol Chem,* 281**,** 19449-56.

KRUEGER, G. G. 2000. Fibroblasts and dermal gene therapy: a minireview. *Hum Gene Ther,* 11**,** 2289-96.

KUHN, U., TERUNUMA, A., PFUTZNER, W., FOSTER, R. A. & VOGEL, J. C. 2002. In vivo assessment of gene delivery to keratinocytes by lentiviral vectors. *Journal of virology,* 76**,** 1496-504.

KUMAR, M., KELLER, B., MAKALOU, N. & SUTTON, R. E. 2001. Systematic determination of the packaging limit of lentiviral vectors. *Hum Gene Ther,* 12**,** 1893-905.

LARCHER, F., DELLAMBRA, E., RICO, L., BONDANZA, S., MURILLAS, R., CATTOGLIO, C., MAVILIO, F., JORCANO, J. L., ZAMBRUNO, G. & DEL RIO, M. 2007. Long-term engraftment of single genetically modified human epidermal holoclones enables safety pre-assessment of cutaneous gene therapy. *Molecular therapy : the journal of the American Society of Gene Therapy,* 15**,** 1670-6.

LEAVITT, A. D., ROBLES, G., ALESANDRO, N. & VARMUS, H. E. 1996. Human immunodeficiency virus type 1 integrase mutants retain in vitro integrase activity yet fail to integrate viral DNA efficiently during infection. *J Virol,* 70**,** 721-8.

LECHLER, T. & FUCHS, E. 2005. Asymmetric cell divisions promote stratification and differentiation of mammalian skin. *Nature,* 437**,** 275-80.

LEGRAIN, P. & ROSBASH, M. 1989. Some cis- and trans-acting mutants for splicing target pre-mRNA to the cytoplasm. *Cell,* 57**,** 573-83.

LI, A., SIMMONS, P. J. & KAUR, P. 1998. Identification and isolation of candidate human keratinocyte stem cells based on cell surface phenotype. *Proc Natl Acad Sci U S A,* 95**,** 3902-7.

LI, H., HAURIGOT, V., DOYON, Y., LI, T., WONG, S. Y., BHAGWAT, A. S., MALANI, N., ANGUELA, X. M., SHARMA, R., IVANCIU, L., MURPHY, S. L., FINN, J. D., KHAZI, F. R., ZHOU, S., PASCHON, D. E., REBAR, E. J., BUSHMAN, F. D., GREGORY, P. D., HOLMES, M. C. & HIGH, K. A. 2011. In vivo genome editing restores haemostasis in a mouse model of haemophilia. *Nature,* 475**,** 217-21.

LIU, J., GAJ, T., WALLEN, M. C. & BARBAS, C. F., 3RD 2015. Improved cell-penetrating zinc-finger nuclease proteins for precision genome engineering. *Mol Ther Nucleic Acids,* 4**,** e232.

LIU, Q., SEGAL, D. J., GHIARA, J. B. & BARBAS, C. F., 3RD 1997. Design of polydactyl zinc-finger proteins for unique addressing within complex genomes. *Proc Natl Acad Sci U S A,* 94**,** 5525-30.

LOMBARDO, A., GENOVESE, P., BEAUSEJOUR, C. M., COLLEONI, S., LEE, Y. L., KIM, K. A., ANDO, D., URNOV, F. D., GALLI, C., GREGORY, P. D., HOLMES, M. C. & NALDINI, L. 2007. Gene editing in human stem cells using zinc finger nucleases and integrase-defective lentiviral vector delivery. *Nat Biotechnol,* 25**,** 1298-306.

LUNSTRUM, G. P., KUO, H. J., ROSENBAUM, L. M., KEENE, D. R., GLANVILLE, R. W., SAKAI, L. Y. & BURGESON, R. E. 1987. Anchoring fibrils contain the carboxyl-terminal globular domain of type VII procollagen, but lack the amino-terminal globular domain. *The Journal of biological chemistry,* 262**,** 13706-12.

MAEDER, M. L., THIBODEAU-BEGANNY, S., OSIAK, A., WRIGHT, D. A., ANTHONY, R. M., EICHTINGER, M., JIANG, T., FOLEY, J. E., WINFREY, R. J., TOWNSEND, J. A., UNGER-WALLACE, E., SANDER, J. D., MULLER-LERCH, F., FU, F., PEARLBERG, J., GOBEL, C., DASSIE, J. P., PRUETT-MILLER, S. M., PORTEUS, M. H., SGROI, D. C., IAFRATE, A. J., DOBBS, D., MCCRAY, P. B., JR., CATHOMEN, T., VOYTAS, D. F. & JOUNG, J. K. 2008. Rapid "open-source" engineering of customized zinc-finger nucleases for highly efficient gene modification. *Mol Cell,* 31**,** 294-301.

MAERTENS, G., CHEREPANOV, P., DEBYSER, Z., ENGELBORGHS, Y. & ENGELMAN, A. 2004. Identification and characterization of a functional nuclear localization signal in the HIV-1 integrase interactor LEDGF/p75. *J Biol Chem,* 279**,** 33421-9.

MAIER, D. A., BRENNAN, A. L., JIANG, S., BINDER-SCHOLL, G. K., LEE, G., PLESA, G., ZHENG, Z., COTTE, J., CARPENITO, C., WOOD, T., SPRATT, S. K., ANDO, D., GREGORY, P., HOLMES, M. C., PEREZ, E. E., RILEY, J. L., CARROLL, R. G., JUNE, C. H. & LEVINE, B. L. 2013. Efficient clinical scale gene modification via zinc finger nuclease-targeted disruption of the HIV co-receptor CCR5. *Hum Gene Ther,* 24**,** 245-58.

MALIM, M. H. & CULLEN, B. R. 1993. Rev and the fate of pre-mRNA in the nucleus: implications for the regulation of RNA processing in eukaryotes. *Mol Cell Biol,* 13**,** 6180-9.

MARTINS, V. L., VYAS, J. J., CHEN, M., PURDIE, K., MEIN, C. A., SOUTH, A. P., STOREY, A., MCGRATH, J. A. & O'TOOLE, E. A. 2009. Increased invasive behaviour in cutaneous squamous cell carcinoma with loss of basement-membrane type VII collagen. *Journal of cell science,* 122**,** 1788-99.

MARUGGI, G., PORCELLINI, S., FACCHINI, G., PERNA, S. K., CATTOGLIO, C., SARTORI, D., AMBROSI, A., SCHAMBACH, A., BAUM, C., BONINI, C.,

BOVOLENTA, C., MAVILIO, F. & RECCHIA, A. 2009. Transcriptional enhancers induce insertional gene deregulation independently from the vector type and design. *Mol Ther,* 17**,** 851-6.

MATRAI, J., CANTORE, A., BARTHOLOMAE, C. C., ANNONI, A., WANG, W., ACOSTA-SANCHEZ, A., SAMARA-KUKO, E., DE WAELE, L., MA, L., GENOVESE, P., DAMO, M., ARENS, A., GOUDY, K., NICHOLS, T. C., VON KALLE, C., MK, L. C., RONCAROLO, M. G., SCHMIDT, M., VANDENDRIESSCHE, T. & NALDINI, L. 2011. Hepatocyte-targeted expression by integrase-defective lentiviral vectors induces antigen-specific tolerance in mice with low genotoxic risk. *Hepatology,* 53**,** 1696-707.

MATRAI, J., CHUAH, M. K. & VANDENDRIESSCHE, T. 2010. Recent advances in lentiviral vector development and applications. *Mol Ther,* 18**,** 477-90.

MAVILIO, F., PELLEGRINI, G., FERRARI, S., DI NUNZIO, F., DI IORIO, E., RECCHIA, A., MARUGGI, G., FERRARI, G., PROVASI, E., BONINI, C., CAPURRO, S., CONTI, A., MAGNONI, C., GIANNETTI, A. & DE LUCA, M. 2006. Correction of junctional epidermolysis bullosa by transplantation of genetically modified epidermal stem cells. *Nature medicine,* 12**,** 1397-402.

MCGINLEY, L., MCMAHON, J., STRAPPE, P., BARRY, F., MURPHY, M., O'TOOLE, D. & O'BRIEN, T. 2011. Lentiviral vector mediated modification of mesenchymal stem cells & enhanced survival in an in vitro model of ischaemia. *Stem Cell Res Ther,* 2**,** 12.

MCGRATH, J. A., EADY, R. A. J. AND POPE, F. M. 2008. *Anatomy and Organization of Human Skin,* Malden, Massachusetts, USA, Blackwell Publishing, Inc.

MCGRATH, J. A., SCHOFIELD, O. M., ISHIDA-YAMAMOTO, A., O'GRADY, A., MAYOU, B. J., NAVSARIA, H., LEIGH, I. M. & EADY, R. A. 1993. Cultured keratinocyte allografts and wound healing in severe recessive dystrophic epidermolysis bullosa. *J Am Acad Dermatol,* 29**,** 407-19.

MCKENNA, K. E., WALSH, M. Y. & BINGHAM, E. A. 1992. Epidermolysis bullosa in Northern Ireland. *Br J Dermatol,* 127**,** 318-21.

MILLER, J. C., HOLMES, M. C., WANG, J., GUSCHIN, D. Y., LEE, Y. L., RUPNIEWSKI, I., BEAUSEJOUR, C. M., WAITE, A. J., WANG, N. S., KIM, K. A., GREGORY, P. D., PABO, C. O. & REBAR, E. J. 2007. An improved zinc-finger nuclease architecture for highly specific genome editing. *Nat Biotechnol,* 25**,** 778-85.

MILLER, M. D., FARNET, C. M. & BUSHMAN, F. D. 1997. Human immunodeficiency virus type 1 preintegration complexes: studies of organization and composition. *J Virol,* 71**,** 5382-90.

MINER, J. H. & YURCHENCO, P. D. 2004. Laminin functions in tissue morphogenesis. *Annu Rev Cell Dev Biol,* 20**,** 255-84.

MITCHELL, R. S., BEITZEL, B. F., SCHRODER, A. R., SHINN, P., CHEN, H., BERRY, C. C., ECKER, J. R. & BUSHMAN, F. D. 2004. Retroviral DNA integration: ASLV, HIV, and MLV show distinct target site preferences. *PLoS biology,* 2**,** E234.

MIYOSHI, H., BLOMER, U., TAKAHASHI, M., GAGE, F. H. & VERMA, I. M. 1998. Development of a self-inactivating lentivirus vector. *J Virol,* 72**,** 8150-7.

MOEHLE, E. A., ROCK, J. M., LEE, Y. L., JOUVENOT, Y., DEKELVER, R. C., GREGORY, P. D., URNOV, F. D. & HOLMES, M. C. 2007. Targeted gene addition into a specified location in the human genome using designed zinc finger nucleases. *Proc Natl Acad Sci U S A,* 104**,** 3055-60.

MOHRI, H., YOSHIOKA, A., ZIMMERMAN, T. S. & RUGGERI, Z. M. 1989. Isolation of the von Willebrand factor domain interacting with platelet glycoprotein Ib, heparin, and collagen and characterization of its three distinct functional sites. *The Journal of biological chemistry,* 264**,** 17361-7.

MOHRIN, M., BOURKE, E., ALEXANDER, D., WARR, M. R., BARRY-HOLSON, K., LE BEAU, M. M., MORRISON, C. G. & PASSEGUE, E. 2010. Hematopoietic stem cell quiescence promotes error-prone DNA repair and mutagenesis. *Cell Stem Cell,* 7**,** 174-85.

MOIANI, A., PALEARI, Y., SARTORI, D., MEZZADRA, R., MICCIO, A., CATTOGLIO, C., COCCHIARELLA, F., LIDONNICI, M. R., FERRARI, G. & MAVILIO, F. 2012. Lentiviral vector integration in the human genome induces alternative splicing and generates aberrant transcripts. *J Clin Invest,* 122**,** 1653-66.

MOLL, R., FRANKE, W. W., SCHILLER, D. L., GEIGER, B. & KREPLER, R. 1982. The catalog of human cytokeratins: patterns of expression in normal epithelia, tumors and cultured cells. *Cell,* 31**,** 11-24.

MONTINI, E., CESANA, D., SCHMIDT, M., SANVITO, F., BARTHOLOMAE, C. C., RANZANI, M., BENEDICENTI, F., SERGI, L. S., AMBROSI, A., PONZONI, M., DOGLIONI, C., DI SERIO, C., VON KALLE, C. & NALDINI, L. 2009. The genotoxic potential of retroviral vectors is strongly modulated by vector design and integration site selection in a mouse model of HSC gene therapy. *The Journal of clinical investigation,* 119**,** 964-75.

MORENO-CARRANZA, B., GENTSCH, M., STEIN, S., SCHAMBACH, A., SANTILLI, G., RUDOLF, E., RYSER, M. F., HARIA, S., THRASHER, A. J., BAUM, C., BRENNER, S. & GREZ, M. 2009. Transgene optimization significantly improves SIN vector titers, gp91phox expression and reconstitution of superoxide production in X-CGD cells. *Gene Ther,* 16**,** 111-8.

MORGAN, R. A., DUDLEY, M. E., WUNDERLICH, J. R., HUGHES, M. S., YANG, J. C., SHERRY, R. M., ROYAL, R. E., TOPALIAN, S. L., KAMMULA, U. S., RESTIFO, N. P., ZHENG, Z., NAHVI, A., DE VRIES, C. R., ROGERS-FREEZER, L. J., MAVROUKAKIS, S. A. & ROSENBERG, S. A. 2006. Cancer regression in patients after transfer of genetically engineered lymphocytes. *Science,* 314**,** 126-9.

MORRIS, N. P., KEENE, D. R., GLANVILLE, R. W., BENTZ, H. & BURGESON, R. E. 1986. The tissue form of type VII collagen is an antiparallel dimer. *The Journal of biological chemistry,* 261**,** 5638-44.

MURATA, T., MASUNAGA, T., ISHIKO, A., SHIMIZU, H. & NISHIKAWA, T. 2004. Differences in recurrent COL7A1 mutations in dystrophic epidermolysis bullosa: ethnic-specific and worldwide recurrent mutations. *Archives of dermatological research,* 295**,** 442-7.

MURAUER, E. M., GACHE, Y., GRATZ, I. K., KLAUSEGGER, A., MUSS, W., GRUBER, C., MENEGUZZI, G., HINTNER, H. & BAUER, J. W. 2011. Functional correction of

type VII collagen expression in dystrophic epidermolysis bullosa. *The Journal of investigative dermatology,* 131**,** 74-83.

NABEL, G. & BALTIMORE, D. 1987. An inducible transcription factor activates expression of human immunodeficiency virus in T cells. *Nature,* 326**,** 711-3.

NAGY, N., ALMAANI, N., TANAKA, A., LAI-CHEONG, J. E., TECHANUKUL, T., MELLERIO, J. E. & MCGRATH, J. A. 2011. HB-EGF induces COL7A1 expression in keratinocytes and fibroblasts: possible mechanism underlying allogeneic fibroblast therapy in recessive dystrophic epidermolysis Bullosa. *The Journal of investigative dermatology,* 131**,** 1771-4.

NALDINI, L. 1998. Lentiviruses as gene transfer agents for delivery to non-dividing cells. *Current opinion in biotechnology,* 9**,** 457-63.

NALDINI, L., BLOMER, U., GAGE, F. H., TRONO, D. & VERMA, I. M. 1996a. Efficient transfer, integration, and sustained long-term expression of the transgene in adult rat brains injected with a lentiviral vector. *Proceedings of the National Academy of Sciences of the United States of America,* 93**,** 11382-8.

NALDINI, L., BLOMER, U., GALLAY, P., ORY, D., MULLIGAN, R., GAGE, F. H., VERMA, I. M. & TRONO, D. 1996b. In vivo gene delivery and stable transduction of nondividing cells by a lentiviral vector. *Science,* 272**,** 263-7.

NELSON, W. G. & SUN, T. T. 1983. The 50- and 58-kdalton keratin classes as molecular markers for stratified squamous epithelia: cell culture studies. *J Cell Biol,* 97**,** 244-51.

NG, Y. Z., POURREYRON, C., SALAS-ALANIS, J. C., DAYAL, J. H., CEPEDA-VALDES, R., YAN, W., WRIGHT, S., CHEN, M., FINE, J. D., HOGG, F. J., MCGRATH, J. A., MURRELL, D. F., LEIGH, I. M., LANE, E. B. & SOUTH, A. P. 2012. Fibroblast-derived dermal matrix drives development of aggressive cutaneous squamous cell carcinoma in patients with recessive dystrophic epidermolysis bullosa. *Cancer Res,* 72**,** 3522-34.

NIGHTINGALE, S. J., HOLLIS, R. P., PEPPER, K. A., PETERSEN, D., YU, X. J., YANG, C., BAHNER, I. & KOHN, D. B. 2006. Transient gene expression by nonintegrating lentiviral vectors. *Mol Ther,* 13**,** 1121-32.

NISHIE, W., NATSUGA, K., NAKAMURA, H., ITO, T., TOYONAGA, E., SATO, H. & SHIMIZU, H. 2014. A recurrent 'hot spot' glycine substitution mutation, G2043R in COL7A1, induces dominant dystrophic epidermolysis bullosa associated with intracytoplasmic accumulation of pro-collagen VII. *J Dermatol Sci,* 75**,** 69-71.

NIU, Y., SHEN, B., CUI, Y., CHEN, Y., WANG, J., WANG, L., KANG, Y., ZHAO, X., SI, W., LI, W., XIANG, A. P., ZHOU, J., GUO, X., BI, Y., SI, C., HU, B., DONG, G., WANG, H., ZHOU, Z., LI, T., TAN, T., PU, X., WANG, F., JI, S., ZHOU, Q., HUANG, X., JI, W. & SHA, J. 2014. Generation of gene-modified cynomolgus monkey via Cas9/RNA-mediated gene targeting in one-cell embryos. *Cell,* 156**,** 836-43.

NYSTROM, A., VELATI, D., MITTAPALLI, V. R., FRITSCH, A., KERN, J. S. & BRUCKNER-TUDERMAN, L. 2013. Collagen VII plays a dual role in wound healing. *J Clin Invest,* 123**,** 3498-509.

ORLANDO, S. J., SANTIAGO, Y., DEKELVER, R. C., FREYVERT, Y., BOYDSTON, E. A., MOEHLE, E. A., CHOI, V. M., GOPALAN, S. M., LOU, J. F., LI, J., MILLER, J. C.,

HOLMES, M. C., GREGORY, P. D., URNOV, F. D. & COST, G. J. 2010. Zinc-finger nuclease-driven targeted integration into mammalian genomes using donors with limited chromosomal homology. *Nucleic Acids Res,* 38**,** e152.

ORTIZ-URDA, S., GARCIA, J., GREEN, C. L., CHEN, L., LIN, Q., VEITCH, D. P., SAKAI, L. Y., LEE, H., MARINKOVICH, M. P. & KHAVARI, P. A. 2005. Type VII collagen is required for Ras-driven human epidermal tumorigenesis. *Science,* 307**,** 1773-6.

ORTIZ-URDA, S., LIN, Q., GREEN, C. L., KEENE, D. R., MARINKOVICH, M. P. & KHAVARI, P. A. 2003. Injection of genetically engineered fibroblasts corrects regenerated human epidermolysis bullosa skin tissue. *The Journal of clinical investigation,* 111**,** 251-5.

ORTIZ-URDA, S., THYAGARAJAN, B., KEENE, D. R., LIN, Q., FANG, M., CALOS, M. P. & KHAVARI, P. A. 2002. Stable nonviral genetic correction of inherited human skin disease. *Nat Med,* 8**,** 1166-70.

OSBORN, M. J., STARKER, C. G., MCELROY, A. N., WEBBER, B. R., RIDDLE, M. J., XIA, L., DEFEO, A. P., GABRIEL, R., SCHMIDT, M., VON KALLE, C., CARLSON, D. F., MAEDER, M. L., JOUNG, J. K., WAGNER, J. E., VOYTAS, D. F., BLAZAR, B. R. & TOLAR, J. 2013. TALEN-based gene correction for epidermolysis bullosa. *Molecular therapy : the journal of the American Society of Gene Therapy,* 21**,** 1151-9.

OTT, M. G., SCHMIDT, M., SCHWARZWAELDER, K., STEIN, S., SILER, U., KOEHL, U., GLIMM, H., KUHLCKE, K., SCHILZ, A., KUNKEL, H., NAUNDORF, S., BRINKMANN, A., DEICHMANN, A., FISCHER, M., BALL, C., PILZ, I., DUNBAR, C., DU, Y., JENKINS, N. A., COPELAND, N. G., LUTHI, U., HASSAN, M., THRASHER, A. J., HOELZER, D., VON KALLE, C., SEGER, R. & GREZ, M. 2006. Correction of X-linked chronic granulomatous disease by gene therapy, augmented by insertional activation of MDS1-EVI1, PRDM16 or SETBP1. *Nature medicine,* 12**,** 401-9.

PALLARI, H. M. & ERIKSSON, J. E. 2006. Intermediate filaments as signaling platforms. *Sci STKE,* 2006**,** pe53.

PARENTE, M. G., CHUNG, L. C., RYYNANEN, J., WOODLEY, D. T., WYNN, K. C., BAUER, E. A., MATTEI, M. G., CHU, M. L. & UITTO, J. 1991. Human type VII collagen: cDNA cloning and chromosomal mapping of the gene. *Proceedings of the National Academy of Sciences of the United States of America,* 88**,** 6931-5.

PAVLETICH, N. P. & PABO, C. O. 1991. Zinc finger-DNA recognition: crystal structure of a Zif268-DNA complex at 2.1 A. *Science,* 252**,** 809-17.

PAXTON, W., CONNOR, R. I. & LANDAU, N. R. 1993. Incorporation of Vpr into human immunodeficiency virus type 1 virions: requirement for the p6 region of gag and mutational analysis. *J Virol,* 67**,** 7229-37.

PEARSON, R. W. 1962. Studies on the pathogenesis of epidermolysis bullosa. *The Journal of investigative dermatology,* 39**,** 551-75.

PERDONI, C., OSBORN, M. J. & TOLAR, J. 2015. Gene editing toward the use of autologous therapies in recessive dystrophic epidermolysis bullosa. *Transl Res*.

PEREZ, E. E., WANG, J., MILLER, J. C., JOUVENOT, Y., KIM, K. A., LIU, O., WANG, N., LEE, G., BARTSEVICH, V. V., LEE, Y. L., GUSCHIN, D. Y., RUPNIEWSKI, I.,

WAITE, A. J., CARPENITO, C., CARROLL, R. G., ORANGE, J. S., URNOV, F. D., REBAR, E. J., ANDO, D., GREGORY, P. D., RILEY, J. L., HOLMES, M. C. & JUNE, C. H. 2008. Establishment of HIV-1 resistance in CD4+ T cells by genome editing using zinc-finger nucleases. *Nat Biotechnol,* 26**,** 808-16.

PETROF, G., MARTINEZ‐QUEIPO, M., MELLERIO, J., KEMP, P. & MCGRATH, J. 2013. Fibroblast cell therapy enhances initial healing in recessive dystrophic epidermolysis bullosa wounds: results of a randomized, vehicle‐controlled trial. *British Journal of Dermatology,* 169**,** 1025-1033.

PFENDNER, E. G. & BRUCKNER, A. L. 1993. Epidermolysis Bullosa Simplex. *In:* PAGON, R. A., BIRD, T. D., DOLAN, C. R., STEPHENS, K. & ADAM, M. P. (eds.) *GeneReviews.* Seattle (WA).

PFENDNER, E. G. & LUCKY, A. W. 1993a. Dystrophic Epidermolysis Bullosa. *In:* PAGON, R. A., BIRD, T. D., DOLAN, C. R., STEPHENS, K. & ADAM, M. P. (eds.) *GeneReviews.* Seattle (WA).

PFENDNER, E. G. & LUCKY, A. W. 1993b. Junctional Epidermolysis Bullosa. *In:* PAGON, R. A., BIRD, T. D., DOLAN, C. R., STEPHENS, K. & ADAM, M. P. (eds.) *GeneReviews.* Seattle (WA).

PORTEUS, M. H. 2006. Mammalian gene targeting with designed zinc finger nucleases. *Mol Ther,* 13**,** 438-46.

POTTS, R. O. & FRANCOEUR, M. L. 1991. The influence of stratum corneum morphology on water permeability. *J Invest Dermatol,* 96**,** 495-9.

POURREYRON, C., COX, G., MAO, X., VOLZ, A., BAKSH, N., WONG, T., FASSIHI, H., ARITA, K., O'TOOLE, E. A., OCAMPO-CANDIANI, J., CHEN, M., HART, I. R., BRUCKNER-TUDERMAN, L., SALAS-ALANIS, J. C., MCGRATH, J. A., LEIGH, I. M. & SOUTH, A. P. 2007. Patients with recessive dystrophic epidermolysis bullosa develop squamous-cell carcinoma regardless of type VII collagen expression. *The Journal of investigative dermatology,* 127**,** 2438-44.

PROCKOP, D. J. 1997. Marrow stromal cells as stem cells for nonhematopoietic tissues. *Science,* 276**,** 71-4.

PROVASI, E., GENOVESE, P., LOMBARDO, A., MAGNANI, Z., LIU, P. Q., REIK, A., CHU, V., PASCHON, D. E., ZHANG, L., KUBALL, J., CAMISA, B., BONDANZA, A., CASORATI, G., PONZONI, M., CICERI, F., BORDIGNON, C., GREENBERG, P. D., HOLMES, M. C., GREGORY, P. D., NALDINI, L. & BONINI, C. 2012. Editing T cell specificity towards leukemia by zinc finger nucleases and lentiviral gene transfer. *Nat Med,* 18**,** 807-15.

PULE, M., FINNEY, H. & LAWSON, A. 2003. Artificial T-cell receptors. *Cytotherapy,* 5**,** 211-26.

PULLAR, C. E., BAIER, B. S., KARIYA, Y., RUSSELL, A. J., HORST, B. A., MARINKOVICH, M. P. & ISSEROFF, R. R. 2006. beta4 integrin and epidermal growth factor coordinately regulate electric field-mediated directional migration via Rac1. *Mol Biol Cell,* 17**,** 4925-35.

QIN, J. Y., ZHANG, L., CLIFT, K. L., HULUR, I., XIANG, A. P., REN, B. Z. & LAHN, B. T. 2010. Systematic comparison of constitutive promoters and the doxycycline-inducible promoter. *PLoS One,* 5**,** e10611.

RAMIREZ, C. L., CERTO, M. T., MUSSOLINO, C., GOODWIN, M. J., CRADICK, T. J., MCCAFFREY, A. P., CATHOMEN, T., SCHARENBERG, A. M. & JOUNG, J. K. 2012. Engineered zinc finger nickases induce homology-directed repair with reduced mutagenic effects. *Nucleic Acids Res,* 40**,** 5560-8.

RAMSHAW, J. A., SHAH, N. K. & BRODSKY, B. 1998. Gly-X-Y tripeptide frequencies in collagen: a context for host-guest triple-helical peptides. *Journal of structural biology,* 122**,** 86-91.

RAN, F. A., HSU, P. D., WRIGHT, J., AGARWALA, V., SCOTT, D. A. & ZHANG, F. 2013. Genome engineering using the CRISPR-Cas9 system. *Nat Protoc,* 8**,** 2281-308.

RATTENHOLL, A., PAPPANO, W. N., KOCH, M., KEENE, D. R., KADLER, K. E., SASAKI, T., TIMPL, R., BURGESON, R. E., GREENSPAN, D. S. & BRUCKNER-TUDERMAN, L. 2002. Proteinases of the bone morphogenetic protein-1 family convert procollagen VII to mature anchoring fibril collagen. *The Journal of biological chemistry,* 277**,** 26372-8.

RATUSHNY, V., GOBER, M. D., HICK, R., RIDKY, T. W. & SEYKORA, J. T. 2012. From keratinocyte to cancer: the pathogenesis and modeling of cutaneous squamous cell carcinoma. *J Clin Invest,* 122**,** 464-72.

REMINGTON, J., WANG, X., HOU, Y., ZHOU, H., BURNETT, J., MUIRHEAD, T., UITTO, J., KEENE, D. R., WOODLEY, D. T. & CHEN, M. 2009. Injection of recombinant human type VII collagen corrects the disease phenotype in a murine model of dystrophic epidermolysis bullosa. *Molecular therapy : the journal of the American Society of Gene Therapy,* 17**,** 26-33.

REMY, S., TESSON, L., MENORET, S., USAL, C., DE CIAN, A., THEPENIER, V., THINARD, R., BARON, D., CHARPENTIER, M., RENAUD, J. B., BUELOW, R., COST, G. J., GIOVANNANGELI, C., FRAICHARD, A., CONCORDET, J. P. & ANEGON, I. 2014. Efficient gene targeting by homology-directed repair in rat zygotes using TALE nucleases. *Genome Res,* 24**,** 1371-83.

RICE, R. H. & GREEN, H. 1979. Presence in human epidermal cells of a soluble protein precursor of the cross-linked envelope: activation of the cross-linking by calcium ions. *Cell,* 18**,** 681-94.

RODECK, U. & UITTO, J. 2007. Recessive Dystrophic Epidermolysis Bullosa–Associated Squamous-Cell Carcinoma: An Enigmatic Entity with Complex Pathogenesis. *Journal of Investigative Dermatology,* 127**,** 2295-2296.

ROUSSELLE, P., KEENE, D. R., RUGGIERO, F., CHAMPLIAUD, M.-F., VAN DER REST, M. & BURGESON, R. E. 1997. Laminin 5 binds the NC-1 domain of type VII collagen. *The Journal of cell biology,* 138**,** 719-728.

RUGG, E. L., HORN, H. M., SMITH, F. J., WILSON, N. J., HILL, A. J., MAGEE, G. J., SHEMANKO, C. S., BATY, D. U., TIDMAN, M. J. & LANE, E. B. 2007. Epidermolysis bullosa simplex in Scotland caused by a spectrum of keratin mutations. *The Journal of investigative dermatology,* 127**,** 574-80.

RUGGIERO, F., ROULET, M. & BONOD-BIDAUD, C. 2005. [Dermis collagens: beyond their structural properties]. *J Soc Biol,* 199**,** 301-11.

RYYNANEN, J., SOLLBERG, S., PARENTE, M. G., CHUNG, L. C., CHRISTIANO, A. M. & UITTO, J. 1992. Type VII collagen gene expression by cultured human cells and in fetal skin. Abundant mRNA and protein levels in epidermal keratinocytes. *J Clin Invest,* 89**,** 163-8.

SAKAI, L. Y., KEENE, D. R., MORRIS, N. P. & BURGESON, R. E. 1986. Type VII collagen is a major structural component of anchoring fibrils. *The Journal of cell biology,* 103**,** 1577-86.

SAKODA, T., KASAHARA, N., HAMAMORI, Y. & KEDES, L. 1999. A high-titer lentiviral production system mediates efficient transduction of differentiated cells including beating cardiac myocytes. *Journal of molecular and cellular cardiology,* 31**,** 2037-47.

SALMON, P., KINDLER, V., DUCREY, O., CHAPUIS, B., ZUBLER, R. H. & TRONO, D. 2000. High-level transgene expression in human hematopoietic progenitors and differentiated blood lineages after transduction with improved lentiviral vectors. *Blood,* 96**,** 3392-8.

SANDER, J. D., DAHLBORG, E. J., GOODWIN, M. J., CADE, L., ZHANG, F., CIFUENTES, D., CURTIN, S. J., BLACKBURN, J. S., THIBODEAU-BEGANNY, S., QI, Y., PIERICK, C. J., HOFFMAN, E., MAEDER, M. L., KHAYTER, C., REYON, D., DOBBS, D., LANGENAU, D. M., STUPAR, R. M., GIRALDEZ, A. J., VOYTAS, D. F., PETERSON, R. T., YEH, J. R. & JOUNG, J. K. 2011. Selection-free zinc-finger-nuclease engineering by context-dependent assembly (CoDA). *Nat Methods,* 8**,** 67-9.

SANJANA, N. E., SHALEM, O. & ZHANG, F. 2014. Improved vectors and genome-wide libraries for CRISPR screening. *Nat Methods,* 11**,** 783-4.

SCHAMBACH, A., BOHNE, J., BAUM, C., HERMANN, F., EGERER, L., VON LAER, D. & GIROGLOU, T. 2005. Woodchuck hepatitis virus post-transcriptional regulatory element deleted from X protein and promoter sequences enhances retroviral vector titer and expression. *Gene therapy,* 13**,** 641-645.

SCHRODER, A. R., SHINN, P., CHEN, H., BERRY, C., ECKER, J. R. & BUSHMAN, F. 2002. HIV-1 integration in the human genome favors active genes and local hotspots. *Cell,* 110**,** 521-9.

SCHWANK, G., KOO, B. K., SASSELLI, V., DEKKERS, J. F., HEO, I., DEMIRCAN, T., SASAKI, N., BOYMANS, S., CUPPEN, E., VAN DER ENT, C. K., NIEUWENHUIS, E. E., BEEKMAN, J. M. & CLEVERS, H. 2013. Functional repair of CFTR by CRISPR/Cas9 in intestinal stem cell organoids of cystic fibrosis patients. *Cell Stem Cell,* 13**,** 653-8.

SEBASTIANO, V., MAEDER, M. L., ANGSTMAN, J. F., HADDAD, B., KHAYTER, C., YEO, D. T., GOODWIN, M. J., HAWKINS, J. S., RAMIREZ, C. L., BATISTA, L. F., ARTANDI, S. E., WERNIG, M. & JOUNG, J. K. 2011. In situ genetic correction of the sickle cell anemia mutation in human induced pluripotent stem cells using engineered zinc finger nucleases. *Stem Cells,* 29**,** 1717-26.

SEBASTIANO, V., ZHEN, H. H., DERAFSHI, B. H., BASHKIROVA, E., MELO, S. P., WANG, P., LEUNG, T. L., SIPRASHVILI, Z., TICHY, A. & LI, J. 2014. Human

COL7A1-corrected induced pluripotent stem cells for the treatment of recessive dystrophic epidermolysis bullosa. *Science translational medicine,* 6**,** 264ra163.

SEGAL, D. J., DREIER, B., BEERLI, R. R. & BARBAS, C. F., 3RD 1999. Toward controlling gene expression at will: selection and design of zinc finger domains recognizing each of the 5'-GNN-3' DNA target sequences. *Proc Natl Acad Sci U S A,* 96**,** 2758-63.

SEHGAL, B. U., DEBIASE, P. J., MATZNO, S., CHEW, T. L., CLAIBORNE, J. N., HOPKINSON, S. B., RUSSELL, A., MARINKOVICH, M. P. & JONES, J. C. 2006. Integrin beta4 regulates migratory behavior of keratinocytes by determining laminin-332 organization. *J Biol Chem,* 281**,** 35487-98.

SHAHARABANY, M. & HIZI, A. 1991. The DNA-dependent and RNA-dependent DNA polymerase activities of the reverse transcriptases of human immunodeficiency viruses types 1 and 2. *AIDS Res Hum Retroviruses,* 7**,** 883-8.

SHI, Y. & BERG, J. M. 1995. A direct comparison of the properties of natural and designed zinc-finger proteins. *Chem Biol,* 2**,** 83-9.

SHIMIZU, H. 1998. New insights into the immunoultrastructural organization of cutaneous basement membrane zone molecules. *Exp Dermatol,* 7**,** 303-13.

SHIMIZU, H., ISHIKO, A., MASUNAGA, T., KURIHARA, Y., SATO, M., BRUCKNER-TUDERMAN, L. & NISHIKAWA, T. 1997. Most anchoring fibrils in human skin originate and terminate in the lamina densa. *Laboratory investigation,* 76**,** 753-763.

SHULTZ, L. D., LYONS, B. L., BURZENSKI, L. M., GOTT, B., CHEN, X., CHALEFF, S., KOTB, M., GILLIES, S. D., KING, M., MANGADA, J., GREINER, D. L. & HANDGRETINGER, R. 2005. Human lymphoid and myeloid cell development in NOD/LtSz-scid IL2R gamma null mice engrafted with mobilized human hemopoietic stem cells. *J Immunol,* 174**,** 6477-89.

SIPRASHVILI, Z., NGUYEN, N. T., BEZCHINSKY, M. Y., MARINKOVICH, M. P., LANE, A. T. & KHAVARI, P. A. 2010. Long-term type VII collagen restoration to human epidermolysis bullosa skin tissue. *Human gene therapy,* 21**,** 1299-310.

SMOLLER, B. R., KRUEGER, J., MCNUTT, N. S. & HSU, A. 1990. "Activated" keratinocyte phenotype is unifying feature in conditions which predispose to squamous cell carcinoma of the skin. *Mod Pathol,* 3**,** 171-5.

SOLDNER, F., LAGANIERE, J., CHENG, A. W., HOCKEMEYER, D., GAO, Q., ALAGAPPAN, R., KHURANA, V., GOLBE, L. I., MYERS, R. H., LINDQUIST, S., ZHANG, L., GUSCHIN, D., FONG, L. K., VU, B. J., MENG, X., URNOV, F. D., REBAR, E. J., GREGORY, P. D., ZHANG, H. S. & JAENISCH, R. 2011. Generation of isogenic pluripotent stem cells differing exclusively at two early onset Parkinson point mutations. *Cell,* 146**,** 318-31.

STERNBERG, S. H., REDDING, S., JINEK, M., GREENE, E. C. & DOUDNA, J. A. 2014. DNA interrogation by the CRISPR RNA-guided endonuclease Cas9. *Nature,* 507**,** 62-7.

SYED, F., SANGANEE, H. J., BAHL, A. & BAYAT, A. 2013. Potent dual inhibitors of TORC1 and TORC2 complexes (KU-0063794 and KU-0068650) demonstrate in vitro and ex vivo anti-keloid scar activity. *Journal of Investigative Dermatology,* 133**,** 1340-1350.

SYED, F., SHERRIS, D., PAUS, R., VARMEH, S., PANDOLFI, P. P. & BAYAT, A. 2012. Keloid disease can be inhibited by antagonizing excessive mTOR signaling with a novel dual TORC1/2 inhibitor. *Am J Pathol,* 181**,** 1642-1658.

SZCZEPEK, M., BRONDANI, V., BUCHEL, J., SERRANO, L., SEGAL, D. J. & CATHOMEN, T. 2007. Structure-based redesign of the dimerization interface reduces the toxicity of zinc-finger nucleases. *Nat Biotechnol,* 25**,** 786-93.

TAGHIAN, D. G. & NICKOLOFF, J. A. 1997. Chromosomal double-strand breaks induce gene conversion at high frequency in mammalian cells. *Mol Cell Biol,* 17**,** 6386-93.

TAMAI, K., YAMAZAKI, T., CHINO, T., ISHII, M., OTSURU, S., KIKUCHI, Y., IINUMA, S., SAGA, K., NIMURA, K., SHIMBO, T., UMEGAKI, N., KATAYAMA, I., MIYAZAKI, J., TAKEDA, J., MCGRATH, J. A., UITTO, J. & KANEDA, Y. 2011. PDGFRalpha-positive cells in bone marrow are mobilized by high mobility group box 1 (HMGB1) to regenerate injured epithelia. *Proceedings of the National Academy of Sciences of the United States of America,* 108**,** 6609-14.

TEBAS, P., STEIN, D., TANG, W. W., FRANK, I., WANG, S. Q., LEE, G., SPRATT, S. K., SUROSKY, R. T., GIEDLIN, M. A., NICHOL, G., HOLMES, M. C., GREGORY, P. D., ANDO, D. G., KALOS, M., COLLMAN, R. G., BINDER-SCHOLL, G., PLESA, G., HWANG, W. T., LEVINE, B. L. & JUNE, C. H. 2014. Gene editing of CCR5 in autologous CD4 T cells of persons infected with HIV. *N Engl J Med,* 370**,** 901-10.

TERHEGGEN, H. G., LOWENTHAL, A., LAVINHA, F., COLOMBO, J. P. & ROGERS, S. 1975. Unsuccessful trial of gene replacement in arginase deficiency. *Z Kinderheilkd,* 119**,** 1-3.

THOMAS, K. R., FOLGER, K. R. & CAPECCHI, M. R. 1986. High frequency targeting of genes to specific sites in the mammalian genome. *Cell,* 44**,** 419-28.

TITEUX, M., PENDARIES, V., ZANTA-BOUSSIF, M. A., DECHA, A., PIRONON, N., TONASSO, L., MEJIA, J. E., BRICE, A., DANOS, O. & HOVNANIAN, A. 2010. SIN retroviral vectors expressing COL7A1 under human promoters for ex vivo gene therapy of recessive dystrophic epidermolysis bullosa. *Molecular therapy : the journal of the American Society of Gene Therapy,* 18**,** 1509-18.

TOLAR, J., ISHIDA-YAMAMOTO, A., RIDDLE, M., MCELMURRY, R. T., OSBORN, M., XIA, L., LUND, T., SLATTERY, C., UITTO, J., CHRISTIANO, A. M., WAGNER, J. E. & BLAZAR, B. R. 2009. Amelioration of epidermolysis bullosa by transfer of wild-type bone marrow cells. *Blood,* 113**,** 1167-74.

TOLAR, J., MCGRATH, J. A., XIA, L., RIDDLE, M. J., LEES, C. J., EIDE, C., KEENE, D. R., LIU, L., OSBORN, M. J., LUND, T. C., BLAZAR, B. R. & WAGNER, J. E. 2014. Patient-specific naturally gene-reverted induced pluripotent stem cells in recessive dystrophic epidermolysis bullosa. *J Invest Dermatol,* 134**,** 1246-54.

TOLAR, J. & WAGNER, J. E. 2015. A biologic Velcro patch. *N Engl J Med,* 372**,** 382-4.

TOLAR, J., XIA, L., RIDDLE, M. J., LEES, C. J., EIDE, C. R., MCELMURRY, R. T., TITEUX, M., OSBORN, M. J., LUND, T. C., HOVNANIAN, A., WAGNER, J. E. & BLAZAR, B. R. 2011. Induced pluripotent stem cells from individuals with recessive dystrophic epidermolysis bullosa. *The Journal of investigative dermatology,* 131**,** 848-56.

TORIKAI, H., REIK, A., LIU, P. Q., ZHOU, Y., ZHANG, L., MAITI, S., HULS, H., MILLER, J. C., KEBRIAEI, P., RABINOVITCH, B., LEE, D. A., CHAMPLIN, R. E., BONINI, C., NALDINI, L., REBAR, E. J., GREGORY, P. D., HOLMES, M. C. & COOPER, L. J. 2012. A foundation for universal T-cell based immunotherapy: T cells engineered to express a CD19-specific chimeric-antigen-receptor and eliminate expression of endogenous TCR. *Blood,* 119**,** 5697-705.

TRABALZA, A., GEORGIADIS, C., ELEFTHERIADOU, I., HISLOP, J. N., ELLISON, S. M., KARAVASSILIS, M. E. & MAZARAKIS, N. D. 2013. Venezuelan equine encephalitis virus glycoprotein pseudotyping confers neurotropism to lentiviral vectors. *Gene Ther,* 20**,** 723-32.

TSURUTA, D., HASHIMOTO, T., HAMILL, K. J. & JONES, J. C. 2011. Hemidesmosomes and focal contact proteins: functions and cross-talk in keratinocytes, bullous diseases and wound healing. *J Dermatol Sci,* 62**,** 1-7.

TSURUTA, D., KOBAYASHI, H., IMANISHI, H., SUGAWARA, K., ISHII, M. & JONES, J. C. 2008. Laminin-332-integrin interaction: a target for cancer therapy? *Curr Med Chem,* 15**,** 1968-75.

TURCZYNSKI, S., TITEUX, M., PIRONON, N. & HOVNANIAN, A. 2012. Antisense-mediated exon skipping to reframe transcripts. *Methods Mol Biol,* 867**,** 221-38.

UITTO, J., BAUER, E. A. & MOSHELL, A. N. 1992. Symposium on epidermolysis bullosa: molecular biology and pathology of the cutaneous basement membrane zone. Jefferson Medical College, Philadelphia, Pennsylvania, October 4 and 5, 1991. *The Journal of investigative dermatology,* 98**,** 391-5.

UITTO, J. & CHRISTIANO, A. M. 1992. Molecular genetics of the cutaneous basement membrane zone. Perspectives on epidermolysis bullosa and other blistering skin diseases. *The Journal of clinical investigation,* 90**,** 687-92.

UITTO, J., MCGRATH, J. A., RODECK, U., BRUCKNER-TUDERMAN, L. & ROBINSON, E. C. 2010. Progress in epidermolysis bullosa research: toward treatment and cure. *The Journal of investigative dermatology,* 130**,** 1778-84.

UMEGAKI-ARAO, N., PASMOOIJ, A. M., ITOH, M., CERISE, J. E., GUO, Z., LEVY, B., GOSTYNSKI, A., ROTHMAN, L. R., JONKMAN, M. F. & CHRISTIANO, A. M. 2014. Induced pluripotent stem cells from human revertant keratinocytes for the treatment of epidermolysis bullosa. *Sci Transl Med,* 6**,** 264ra164.

URBINATI, F., ARUMUGAM, P., HIGASHIMOTO, T., PERUMBETI, A., MITTS, K., XIA, P. & MALIK, P. 2009. Mechanism of reduction in titers from lentivirus vectors carrying large inserts in the 3'LTR. *Mol Ther,* 17**,** 1527-36.

URNOV, F. D., MILLER, J. C., LEE, Y. L., BEAUSEJOUR, C. M., ROCK, J. M., AUGUSTUS, S., JAMIESON, A. C., PORTEUS, M. H., GREGORY, P. D. & HOLMES, M. C. 2005. Highly efficient endogenous human gene correction using designed zinc-finger nucleases. *Nature,* 435**,** 646-51.

URNOV, F. D., REBAR, E. J., HOLMES, M. C., ZHANG, H. S. & GREGORY, P. D. 2010. Genome editing with engineered zinc finger nucleases. *Nature reviews. Genetics,* 11**,** 636-46.

VAN SLUIS, M. & MCSTAY, B. 2015. A localized nucleolar DNA damage response facilitates recruitment of the homology-directed repair machinery independent of cell cycle stage. *Genes Dev,* 29**,** 1151-63.

VANDEGRAAFF, N. & ENGELMAN, A. 2007. Molecular mechanisms of HIV integration and therapeutic intervention. *Expert Rev Mol Med,* 9**,** 1-19.

VARKI, R., SADOWSKI, S., PFENDNER, E. & UITTO, J. 2006. Epidermolysis bullosa. I. Molecular genetics of the junctional and hemidesmosomal variants. *Journal of medical genetics,* 43**,** 641-52.

VARKI, R., SADOWSKI, S., UITTO, J. & PFENDNER, E. 2007. Epidermolysis bullosa. II. Type VII collagen mutations and phenotype-genotype correlations in the dystrophic subtypes. *Journal of medical genetics,* 44**,** 181-92.

VENUGOPAL, S. S., YAN, W., FREW, J. W., COHN, H. I., RHODES, L. M., TRAN, K., MELBOURNE, W., NELSON, J. A., STURM, M. & FOGARTY, J. 2013. A phase II randomized vehicle-controlled trial of intradermal allogeneic fibroblasts for recessive dystrophic epidermolysis bullosa. *Journal of the American Academy of Dermatology,* 69**,** 898-908. e7.

VERPLANCKE, P., BEELE, H., MONSTREY, S. & NAEYAERT, J. M. 1997. Treatment of dystrophic epidermolysis bullosa with autologous meshed split-thickness skin grafts and allogeneic cultured keratinocytes. *Dermatology,* 194**,** 380-2.

VILLONE, D., FRITSCH, A., KOCH, M., BRUCKNER-TUDERMAN, L., HANSEN, U. & BRUCKNER, P. 2008. Supramolecular interactions in the dermo-epidermal junction zone: anchoring fibril-collagen VII tightly binds to banded collagen fibrils. *The Journal of biological chemistry,* 283**,** 24506-13.

VINCENT, N., RAGOT, T., GILGENKRANTZ, H., COUTON, D., CHAFEY, P., GREGOIRE, A., BRIAND, P., KAPLAN, J. C., KAHN, A. & PERRICAUDET, M. 1993. Long-term correction of mouse dystrophic degeneration by adenovirus-mediated transfer of a minidystrophin gene. *Nat Genet,* 5**,** 130-4.

VUORIO, E. & DE CROMBRUGGHE, B. 1990. The family of collagen genes. *Annual review of biochemistry,* 59**,** 837-72.

WAGNER, J. E., ISHIDA-YAMAMOTO, A., MCGRATH, J. A., HORDINSKY, M., KEENE, D. R., WOODLEY, D. T., CHEN, M., RIDDLE, M. J., OSBORN, M. J. & LUND, T. 2010. Bone marrow transplantation for recessive dystrophic epidermolysis bullosa. *New England Journal of Medicine,* 363**,** 629-639.

WALLER, J. M. & MAIBACH, H. I. 2006. Age and skin structure and function, a quantitative approach (II): protein, glycosaminoglycan, water, and lipid content and structure. *Skin Res Technol,* 12**,** 145-54.

WANG, J., FRIEDMAN, G., DOYON, Y., WANG, N. S., LI, C. J., MILLER, J. C., HUA, K. L., YAN, J. J., BABIARZ, J. E., GREGORY, P. D. & HOLMES, M. C. 2012. Targeted gene addition to a predetermined site in the human genome using a ZFN-based nicking enzyme. *Genome Res,* 22**,** 1316-26.

WANG, X., GHASRI, P., AMIR, M., HWANG, B., HOU, Y., KHILILI, M., LIN, A., KEENE, D., UITTO, J., WOODLEY, D. T. & CHEN, M. 2013. Topical application of recombinant type VII collagen incorporates into the dermal-epidermal junction and

promotes wound closure. *Molecular therapy : the journal of the American Society of Gene Therapy,* 21**,** 1335-44.

WANG, Y., CHEN, X., CAO, W. & SHI, Y. 2014. Plasticity of mesenchymal stem cells in immunomodulation: pathological and therapeutic implications. *Nat Immunol,* 15**,** 1009-16.

WATERMAN, E. A., SAKAI, N., NGUYEN, N. T., HORST, B. A., VEITCH, D. P., DEY, C. N., ORTIZ-URDA, S., KHAVARI, P. A. & MARINKOVICH, M. P. 2007. A laminin-collagen complex drives human epidermal carcinogenesis through phosphoinositol-3-kinase activation. *Cancer Res,* 67**,** 4264-70.

WEISS, C. D., BARNETT, S. W., CACALANO, N., KILLEEN, N., LITTMAN, D. R. & WHITE, J. M. 1996. Studies of HIV-1 envelope glycoprotein-mediated fusion using a simple fluorescence assay. *AIDS,* 10**,** 241-6.

WENZEL, D., BAYERL, J., NYSTROM, A., BRUCKNER-TUDERMAN, L., MEIXNER, A. & PENNINGER, J. M. 2014. Genetically corrected iPSCs as cell therapy for recessive dystrophic epidermolysis bullosa. *Sci Transl Med,* 6**,** 264ra165.

WOLLINA, U., KONRAD, H. & FISCHER, T. 2001. Recessive epidermolysis bullosa dystrophicans (Hallopeau-Siemens)--improvement of wound healing by autologous epidermal grafts on an esterified hyaluronic acid membrane. *J Dermatol,* 28**,** 217-20.

WONG, T., GAMMON, L., LIU, L., MELLERIO, J. E., DOPPING-HEPENSTAL, P. J., PACY, J., ELIA, G., JEFFERY, R., LEIGH, I. M. & NAVSARIA, H. 2008. Potential of fibroblast cell therapy for recessive dystrophic epidermolysis bullosa. *Journal of Investigative Dermatology,* 128**,** 2179-2189.

WOODLEY, D. T., HOU, Y., MARTIN, S., LI, W. & CHEN, M. 2008. Characterization of molecular mechanisms underlying mutations in dystrophic epidermolysis bullosa using site-directed mutagenesis. *The Journal of biological chemistry,* 283**,** 17838-45.

WOODLEY, D. T., KEENE, D. R., ATHA, T., HUANG, Y., LIPMAN, K., LI, W. & CHEN, M. 2004a. Injection of recombinant human type VII collagen restores collagen function in dystrophic epidermolysis bullosa. *Nature medicine,* 10**,** 693-5.

WOODLEY, D. T., KEENE, D. R., ATHA, T., HUANG, Y., RAM, R., KASAHARA, N. & CHEN, M. 2004b. Intradermal injection of lentiviral vectors corrects regenerated human dystrophic epidermolysis bullosa skin tissue in vivo. *Molecular Therapy,* 10**,** 318-326.

WOODLEY, D. T., KRUEGER, G. G., JORGENSEN, C. M., FAIRLEY, J. A., ATHA, T., HUANG, Y., CHAN, L., KEENE, D. R. & CHEN, M. 2003. Normal and gene-corrected dystrophic epidermolysis bullosa fibroblasts alone can produce type VII collagen at the basement membrane zone. *The Journal of investigative dermatology,* 121**,** 1021-8.

WOODLEY, D. T., REMINGTON, J. & CHEN, M. 2007a. Autoimmunity to type VII collagen: epidermolysis bullosa acquisita. *Clinical reviews in allergy & immunology,* 33**,** 78-84.

WOODLEY, D. T., REMINGTON, J., HUANG, Y., HOU, Y., LI, W., KEENE, D. R. & CHEN, M. 2007b. Intravenously injected human fibroblasts home to skin wounds, deliver type VII collagen, and promote wound healing. *Molecular therapy : the journal of the American Society of Gene Therapy,* 15**,** 628-35.

WOODLEY, D. T., WANG, X., AMIR, M., HWANG, B., REMINGTON, J., HOU, Y., UITTO, J., KEENE, D. & CHEN, M. 2013. Intravenously injected recombinant human type VII collagen homes to skin wounds and restores skin integrity of dystrophic epidermolysis bullosa. *Journal of investigative dermatology,* 133**,** 1910-1913.

WU, X., LI, Y., CRISE, B. & BURGESS, S. M. 2003. Transcription start regions in the human genome are favored targets for MLV integration. *Science,* 300**,** 1749-51.

YASUKAWA, K., SAWAMURA, D., GOTO, M., NAKAMURA, H., JUNG, S. Y., KIM, S. C. & SHIMIZU, H. 2006. Epidermolysis bullosa simplex in Japanese and Korean patients: genetic studies in 19 cases. *The British journal of dermatology,* 155**,** 313-7.

YI, G., CHOI, J. G., BHARAJ, P., ABRAHAM, S., DANG, Y., KAFRI, T., ALOZIE, O., MANJUNATH, M. N. & SHANKAR, P. 2014. CCR5 Gene Editing of Resting CD4(+) T Cells by Transient ZFN Expression From HIV Envelope Pseudotyped Nonintegrating Lentivirus Confers HIV-1 Resistance in Humanized Mice. *Mol Ther Nucleic Acids,* 3**,** e198.

YUSA, K., RASHID, S. T., STRICK-MARCHAND, H., VARELA, I., LIU, P. Q., PASCHON, D. E., MIRANDA, E., ORDONEZ, A., HANNAN, N. R., ROUHANI, F. J., DARCHE, S., ALEXANDER, G., MARCINIAK, S. J., FUSAKI, N., HASEGAWA, M., HOLMES, M. C., DI SANTO, J. P., LOMAS, D. A., BRADLEY, A. & VALLIER, L. 2011. Targeted gene correction of alpha1-antitrypsin deficiency in induced pluripotent stem cells. *Nature,* 478**,** 391-4.

ZANTA-BOUSSIF, M. A., CHARRIER, S., BRICE-OUZET, A., MARTIN, S., OPOLON, P., THRASHER, A. J., HOPE, T. J. & GALY, A. 2009. Validation of a mutated PRE sequence allowing high and sustained transgene expression while abrogating WHV-X protein synthesis: application to the gene therapy of WAS. *Gene Ther,* 16**,** 605-19.

ZOU, J., MALI, P., HUANG, X., DOWEY, S. N. & CHENG, L. 2011a. Site-specific gene correction of a point mutation in human iPS cells derived from an adult patient with sickle cell disease. *Blood,* 118**,** 4599-608.

ZOU, J., SWEENEY, C. L., CHOU, B. K., CHOI, U., PAN, J., WANG, H., DOWEY, S. N., CHENG, L. & MALECH, H. L. 2011b. Oxidase-deficient neutrophils from X-linked chronic granulomatous disease iPS cells: functional correction by zinc finger nuclease-mediated safe harbor targeting. *Blood,* 117**,** 5561-72.

ZUFFEREY, R., DONELLO, J. E., TRONO, D. & HOPE, T. J. 1999. Woodchuck hepatitis virus posttranscriptional regulatory element enhances expression of transgenes delivered by retroviral vectors. *J Virol,* 73**,** 2886-92.

ZUFFEREY, R., DULL, T., MANDEL, R. J., BUKOVSKY, A., QUIROZ, D., NALDINI, L. & TRONO, D. 1998. Self-inactivating lentivirus vector for safe and efficient in vivo gene delivery. *Journal of virology,* 72**,** 9873-80.

Lentiviral Engineered Fibroblasts Expressing Codon-Optimized *COL7A1* Restore Anchoring Fibrils in RDEB

Christos Georgiadis[1,7], Farhatullah Syed[1,7], Anastasia Petrova[1], Alya Abdul-Wahab[2], Su M. Lwin[2], Farzin Farzaneh[4], Lucas Chan[4], Sumera Ghani[1], Roland A. Fleck[3], Leanne Glover[3], James R. McMillan[5], Mei Chen[6], Adrian J. Thrasher[1], John A. McGrath[2], Wei-Li Di[1,8] and Waseem Qasim[1,8]

Cells therapies, engineered to secrete replacement proteins, are being developed to ameliorate otherwise debilitating diseases. Recessive dystrophic epidermolysis bullosa (RDEB) is caused by defects of type VII collagen, a protein essential for anchoring fibril formation at the dermal-epidermal junction. Whereas allogeneic fibroblasts injected directly into the dermis can mediate transient disease modulation, autologous gene-modified fibroblasts should evade immunological rejection and support sustained delivery of type VII collagen at the dermal-epidermal junction. We demonstrate the feasibility of such an approach using a therapeutic grade, self-inactivating-lentiviral vector, encoding codon-optimized *COL7A1*, to transduce RDEB fibroblasts under conditions suitable for clinical application. Expression and secretion of type VII collagen was confirmed with transduced cells exhibiting supranormal levels of protein expression, and ex vivo migration of fibroblasts was restored in functional assays. Gene-modified RDEB fibroblasts also deposited type VII collagen at the dermal-epidermal junction of human RDEB skin xenografts placed on NOD-*scid* IL2Rgamma^{null} recipients, with reconstruction of human epidermal structure and regeneration of anchoring fibrils at the dermal-epidermal junction. Fibroblast-mediated restoration of protein and structural defects in this RDEB model strongly supports proposed therapeutic applications in man.

Journal of Investigative Dermatology (2016) **136,** 284-292; doi:10.1038/JID.2015.364

INTRODUCTION

Recessive dystrophic epidermolysis bullosa (RDEB) is a debilitating genodermatosis caused by loss-of-function mutations in *COL7A1* (Fine et al., 2014). Type VII collagen (C7) is essential for anchoring fibril (AF) formation at the dermal-epidermal junction (DEJ), and in RDEB, malformed, reduced, or absent AFs are a direct consequence of *COL7A1* mutations (Hovnanian et al., 1997). C7 is one of the main contributors of dermal-epidermal adhesion, forming "wheat-stack"-shaped, centrosymmetrically banded, semicircular loop structures known as AFs after antiparallel dimerization of two fibrils at their carboxyl (C)-termini (Burgeson et al., 1990). These can be seen extending from their amino (N)-termini that indirectly bind to hemidesmosomal α6β4 integrin via the bridging activity of laminin-332 in the lamina densa (Rousselle et al., 1997), where they protrude down to the papillary dermis encircling dermal type I and III collagen amongst other fibrous elements before terminating back in the lamina densa (Shimizu et al., 1997). Loss-of-function mutations in C7 lead to fragility of AF structures, thereby compromising the integrity of the DEJ resulting in severe sublamina densa blistering and tissue cleavage.

Clinically, skin blistering can follow even minor mechanical stress causing skin erosions from birth in many subtypes of RDEB. Moreover, chronic erosions with secondary infections that can progress to widespread, mutilating scars and joint contractures, and aggressive squamous cell carcinomas, typify the severe generalized forms of RDEB (Fine and Mellerio, 2009; Rodeck and Uitto, 2007). RDEB has a profound medical and socioeconomic impact on patients and their families (Tabolli et al., 2009). There are no curative therapies for RDEB, and supportive care, with daily dressings, meticulous wound care, nutritional support, and iron supplementation for chronic anemia are the mainstay of clinical management (Grocott et al., 2013; Mellerio et al., 2007).

Experimental therapies under development include recombinant C7 protein (Remington et al., 2008; Woodley et al., 2004, 2013), infusion of allogeneic mesenchymal cells (Conget et al., 2010), hematopoietic–stem cell transplantation (Tolar and Wagner, 2012; Wagner et al., 2010),

[1]*UCL Institute of Child Health, Molecular and Cellular Immunology Section & Great Ormond Street Hospital NHS Foundation Trust, London, United Kingdom;* [2]*St John's Institute of Dermatology, King's College London (Guy's campus), London, United Kingdom;* [3]*Centre for Ultrastructural Imaging, King's College London, London, United Kingdom;* [4]*Department of Haematological Medicine, King's College London, The Rayne Institute, London, United Kingdom;* [5]*The Robin Eady National Diagnostic Epidermolysis Bullosa Laboratory, Viapath LLP, St Thomas' Hospital, London, United Kingdom and* [6]*Department of Dermatology, University of Southern California, Los Angeles, California, USA*

[7] *These authors have contributed equally to this work.*

[8] *These authors have contributed equally to this work.*

Correspondence: Waseem Qasim, Reader in Cell & Gene Therapy, UCL Institute of Child Health & Great Ormond Street Hospital NHS Foundation Trust, 30 Guilford Street, London WC1N 1EH, United Kingdom. E-mail: W.Qasim@ucl.ac.uk

Abbreviations: AF, anchoring fibril; DEJ, dermalepidermal junction; LV, lentiviral; RDEB, recessive dystrophic epidermolysis bullosa; C7, type VII collagen

Received 7 May 2015; revised 27 July 2015; accepted 3 August 2015; accepted manuscript published online 22 September 2015

and gene therapies (Droz-Georget Lathion et al., 2015; Osborn et al., 2013; Sebastiano et al., 2014; Titeux et al., 2010). We have investigated the feasibility of ex vivo gene-modified cell-based delivery of C7 to restore AFs at the DEJ of affected skin. Although both keratinocytes and fibroblasts are involved in the production and secretion of C7, fibroblasts are generally more robust and easier to maintain in culture, making them an attractive target for such an approach (Goto et al., 2006). In addition, alternative approaches based on transduction of keratinocytes and production of engineered skin grafts may not be suitable for RDEB where the abnormal DEJ may compromise adhesion of engineered epidermal sheets. In previous studies, intradermal injections of allogeneic fibroblasts from healthy donors supported increased levels of *COL7A1* expression in patients with RDEB for several months (Nagy et al., 2011; Wong et al., 2008). However, a recent phase II double-blind randomized trial demonstrated the importance of intradermal control injections. These comprised placebo (vehicle only) reagents and resulted in similar levels of wound healing as with mismatched allogeneic fibroblasts (Venugopal et al., 2013). A significant difference between injection of vehicle and allogeneic fibroblasts was only noted at day 7 (of 28 days) in a separate trial (Petrof et al., 2013). Although the mechanism is unclear, a localized anti-inflammatory effect and upregulation of *COL7A1* from intradermal inoculation of the vehicle solution or injection needle itself (commonly used in scar remodeling) has been postulated (Nagy et al., 2011; Petrof et al., 2013; Venugopal et al., 2013). Irrespective of the mechanism, a major limitation of allogeneic injections is the immunological rejection of HLA-mismatched donor fibroblasts (Larcher and Del Río, 2015; Venugopal et al., 2013; Wong et al., 2008). An autologous approach using genetically modified RDEB fibroblasts should circumvent the risk of rejection and provide a source of locally synthesized C7. Previous reports have established the feasibility of modifying fibroblasts with a variety of vectors, including phage (Ortiz-Urda et al., 2003), gamma retrovirus (Goto et al., 2006; Titeux et al., 2010; Woodley et al., 2007), and lentivirus (Chen et al., 2002; Woodley et al., 2003), and local or systemic injection into recipient mice has provided varying degrees of evidence of restoration of skin integrity (Woodley et al., 2004, 2007). We have developed a self-inactivating-lentiviral (LV) platform combined with a human phosphoglycerate kinase promoter and codon-optimized *COL7A1* for the engineering of autologous RDEB fibroblasts and have shown definitive evidence of AF reconstruction at the DEJ in a human:murine xenograft model. The production and validation of good-manufacturing-practice compliant reagents and a robust process for manufacturing engineered fibroblasts have enabled the submission of applications for regulatory approval for first-in-man testing of this therapy.

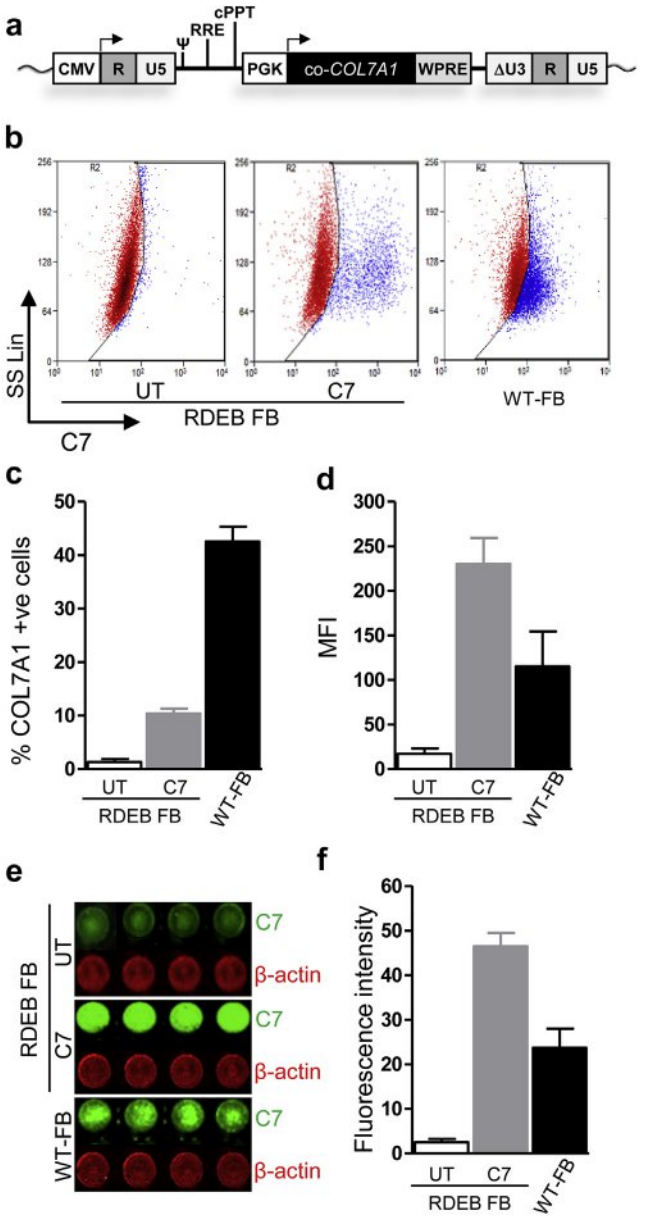

Figure 1. Expression of C7 in gene-corrected RDEB fibroblasts using a SIN-LV-*COL7A1* vector. (**a**) Configuration of pCCL-PGK-*COL7A1* lentiviral transfer plasmid shows a third-generation, split-packaging SIN vector with the deleted U3 region of the 3′LTR, internal PGK promoter, mutated woodchuck hepatitis virus posttranscriptional regulatory element (WPRE), and central polypurine tract (cPPT). Transgene *COL7A1* was codon-optimized (co-*COL7A1*) encoding the full-length *COL7A1* sequence. (**b**, **c**) Average expression of C7 in LV-*COL7*-transduced and untransduced (UT) primary RDEB-1 and -2 fibroblasts by intracellular staining and flow cytometry with corresponding mean fluorescence intensity (MFI) (**d**). (**e**) In situ expression of C7 in RDEB-1 and -2 LV-*COL7* fibroblasts using in-cell Western blotting (ICWB). Green lanes represent C7 expression; red lanes represent loading control (β-actin) expression with average immunoreactivity (**f**). LTR, long terminal repeat; LV, lentiviral; PGK, phosphoglycerate kinase; RDEB, recessive dystrophic epidermolysis bullosa; SD , standard deviation; SIN, self-inactivating. Error bars represent SD of four replicates.

RESULTS

Restoration of C7 expression in LV-*COL7A1*-transduced RDEB primary fibroblasts

Primary fibroblasts from patients with RDEB lacking C7 expression were transduced with a third-generation self-inactivating-LV vector encoding codon-optimized C7 (LV-*COL7*) under current good-manufacturing-practice compliant conditions using a single round of exposure at a multiplicity of infection 5 (Figure 1a). After 3 weeks of culture and expansion, flow cytometric analysis showed 9.3−12.8% of fibroblasts expressing C7 (Figure 1b−d), and this

corresponded to an integrated proviral copy number of 0.12−0.14 copies/cell. In-cell Western blotting showed overexpression of C7 in transduced RDEB fibroblasts compared with untransduced and wild-type (WT) fibroblasts as measured by mean fluorescence intensity (Figure 1e and f). In situ cytostaining also detected C7 protein expression in transduced RDEB fibroblasts (Figure 2a), whereas there was no expression in untransduced RDEB fibroblasts. These results were further confirmed by Western blot analysis using a purified C7 antibody (a gift from Professor Mei Chen). Cell lysates from transduced RDEB fibroblasts revealed the expression of an approximately 290 kDa protein band corresponding to full-length C7 (Figure 2b) and expression was stable when reassessed after 8 weeks. Full-length protein was also detected in media harvested from cultured transduced RDEB fibroblasts (Figure 2c) indicating effective secretion of the recombinant protein. In view of previous reports that around a quarter of gamma retroviral vector integrants, particularly in keratinocytes, may encode truncated forms of the *COL7A1* transgene, we screened cultures for aberrant protein forms, and found that only 3 of 49 single-cell clonal populations expressed abnormally sized protein. This greatly reduced frequency was attributed to our codon optimization of the transgene, with residual low-level recombination events during reverse transcription linked to a small number of persisting repeat sequences.

Functional recovery in LV-*COL7*-transduced RDEB fibroblasts

LV-*COL7*-transduced fibroblasts were assessed for viability and metabolic activity using a water-soluble tetrazolium salt-1 assay, with no differences observed compared with non-corrected RDEB fibroblasts (Supplementary Figure S1 online).

In migration assays, the loss of C7 in RDEB cells has been previously correlated with adverse functional effects on the kinetics of wound closure compared with WT cells. Reports have separately described both increased or decreased migration associated with loss of C7, but with normalization to WT levels after the reconstitution of C7 expression (Chen et al., 2002; Martins et al., 2009; Nystrom et al., 2013). Functional recovery in transduced RDEB fibroblasts was examined by using a two-dimensional assay of fibroblast migration across "wounds" created by cell-seeding stoppers (Syed et al., 2013). RDEB fibroblasts had reduced ($P < 0.05$) migration compared with WT fibroblasts, which was restored by transduction with LV-*COL7* (Figure 3a). The number of cells within the 2 mm migration zone was analyzed using ImageJ and revealed a significant increase in transduced compared with nontransduced RDEB fibroblasts ($P < 0.01$), with numbers similar to healthy donor fibroblasts ($P > 0.05$) (Figure 3b).

Morphological correction of the DEJ in an RDEB human:murine skin graft model

To determine whether secreted C7 produced from LV-*COL7*-transduced fibroblasts can contribute toward the deposition and incorporation of C7 into the DEJ in vivo, a modified human:murine xenograft skin model was developed using previously described procedures (Di et al., 2011, 2012; Larcher et al., 2007). Primary RDEB fibroblasts were transduced with LV-*COL7* and seeded in a supporting fibrin matrix composed of porcine plasma and human thrombin on which primary keratinocytes were further seeded, generating a bioengineered skin graft. Control grafts carrying combinations of primary healthy or untransduced RDEB keratinocytes and fibroblasts were prepared alongside under the same conditions. The bioengineered skin grafts were grafted on NOD-*scid* IL2Rgamma^{null} mice in duplicate for each condition and allowed to mature over a period of 8 weeks. This provided an opportunity to monitor two full cycles of human keratinocyte and fibroblast development in vivo. At that point the grafts were harvested and processed for cryosectioning and transmission electron microscopy (TEM). Hematoxylin and eosin staining showed distinct and fully differentiated human epidermis with visible stratification and formation of a thick cornified layer that was readily distinguishable from murine tissue (Figure 4a−c and Supplementary Figure S2a−c online). The human derivation of the grafted area was confirmed by species-specific staining for human C7 and mitochondrial markers (complex IV subunit II) and showed clearly demarcated human:murine borders (Figure 4d−f and g−i). Human-specific staining for desmoglein further verified the human origin of the graft (Supplementary Figure S2d−e online). Epidermal proliferation and differentiation was confirmed by staining of keratin 10 and involucrin in suprabasal layers and the upper epidermal strata of terminally differentiated keratinocytes, respectively (Figure 4j−l and m−o). Taken together, these data support the adoption of a NOD-*scid* IL2Rgamma^{null} xenograft model for the reconstruction of human epidermal structures pertinent to human RDEB modeling. Severe blistering was observed in the RDEB grafts derived from untransduced fibroblasts in combination with untransduced keratinocytes and closely resembled the human disease phenotype (Figure 4b). Tissue cleavage at the junction between basal keratinocytes and the underlying dermis resulted in blister formation and epidermal sloughing upon mechanical stress. On the contrary, there was no blistering observed using the healthy donor fibroblast in combination with healthy donor keratinocytes (Figure 4a). Importantly, in grafts comprising vector-transduced RDEB fibroblasts with untransduced keratinocytes, there was also no indication of blister formation, consistent with restoration of the DEJ (Figure 4c and Supplementary Figure S2a−c) and supported by the detection of C7 expression. Robust expression of human-specific C7 was seen only in grafts incorporating transduced fibroblasts, with the deposition of the protein throughout the DEJ at levels comparable with healthy donor grafts (Figure 5a and c). C7 expression could also be detected in fibroblasts in the dermis by punctate staining in corrected RDEB grafts and healthy donor grafts, but not in untransduced RDEB cell combinations (Figure 5a−c). Collectively, these data provide compelling evidence that human C7 expression can be restored in vivo at the DEJ by RDEB fibroblasts transduced with LV-*COL7*.

LV-*COL7*-mediated restoration of AFs at the DEJ of RDEB skin grafts

To evaluate whether the C7 expression confirmed in grafts incorporating LV-*COL7*-transduced RDEB fibroblasts extended to the formation of AFs, ultrathin sections of each graft were imaged by TEM. The micrographs revealed an abundance sublamina densa fibrillary structures that bore the

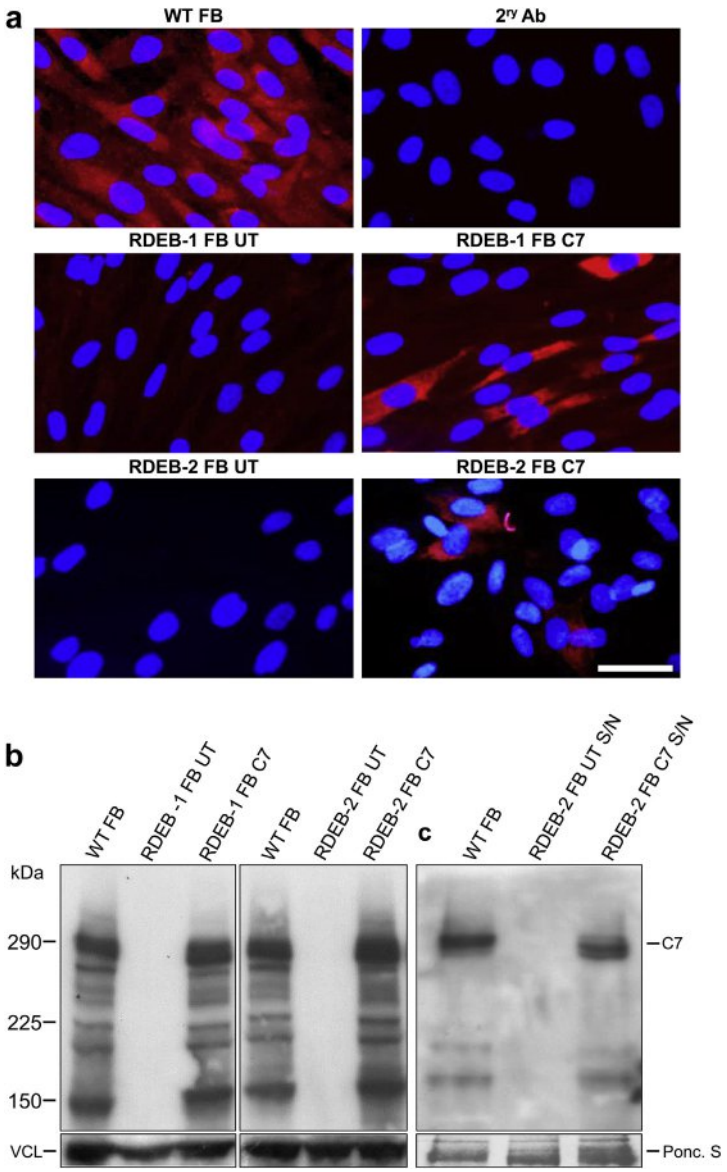

Figure 2. Restoration of full-length C7 protein expression in RDEB fibroblasts. (**a**) In situ immunocytochemistry for type VII collagen expression (C7) (red) and nuclear stain 4′.6-diamidino-2-phenylindole (blue) of either healthy primary (WT) or RDEB-1 and -2 patient untransduced (UT) or LV-*COL7* fibroblasts. C7 expression restored after LV-*COL7* transduction at MOI 5. Bar = 25 μm. (**b**) RDEB-1 and -2 fibroblast pellets were lysed before assessment by SDS-PAGE. Restoration of full-length C7 expression visualized at 290 kDa in LV-*COL7* and WT fibroblasts. The complete absence of C7 expression was seen in both RDEB-1 and -2 UT samples. Vinculin represents internal loading control. (**c**) Culture supernatant from WT, RDEB-2 UT, and LV-*COL7* fibroblasts showing secreted C7 protein at 290 kDa after lentiviral transduction. Ponceau S used as internal loading control. LV, lentiviral; MOI, multiplicity of infection; RDEB, recessive dystrophic epidermolysis bullosa; UT, untransduced; WT, wild-type.

ultrastructural characteristics of normal AFs. These appeared similar to the AFs seen in healthy donor control grafts, exhibiting cross-banding and extending approximately 200 nm into the dermis, looping around type I and III dermal collagen fibers (Figure 5d, h and f, i). The morphological features of hemidesmosomes, subbasal dense plates, and anchoring filaments also resembled control skin. In addition, there was an abundance of plasmalemmal vesicles within the finger-like protrusions of the basal keratinocytes in close proximity to the basement membrane zone. In both control and transduced grafts, there was no blistering or tissue cleavage at the DEJ and a robust lamina densa throughout, consistent with the functional correction of the DEJ with restoration of dermal-epidermal adhesion by AFs (Figure 5d, h and f, i). In contrast, the nonmodified RDEB grafts had a blistering phenotype and an extensive splitting of sublamina densa leading to complete separation of the epidermis from the underlying dermis (Figure 5e and h). Moreover, the hemidesmosomes were reduced in number, smaller and, in some cases, internalized. There were no clearly discernible AFs at the DEJ, in keeping with an absence of C7 by immunofluorescent staining (Figure 5b). Overall, the data suggest that C7 secreted by a modest proportion of engineered fibroblasts is sufficient for the generation of robust AFs and the amelioration of blistering at the DEJ.

DISCUSSION

RDEB is a serious, painful, and disabling condition with limited therapeutic options. Based on recent experience with allogeneic fibroblasts (Wong et al., 2008), there is a strong rationale to develop a therapy for RDEB using autologous gene-engineered fibroblasts. Wong et al. reported allogeneic fibroblast cell therapy for RDEB-supported twofold increases in C7 immunostaining at the sites injected with donor fibroblasts, although it has been postulated that autocrine effects exerted on recipient keratinocytes by inflammation-induced heparin-binding EGF may also indirectly lead to increased

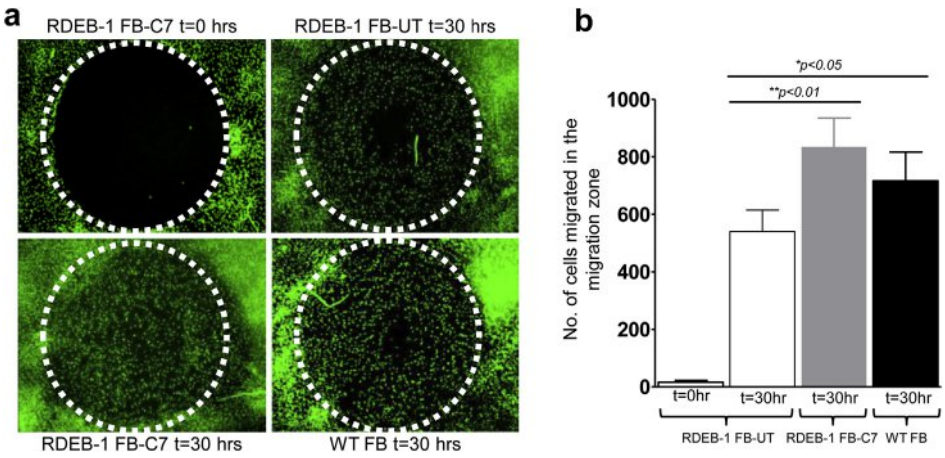

Figure 3. Human RDEB fibroblasts corrected for C7 showed improved migration and "wound" closure in vitro. (**a**) Representative micrographs of RDEB-1 fibroblasts corrected for C7 from three independent experiments show the migration pattern in a 2 mm migration zone at 30 hours ($T = 30$). (**b**) Bar graph showing normalization of migration of C7 corrected primary RDEB-1 fibroblasts toward WT values compared with uncorrected (UT) primary RDEB fibroblasts at 30 hours. Statistical analysis carried out using Student's *t*-test. C7, type VII collagen; RDEB, recessive dystrophic epidermolysis bullosa; SD, standard deviation; WT, wild-type. Error bars represent SD of four replicates.

synthesis and secretion of endogenous C7 (Nagy et al., 2011; Wong et al., 2008). An unexpected indirect upregulation of *COL7A1* was also found after intradermal injection of placebo suspension solution alone (Nagy et al., 2011; Venugopal et al., 2010), with further confirmation in a randomized clinical trial (Venugopal et al., 2010), although the precise mechanism remains unclear. In any case, such a therapy has potential advantages over gene-modified epidermal graft approaches in RDEB (Siprashvili et al., 2010), where there is concern that grafts may fail because of the nature of the DEJ defects. Localized injections of engineered fibroblasts could be used to treat troublesome blistering lesions, and systemic delivery may deliver more generalized benefit. The demonstration of safety of vector-modified cells in a localized setting would provide valuable data for subsequent systemic therapies using the same vector platform.

Whereas allogeneic fibroblasts mediated only transient benefits and were rejected over a matter of weeks, engineered autologous cells should provide longer lasting effects. This may be partly mediated through local effects triggered by the intradermal injections, but more importantly by the secretion of recombinant C7 produced in situ by a subpopulation of transduced cells. Effective fibroblast transduction has previously been reported using a variety of methods (Chen et al., 2002; Ortiz-Urda et al., 2003; Woodley et al., 2003) with a γ-retroviral delivery developed with clinical applications in mind, but troubled by low vector titer and high frequency of abnormal, shortened collagen forms (Titeux et al., 2010). Our LV platform was developed with clinical applications in mind and includes a human phosphoglycerate kinase internal promoter and co-*COL7A1* transgene with eliminated cryptic splice sites. All reagents, including sera and enzymes, were sourced for their certificates of analysis and transmissible spongiform encephalopathie compliance. Vector titer was modest, reflecting the large cargo size, and we found a greatly reduced frequency of truncated, or variant, C7 forms arising because of recombination events during reverse transcription. Our data indicate that ex vivo gene transfer to a modest number of fibroblasts using this vector results in high levels of C7 expression at the DEJ. The vector supports supranormal levels of protein expression in transduced cells, as indicated by the high intensities of C7 detected by Western blot, in-cell assays and flow cytometry. Critically, the reconstitution of C7 at the DEJ supported the regeneration of ultrastructural features including AFs.

We found that the NOD-*scid* IL2Rgamma^{null} immunodeficient mouse strain was amenable to human skin grafting without the need for irradiation or additional immunosuppression. These animals are devoid of T, B, and NK cells with additional defects of innate immunity and, thus, unable to mount effective rejection of human xenografts. Previous studies of human skin grafting (Di et al., 2011; Larcher et al., 2007) adopted the Foxn1^{nu} *nude* mouse strain, which is athymic and deficient of T cells but can retain NK and other aspects of the immune repertoire. Importantly, the grafts recovered from our model had clearly demarcated human:-murine junctional boundaries, and characteristic epidermal structural features of healthy or RDEB skin, including a predisposition for epidermal detachment and blistering.

Our experiments used ex vivo transduction and graft preparation and were specifically designed to circumvent the triggering of localized paracrine effects that may be induced by injection into the epidermis. Whereas previous reports suggested that residual or baseline expression of C7 by keratinocytes may be necessary to secure a therapeutic effect (Kern et al., 2009; Wagner et al., 2010; Wong et al., 2008), we found that the restoration of C7 expression at the DEJ and AF formation was mediated by transduced fibroblasts even in combination with non-C7-expressing keratinocytes. This translated to eradication of subepidermal cleavage seen in noncorrected grafts.

With regard to future clinical translation, we have completed the production and release of a clinical batch of LV-*COL7* and demonstrated engineering of human RDEB fibroblasts under good-manufacturing-practice conditions. UK regulatory and ethics committee approval has recently been secured for a first-in-man study, designed in the first instance as a single-arm, open-label study to confirm the feasibility and safety of an approach using the localized intradermal injection of fibroblasts. If successful, comparison against control injections will follow and further systemic therapies

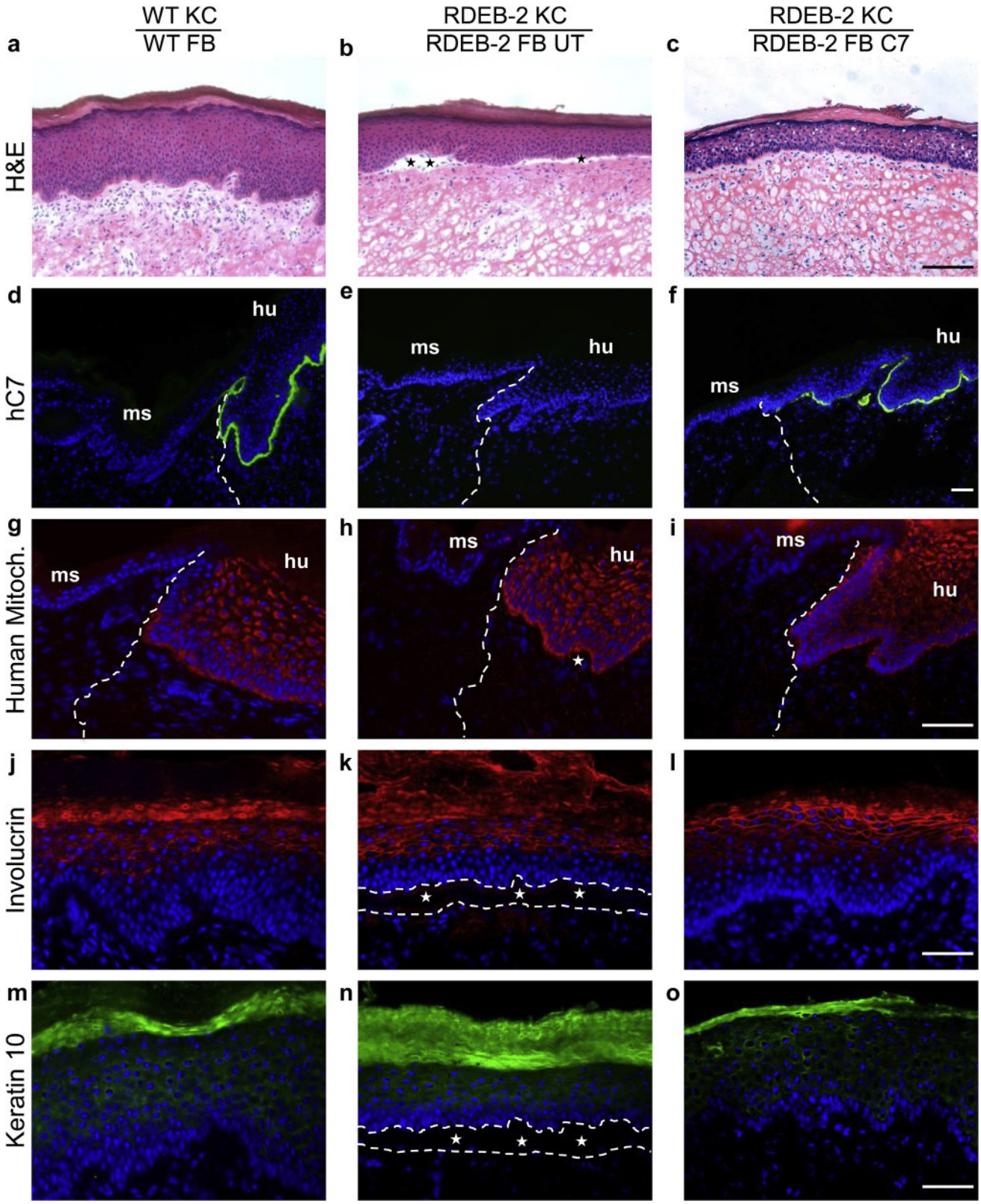

Figure 4. Visualization of human origin and epidermal cytoarchitecture of bioengineered skin sheets generated on NOD-*scid* IL2Rgamma^{null} mice. (**a**–**c**) H&E staining of WT, RDEB-2 untransduced (UT), or LV-*COL7* fibroblast (FB) graft combination seeded with WT or RDEB-2 UT patient keratinocytes (KC). Blistering seen in RDEB-2 UT combination (stars). Bar = 50 μm. Human-specific anti-C7 antibody showing expression in healthy and LV-*COL7* grafts (**d**, **f**) but not in untreated RDEB grafts (**e**). Bar = 50 μm. (**g**–**i**) Human-specific mitochondrial marker identifies the human:mouse junction: the border between mouse (ms) and bioengineered human (hu) skin (dotted line). Bar = 25 μm. Involucrin staining reveals cornification (**j**–**l**); keratin 10 shows a later stage of KC differentiation (**m**–**o**). Epidermal-dermal tissue cleavage in RDEB-2 patient UT combination (dotted lines). C7, type VII collagen; H&E, hematoxylin and eosin; LV, lentiviral; RDEB, recessive dystrophic epidermolysis bullosa; WT, wild-type. Bar = 25 μm.

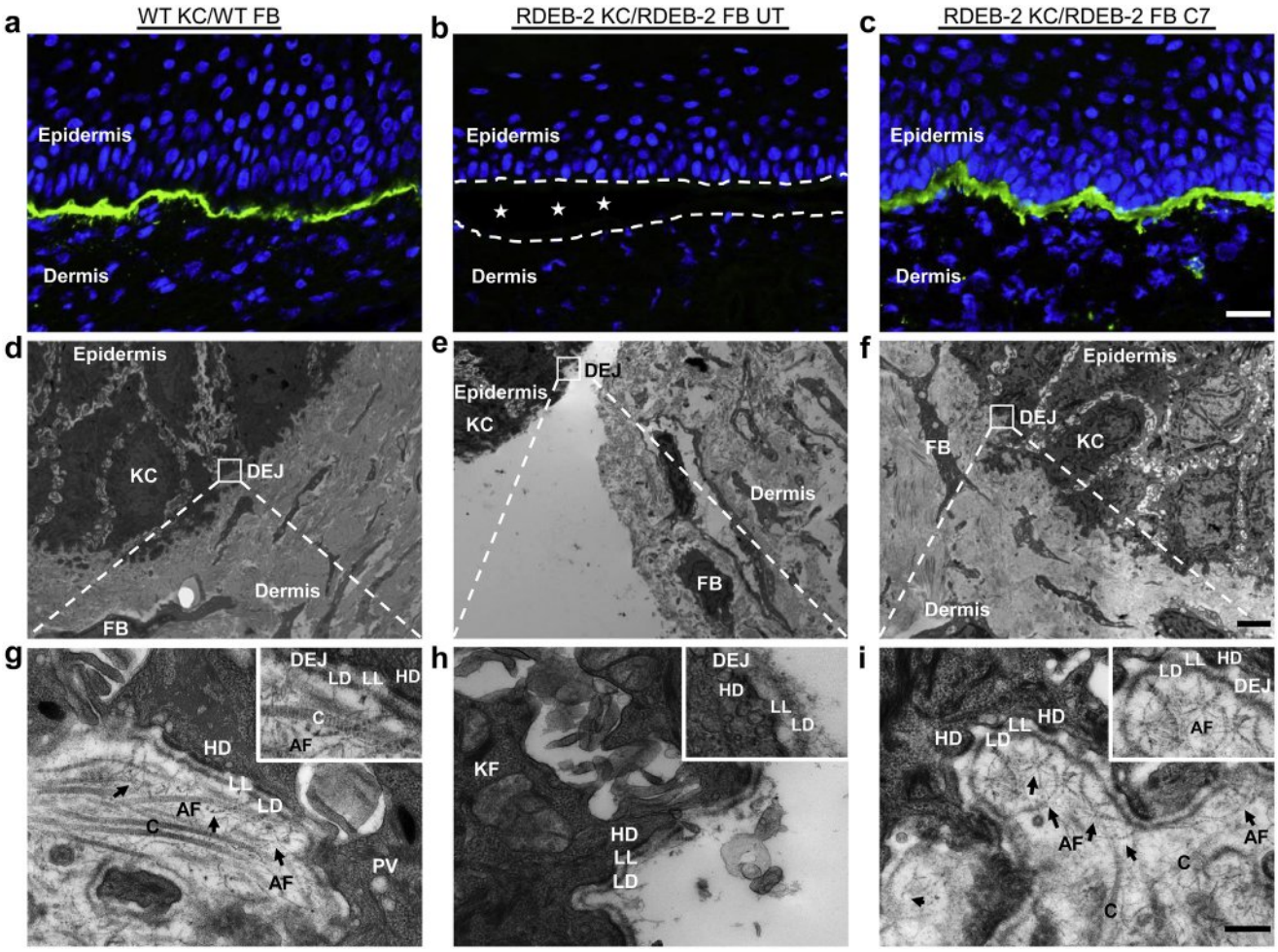

Figure 5. In vivo functional correction through LV-*COL7*-mediated restoration of type VII collagen anchoring fibrils (AFs). C7 overexpression over WT (**a**) visible in LV-*COL7* RDEB-2 fibroblast (FB) containing graft (**c**), no protein deposition seen in untransduced (UT) graft (**b**). Bar = 25 μm. TEM micrographs of WT (**d**), RDEB-2 patient UT (**e**), and LV-C*OL7* (**f**) grafts. Bar = 5 μm. (**g**) WT human keratinocyte (KC) and/or FB combination showing thick, cross-banded AFs (arrows). (**h**) Loss of AFs causes extensive tissue cleavage at the dermal-epidermal junction (DEJ) of UT RDEB-2 KC and/or FB combination with lamina densa (LD) reduplication. (**i**) UT RDEB-2 KC and/or LV-*COL7* FB combination reveals restoration of dermal-epidermal adhesion. C, collagen type I and III; C7, type VII collagen; HD, hemidesmosome; KF, keratin filament; LL, lamina lucida; LV, lentiviral; PV, plasmalemmal vesicle; RDEB, recessive dystrophic epidermolysis bullosa; TEM, transmission electron microscopy; WT, wild-type. Bar = 300 nm.

will be envisaged using the same vector platform for the treatment of RDEB and other debilitating skin diseases.

MATERIALS AND METHODS

RDEB skin biopsies and isolation and propagation of primary fibroblasts

A 6-mm RDEB skin biopsy was obtained with authorization from the National Research Ethics Services, Westminster (07/H0802/104), and with written informed consent from patients with RDEB-1 ((+/−) c.1732C>T p.R578X)/(+/−) c.2710+2T>C IVS20+2T.C) and RDEB-2 ((+/+) c.425A>G p.K142R). Excess connective tissue was removed using a sterile blade and the sample was incubated in neutral protease NB (1 unit/ml; SERVA Electrophoresis, Heidelberg, Germany) at 37 °C for 3 hours until the epidermis peeled off. The remaining dermis was fragmented and treated with collagenase NB6 (0.45 units/ml; SERVA Electrophoresis). The resulting cell suspension was seeded into a T25 flask and cultured at 37 °C in a 5% CO_2 incubator.

Production of third-generation *COL7A1*-expressing-LV vectors with human phosphoglycerate kinase promoter

pCCL is a self-inactivating-LV vector (Figure 1a) derived from HIV-1 as described previously (Dull et al., 1998). Self-inactivation was achieved through a 400 bp deletion in the 3′HIV-1 long terminal repeat and a 516 bp promoter sequence from human internal phosphoglycerate kinase promoter was included as an internal promoter (Ginn et al., 2010; Huston et al., 2011). A mutated woodchuck hepatitis virus posttranscriptional regulatory element sequence devoid of the hepadnaviral-X protein open reading frame (WPREmut6) was cloned (Marangoni et al., 2009) downstream of a full-length codon-optimized *COL7A1* transgene (Geneart, Regensburg, Germany). The vector was pseudotyped with vesicular stomatitis virus glycoprotein using a split packaging system and concentrated by ultracentrifugation. High-grade plasmids were produced, characterized, and released (PlasmidFactory, Bielefeld, Germany) for the production of good-manufacturing-practice vector stocks.

Vector titer

The titer of concentrated LV-*COL7* virus was determined by exposing 293 T cells with serial dilutions of concentrated LV-*COL7*. Three days after transduction, cells were harvested and copies of HIV Psi packaging element (Ψ) were determined by quantitative polymerase chain reaction. Proviral integrant copy number per transduced cell was determined after normalization of Ψ with housekeeping gene albumin accounting for two albumin alleles per cell. Qualified plasmid standards encoding Ψ and human albumin sequences were used.

Bioengineered skin preparation and grafting on immunodeficient mice

The methods for preparing and grafting bioengineered skin on immunodeficient *nude* mice have been described previously (Larcher et al., 2007). Our approach was similar, except the recipient strain was NOD-*scid* IL2Rgamma^{null}. In brief, fibrinogen solution (cryoprecipitate derived from a porcine plasma source) containing 1.5 $\times 10^6$ WT, RDEB-2 patient ((+/+) c.425A>G, p.K142R) or RDEB-2 LV-*COL7*-transduced human dermal fibroblasts was combined with 0.025 mmol/l $CaCl_2$ (Sigma-Aldrich, Gillingham, UK) and 11 IU of bovine thrombin (Sigma-Aldrich). The mixture was poured in two 35-mm wells and allowed to solidify at 37 °C for 1 hour. WT or RDEB patient human keratinocytes (1.2×10^6 cells per well) were then seeded on the fibrin matrix to form the epidermal layer of the bioengineered skin. When confluent (3 days), bioengineered skins were manually detached from tissue culture wells and grafted onto immunodeficient mice. All animal procedures were performed in accordance with the United Kingdom Animals Scientific Procedures Act (1986) and associated guidelines. Grafting was performed under sterile conditions using 6-week-old female immunodeficient mice (NOD-*scid* IL2Rgamma^{null}) housed under protective conditions. In brief, mice were aseptically cleansed and anesthetized, and full-thickness 35-mm-diameter circular wounds were then created on the dorsum of the mice. Bioengineered equivalents were placed orthotopically on the wound. The mouse skin removed to generate the wound was devitalized by three repeated cycles of freezing and thawing and used as a biological bandage and fixed with sutures to protect and hold the skin substitute in place during the take process. Dead mouse skin typically sloughed off within 15–20 days after grafting. Eight weeks after grafting, bioengineered human skins were harvested postmortem preserving a surrounding border of mouse epithelial tissue, snap frozen in LN_2, embedded in optimum cutting temperature (Sakura Finetek, Alphen aan den Rijn, The Netherlands) and cryosectioned at 7 μm for histological and immunohistochemical examinations. A central portion of the human graft was placed in TEM fixative for ultrastructural imaging.

Immunostaining of bioengineered grafted tissue

Immunofluorescence staining was performed on frozen graft tissue sections after 10-min fixation with ice-cold acetone and/or methanol (7 μm thickness). Sections were blocked for 1 hour at room temperature (RT) with 3% fetal bovine serum in phosphate buffered saline before incubation with primary antibodies against hC7 LH7.2 (Sigma-Aldrich) in a 1:500 dilution (Supplementary Table S1 online), desmoglein-1 (Fitzerald Industries, Acton, MA), involucrin (Sigma-Aldrich), keratin 10 (in-house), complex IV subunit II MTCO2 (Abcam, Cambridge, UK) overnight at 4 °C. Secondary antibody incubation with Alexa Fluor goat antimouse 488 (Invitrogen, Paisley, UK), goat antirabbit Cy3 (Life Technologies, Paisley, UK), and strep 488 was followed for 1 hour at RT. Sections were stained with 4′.6-diamidino-2-phenylindole (5 mg/ml) and mounted using a ProLong Gold antifade agent (Life Technologies). These were also stained by a hematoxylin and eosin histochemical technique. Staining was visualized and imaged using a Leica DMLB upright microscope (Leica Microsystems CMS, Wetzlar, Germany) and a Zeiss Axiophot 2 (Zeiss, Oberkochen, Germany) and processed using Image-Pro 6.2 (MediaCybernetics, Rockville, MD). Confocal imaging was carried out on a Zeiss LSM 510 Meta laser confocal microscope (Zeiss). Postprocessing was carried out using ImageJ.

Preparation of skin grafts for TEM

For TEM, the central piece (approximately 3×3 mm^2) of each skin graft was dissected out and fixed with half strength Karnovsky's fixative (2% [v/v] paraformaldehyde, 2.5% [v/v] glutaraldehyde in 0.1 M phosphate buffer [pH 7.4]) for 3–5 hours at RT and kept at 4 °C until further processing. After the initial fixation, tissue samples were rinsed several times in phosphate buffer and postfixed with 1.3% osmium tetroxide in double distilled water for 2 hours at RT. Samples were then washed, en bloc stained with 2% uranyl acetate in 50% ethanol and dehydrated in a graded series of ethanols. Tissue samples were further equilibrated with propylene oxide before infiltration with TAAB epoxy resin, embedded, and polymerized at 70 °C for 24 hours. Ultrathin sections (70–90 nm) were prepared using a Reichert-Jung Ultracut E ultramicrotome (Eeichert-Jung, Vienna, Austria), mounted on 150 mesh copper grids (Gilder, Grantham, UK), contrasted using uranyl acetate and lead citrate and examined on a FEI Tecnai 12 (FEI, Hillsboro, OR) transmission microscope operated at 120 kV. Images were acquired with an AMT 16000M camera (Advanced Microscopy Techniques, Woburn, MA). Morphological examination and AF scoring of the TEM slides was blinded and performed by an ultrastructural microscopy specialist.

CONFLICT OF INTEREST

The authors state no conflict of interest.

ACKNOWLEDGMENTS

Funding was received from DEBRA International and Sohana Research Fund, and GOSH/NIHR Biomedical Research Centre. CG received an IMPACT PhD studentship. WQ is supported by GOSH charity special trustees. AJT is a Wellcome principal fellow.

SUPPLEMENTARY MATERIAL

Supplementary material is linked to the online version of the paper at www.jidonline.org, and at http://dx.doi.org/10.1038/JID.2015.364.

REFERENCES

Burgeson RE, Lunstrum GP, Rokosova B, et al. The structure and function of type VII collagen. Ann N Y Acad Sci 1990;580:32–43.

Chen M, Kasahara N, Keene DR, et al. Restoration of type VII collagen expression and function in dystrophic epidermolysis bullosa. Nat Genet 2002;32:670–5.

Conget P, Rodriguez F, Kramer S, et al. Replenishment of type VII collagen and re-epithelialization of chronically ulcerated skin after intradermal administration of allogeneic mesenchymal stromal cells in two patients with recessive dystrophic epidermolysis bullosa. Cytotherapy 2010;12:429–31.

Di WL, Larcher F, Semenova E, et al. Ex-vivo gene therapy restores LEKTI activity and corrects the architecture of Netherton syndrome-derived skin grafts. Mol Ther 2011;19:408–16.

Di WL, Semenova E, Larcher F, et al. Human involucrin promoter mediates repression-resistant and compartment-specific LEKTI expression. Hum Gene Ther 2012;23:83–90.

Droz-Georget Lathion S, Rochat A, Knott G, et al. A single epidermal stem cell strategy for safe ex vivo gene therapy. EMBO Mol Med 2015;7:380–93.

Dull T, Zufferey R, Kelly M, et al. A third-generation lentivirus vector with a conditional packaging system. J Virol 1998;72:8463–71.

Fine J-D, Bruckner-Tuderman L, Eady RA, et al. Inherited epidermolysis bullosa: updated recommendations on diagnosis and classification. J Am Acad Dermatol 2014;70:1103–26.

Fine J-D, Mellerio JE. Extracutaneous manifestations and complications of inherited epidermolysis bullosa: part I. Epithelial associated tissues. J Am Acad Dermatol 2009;61:367–84.

Ginn SL, Liao SH, Dane AP, et al. Lymphomagenesis in SCID-X1 mice following lentivirus-mediated phenotype correction independent of insertional mutagenesis and γc overexpression. Mol Ther 2010;18:965–76.

Goto M, Sawamura D, Ito K, et al. Fibroblasts show more potential as target cells than keratinocytes in COL7A1 gene therapy of dystrophic epidermolysis bullosa. J Invest Dermatol 2006;126:766–72.

Grocott P, Blackwell R, Weir H, et al. Living in dressings and bandages: findings from workshops with people with epidermolysis bullosa. Int Wound J 2013;10:274–84.

Hovnanian A, Rochat A, Bodemer C, et al. Characterization of 18 new mutations in COL7A1 in recessive dystrophic epidermolysis bullosa provides evidence for distinct molecular mechanisms underlying defective anchoring fibril formation. Am J Hum Genet 1997;61:599–610.

Huston MW, van Til NP, Visser TP, et al. Correction of murine SCID-X1 by lentiviral gene therapy using a codon-optimized IL2RG gene and minimal pretransplant conditioning. Mol Ther 2011;19:1867–77.

Kern JS, Loeckermann S, Fritsch A, et al. Mechanisms of fibroblast cell therapy for dystrophic epidermolysis bullosa: high stability of collagen VII favors long-term skin integrity. Mol Ther 2009;17:1605–15.

Larcher F, Del Río M. Innovative therapeutic strategies for recessive dystrophic epidermolysis bullosa. Actas Dermosifiliogr 2015;106:376–82.

Larcher F, Dellambra E, Rico L, et al. Long-term engraftment of single genetically modified human epidermal holoclones enables safety preassessment of cutaneous gene therapy. Mol Ther 2007;15:1670–6.

Marangoni F, Bosticardo M, Charrier S, et al. Evidence for long-term efficacy and safety of gene therapy for Wiskott-Aldrich syndrome in preclinical models. Mol Ther 2009;17:1073–82.

Martins VL, Vyas JJ, Chen M, et al. Increased invasive behaviour in cutaneous squamous cell carcinoma with loss of basement-membrane type VII collagen. J Cell Sci 2009;122:1788–99.

Mellerio JE, Weiner M, Denyer JE, et al. Medical management of epidermolysis bullosa: proceedings of the IInd international symposium on epidermolysis bullosa, Santiago, Chile, 2005. Int J Dermatol 2007;46:795–800.

Nagy N, Almaani N, Tanaka A, et al. HB-EGF induces COL7A1 expression in keratinocytes and fibroblasts: possible mechanism underlying allogeneic fibroblast therapy in recessive dystrophic epidermolysis bullosa. J Invest Dermatol 2011;131:1771–4.

Nystrom A, Velati D, Mittapalli VR, et al. Collagen VII plays a dual role in wound healing. J Clin Invest 2013;123:3498–509.

Ortiz-Urda S, Lin Q, Green CL, et al. Injection of genetically engineered fibroblasts corrects regenerated human epidermolysis bullosa skin tissue. J Clin Invest 2003;111:251–5.

Osborn MJ, Starker CG, McElroy AN, et al. TALEN-based gene correction for epidermolysis bullosa. Mol Ther 2013;21:1151–9.

Petrof G, Martinez-Queipo M, Mellerio J, et al. Fibroblast cell therapy enhances initial healing in recessive dystrophic epidermolysis bullosa wounds: results of a randomized, vehicle-controlled trial. Br J Dermatol 2013;169:1025–33.

Remington J, Wang X, Hou Y, et al. Injection of recombinant human type VII collagen corrects the disease phenotype in a murine model of dystrophic epidermolysis bullosa. Mol Ther 2008;17:26–33.

Rodeck U, Uitto J. Recessive dystrophic epidermolysis bullosa–associated squamous-cell carcinoma: an enigmatic entity with complex pathogenesis. J Invest Dermatol 2007;127:2295–6.

Rousselle P, Keene DR, Ruggiero F, et al. Laminin 5 binds the NC-1 domain of type VII collagen. J Cell Biol 1997;138:719–28.

Sebastiano V, Zhen HH, Derafshi BH, et al. Human COL7A1-corrected induced pluripotent stem cells for the treatment of recessive dystrophic epidermolysis bullosa. Sci Transl Med 2014;6:264ra163.

Shimizu H, Ishiko A, Masunaga T, et al. Most anchoring fibrils in human skin originate and terminate in the lamina densa. Lab Invest 1997;76:753–63.

Siprashvili Z, Nguyen NT, Bezchinsky MY, et al. Long-term type VII collagen restoration to human epidermolysis bullosa skin tissue. Hum Gene Ther 2010;21:1299–310.

Syed F, Sanganee HJ, Bahl A, et al. Potent dual inhibitors of TORC1 and TORC2 complexes (KU-0063794 and KU-0068650) demonstrate in vitro and ex vivo anti-keloid scar activity. J Invest Dermatol 2013;133:1340–50.

Tabolli S, Sampogna F, Di Pietro C, et al. Quality of life in patients with epidermolysis bullosa. Br J Dermatol 2009;161:869–77.

Titeux M, Pendaries V, Zanta-Boussif MA, et al. SIN retroviral vectors expressing COL7A1 under human promoters for ex vivo gene therapy of recessive dystrophic epidermolysis bullosa. Mol Ther 2010;18:1509–18.

Tolar J, Wagner JE. Management of severe epidermolysis bullosa by haematopoietic transplant: principles, perspectives and pitfalls. Exp Dermatol 2012;21:896–900.

Venugopal SS, Yan W, Frew JW, et al. First double-blind randomized clinical trial of intradermal allogeneic fibroblast therapy for severe generalized recessive dystrophic epidermolysis bullosa randomized against placebo injections resulted in similar wound healing that is independent of collagen VII expression. J Invest Dermatol 2010;130(Suppl 2):S67.

Venugopal SS, Yan W, Frew JW, et al. A phase II randomized vehicle-controlled trial of intradermal allogeneic fibroblasts for recessive dystrophic epidermolysis bullosa. J Am Acad Dermatol 2013;69:898–908.

Wagner JE, Ishida-Yamamoto A, McGrath JA, et al. Bone marrow transplantation for recessive dystrophic epidermolysis bullosa. N Engl J Med 2010;363:629–39.

Wong T, Gammon L, Liu L, et al. Potential of fibroblast cell therapy for recessive dystrophic epidermolysis bullosa. J Invest Dermatol 2008;128:2179–89.

Woodley DT, Keene DR, Atha T, et al. Intradermal injection of lentiviral vectors corrects regenerated human dystrophic epidermolysis bullosa skin tissue in vivo. Mol Ther 2004;10:318–26.

Woodley DT, Krueger GG, Jorgensen CM, et al. Normal and gene-corrected dystrophic epidermolysis bullosa fibroblasts alone can produce type VII collagen at the basement membrane zone. J Invest Dermatol 2003;121:1021–8.

Woodley DT, Remington J, Huang Y, et al. Intravenously injected human fibroblasts home to skin wounds, deliver type VII collagen, and promote wound healing. Mol Ther 2007;15:628–35.

Woodley DT, Wang X, Amir M, et al. Intravenously injected recombinant human type VII collagen homes to skin wounds and restores skin integrity of dystrophic epidermolysis bullosa. J Invest Dermatol 2013;133:1910–3.